,,,,,

UNIVERSITY OF SOUTHAMPTON

Faculty of Engineering and Physical Science
School of Electronics and Computer Science

UAV-Assisted Wireless Communications

DOI: 10.5258/SOTON/D2373

by

Mingze Zhang
B.Eng., M.Sc.
ORCiD: 0000-0003-4798-2526

A thesis for the degree of
Doctor of Philosophy

September 2022

University of Southampton

Abstract

Faculty of Engineering and Physical Science
School of Electronics and Computer Science

Doctor of Philosophy

UAV-Assisted Wireless Communications

by Mingze Zhang

Unmanned aerial vehicles (UAVs) have been attracting a lot of attention in recent years for its potential in numerous applications. Due to the flexibility and mobility of UAVs, UAV-mounted base stations are effective and cost-efficient to provide wireless connectivity and to improve the performance of terrestrial wireless network when fixed infrastructure is not available. In particular, UAVs can timely adjust their locations according to the movement of ground users (GUs).

Against this background, we firstly propose a method to apply mobile edge caching on UAVs in wireless communication systems. By investigating the user request preference with the aid of latent Dirichlet allocation (LDA), the caching strategy can be optimized. In the proposed system, we consider the design of intelligent caching strategies when a number of UAVs are deployed to serve the GUs, where each UAV has a limited storage capacity for caching useful user contents. We use LDA to extract the user request preferences in order to intelligently caching data in the UAVs, while the k-means clustering is utilized to classify GUs and to assist in deploying the UAVs. Additionally, we consider three user-UAV association criteria, namely the user received signal to noise ratio (SNR), user preferences and the delay. Our simulation results show that, when compared to random caching, the average caching efficiency could be significantly improved from 50% to 70%, while the latency of our proposed system can also be greatly reduced.

Then, we propose an optimized UAV-user association technique that can mitigate the challenge of the existence of "outliers" caused by limited UAV resources. More specifically, in order to solve the sudden-shift of UAVs position, which is a challenge for traditional deployment algorithm such as the k-means clustering, we propose a reinforcement learning based method to eliminate the challenge of sudden-shift requirement as well as to provide an improved performance, when we have limited UAV resources. Our simulation results show that the proposed UAV-user association can provide a solution for the "outliers" problem. Meanwhile, the average downlink rate of the system, which employs the proposed deep Q-learning (DQL) based UAV deployment, is close

to the ideal system that employs a k-means clustering with infinite UAV speed. Additionally, we show that the DQL provides an improved performance, when the number of UAV is limited for a given coverage area.

On the other hand, given the limited availability of on-board energy, we design an energy efficient communication scheme. Explicitly, we propose a method that combines the concept of index modulation (IM) with the UAV communications systems, which we refer to as IM-UAV, to attain an improved energy efficiency (EE). Furthermore, based on the proposed IM-UAV communication system, a gradient descent based UAV deployment scheme is designed to maximize the sum rate of the GUs in the target area. Additionally, the maximum likelihood detection for the IM-UAV requires a high computational complexity for detection at the GUs, while providing the best possible performance. Hence, we propose a low-complexity detection scheme that can separately detect the index symbols and data symbols to reduce the computational complexity at the receiver side. The simulation results demonstrate that the proposed deployment method is capable of attaining the appropriate positions to deploy the UAVs, while the EE is also improved by combining IM with UAV communication system.

Finally, we consider a content-aware scenario that employs UAVs as aerial base stations to transmit data to GUs via air to ground communication links. Furthermore, inspired by the concept of rate splitting (RS), we design two subcarrier-sharing (SS) data transmission schemes to improve the average data rate of the GUs. Additionally, based on the proposed transmission schemes, we design the UAV deployment schemes, namely the fixed-point deployment scheme and traverse-search deployment scheme. The simulation results demonstrate that our proposed data transmission techniques significantly increase the average data rate, while the deployment schemes are capable of optimizing the data rate in the respective application scenarios.

Contents

List of Figures

List of Tables

Declaration of Authorship

I declare that this thesis and the work presented in it is my own and has been generated by me as the result of my own original research.

I confirm that:

1. This work was done wholly or mainly while in candidature for a research degree at this University;
2. Where any part of this thesis has previously been submitted for a degree or any other qualification at this University or any other institution, this has been clearly stated;
3. Where I have consulted the published work of others, this is always clearly attributed;
4. Where I have quoted from the work of others, the source is always given. With the exception of such quotations, this thesis is entirely my own work;
5. I have acknowledged all main sources of help;
6. Where the thesis is based on work done by myself jointly with others, I have made clear exactly what was done by others and what I have contributed myself;
7. Parts of this work have been published as:

Signed:..... Date:.....

Acknowledgements

I would like to express my heartfelt gratitude to Dr. Mohammed El-Hajjar and Prof. Soon Xin Ng for their outstanding supervision and support throughout my research. Without their patient instruction, insightful criticism and expert guidance, my research would not have been done successfully. Thank Dr. Mohammed El-Hajjar for not only offering me valuable suggestions in the academic studies but also teaching me the attitude of "step by step". In a word, their guidance, inspiration and encouragement have greatly benefited me not only in work but also in life. Most importantly, I would like to thank them for their invaluable friendship.

Many thanks also to my colleagues and the staff of the Next Generation Wireless Research Group, both past and present, for their support, help and discussions throughout my research. Special thanks to my colleagues, Prof. Lajos Hanzo, Prof. Sheng Chen, Prof. Lie-Liang Yang, Prof. Rob Maunder, Dr. Chao Xu, Dr. Jiankang Zhang, Dr. Yifeng Xiong, Dr. Luping Xiang, Dr. Xiaoyu Zhang, Dr. Siyao Lu, Dr. Yusha Liu and Dr. Shuai Shao for their kindly provided technical support and collaborative work. Thanks to my friends I have during my PhD years, too numerous to mention here explicitly.

Finally, I would like to express my strongest gratitudes to my father, Wei Zhang, who dedicated his life and love to my success in my life, supporting me endlessly and selflessly, leading me to a bright future, and my mother, Chune Bian, who contributes her encouragement and faith to me, nurturing and supporting me. I am forever grateful they bring me into this world and let me follow my dream.

List of Publications

1. **M. Zhang**, M. El-Hajjar and S. X. Ng, "Intelligent Caching in UAV-Aided Networks", IEEE Transactions on Vehicular Technology,vol.71,pp.739-752,2021.

2. **M. Zhang**, M. El-Hajjar and S. X. Ng, "Deep Q-learning for UAV Deployment in Dynamic Environments with Optimized UAV-user Association", submitted to IEEE Transactions on Vehicular Technology.

3. **M. Zhang**, Y. Xiong, M. El-Hajjar and S. X. Ng, "Deployment of Energy-Efficient Aerial Communication Platforms with Low-Complexity Detection", submitted to IEEE Transactions on Vehicular Technology.

4. **M. Zhang**, Y. Xiong, M. El-Hajjar and S. X. Ng, "Content-Aware Transmission in UAV-Assisted Multicast Communication", submitted to IEEE Transactions on Broadcasting.

5. **M. Zhang**, M. El-Hajjar and S. X. Ng, "UAV-based 6G Communication for Net-Zero", book chapter in "The Role of 6G and Beyond on the Road to Net-Zero Carbon", in preparation.

List of Abbreviations

1G	First generation
2D	Two dimensional
3D	Three dimensional
5G	Fifth generation
5G PPP	5G Infrastructure Public Private Partnership
6G	Sixth generation
A2A	Air-to-air
A2G	Air-to-ground
ABS	Aerial base station
AMC	Automatic modulation classification
ANN	Artificial neural network
AP	Access point
BS	Base station
BBU	Baseband unit
BER	Bit error rate
CCS	Common content sharing
CDMA	Code division multiple access
CNN	Convolutional neural network
C-RAN	Cloud radio access network
CRT	Click-through rate
CSI	Channel state information
D2D	Device to device
DDCS	Dynamic duty circle selection
DFT	Discrete Fourier transform
DQL	Deep Q-learning
DQN	Deep Q-network
DRL	Deep reinforcement learning
EE	Energy efficiency
ESN	Echo state network
FBS	Femto base station
FDM	Frequency division multiplexing
FFT	Fast Fourier transform

F-RAN	Fog radio access network
GAK-means	Genetic algorithm based k-means
GP	Gaussian process
GSM	Generalised spatial modulation
GU	Ground user
HetNet	Heterogeneous network
IDFT	Inverse discrete Fourier transform
IM	Index modulation
IoTs	Internet of Things
KNN	K nearest neighbour
LDA	Latent Dirichlet allocation
LiDAR	Light detection and ranging
LoS	Line of sight
LSTM	Long short-term memory
LTE-U	LTE-Unlicensed
M2M	Machine to machine
MA-SM	Multiple-active spatial modulation
MBS	Macro base station
MCC	Mobile cloud computing
MDP	Markov decision process
MEN	Mobile edge network
MIMO	Multiple input multiple output
ML	Machine learning
MOS	Mean opinion score
MPC	Multipath component
M-PSK	M-ary phase shift keying
M-QAM	M-ary quadrature amplitude modulation
NLoS	Non line of sight
NMPC	Nonlinear model predictive control
NN	Neural network
OFDM	Orthogonal frequency division multiplexing
OFDMA	Orthogonal frequency division multiple access
PBS	Pico base station
PCS	Private content sharing
QL	Q-learning
QoE	Quality of experience
QoS	Quality of service
RAIM	Resource allocation and interference management
RandF	Random forest
RBL	Regret-based learning
RL	Reinforcement learning

RRH	Remote radio head
RS	Rate splitting
RSS	Received signal strength
RU	Resource unit
SE	Spectrum efficiency
SBS	Small base station
SINR	Signal to interference plus noise ratio
SM	Spatial modulation
SNR	Signal to noise ratio
CS	Content sharing
STC	Space-time coding
TBS	Terrestrial base station
TD	Temporal difference
TDMA	Time division multiple access
UAV	Unmanned aerial vehicle
UE	User equipment
ULA	Uniform linear array
V-BLAST	Vertical Bell Laboratories layered space-time

List of Symbols

A_i	Coefficient dedicated for the i^{th} subcarrier
A_u	Coefficient dedicated for the u^{th} GU
b_i	The i^{th} independent binary random variables
B	Bandwidth
c	Speed of light
C_d^i	The i^{th} content cached in the d^{th} UAV
$C_n^m(\cdot)$	Capacity of the n^{th} GU and the m^{th} UAV link
C_p	Parasitic capacitance of each switch
C_t^u	Capacity of the u^{th} GU at the t^{th} time slot
d	Distance between the transmitter and receiver
d_i^j	Distance from the j^{th} transmitter antenna to the i^{th} receiver antenna
$d_m^n(\cdot)$	The A2G distance between the n^{th} GU and the m^{th} UAV
d_u	Distance between the u^{th} GU and the UAV
$\boldsymbol{D}$	Distance matrix
D_r	Request delay from BSs to UAVs
D_{sum}^c	The current total distance
D_{sum}^s	The total distance after exchange
e	Euler number
f_c	Carrier frequency
f_{cor}	Corner frequency
f_s	Sampling frequency
F	Flag used for parity check
$F_n(\cdot)$	Flag to indicate if $\gamma_n^m(\cdot)$ can support basic communication
$\boldsymbol{F}_i$	Filter vector for the i^{th} subcarrier
$\boldsymbol{F}_u$	Filter vector for the u^{th} GU
$\boldsymbol{G}$	The coordinate of the UAV
$\tilde{\boldsymbol{G}}$	The terrestrial coordinate of the UAV
h	Normalised complex Rician channel
h_d	Flying height of UAV
h_i	The channel of the i^{th} GU at the i^{th} subcarrier
h_i^j	Channel from the j^{th} transmitter antenna to the i^{th} receiver antenna

h_T	Channel threshold
h_{LoS}	Deterministic LoS component
h_{NLoS}	Stochastic NLoS component
$\boldsymbol{H}$	$N_r \times N_t$ Rician channel matrix
$\boldsymbol{H}_{\text{LoS}}$	$N_r \times N_t$ Deterministic LoS channel matrix
$\boldsymbol{H}_{\text{NLoS}}$	$N_r \times N_t$ Stochastic NLoS channel matrix
I_o	Total output current
I_u	Unit current source
$I_0(\cdot)$	0^{th} order modified Bessel function of the first kind
$\boldsymbol{I}$	Number of bits used for index symbols
$\boldsymbol{I}_{N_r}$	N_r dimensional identity matrix
k	Total number of I_u
K	Power ratio of the LoS path and the NLoS path
K_{N_a}	Number of all possible activated combinations
l_m	The size of mini-batch
l_r	Learning rate of gradient descent
l_u	The length of buffer
L	The length of target area
M	Modulation order
$\boldsymbol{M}$	Number of incoming bits
n_c	Size of each content
n_i	Noise at the i^{th} subcarrier
n_m	Memory size of UAVs
N	Resolution of DAC
N_a	Number of activated UAVs
N_c	Number of contents considered in the system
N_d	Number of UAVs considered in the system
N_{ds}	Number of data subcarriers
N_e	Number of epochs
N_h	Number of possible combinations of the channels
N_l	Number of layers in neural network
N_m	Number of GUS allocated to m^{th} UAV
N_m^a	Number of GUS successfully associated to the m^{th} UAV
N_n	The size of layers in neural network
$N_o(\cdot)$	Number of outage GUs
N_q	Number of words in the q^{th} document
N_r	Number of receiver antennas
N_s	Number of subcarriers
N_t	Number of transmitter antennas
N_u	Number of GUs considered in the system
N_0	Noise power spectral density

p_e	The optimum value of power allocation coefficient p_i
p_i	Power allocation coefficient of the common message in the i^{th} subcarrier
$P(\cdot)$	Penalty of collision
P_a	Power consumption of power amplifier
P_c	Power consumption of other circuit blocks
P_d	Dynamic power consumption
$P_d(\cdot)$	PDF of UAV-content
$\boldsymbol{P}_d(\cdot)$	Coordinate matrix of the UAVs
P_{DAC}	Power consumption of the DAC
P_{Filt}	Power consumption of the filter
P_l	Propagation pathloss
P_{Mix}	Power consumption of the mixer
P_r	Received signal power
$\boldsymbol{P}_r$	N_t-dimensional diagonal matrix of received power
P_s	Static power consumption
P_{sum}	Total power consumption by the UAVs
P_{Syn}	Power consumption of the frequency synthesizer
P_t	Transmission power
$P_u(\cdot)$	PDF of user-content
$\boldsymbol{P}_u(\cdot)$	Coordinate matrix of the u^{th} GU's receiver antennas
$PL_n^m(\cdot)$	Pathloss between the n^{th} GU and the m^{th} UAV
Q	Number of documents collected by UAVs
$\boldsymbol{Q}$	Precoding matrix for index modulation
$\boldsymbol{Q}_i$	The i^{th} precoding matrix of set $\mathcal{Q}$
$r_n^m(\cdot)$	Horizontal distance between the n^{th} GU and the m^{th} UAV
$\boldsymbol{r}_g$	Number of bits transmitted from g^{th} UAV
$\boldsymbol{R}$	Number of bits used for data symbols
$R(\cdot)$	Sum rate of all successfully associated GUs
$R_a(\cdot)$	Average transmission rate
R_A	Average rate of all GUs
R_c^i	Common rate of the i^{th} subcarrier
$R_{\min}$	The rate constraint set for CSS method
R_i	The rate of the i^{th} subcarrier in CSS scheme
R_p^i	Private rate of the i^{th} subcarrier
$R_v(\cdot)$	The valid average transmission rate
R_L^M	Lower bound of the achievable rate
R_s^i	Sum rate of the i^{th} subcarrier
R_u^i	The rate of the u^{th} GU
$\boldsymbol{s}$	Multiple data streams
s_{ju}	The flag of j^{th} content from the u^{th} GU
$\boldsymbol{S}$	Selection matrix

T	Number of topics considered in the system
U_d	Number of GUs associated with the d^{th} UAV
$\boldsymbol{U}_u$	The coordinate of the u^{th} GU
$\tilde{\boldsymbol{U}}_u$	The terrestrial coordinate of the u^{th} GU
$\boldsymbol{v}$	N_r-dimensional i.i.d zero-mean complex Gaussian noise vector
v_d	Velocity of UAVs
$v_{\max}$	Maximum speed of GUs
v_n	Velocity of GUs
V_{dd}	Power supply voltage
V_i	The i^{th} covariance matrix of transmitted vector
$\boldsymbol{w}$	Weight vector for deep Q-learning
w_{ci}	The weight of the c^{th} content in the i^{th} subcarrier
w_{ij}	The weight of the j^{th} content in the i^{th} subcarrier
$\boldsymbol{W}_c$	The weight vector of the c^{th} content in each subcarrier
$\boldsymbol{W}_i$	The weight vector of each content in the i^{th} subcarrier
$\boldsymbol{W}_u$	The weight vector of the u^{th} GU
$\boldsymbol{x}$	N_t-dimensional transmitted vector
$\hat{\boldsymbol{x}}$	The set of possible transmitted signals at the receiver side
$\boldsymbol{x}(\cdot)$	Frequency domain OFDM block
x_c	Common message
x_p	Private message
$\boldsymbol{X}(\cdot)$	Time domain OFDM block
$\boldsymbol{y}$	N_r-dimensional received symbol vector
y_u^i	The received signal of the u^{th} GU at the i^{th} subcarrier
α	Pathloss exponent
α_l	Learning rate of deep Q-learning
α_s	Start phase
α_v	Valid phase range
γ	Discount factor
$\gamma_{\min}$	Minimum SNR that can support basic communication
$\gamma_n^m(\cdot)$	The received SNR of the n^{th} GU from the m^{th} UAV
η	Drain efficiency
η_d	Caching efficiency of the d^{th} UAV
λ	Free space wavelength
π	The ratio of a circle's circumference to its diameter
ρ	Signal to noise ratio
σ^2	The variance of AWGN
β	Correcting factor
θ_d	Phase difference between the received symbol and the constellation symbol
θ_r	Phase of the received symbol
$\boldsymbol{\Sigma}_i$	The i^{th} covariance matrix of the received vector

τ	Smoothing factor
Ω	Total power from both LoS and NLoS paths
$\Im$	Imaginary part of complex value
$\Re$	Real part of complex value
$\mathcal{H}$	The set of possible combinations of the channels
$\mathcal{O}(\cdot)$	The computational complexity order
$\mathcal{Q}$	The set of procoding matrix
$\mathcal{V}$	The set of covariance matrix
$\mathcal{W}_C$	The set of weight vector based on content
$\mathcal{W}_S$	The set of weight vector based on subcarrier

Chapter 1

Introduction

Given the worldwide growth of smart devices and the continuous introduction of new applications, the data traffic has increased dramatically in the past two decades and will keep growing during the next decades [10]. Meanwhile, the communication technology has evolved from the 1st generation (1G) to the present 5th generation (5G). Although the capacity and the data rate of our communication system have been significantly improved by means of the physical layer techniques, such as code division multiple access (CDMA), orthogonal frequency division multiplexing (OFDM), multiple input multiple output (MIMO) and so on [5], an ever-increasing data traffic of mobile devices motivates the development of new architectures of the mobile network to overcome the heavy load on backhaul links and long latency of the conventional centralized network. According to the white paper published by Cisco [11], global mobile data traffic will increase seven-fold between 2017 and 2022 at a rate of 46% annually. Furthermore, our wearable devices are becoming smarter and smarter in the computing capabilities and hence, there is the challenge of supporting massive machine to machine (M2M) connections [12]. On the other hand, unmanned aerial vehicles (UAVs) which are commonly known as drones have raised a lot of interests over the past few years, due to their mobility, flexibility, and wide range of application perspectives. Typical application scenarios of UAVs for Military are border surveillance, reconnaissance, and strike, while potential civilian and commercial use of UAVs are numerous, such as traffic monitoring, disaster warnings, and global climate observation [13, 14, 15]. In wireless communication systems, UAVs are also predicted to bring fresh and meritorious opportunities to the 6th generation (6G) and beyond cellular network [16, 17].

1.1 Motivations and Challenges

Along with the development of Internet of Things (IoTs) and mobile communication technologies, it brings great challenges to design a mobile wireless network that can

provide ultra-high data rate and extremely low latency. Meanwhile, The current centralized architecture of the mobile network cannot cope with the explosively growing data traffic [18]. Although the remote cloud server could offer powerful computing and caching resources, it has the challenge of degrading the user's experience due to the long latency and transmission cost [19]. Therefore, mobile edge computing and caching are the promising paradigm which allows data to be processed and cached by the device itself or by a local server rather than being transmitted to a remote data center via computation offloading and distributed content caching [20], which helps reduce the task processing latency [21]. Besides, it also adds a layer of security for sensitive data without sending it to a public cloud.

On the other hand, due to their high agility and a broad range of applications, UAVs have attracted an increasing attention in recent years [22]. UAVs can be rapidly deployed without considering the geography when compared to conventional terrestrial infrastructures [10]. For instance, UAVs can act as flying base stations (BSs) to cover more wireless areas and enhance throughput [23, 24]. Additionally, UAVs are able to serve as small BSs (SBSs) to improve users' throughput and reduce transmission delay by dynamically caching the popular contents and track the moving patterns of corresponding users [24, 25]. Also, caching complexity could be significantly reduced compared to traditional fixed base stations.

Moreover, by exploiting the property of contents reuse, multicast communication becomes one of the promising solutions for the explosively growing content-centric applications [26]. The authors of [27] proposed a rate adaptive resource allocation scheme for multi-user OFDM systems based on the perceptual quality aspects of the transmitted video. In [28], a content-aware cooperative transmission strategy is proposed to improve the transmission data rate by offloading users from macro BSs to SBSs. Besides, a content and computation-aware communication control framework was proposed in [29] based on the software defined network paradigm to realise an adaptable and programmable user-controlled platform. Moreover, the authors of [30] jointly optimized the locations and beamforming of cache-enabled UAVs to maximize the user admission, while the authors of [31] considered a practical operational constraint of limited storage capacity for UAVs to meet the demand of minimum rate required by users.

However, UAVs have their inherent limitations. Due to the limited communication range, a large number of UAVs would be required to provide wireless coverage to a large geographical area throughout the considered period but this might not be possible because of the relatively high cost [32]. Therefore, a limited number of UAVs need to be utilized to provide wireless coverage in a large geographical area to support a large number of ground users (GUs). Nevertheless, the constraints on the available energy makes it vital to optimally utilize energy to serve users and to prolong the network lifetime. In terms of open problems for UAV deployment, there is a need for new solutions for the optimal three-dimensional (3D) placement of UAVs while accounting for

their unique features. For example, it is necessary to study the optimal 3D deployment in the presence of terrestrial networks because of the mutual interference between such aerial and terrestrial system. Other key problems in deployment include: 1) joint optimization of deployment and bandwidth allocation for low latency communications, 2) joint optimal 3D deployment and cell association for flight time minimization, and 3) obstacle-aware deployment of UAVs for maximizing wireless coverage [33].

Additionally, the performance of UAV communication system is fundamentally limited by the on-board energy, which is closely related to the size and weight of the UAVs. In [34], the authors investigated energy-saving communication links in a downlink air-to-ground wiretap system by formulating the power minimization and allocation problem with constraints to satisfy the effectiveness of the legitimate link and to meet the security requirement of the communications link. In [35], the authors also investigated the downlink transmission with specific security requirements, where an energy-efficient transmission was proposed by considering user scheduling and power allocation. Therefore, it is important to design an energy-efficient UAV communication model to reduce the energy consumed per information bit.

1.2 Novel Contributions

The novel contributions of this thesis are summarized as follow:

1. We propose a UAV-aided intelligent strategy for mobile edge caching in the wireless communication system by employing latent Dirichlet allocation (LDA) algorithm, which aims to minimize the system delay and hence improve the quality of experience (QoE).

2. Then, a deep reinforcement learning based algorithm is proposed to enable multiple UAVs in a target area to automatically update their locations according to the distribution of moving GUs and an optimal association algorithm has been designed to fix the issue of "outliers" that could occur in the traditional greedy association method.

3. Afterwards, we propose an index modulation (IM) based UAV wireless communication system, which aims to increase the energy-efficiency (EE) of power-limited UAV platforms. Meanwhile, a multi-UAV deployment scheme has been designed to maximize the downlink sum rate of all GUs based on the proposed IM-UAV communication system. Additionally, a low-complexity detection scheme to separately detect the index symbols and the data symbols is designed for this IM-UAV communication system.

4. Finally, we propose two subcarrier-sharing (CS) transmission schemes, namely private CS (PCS) and common CS (CCS), in a content-aware UAV-assisted wireless communication system, which aims to increase the average data rate of GUs. Besides, we design two deployment schemes to find the appropriate UAV position that maximizes the average data rate of GUs based on the proposed PCS and CCS scheme.

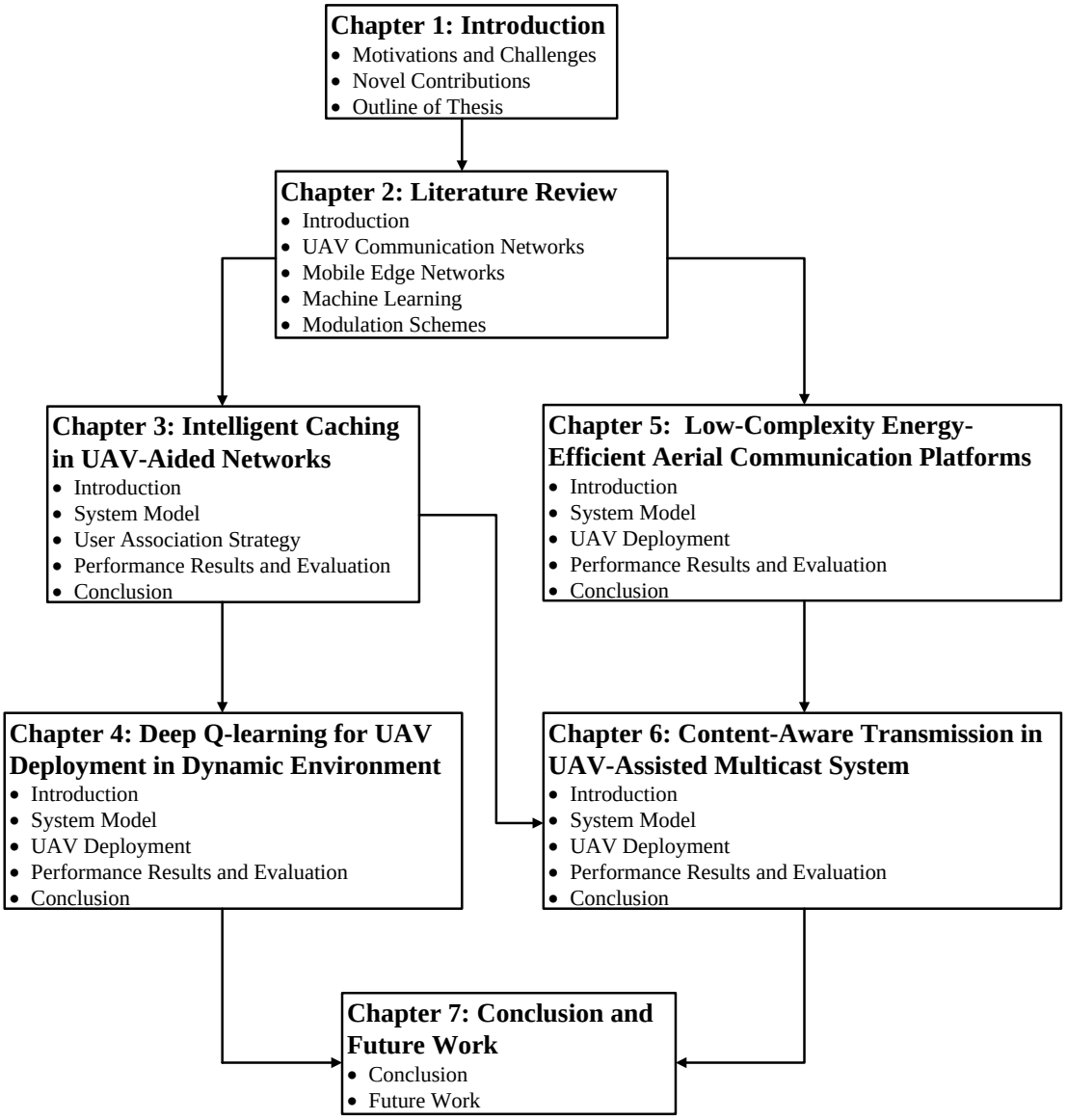

Figure 1.1: Outline of the Thesis.

1.3 Outline of Thesis

The structure of the thesis is illustrated by Fig. 1.1. In Chapter 1, we give a brief background of the emergence of UAV assisted wireless communication system. Then, the

motivations and the challenges related to the design of UAV assisted communication system are given followed by the novel contributions. Afterwards, Chapter 2 presents a detailed literature review of related works and research backgrounds. Then, Chapter 3 introduces our proposed UAV-aided mobile edge caching system and its performance has been studied under different scenarios. Also, Chapter 4 presents the structure of our proposed UAV deployment methods with the help of ML scheme, including detailed results and analysis. Moreover, we propose a method that combines the concept of IM with the UAV communications systems to attain an improved EE in Chapter 5. Furthermore, we propose two subcarrier-sharing transmission schemes based on the OFDMA scheme, which is employed in Chapter 5, by considering the the content-aware scenario in Chapter 3 with the aim to further improve the sum rate of GUs. Finally, Chapter 7 concludes the thesis and presents further research development ideas.

Chapter 2

Literature Review

2.1 Introduction

In this chapter, we present a review of the UAV-assisted wireless communication systems including channel modelling, UAV deployment, and user association at first. Then, the mobile edge network structure is introduced to handle part of the tasks from the centric network to the mobile edge, which could help meet the demand for low-latency transmission and high-speed data rate in today's wireless network. More specifically, both mobile edge computing and mobile edge caching, are included to illustrate the functions of mobile edge networks. Afterwards, several widely applied machine learning (ML) techniques are presented as a tool that has been applied in many applications. This includes two numerical optimization algorithms: fixed-point iteration and gradient descent algorithm, as well as two classification algorithms: k-means clustering and latent Dirichlet allocation (LDA). Furthermore, the concept of reinforcement learning (RL)and two modulation schemes, namely orthogonal frequency division multiplexing (OFDM) and spatial modulation (SM), are also introduced.

2.2 UAV Communication Networks

UAVs, also known as drones, have attracted a lot of attention over the past few years due to their wide range of application areas. UAVs can be utilized for military, public and civil applications. Military use includes strikes, surveillance and monitoring, while for public use, they could be employed for public safety and transportation management. Besides, UAVs can assist in disaster warnings and rescue operations. In particular, there are several potential applications that UAVs could be applied in wireless networks, where UAVs can work as aerial user equipment (UE), which is connected to cellular networks, called cellular-connected UAVs, to coexist with ground users (GUs)

supported by the terrestrial base station (TBS) [36]. Besides, they can also play the role of a mobile relay in flying ad-hoc networks [37, 38] or as aerial base stations (ABSs) to provide reliable and cost-effective communications for various scenarios, which significantly enhances the existing communication system [39, 40]. Moreover, UAVs can also assist in wireless backhaul links [41] and smart cities [42]. This section will review several key challenges of wireless communications in the UAV scenario from the aspects of channel model, UAV deployment and user association.

2.2.1 Channel Model for UAV Communication

UAVs play an increasingly vital role in broad wireless connection and high data rate transmission for future communication systems as essential aerial platforms. Notably, UAV communications comprise a variety of communication situations, including intercommunications between UAVs and communications with ground UEs and cellular BSs. This section focuses on the fundamentals of air-to-air (A2A) and air-to-ground (A2G) channels in UAV communications.

In wireless communications with UAVs, three typical communication scenarios are included [43]:

- **UAV to UE**: The rotary-wing UAV can act as a temporary static ABS in disaster zones and to enhance hotspot coverage to fulfil overloaded quality-of-service needs from mobile UE on the ground; this is known as a UAV-assisted network.
- **UAV to TBS**: UAVs are intended to be aerial users of TBSs in cellular networks to ensure reliable beyond line-of-sight (LoS) communication links in long-distance flights, known as cellular-connected UAV communications [44].
- **UAV to UAV**: Intercommunication between UAVs is required for numerous use cases, including aerial relay and flying ad hoc networks. UAV-to-UAV communication has other challenges than regular vehicle communication since drones can fly in three-dimensional (3D) space at highly changeable heights. On the other hand, vehicles usually follow a linear trajectory in the two-dimensional (2D) plane.

The features of UAV channel are quite different from that of terrestrial communication channels. In reality, any movement of UAVs would change the channel characteristics [33]. Besides, type of UAVs, altitude, elevation angle and propagation environment are the key factors to determine the channel conditions. The works in [45, 46, 47] characterise the direct path and the multipath elements by a model of tapped delay line. Then, according to the channel impulse response, parameters of wideband frequency selective channel could be derived. In [48], considering the scenario of urban environment,

the authors derived the likelihood of LoS links from A2G as a function of elevation angle and the average height of obstacles. Similarly, the authors in [49] considered the links between high altitude platforms and GUs by two cases: LoS and non line-of-sight (NLoS), and further derived the probability of occurrence of each link. The unique features that differentiate between UAV communication system and traditional wireless communication system are summarized as follow [50]:

- The special channel conditions: A2G and A2A channels.
- The variation on space and time in variable channel.
- The shadowing caused by the fuselage structure and the maneuverability of UAVs.

These features become more challenging in a diverse propagation scenario of UAV channel. Empirical and analytical models have well established the channel characteristics of classical ground communication. Besides, in [51] and [52], the links of satellite for mobile GUs were investigated. Nevertheless, all these models cannot be directly applied to characterise the UAV channels due to the unique needs mentioned before. Also, the A2G channel suffers more blockages when compared with A2A communication links which experience LoS in most of the time. Thus, an accurate A2G channel model needs to be settled for a board range of UAV-aided applications.

Channel models generate formulated expressions which can be used directly in system design and evaluation. As a result, we will concentrate on fundamental channel models for UAV communications, such as the pathloss model, small-scale fading model, and multipath components (MPCs) model. The most common pathloss models are log-distance [47], modified free-space [53], close-in [54], floating intercept [44] and excess loss models [55]. The log-distance model is the most widely used in these channel models for both A2A and A2G channels. However, it is worth noting that the excess loss model can only be used in A2G channels since it divides total loss into terrestrial and aerial components.

The small-scale fading model, which can represent both narrowband fading channels and individual MPCs in wideband channels, basically reflects the probability distribution of the envelope of small-scale fading. Popular probability distributions include the Rician, Rayleigh, and Nakagami-m distributions. Besides, numerous measurements have shown that A2A and A2G channels are more likely to exhibit Rician fading in most situations due to a strong LoS path [45, 47, 54]. Nakagami-m, on the other hand, can be a more broad representation with increasing multipath, as shown in [53]. Rayleigh fading is uncommon in existing works; nonetheless, research in [56] reveals that Rayleigh fading occurs in A2G channels under NLoS environments at low altitudes.

Wideband measurements and simulations make it simpler to detect and characterise MPCs, allowing for a more accurate reconstruction of the channel impulse response.

The two-ray propagation model has an intuitive description of the UAV channel. However, more MPCs were detected in measurements, where a three-ray model was shown to accurately model A2G channels in an over-water environment, although the third ray is intermittent and must be stated probabilistically [45]. Additionally, over-three-ray models were discovered to simulate both A2A and A2G channels in built-up environments, where rays impinging on building walls result in additional MPCs. For example, MPCs for A2G channels have been observed to reach nine in a suburban area [47]. Furthermore, the most recent A2A channel measurements and ray-tracing simulations in the rebuilt suburban environment revealed a total of seven MPCs, consisting of the LoS, the ground reflection, four single-bounce wall reflections, and one double-bounce wall reflection [57].

2.2.2 UAV Deployment

Among all challenges in the UAV scenario, the most fundamental issue is the schedule for UAV deployment. A UAV deployment involves various scheduling problems ranging from resource allocation to routing problems. Early works have studied the deployment of a single UAV by maximizing the radio coverage on GUs [58, 59] or maximizing the number of users with minimum transmission power [60]. As the research progressed, the UAV-assisted system draws more attention and has been combined with many other promising technologies. For instance, authors of [61, 62, 63] employed non-orthogonal multiple access to improve the performance of the UAV-assisted communication system, which outperforms orthogonal multiple access. UAV-aided device-to-device (D2D) communication has been investigated in [64], where they analyzed the trade-off between the coverage area and the time needed to cover the target area by UAV-aided acquisition. In [65], the authors proposed a framework to maximize the average data rate provided for users with static UAVs while also considering the fairness amongst users. The authors of [66] jointly maximize both the total coverage area and the battery operating period of UAVs by determining the most appropriate location using the sphere packing theory.

On the other hand, mobile UAVs can provide better coverage than static UAVs. However, existing works are mainly considered static users on the ground [67, 68]. By applying the classic block coordinate descent and successive convex optimization techniques, the authors of [69] invoked an iterative algorithm for solving the resultant non-convex optimization problem between UAV trajectory and transmit power. In [70], by jointly considering the communication throughput and the energy consumption, a new design paradigm was proposed to determine the trajectory of the UAV, including its initial or final location, velocities as well as maximum/minimum speed and acceleration. The authors of [67] assumed two practical trajectories named straight flight and circular

flight for collecting a given amount of data from a fixed ground terminal by considering the trade-off of associated energy dissipation. Additionally, [68] employed a novel cyclical trajectory to serve users via time division multiple access (TDMA), and a significant throughput gain could be achieved. In [71], a concise circular trajectory was exploited to maximize the minimum average throughput of users. The work of [72] was to minimize the UAV's operation time by optimizing its trajectory in a scenario where the UAV flew from one start point to a destination, while maintaining a reliable connection with the cellular network by associating with one of the ground BSs at each time instant.

2.2.3 User Association

User association is defined as a set of rules for assigning users to different BSs available in the system. A decision to associate a user with one BS will affect the throughput seen by that user and others associated with that BS. In traditional homogeneous cellular networks, user association is related to the downlink received signal strength (RSS). Many works have been proposed that outperform the conventional rules in heterogeneous network (HetNets) [73, 74, 75]. However, it is hard to tell which one is better since each study is based on different resource allocation schemes and assumptions.

Typically, HetNets are based on OFDM, where the HetNet is considered as a whole and allocated a frequency band, which is divided into several orthogonal sub-channels where each sub-channel has a bandwidth. Therefore, one of the resources to allocate among different BSs is sub-channels. Besides, transmission power is also a significant resource that needs to be considered in the network. Given all that, a resource allocation and interference management (RAIM) scheme can determine how to allocate channels among BSs and how to use the power budget on the allocated channels at each BS. Hence, in its most complex form, a RAIM scheme is a centralized scheduling to decide which BS should transmit, which user to tranmit to, which channel to use, and what transmit power to apply. Even in a static scenario where channel gains are known and fixed, and the association is given, this issue is not tractable due to the very large number of parameters. In its simplest form, a RAIM scheme might allow each BS to transmit continuously on all sub-channels (and to cope with the resulting interference) using the same power on each channel. In that case, for a given association rule, each BS can locally schedule its own users without any coordination with the other BSs. Clearly, even in this simple case, one would expect different performances for different association rules.

In traditional terrestrial wireless communication system, many works have been presented on user association schemes under different models and assumptions. Basically, two metrics are considered for selecting the serving BS. The first one is the received signal quality, such as pilot signal strength, signal to interference plus noise ratio (SINR)

or the corresponding achievable rate, while the second is cell traffic load. The authors of [76] proposed a user association policy, which was focused on load balancing, while the authors of [77] further considered the operational power consumption of BSs as the user association metric, so that mobile users are likely to be associated with energy-efficient BSs. The possibility of energy saving has been studied in [78]. The authors of [79] conceived a predefined sleep pattern of BS for a deterministic traffic profile over one day. However, under the setting where traffic patterns are not predictable from day to day, the authors of [80, 81] proposed dynamic BSs switching algorithms. Additionally, a sharing method was introduced by [82], in which different operators pool their BSs together to conserve energy further.

On the other hand, the user association schemes in a UAV-assisted wireless communication system can be different due to the mobility and flexibility of UAVs. The works of [83] studied a simultaneous UAV-user association and 3D placement problem in multi-UAV enabled wireless networks, where a map-based approach for the optimal placement of multiple UAV-based was proposed. In [84], the authors investigated a joint user association and UAV location optimization problem for UAV-aided communications by maximizing users' total achievable data rates and UAV's fair coverage under constraints of users' required data rates and UAV's service capability. Besides, a joint optimization of user association, UAV trajectory, and uploading power of each UE to maximize sum bits offloaded from all UEs to the UAV was investigated in [85] by employing an UAV as the edge computing server. Additionally, the user association for a dual UAV-enabled wireless network with the help of D2D connections in disasters was considered in [86], where two low-complexity algorithms, the cluster-based algorithm and the relaxed optimization algorithm, were proposed to maximize the weighted sum rate of the UAV-served users and the total number of D2D-connected users. Afterwards, the authors of [87] investigated the UAV location and user association problem from a load balancing perspective, the target of this work is to make the traffic loads of UAVs almost equal so that the networks can be stable and robust to unexpected events by alternately invoking user association and location algorithms. Moreover, a distributed algorithm that allows UAVs to dynamically learn their optimal 3D locations and associate with GUs while maximizing the network's sum rate was proposed in [88].

2.3 Mobile Edge Networks

In the past three decades, mobile cellular networks have experienced five generations of information and telecommunications technology advancements. Meanwhile, the explosive growth of smart devices and mobile users also brings new challenges to mobile wireless communication networks, such as high-speed data rates and low-latency

transmission. However, the traditional BS centric architecture cannot meet these demands anymore. Thus, a new paradigm that moves the centre of gravity from the core network to the edge [89], which transforms the architecture of the network from BS-centric to device-centric and content-centric, is a promising solution to break the bottleneck of massive content delivery. The concept of a mobile edge network (MEN) brings networks' functions, contents and resources to the network edge, making it close to users. The network resources include computing, caching and communication resources [12]. While caching is also considered as a part of a computing resource in [90]. Based on the above discussion, we will discuss MEN by separately considering computing and caching since the service types and problems they focus on are different.

2.3.1 Mobile Edge Computing

A 2-level hierarchy named "Client" and "Server" was first investigated for the mobile computing scheme [91]. Afterwards, a concept called "Cloud" was used to describe a cluster of servers that provide storage, computing and network resources for mobile devices, and this gave rise to the study on mobile cloud computing (MCC) [92]. However, MCC faces inevitable challenges like long latency and bandwidth limitation caused by the long-distance backhaul links between mobile devices and the cloud. Therefore, mobile edge computing (MEC) [93] [94] is a promising solution to this problem by deploying cloud servers close to users. In this case, the computational capability is much closer to mobile devices [95], which can reduce the service response time and improve the user experience.

Moreover, edge servers could easily obtain network status information, which helps to offer better services. Due to the superiority of low latency, high bandwidth and proximity, MEC is considered as one key technology for the 5G networks by 5G Infrastructure Public Private Partnership (5G PPP) [96]. As shown in Figure 2.1, MEC is settled between the cloud and the mobile devices to comply with cloud computing for supporting and enhancing the performance of the end devices [97]. Therefore, a three-layer hierarchy, cloud, MEC and mobile devices, composes the cellular network communication system infrastructure.

2.3.2 Mobile Edge Caching

A centralized network is established for traditional network architecture where the central server deals with all the major processing. At the same time, end users with less power have to submit their requests to the central server instead of performing operations locally. Unfortunately, a waste of network resources could occur due to duplicate transmission of the same content in the whole network [98, 99, 100]. Therefore, researchers have been investigating effective solutions to reduce the transmissions of

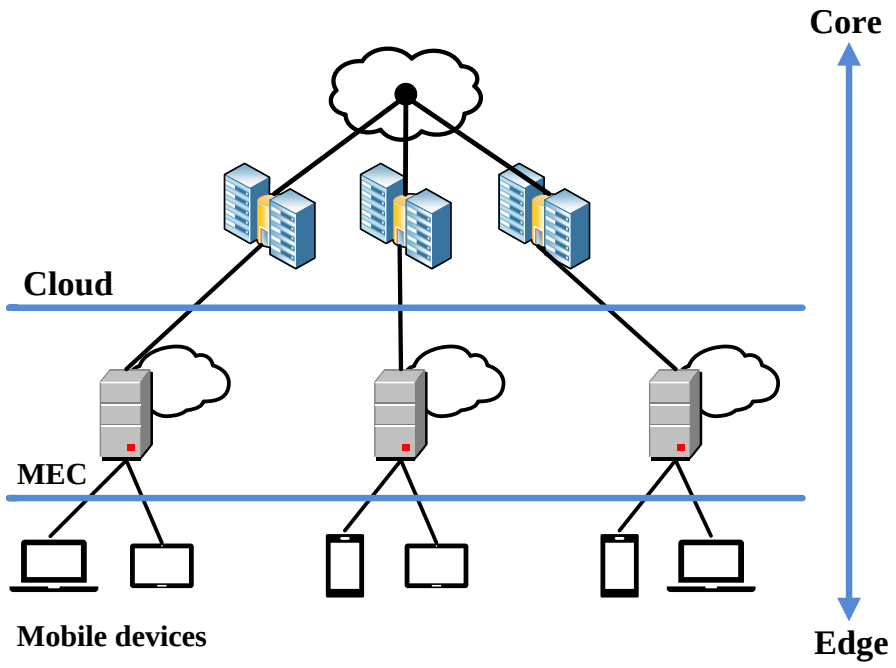

Figure 2.1: Three-layer architecture [1].

duplicate requested contents by caching popular contents (e.g., popular videos) at the mobile edge (e.g., gateways) with intelligent caching strategies [101, 102, 103]. The MEC servers can be utilized as caching nodes to store requested popular contents from users, and this method is referred to as mobile edge caching [90]. The mobile edge caching helps to reduce the content delivery latency and also to alleviate the traffic load by utilizing the cache-enabled edge servers to store popular contents and directly send them to the user equipments, instead of transmitting them from a remote cloud or server [104]. Consequently, the traffic load of the backhaul links could be largely reduced.

Unlike a central cloud server with significant computing, memory and storage resources, the edge server has limited computing capability due to its limited resources. Additionally, mobile users have a variety of requests, which introduces a challenge to utilize the mobile edge resources efficiently. Note that caching in wireless networks faces the challenge of dynamic traffic loads caused by the user mobility [105], where the network traffic is highly related to users' mobility patterns. For caching at mobile edge servers, the content popularity distribution is one key factor that the BSs need to consider. Nevertheless, since the requested content from each BS will change over time, the distributions of content popularity in individual BS may also change in space and time [106]. On the other hand, users may also request contents from their corresponding BSs based on content availability [107].

Additionally, there are several caching criteria available for consideration when designing a caching scheme [105]:

- **Cache Hit Probability**: The ratio of the number of cached files requested by users to the total number of files in the caches is known as the cache hit probability. A greater cache hit probability indicates that the cached information satisfy more user requests. Increased cache size can enhance cache hit probability while lowering backhaul bandwidth requirements. As a result, there is a tradeoff between cache size and required backhaul capacity.

- **Spectrum Efficiency**: The spectrum efficiency (SE) is the supported data rate over a given frequency bandwidth. Network densification by deploying more SBSs in a macro cell has been used to improve the area SE. Caching can also improve SE by reducing network traffic and improving network throughput.

- **Energy Efficiency**: Energy efficiency (EE) is a key performance indicator for 5G cellular networks, defined as the supported data rate per unit of energy consumed. Turning BSs into sleep mode without traffic load can save energy in typical cellular networks. Caching at the mobile edge can assist reduce energy consumption by preventing duplicate transmissions.

- **Network Throughput**: The network throughput is defined as the maximum data rate the network can provide and affects the network performance. A more significant network throughput leads to lower content download delay. Caching schemes should maximize network throughput by caching more data closer to the users. The network throughput is also highly related to the caching storage capacities.

- **Content Retrieving Delay**: The quality of service (QoS) of a user is directly related to the content retrieving delay, which is often defined as the roundtrip time for acquiring content by users. The wireless transmission delay from BSs to UEs and the backhaul delay from BSs to the mobile core network are commonly included. Backhaul delay is determined by link length, traffic load, and the number of BSs connected to the mobile core network, while wireless transmission delay is determined by bandwidth and SINR. With varying latency, users can retrieve content from local UEs, BSs, or the mobile core network.

- **Offloaded Traffic**: Mobile edge caching can offload the traffic from backhaul links. Maximizing traffic offloading leads to better-caching performance.

2.3.2.1 Where to Cache

In mobile networks, caching can be used in a variety of ways. Given the importance of D2D communication in 5G networks, caching in UE by utilizing its storage becomes an attractive option for improving the quality of experience (QoE) of users. In the meanwhile, caching at BSs is a way to have a pretty large coverage area and serve

more users. Finally, the contents can be cached in the remote radio head (RRH) and baseband unit (BBU) of the cloud radio access network (C-RAN) [108]. The related works of caching palace on mobile edge caching is summarized in Table 2.1.

Table 2.1: Summary of caching places on mobile edge caching.

Place	Related Work
Caching in UE	[109, 110, 111, 112, 113, 114, 115, 116]
Caching in BSs	[109, 117, 118, 119, 120, 121, 122, 123, 124, 125, 126, 127, 128]
Caching at Relays	[129, 130, 131, 132, 133]
Caching in C-RAN	[134, 135, 136, 137, 138]

Caching in UEs: D2D technology allows direct communication between devices by using licensed-band or unlicensed-band protocols [105]. The devices are separated into groups according to their locations and controlled by base stations. In this scheme, a user's content requests can only be obtained from other users in the same group [139]. The authors of [114] proposed content caching strategies for mobile D2D networks based on reinforcement learning that exploits the knowledge of content demand history. Besides, a novel policy was proposed in [112] for device caching that combines the emerging technologies of D2D and millimeter wave communication to enhance the offloading and the delay performance of the cellular network. Moreover, the authors of [115] proposed a data caching scheme in a D2D enabled fog radio access network (F-RAN) from the social point of view. Furthermore, Internet of Things (IoT) devices are considered as caching helpers in [116] to provide caching services for users.

Caching at Relays: Wireless relays are usually deployed to extend the wireless coverages and improve SE. Therefore, they can also be used as urban hot spots where contents can be cached [129]. In [130], the authors designed a relay caching mechanism to improve the EE in cellular networks for multimedia applications. Besides, the author of [140] proposed the cache-at-relay scheme, which jointly optimises content access energy, caching energy and relay deployment costs in three integer linear programming models. Furthermore, the works of [133] studied a relay network where all nodes, including the central server, relay nodes and users, are equipped with cache memories.

Caching in BSs: HetNet consists of several types of BSs like macro base station (MBS), small base station, pico base station (PBS) and femto base station (FBS). Since MBSs have a larger coverage area and caching memories than SBSs, they are usually used to improve backhaul traffic and network latency [117, 120]. While the SBSs have relatively small caching storages, a cooperative caching can be considered, where SBSs are able to share contents with each other[124]. Besides, in order to make full use of caching memories, caching contents should be updated frequently in accordance with the dynamic change in content popularities.

Caching in C-RAN: C-RAN is proposed as a novel architecture for 5G cellular networks to reduce capital and operating expenditure by adopting cloud computing technology. C-RAN tackles the capacity and coverage challenges by deploying multiple RRHs at cell sites. The computational functionalities of BSs are centralized in a BBU pool. These RRHs serve as distributed antennas, allowing users to interact with one another. RRHs and BBUs are connected by high bandwidth and low latency fronthaul links [141]. Despite the fact that C-RAN can provide powerful computing capabilities by sharing computing and storage resources at the BBU pool, it still has performance constraints due to the limited capacities of fronthaul and backhaul links [142]. To combat this shortage, caching techniques have been deemed a viable approach of alleviating network traffic in both fronthaul and backhaul networks. Cache storage can be deployed at the BBU or RRH levels in the C-RAN architecture. The F-RAN is a C-RAN design that uses distributed edge caching techniques [134]. Besides, the works of [135] presented an information-theoretic analysis of F-RANs by accounting for the total content delivery delay across the fronthaul and wireless segments of the network.

2.3.2.2 How to Cache

Furthermore, several caching schemes, which include proactive caching, distributed caching, cooperative caching, coded caching and probabilistic caching, are introduced in the following paragraphs. The related works of caching schemes on mobile edge caching is summarized in Table 2.2.

Table 2.2: Summary of caching scheme on mobile edge caching.

Scheme	Related Work
Proactive Caching	[114, 115, 119, 124, 125, 126, 127, 128, 130, 140, 143, 144, 145, 146]
Distributed Caching	[110, 113, 118, 136, 137, 138, 147, 148]
Cooperative Caching	[109, 112, 119, 124, 125, 126, 131, 149, 150, 151]
Coded Caching	[132, 133, 152, 153, 154, 155, 156]
Probabilistic Caching	[111, 116, 123, 157, 158, 159, 160, 161]

Proactive Caching: The reactive caching policy governs whether or not to cache requested content. It usually occurs during a peak-traffic hour when the network is unable to cope with the increased demand. A proactive caching policy, on the other hand, determines which contents should be cached before they are requested based on user demand predictions [143]. Proactive caching usually estimates the request patterns (e.g., user mobility patterns, user preferences and social relationships) to improve caching performance and guarantee QoS requirements. As ML and big data analytics get more sophisticated, it becomes more advantageous to cache popular information locally before actual requests occur [144, 147]. Proactive caching improves the caching

efficiency by pre-downloading popular contents during off-peak times and serving predictable peak-hour demands. In [127], the authors proposed an online proactive caching scheme based on a bidirectional deep recurrent neural network (NN) model to predict time-series content requests and update edge caching accordingly. Besides, the works in [128] introduced a predictive caching algorithm that utilises big data analytics to predict user content requests and determine what content items need to be cached in the network.

Distributed Caching: To determine caching techniques, centralized caching employs a central controller with a global view of all network conditions. By extracting and analysing the collected requests, the central controller normally keeps track of user movement patterns and the channel state information (CSI). As a result, centralized caching can achieve optimal performance by making the best judgments (e.g., content placement). Obtaining entire network information, on the other hand, is difficult, especially in dynamic 5G wireless networks, which are expected to support a growing number of mobile users [148]. Furthermore, the central controller must process a large amount of traffic, putting a tremendous strain on the controller and the links between it and the network entities. In that case, the mobile caching system's bottleneck might be the central controller. Cache nodes in distributed caching, also known as decentralized caching, make choices (such as content placement and update) solely based on their local information and that of neighbouring nodes. Distributed caching is applied in [147] where neighbouring BSs are jointly optimized to increase the cache hit probability. By fetching contents from multiple neighbouring caches, the total cache size seen from the user can be improved. In [118], the authors proposed a distributed caching scheme considering the trade-off between the diversity and redundancy of BSs' cached contents. Besides, the authors of [113] proposed a distributed D2D relay-aided packet caching scheme, which exploits the properties of the diverse packet requests and requirements of physical link success among different UE groups. Afterwards, the works of [137] proposed a dynamic distributed edge caching scheme in ultra-dense F-RANs by considering time-variant user requests. Moreover, an RL-based distributed edge caching method was proposed in [136] for learning and tracking the potential dynamic process of user requests. Similarly, another RL-based distributed edge caching with the content recommendation in F-RANs was investigated in [138]. Furthermore, the authors of [110] developed an online and distributed edge caching and computation approach to realise delay-sensitive Internet of Vehicles services in a cost-efficient way.

Cooperative Caching: Since a BS's caching capacity is limited, designing a caching policy for each BS may result in insufficient cache use. This occurs when certain caches are overcrowded, while others have a large number of empty places. To solve this issue, cooperative caching rules have been proposed to increase caching efficiency. In cooperative caching, BSs can share cached contents [150]. However, the time it takes to look for and get content from other caches may be substantial and should be taken

into account. Furthermore, in order to implement cooperative caching, network nodes must be aware of the caching state of other nodes via information transfers that might result in considerable signalling overheads. Consequently, we need to discover a way to convey the caching status with the least amount of overhead. In [131, 151], a novel approach has been proposed to support cooperative caching in disruption tolerant networks, which enables the sharing and coordination of cached data among multiple nodes and reduces data access delay. Besides, an optimal cooperative content caching and delivery policy has been developed in [109], for which FBSs and UEs are all engaged in local content caching. Moreover, a video popularity based cooperative edge caching along with a proactive cache updating policy was proposed in [119] with an aim to reduce the delay. Additionally, the authors of [124] proposed a learning-based cooperative caching strategy based on mobile edge computing architecture to reduce transmission costs while improving user QoE for future mobile networks. A proactive caching algorithm for collaboration between the cloud and the MEC server to determine the caching status has been investigated in [125]. In [126], the authors proposed the idea of deploying a collaborative caching and processing framework in multi-cell MEC networks, whereby the MEC servers attached to the BSs can assist each other for both caching and transcoding of adaptive bit rate videos.

Coded Caching: In a traditional switching network, the network node forwards packets one after another: two packets are present in the node simultaneously; one of the two packets is forwarded while the other is queued, even though they are both bound for the same destination. Separate transmissions are required by this classical packet forwarding system, which reduces network efficiency. On the other hand, network coding is a technique that combines two separate messages into a single coded message and sends it to the intended recipient. After receiving the coded message, the network node separates them into two original messages. To allow the network coding approach, the transmitted data is encoded at network nodes and then decoded at the destinations. As a result, network coding uses fewer transmissions to deliver all of the data. However, this scheme involves coding and decoding processes, which will increase processing overheads to the network nodes. Therefore, efficient packet transmissions can lower the complexity of network coding [154]. In [152], an online coded caching algorithm termed "coded least-recently sent" was proposed to operate the caches as well as the server such that these requests are satisfied with the minimum number of bits sent over the shared link. Then, the authors of [153] introduced a novel group-based coded caching scheme, which is suitable for caching systems that have more users than the number of popular files in the database. Additionally, the authors extended their works to a scenario where users have distinct cache capacities to improve the delivery rate in [155]. Afterwards, the authors of [132] investigated cache-aided combination networks by utilizing maximum distance separable coding and jointly optimizing both cache placement and delivery phases. Besides, user mobility and distributed storage are incorporated into the proposed coded probabilistic

caching scheme in [156], with the aim of throughput maximization. In [133], the authors designed a centralized caching scheme based on a two-layer file placement and a superposition coding delivery strategy.

Probabilistic Caching: Unlike wired networks with fixed and known topologies, wireless networks face uncertainty about which user will connect to which BS due to indeterminate user locations and the variability of user demands. As a result, when a user travels from one cell to another during content delivery, caching in wireless networks becomes more complicated. A probabilistic caching policy, in which content is stored in caches according to certain random distributions, is one way to overcome this problem [160, 161]. The authors of [157, 158] proposed ProbCache, an algorithm that approximates the capability of paths to cache contents based on path lengths and multiplexes content flows accordingly. Furthermore, in [159], the performance of the probabilistic caching scheme when working with different cache replacement policies has been investigated. Besides, the works of [111] studied probabilistic caching placement in stochastic wireless D2D caching networks for maximizing cache hit probability and maximizing the cache-aided throughput. Moreover, an optimal probabilistic caching scheme for maximizing the successful delivery probability was investigated in [123]. Additionally, the works of [116] focus on the probabilistic caching for contents of different sizes in heterogeneous IoT networks, aiming at improving the offloading rate for backhaul links.

Finally, the content patterns requested by users play a key role in determining the caching strategy. The most common caching files are multimedia files (e.g., software, video and audio), which could be treated as delay tolerant data since files can only be used after delivery. Meanwhile, for the next-generation 5G networks, IoT is one of the primary use cases, which is still increasing and has different characteristics (e.g., more dimensions and shorter lifetime) compared to multimedia data [162]. Hence, we need to be aware of request patterns to make an optimal decision. Request patterns can be extracted and analysed to predict future requests and provide insights into proactive caching. Observation of past request arrivals can be a feasible solution to obtain request patterns. However, it is challenging to predict or model the request arrivals in the real world. Hence, intelligent algorithms based on predictions and stochastic models are required [163, 164].

Besides, content popularity is defined by the ratio of the requested times for a particular content to the total number of requests from users. Generally, it is obtained from a specific region during a given period. The main feature of content popularity is that most people are interested in a few popular contents within a particular period [147]. Hence, these few contents account for major traffic loads. In general, the content popularity distribution changes at a relatively slow speed. Accordingly, the content popularity distribution is usually considered a constant over a long time. In addition, the global

popularity in a large region like in a city or a country is often different from local popularity in a small area within it [143]. Hence, content popularity or user preference must be estimated to determine the probability of a particular content being requested. Several model-based forecasting schemes carried out by ML methods have been proposed (e.g., autoregressive integrated moving average [165], regression models [166] and classification models [167]).

In addition, mobility pattern is also an essential factor in mobile networks because it impacts mobile network topologies, such as the dynamic user-BS association over time [168]. The latency of mobile networks can be attributed to unpredictable topology changes owing to the mobility of users [169]. User mobility also contains much helpful information, such as social relationships and traffic patterns, which improves the caching performance. The user mobility pattern is generally classified into two categories, spatial and temporal properties, which respectively reflect the location-based and time-related characteristics [170].

2.3.3 Caching in UAV

Using UAVs as flying BSs to cache popular data that can serve GUs is a new trend in caching techniques. Due to their limited energy resources, UAVs are typically built to fly within a cell covered by an MBS. Therefore, the UAVs in the system can collaborate with each other as well as the MBS and MEC servers to cache the requested contents and tasks. The UAVs then deliver the contents to the corresponding end users and requesters. In addition, the UAVs gather data from the GUs and either analyse and make decisions locally or cache and transmit the data to cooperate with the MBS and the MEC server. The UAVs can be linked together to establish a robust network that better serves the GUs.

Particularly, in [145], a caching UAV-assisted secure transmission scheme has been proposed in hyper-dense small-cell networks based on interference alignment. Besides, the authors of [146] proposed a novel scheme to overcome the endurance issue for UAV-enabled wireless communications by utilizing the technique of proactive caching. Moreover, a novel scheme has been proposed in [149] to guarantee the security of UAV-relayed wireless networks with caching via jointly optimizing the UAV trajectory and time scheduling. Afterwards, the authors of [171] proposed a caching placement strategy based on the probabilistic caching placement in a heterogeneous wireless network, where there are several types of UAV-BS placed following the independent homogeneous Poisson point process. Moreover, the authors of [172] formulated a joint optimization problem of UAV deployment, caching placement and user association for maximizing the QoE of users. Similarly, the work in [9] also considered the minimization of transmission power used by UAVs. Additionally, the authors of [173] proposed

Table 2.3: Major contribution of caching in UAV-assisted communication system.

Year	Author	Contribution
2017	Chen *et al.* [9]	Proactive deployment of cache-enabled UAVs for optimizing the QoE of wireless devices in a cloud radio access network.
2018	Zhao *et al.* [145]	A caching UAV-assisted secure transmission scheme has been proposed in hyper-dense small-cell networks based on interference alignment.
2019	Cheng *et al.* [149]	A novel scheme to guarantee the security of UAV-relayed wireless networks with caching via jointly optimization of UAV trajectory and time scheduling.
2019	Lin *et al.* [171]	A caching placement strategy was proposed based on the probabilistic caching placement in a heterogeneous wireless network, where there are several types of UAV-BS placed following the independent homogeneous Poisson point process.
2020	Zhang *et al.* [172]	Formulated a joint optimization problem of UAV deployment, caching placement and user association for maximizing QoE of users.
2021	Gu *et al.* [173]	Proposed a coded caching strategy with resource optimization to provide more multicast opportunities for file requesting and reduce the backhaul transmission volume in a cache-enabled satellite-UAV-vehicle integrated network.
2022	Sun *et al.* [174]	A multi-UAV content-caching strategy and cooperative, complementary content transmission among UAVs are jointly studied.

a coded caching strategy with resource optimization to provide more multicast opportunities for file requesting and reduce the backhaul transmission volume in a cache-enabled satellite-UAV-vehicle integrated network. Furthermore, a multi-UAV content-caching strategy and cooperative, complementary content transmission among UAVs are jointly studied in [174]. The major contribution of caching in UAV-assisted communication system is summarized in Table 2.3.

2.4 Overview of Machine Learning

Since its birth several decades ago, the digital computer has continually astounded us with its incredible computing and data storage capability. However, on the other hand, people are very interested in exploring the limits of what a computer can do beyond basic computing and storage capabilities. The fascinating question in this area is whether the human-made hardware of digital computers can do complicated tasks that traditionally need human intelligence. Therefore, the study of this kind of autonomous

learning algorithm has emerged under the name of ML. ML is a fast-expanding field of research that focuses on developing and analysing algorithms that allow computers to learn. It can teach computers to perform a wide range of valuable tasks, including automatic object detection in images, speech recognition, knowledge discovery in the medical sciences, and predictive analytics. However, it is still a young discipline with much more to discover than is currently known. In this section, two classification algorithms, *k*-means clustering and LDA, that are used to distinguish between different types of specific things or to discover the underlying patterns from a collection of data will be introduced. Afterwards, RL, an important ML type that learns through trial and error, is also included. Finally, the application of ML in UAV scenarios will be summarized.

2.4.1 *k*-means Clustering Algorithm

The term "*k*-means" was first proposed in [175], while the standard algorithm of *k*-means clustering was firstly conceived for pulse-code modulation [176] and published later in [177]. It is an iterative approach for partitioning a dataset into K separate non-overlapping clusters, with each data point belonging to just one of these clusters. It aims to make intra-cluster data points as similar as possible while maintaining clusters as distinct as possible. It allocates data points to clusters so that the sum of the squared distance between them and the cluster's centroid is as small as possible. Within a cluster, the less variance there is, the more similar the data points are.

In the *k*-means clustering algorithm, the data points are clustered into k groups according to their pairwise distances. Typically, squared Euclidean distance [178] is used to measure the difference between two N-dimensional feature vectors or points $\boldsymbol{p}_i = [p_{i1}, p_{i2}, \ldots, p_{iN}]$ and $\boldsymbol{p}_j = [p_{j1}, p_{j2}, \ldots, p_{jN}]$, which is defined by:

$$d\left(\boldsymbol{p}_i, \boldsymbol{p}_j\right) = \|\boldsymbol{p}_i - \boldsymbol{p}_j\|_2^2. \tag{2.1}$$

Besides, some other metrics can also be employed here, such as Manhattan distance $d_M = \sum_{n=1}^{N} |p_{in} - p_{jn}|$ [179] and hamming distance for binary data. The algorithm begins with initial estimates for the k centroids, which can be generated or selected at random from the data set points $\{\boldsymbol{p}_1, \boldsymbol{p}_2, \ldots, \boldsymbol{p}_n\}$. Then, the data points will be portioned into K clusters by assigning them to the closets centroids based on squared Euclidean distance. Afterwards, the centroid $\boldsymbol{c}_k$ In each cluster k will be recalculated by:

$$\boldsymbol{c}_k = \frac{1}{N_{\boldsymbol{c}_k}} \sum_{w=1}^{N_{\boldsymbol{c}_k}} \boldsymbol{p}_{\boldsymbol{c}_k}^{(w)}, \tag{2.2}$$

where N_{c_k} is the number of points in k^{th} cluster and $\boldsymbol{p}_{c_k}^{(w)}$ denotes the w^{th} point in that cluster. This procedure is repeated until the data points no longer change their clusters. Finally, the whole procedure is summarized in Algorithm 1.

Algorithm 1 k-means clustering algorithm.

Input: Data set points $\{\boldsymbol{p}_1, \boldsymbol{p}_2, \ldots \boldsymbol{p}_n\}$, number of clusters K
Initialization: Partition the dataset into K initial clusters selected at random
1: **repeat**
2: Associated data points with the closest centroids based on square Euclidean distance
3: Recalculate the new centroids
4: **until** The data points no longer change

In contrast to k-means clustering algorithm, where one entity can only be assigned to one group (hard-clustering), a soft-clustering algorithm, LDA, which allows fuzzy membership will be reviewed in the following section.

2.4.2 Latent Dirichlet Allocation

LDA [180] is a generative probabilistic model that allows sets of observations (e.g., discrete data) to be explained by unobserved groups. The most common use of LDA is for modelling text collections, also known as topic modelling [181]. The topic here is represented by a word probability distribution, which gives us the probability of a collection of words for a given topic. If we consider the topic as a bag of words, then, any word that is not in the bag has a zero chance of getting drawn. While the other words in the bag, on the other hand, have a probability greater than zero.

The basic idea of LDA is that each document is made up of a variety of topics, each of which is made up of a collection of words. This may also be used to generate new documents (if we know the topics in advance) or to infer topics from a group of documents we already have. According to the name of LDA, the model can be explained as follows:

- **Latent**: It means the topic structure is latent, which is hidden in the document.
- **Dirichlet**: The Dirichlet distribution establishes the proportions of topics and words in each document.
- **Allocation**: Words are allocated to a certain topic.

To summarise, the words are allocated to a given topic and the topics are allocated to a given document, we use latent structures in a corpus, with topic distributions in each document and word distributions in each topic based on the Dirichlet distribution. In the following, the generative progress [182] of LDA model will be presented.

2.4.2.1 Generative Process

In this section, the LDA is considered as a generative model [182]. Generative models are approaches that explicitly or implicitly characterise the distribution of inputs and outputs so that synthetic data points in the input space can be generated by sampling from them. This implies that we are able to generate documents containing a variety of topics and words related to those topics. Before generating new documents, the parameters and variables that will be used are summarized as follows [2]:

- K: Total number of topics.
- D: Total number of documents.
- k: Index of the k_{th} topic.
- d: Index of the d^{th} document.
- N : Total number of words in d^{th} document.
- W_{dn}: The n^{th} word of document d.
- Z_{dn}: The topic index selected for the n^{th} word of document d.
- $\vec{\alpha}$: The values of $\vec{\alpha}$ indicate our prior knowledge of the topic mixture in that document. To determine the topic distribution θ of the document, we have to sample from a Dirichlet distribution, which uses α as the input parameter.
- $\vec{\eta}$: The values of $\vec{\eta}$ represent our prior information of the word distribution in a topic. To determine the word distribution θ of a given topic, we have to sample from a Dirichlet distribution, which uses η as the input parameter.
- $\vec{\theta}_d$: $\vec{\theta}_d$ is the topic proportion of a given document d. It will be employed as a parameter in the multinomial distribution to determine the topic of the next word. To be clear, the word distribution of the specified topic will be utilized to choose a word.
- $\vec{\beta}_k$: $\vec{\beta}_k$ is the word distribution of a given topic k. It indicates the probability of each word that will be generated if a topic k is selected.

A graphical model [182] of LDA, which is used to illustrate the generative process of LDA, is shown in Figure 2.2. We firstly generate topic-word distributions β for each word in the vocabulary[1]. The value of β_k, which gives us $p(\beta|\eta)$, is randomly drawn from the Dirichlet distribution Dirichlet(η). Then, we generate the topic mixture θ of the document from the Dirichlet distribution Dirichlet(α), which gives us the distribution of topic in this document $p(\theta|\alpha)$. Afterwards, we use document-topic distribution to

[1]The vocabulary here is composed by the words in all documents.

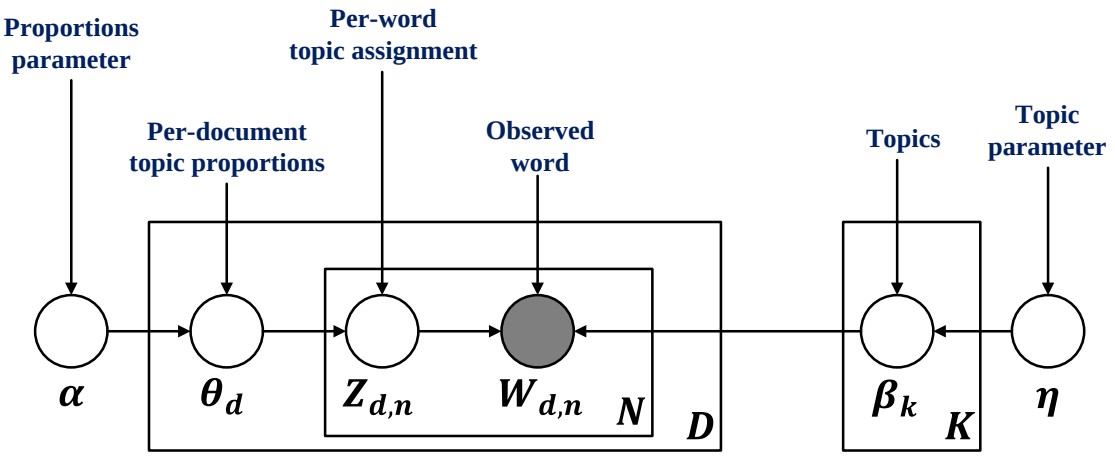

Figure 2.2: The graphical model of LDA [2].

generate a topic for each word $p(Z|\theta)$, and then we use the topic-word distribution to select the word $p(W|\beta)$ for each topic selected before. To sum, the generative process of LDA for document d can be expressed by the following equation [183]:

$$p(W, Z, \theta, \beta|\alpha, \eta) = p(\beta|\eta)p(\theta|\alpha)p(Z|\theta)p(W|\beta_Z). \tag{2.3}$$

Finally, based on the parameters and variables defined above, the generative process of LDA is given in Algorithm 2.

Algorithm 2 The generative model of LDA.

for k from 1 to K, where K is the predefined total number of topics **do**
  Sample the parameters for each topic-word distribution
  $\phi_k \sim$ Dirichlet(η)
end for
for d from 1 to D **do**
  Sample the parameters for document-word distribution
  $\theta_d \sim$ Dirichlet(α)
  for N from 1 to N **do**
    Generate a topic z_{dj} for word W_{dn},
    $Z_{dn} \sim$ Multinomial(θ_d)
    Generate a word based on the topic-word distribution of Z_{dn}
    $W_{dn} \sim$ Multinomial($\phi_{Z_{dn}}$)
  end for
end for

2.4.2.2 Inference of LDA

In Section 2.4.2.1, LDA is considered as the generative model. However, the main use of LDA is to turn the situation around. Usually, we hope to infer the topic of a bunch

of documents and this can be solved with the assumption that the documents are generated by a generative process. Under this assumption, we have to find the solution of

$$p(\theta, \beta, Z|W, \alpha, \eta) = \frac{p(\theta, \beta, Z, W|\alpha, \eta)}{p(W|\alpha, \eta)}. \tag{2.4}$$

(2.4) defines the probability of document-topic distribution θ, topic-word distribution β and topic label in all documents when given all words of all documents and the hyperparameters α and η. More explicitly, our target is to infer the probability of topic Z for a given word and further to estimate θ and β. In this section, the key derivation for LDA inference through Gibbs sampling [184, 185] will be introduced, while the detailed derivation are presented in [181, 183, 186].

Before the mathematical derivations for inference, the known parameters and latent parameters that related to the inference is summarized as follow:

Known parameters

- Document D: It indicates a bunch of documents we hope to estimate the topics in.
- Words in document W: Each document includes a collection of words and word counts.
- Vocabulary V: The list of words that appears in every document.
- Hyperparemeters:
  - $\vec{\alpha}$: The prior assumption of the topic distribution in documents.
  - $\vec{\eta}$: The prior assumption of the word distribution of each topic.

Latent parameters

- Number of topics K: We need to define how many topics we expect to find in the documents [187, 188].
- Topic-word distribution β: The distribution of words in each topic need to be known.
- Document-topic distribution θ: The distribution of topics in each document has to be determined.
- Topic assignment Z: This is the key point of the inference. If the topic assignment of each word is known to us, the topic-word distribution β and the document-topic distribution θ can be obtained.

As mentioned before, the crucial point of LDA inference is to figure out the topic of each word in each document. Here, we define Z_n as the topic of the n^{th} word. Please note that the topic of the current word Z_n depends on the topic assignments of all other words but not including itself, which is defined by $Z_{\neg n}$. Then we have:

$$\begin{aligned} p(Z_n|Z_{\neg n}, \alpha, \eta, W) &= \frac{p(Z_n, Z_{\neg n}, W, \alpha, \eta)}{p(Z_n, W|Z_{\neg n}, \alpha, \eta)}, \\ &\propto p(Z_n, Z_{\neg n}, W, \alpha, \eta), \\ &\propto p(Z, W, \alpha, \eta). \end{aligned} \tag{2.5}$$

It can be seen that $p(Z, W, \alpha, \eta)$ is similar to (2.3), while the difference is the lack of θ and β. Therefore, (2.5) can be obtained from the integration of (2.3) with respect to θ and β.

$$\begin{aligned} p(Z, W, \alpha, \eta) &= \int\int p(W, Z, \theta, \beta|\alpha, \eta) d\theta d\beta, \\ &= \int\int p(\beta|\eta) p(\theta|\alpha) p(Z|\theta) p(W|\beta), \\ &= \int p(\theta|\alpha) p(Z|\theta) d\theta \int p(W|\beta_Z) p(\beta|\eta) d\beta. \end{aligned} \tag{2.6}$$

Afterwards, the first term of (2.6) can be solved by utilizing the features of conjugate prior between the Dirichlet distribution and multinomial. Therefore, the following integration of current document d can be obtained:

$$\int p(\theta|\alpha) p(Z|\theta) d\theta = \prod \frac{\triangle(\vec{n}_d + \vec{\alpha})}{\triangle(\vec{\alpha})}, \tag{2.7}$$

where $\vec{n}_d = \left[n_d^1, n_d^2, \ldots, n_d^k\right]$ is the number of words assigned to each topic in the document d, and $\triangle(\alpha)$[2].

Similarly, the second term of (2.6) is given by:

$$\int p(W|\beta_Z) p(\beta|\eta) d\beta = \prod_k \frac{\triangle(\vec{n}_k + \vec{\eta})}{\triangle(\vec{\eta})}, \tag{2.8}$$

where $\vec{n}_k = \left[n_k^1, n_k^2, \ldots, n_k^v\right]$ is the number of times one word occurred in topic k. Accordingly, the solution for $p(Z, W, \alpha, \eta)$ is:

$$p(Z, W, \alpha, \eta) = \prod_k \frac{\triangle(\vec{n}_d + \vec{\alpha})}{\triangle(\vec{\alpha})} \prod_k \frac{\triangle(\vec{n}_k + \vec{\eta})}{\triangle(\vec{\eta})}. \tag{2.9}$$

[2] $Dirichlet(\vec{p}|\vec{\alpha}) = \frac{\Gamma\left(\sum_{k=1}^K \alpha_k\right)}{\prod_{k=1}^K \Gamma(\alpha_k)} \prod_{k=1}^K p_k^{\alpha_k - 1} = \frac{1}{\triangle(\vec{\alpha})} \prod_{k=1}^K p_k^{\alpha_k - 1}$, where $\vec{\alpha} = [\alpha_1, \alpha_2, \ldots, \alpha_k]$ and $\vec{p} = [p_1, p_2, \ldots, p_k]$.

Now, the equation required for Gibbs sampling can be obtained based on (2.9) through chain rule:

$$\begin{aligned} p(Z_n|Z_{\neg n}, W) &= \frac{p(W,Z)}{W, Z_{\neg n}} = \frac{p(Z)}{p(Z_{\neg n})} \frac{p(W_{\neg n}|Z_{\neg n})}{p(W|Z)p(W_n)}, \\ &\propto \left(n^k_{d,\neg n} + \alpha_k\right) \frac{n^W_{k,\neg n} + \eta_W}{\sum_W n^W_{k,\neg n} + \eta_W}. \end{aligned} \tag{2.10}$$

Finally, the topic-word distribution can be express by:

$$\beta_{k,W} = \frac{n^W_k + \eta_W}{\sum_{W=1}^V n^W_k + \eta_W}, \tag{2.11}$$

while the document-topic distribution is calculated by:

$$\theta_{d,k} = \frac{n^k_d + \alpha_k}{\sum_{k=1}^K n^k_d + \alpha_k}. \tag{2.12}$$

Until now, the word distribution under a topic k and the topic distribution in a document d can be obtained by Gibbs sampling from (2.11) and (2.12). In the following, a ML algorithm, RL, will be discussed. It is commonly used by software or machines to find the optimum behaviour in a given situation.

2.4.3 Reinforcement Learning

RL is a learning paradigm that differs from classical ML. The idea underlying RL is that an agent would learn from their environment by interacting with them and receiving rewards for their actions [189]. It has typically been employed in planning/decision-making applications such as robotics and autonomous driving, which mimics people learning from interactions through trial-and-error. The goal of an RL task is to train an agent that interacts with its environment. The agent will arrive at different scenarios, referred to as states, by performing different actions, which will result in positive or negative rewards and the agent has only one purpose to maximize its total reward across an episode [190]. This episode is anything and everything that happens between the first state and the terminal state within the environment. We reinforce the agent to learn to perform the best actions by experience, which is known as strategy or policy [3].

Firstly, we start by considering an example of news recommendation:

- Users are presented a list of articles that are of potential interest to them, and the user decides to either read or not-read.
- The states are defined by what the user reads.

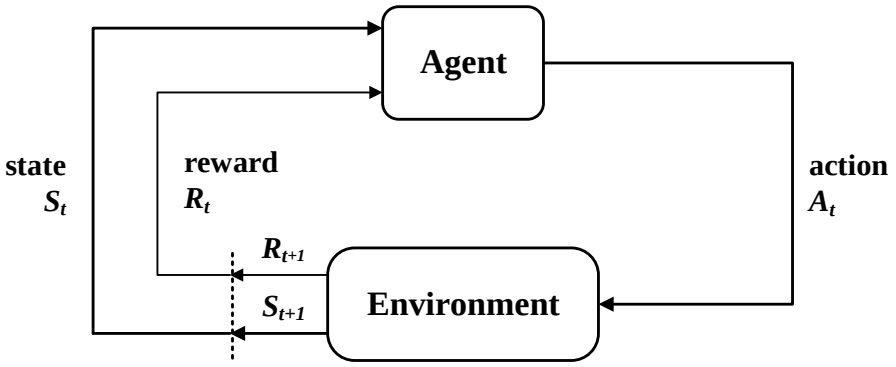

Figure 2.3: Sequential decision process of RL [3].

- An episode is the length of reading.
- Clicking or not-clicking on an article is the action.
- Reward is defined by the click-through rate[3] (CRT).

Thus, in order to maximize the CRT with RL, the agent will consider the sequence of articles already read by users at each state. In other words, the agent are trying to maximize the total future cumulative rewards (clicks) by recommending one article given the fact that the user has already read the first, the second and the third articles. The sequential decision process of RL is shown in Figure 2.3.

The RL is based on the idea of the reward hypothesis. All goals can be described by the maximization of the expected cumulative reward. That means to have the best behaviour, we need to maximize the expected cumulative reward. The cumulative reward at each time step t is represented by [191]:

$$G_t = R_{t+1} + R_{t+2} + \cdots = \sum_{k=0}^{T} R_{t+k+1}. \tag{2.13}$$

However, in reality, we cannot simply add the rewards as in (2.13). This is because rewards at the beginning are more likely to happen since they are more predictable than the long term future reward. Therefore, a discount rate γ between 0 and 1 is defined. The larger the γ, the smaller the discount. This means the learning agent cares more about the long term reward. On the other hand, the smaller the γ, the bigger the discount. This means our agent cares more about the short term reward. Hence, the discounted cumulative expected rewards can be written as [191]:

$$G_t = \sum_{k=0}^{\infty} \gamma^k R_{t+k+1}, \gamma \in [0, 1). \tag{2.14}$$

[3] A metric that measures the number of clicks advertisers receive on their advertisements per number of impressions.

In a word, each reward will be discounted by γ to the exponent of the time step, implying that the likelihood of a future reward decreases as the time step increases.

Besides, the task, episodic or continuous, in RL is defined as the instance of an RL problem. Episodic tasks are the tasks that have a terminal state, which creates an episode composed by a list of states, actions, rewards and new states. For example, the ultra-popular PubG game, an episode begins at the launch of a new game and end when you are killed or all enemies are destroyed. Continuous tasks, on the other hand, are those that go on forever and have no termination. In this case, the agent has to learn how to choose the best action and simultaneously interacts with the environment. Taking stock trading as an example, there is no specific starting state or terminal state. The agent keeps running until people ask it to stop.

Moreover, there are also two ways of learning in RL problem. Monte Carlo approach collects the rewards at the end of each episode and then calculates the maximum expected future reward [192], while temporal difference (TD) learning calculate the rewards at each step [193].

In Monte Carlo, rewards are only received at the end of the episode and the agent looks at the total cumulative reward to see how well it did. Then, we start a new episode with the added knowledge. Therefore, the agent is able to make better decisions after each iteration. The process of Monte Carlo can be described by [194]:

$$V(S_{t+1}) \leftarrow V(S_t) + \alpha[G_t + V(S_t)], \tag{2.15}$$

where $V(S_t)$ is the maximum expected future reward at state S_t, G_t is the discounted cumulative rewards and α is the learning rate.

For TD learning, it will not wait until the end of the episode to update the maximum expected future rewards, where it will update the value $V(S_t)$ for the non-terminal state S_t occurring at that step. Hence, the value function of TD learning is [194]:

$$V(S_{t+1}) \leftarrow V(S_t) + \alpha[R_{t+1} + \gamma V(S_{t+1}) - V(S_t)]. \tag{2.16}$$

At time step $t+1$, it forms a TD target, $R_{t+1} + \gamma V(S_{t+1})$ by the observed reward R_{t+1} and the current estimate $V(S_{t+1})$. TD target is an estimation, where we update the previous estimate $V(S_t)$ towards a one-step target.

Additionally, it can be seen that RL is a training algorithm that keeps interacting with the environment. However, it is highly possible that the agent cannot learn "new skills" anymore after a long period. In this situation, one very important topic in RL is the exploration/exploitation trade-off [195]. Exploration means discovering more information about the environment, while exploitation utilises what we already know to maximize the reward. For instance, consider that someone and his friends are trying to

decide where to eat. They used to go to a Mexican restaurant in the past, and they all enjoyed it. However, one of his friends mentions that a new Lebanese place has opened up down the street this time, and it is supposed to be good. None of them can come to a consensus — should they go to the Mexican restaurant, which they know to be good, or should they try the Lebanese place, which has the potential to be better or worse. Similarly, in real life, the agent should decide whether it is preferable to exploit options that it believes are the best rather than exploring options that may be better or worse (or vice versa).

In the following sections, Q-learning (QL), a well-known RL algorithm that learns the value of an action in a particular state, will be reviewed first. Then, since QL suffers from having large Q-table in a complex environment, deep Q-learning (DQL) will be introduced. Finally, several methods that improve the learning progress of DQL will also be presented.

2.4.3.1 Q-learning

QL was first introduced in [196] as an extension of the dynamic programming paradigm [197]. It is a value-based RL algorithm that relies on Markov decision processes (MDP) [198]. The MDP consists of states s_t that an agent is in and actions a_t that the agent can take to move onto a new state s_{t+1} and receive a reward or a punishment R_{t+1}. QL seeks to learn the corresponding Q-value (quality) of a given action-state pair.

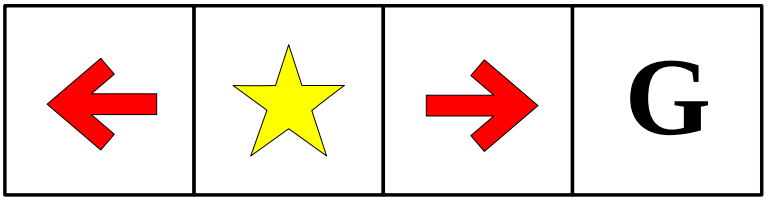

Figure 2.4: Model of simple grid world.

Starting with an example, imagine a simple grid world in Figure 2.4 with two actions: left and right, and four grid spaces with the goal (G) at the far side. If the agent reaches the goal it gets a reward of +1 and the episode ends. Although solving such a small environment is simple, it offers easy visualization of a Q-table. The Q-values in Figure 2.5 are understood as the expected discounted reward the agent will receive if it takes action (left or right in this case) in a given state (1, 2, 3, or 4).

To calculate each value of this Q-table, we use the action-value function (Q-function) to update the Q-value [191]:

$$Q(s_t, a_t) = E\left[R_{t+1} + \gamma R_{t+2} + \gamma^2 R_{t+3} + \cdots | s_t, a_t\right]. \tag{2.17}$$

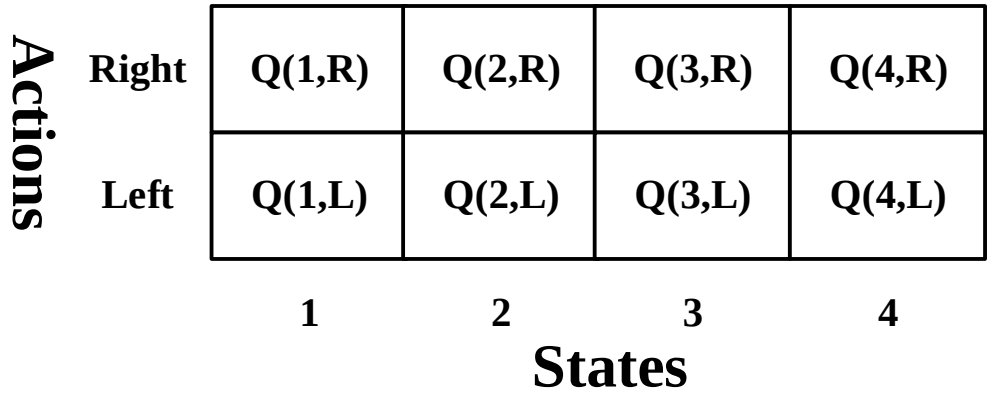

Figure 2.5: Q-table of grid world.

The action-value function (2.17) takes two inputs: state and action, and outputs the expected future reward at that state given that action. The function can be imagined as a reader that scrolls through the Q-table to find the line associated with the state and the column associated with the action. It returns the Q-value from the matching cell. However, before the agent explores the environment, the Q-table must be initialized with arbitrary fixed values. As long as the agent constantly explores the environment, the Q-table will provide a better approximation by iteratively updating $Q(s,a)$ using the Bellman equation [197]:

$$Q(s,a) = Q(s,a) + \alpha[r + \gamma \max_{a'} Q(s',a') - Q(s,a)]. \tag{2.18}$$

Starting from inside the parentheses, we first take the reward r we obtained from the selected action a and add it to the discounted maximum Q-value for the next state s', and subtract it from the current estimation of the Q-value at that state. This step is computing the error between the action just taken, and the action believed to be the best from this new state. Then, scaling the error down by step-size α, also known as the learning rate, adds to our current estimate for $Q(s,a)$. Finally, we obtain the new estimate for $Q(s,a)$. The QL algorithm process is summarized as follow:

1. Initialization of Q-value: A $m \times n$ Q-table will be generated and initialized with zero values, where m is the number of actions and n is the number of states.
2. Stopping condition: Repeating steps 3 to step 5 until a maximum number of episodes has been achieved or manually stopped by people.
3. Select an action: Select an action a at the current state s according to the current estimation of the Q-value.
4. Evaluation: After taking the selected action a, observe the resulting state s' and reward r.
5. Update the Q-value: $Q(s,a) = Q(s,a) + \alpha\,[r + \gamma \max(Q'(s',a')) - Q(s,a)]$.

Recall the exploration/exploitation trade-off mentioned at the end of Section 2.4.3. In step 3, an important issue is what action should be taken when all Q-values are zeros at the initial stage. Here, the ϵ-greedy algorithm [199, 200] is employed to solve this problem. The concept is that a large ϵ is needed at the start of the Q-function training. Then, as the agent gains more confidence in estimating Q-values, it will gradually lower it. Based on the idea of ϵ-greedy algorithm, the strategy is summarized as follow:

1. Since the agent knows nothing about the environment initially, ϵ will be set to 1 to allow a random selection of actions and do as much exploration as possible.
2. The value of ϵ will reduce as time goes on. Meanwhile, a random number δ will be generated to compare with ϵ. If $\delta > \epsilon$, the agent does exploitation, which means the agent will select an action based on the Q-table. Otherwise, the agent will randomly select an action and does exploration.

Hence, the agent can sense the actions returning with the highest reward. However, it will choose a random action from time to time to make sure that it is not missing anything. Accordingly, the machine can converge to the optimal strategy for whatever situation it is trying to learn. However, a limitation of QL is the size of the Q-table, especially when there are hundreds of actions and thousands of states. Therefore, it is hard for machines to traverse all possible conditions in a short time, which largely decrease their efficiency. Hence, the DQL will be reviewed in the following section, which is a deep-learning based QL algorithm, where the neural network [201] has been employed to solve this issue.

2.4.3.2 Deep Q-learning

In the previous section, it was shown that QL is a simple but effective method for creating a cheat sheet for the agent, enabling the agent to determine the optimal action in any given state. However, as we can see, producing and updating a Q-table can become ineffective in big state space environments. As a result, instead of employing a Q-table, a deep Q-network (DQN) can be used in QL to approximate these Q-values.

As shown in Figure 2.6, a neural network is employed to approximate the function of Q-Table in DQL [202]. Here, the state is considered as the input of the neural network and the Q-values of all possible actions are the outcomes of the neural network.

Therefore, the steps involved in RL but using DQN are:

1. All the experience is stored in memory by the user.
2. The maximum output of the DQN determines the following action.

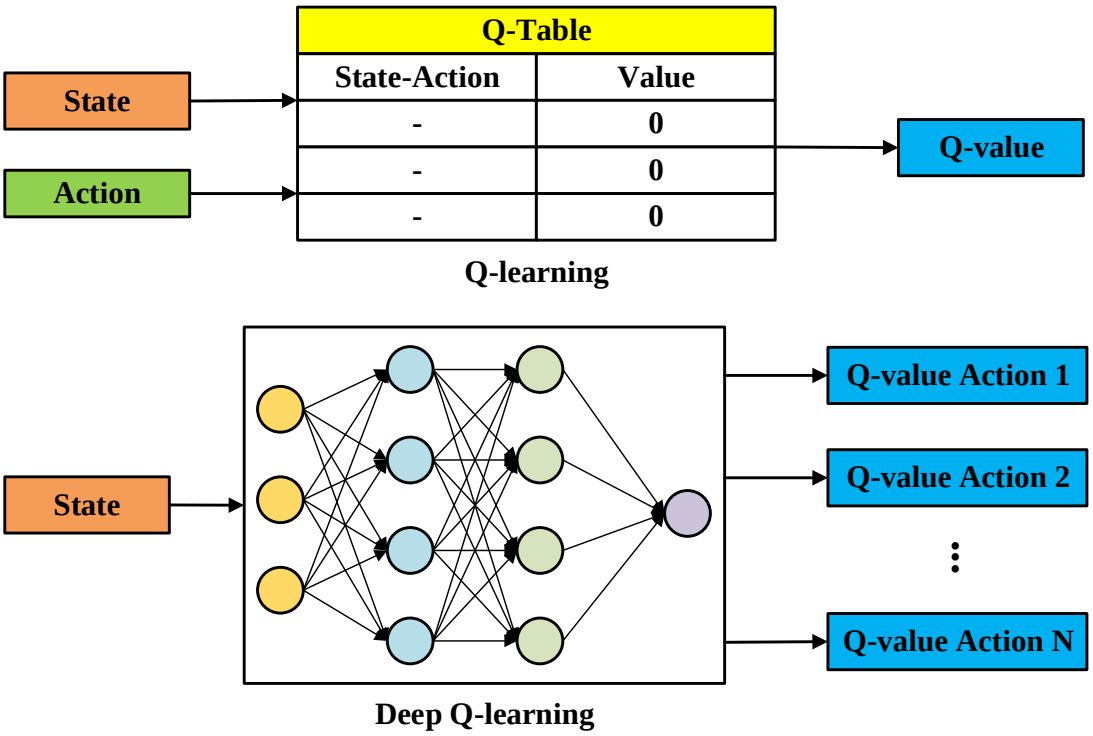

Figure 2.6: Comparison between QL and DQL.

3. Here, the loss function is defined by the mean squared error between the predicted Q-value and the target Q-value, which is a regression problem. However, as illustrated in (2.16), a target should be determined in an RL problem. Therefore, going back to the Q-value update function (2.18):

$$Q(s,a) = Q(s,a) + \alpha \left[\boxed{r + \gamma \max(Q'(s',a'))} - Q(s,a) \right]. \tag{2.19}$$

The target is represented by the section in the box in (2.19). As a result, it may be claimed that it is predicting its own value. However, because r is an unbiased true reward, the network will eventually converge by updating its gradient through back propagation.

Additionally, it can be shown that the target is continuously changing at each step or iteration, which is different from that in deep learning [203]. In deep learning, the target variable will not change and hence the training is stable but this is not true for RL. The same network calculates the predicted and target values, and there could be much divergence between these two. As a result, two neural networks will be employed for learning instead of one. As shown in Figure 2.7, the target network has the same structure as that of the prediction network but with fixed parameters w', where w' and w are the parameters of neurons in each layer of the neural network [204]. The parameters from the prediction network are transferred to the target network every N iterations.

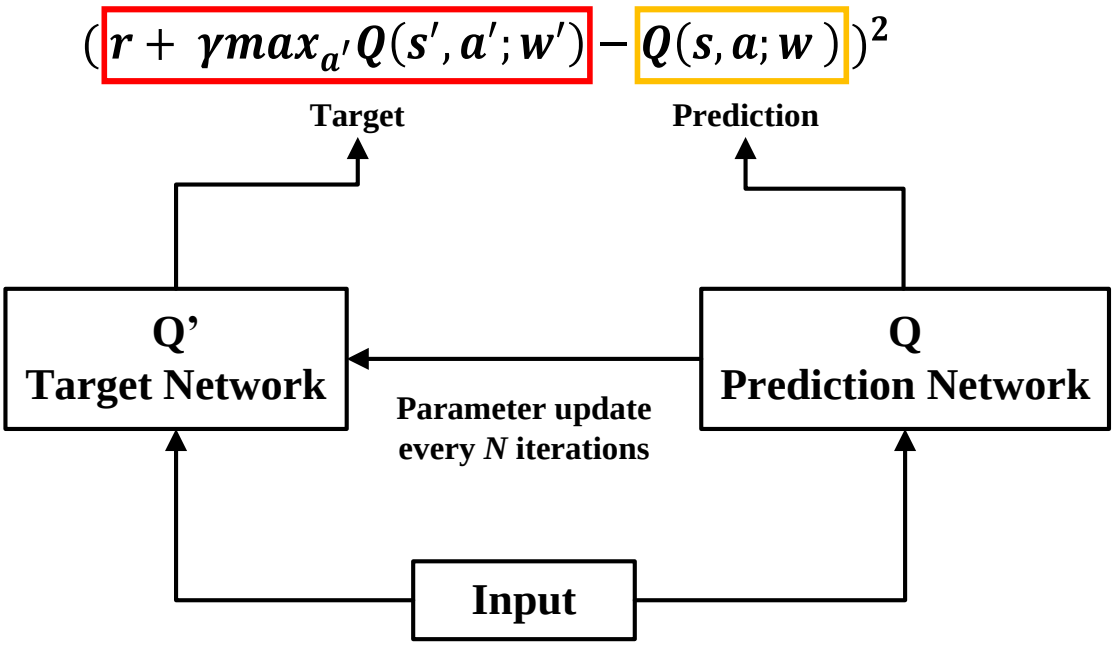

Figure 2.7: The structures of DQL network.

Moreover, the experience replay is also an important strategy to efficiently utilize the observed experience in DQL. Experience replay helps the system remember what it learnt before and reduce the correlation of experience [202]. However, instead of running QL on state-action pairs as they occur, the DQL system stores the data in the format of $[state, action, reward, nextstate]$ in a large buffer. For instance, assume we are attempting to create a video game bot in which each game frame represents a different state. Then, a random batch of frames will be selected from the last, say 10^6 frames, to train the network during training, which prevents the network from only learning about what it has immediately done and avoiding forgetting previous experiences. Besides, this also helps avoid being fixated on one region of the state space and prevents repeatedly reinforcing the same action, which reduces the correlation between experiences.

The concepts listed so far are combined to make the DQL algorithm achieve human-level performance in real life and the steps involved in a DQL system are shown below:

1. Preprocess and feed the state s to DQN, which will return the Q-values of all possible actions in the state.
2. Select an action with the ϵ-greedy algorithm. A random action a will be selected with the probability ϵ, while an action that has a maximum Q-value will be selected with probability $1 - \epsilon$, i.e., $a = \text{argmax}(Q(s, a, w))$.
3. Perform selected action at the state s and move to the next state s' to receive a reward. Then, this transition will be stored in the replay buffer in the format of $< s, a, r, s' >$

4. Randomly ample batch of transitions from the replay buffer and calculate the loss L, which is defined by $L = (r + \gamma \max_{a'} Q(s', a'; w') - Q(s, a; w))^2$.
5. Perform gradient descent with respect to the prediction network parameters w to minimize the loss.
6. Transfer the parameters of prediction network to the target network every N iterations.
7. Repeat for a total of M episodes until convergence is achieved.

So far, the theoretical aspects of DQL have all been reviewed. In the following section, several improvements on DQL will be presented.

2.4.3.3 Improvements of Deep Q-learning

In this section, two improvement methods on DQL, namely double DQL and duelling DQL, will be introduced to solve the issue of overestimation and accelerate the training progress of DQN. Double DQL was introduced in [205] to handle the overestimation issue of Q-values. Firstly, recall the way to calculate the TD target:

$$\underbrace{Q(s, a)}_{Q \text{ target}} = r + \gamma \max_{a'} Q(s', a'). \tag{2.20}$$

Then, there is a fundamental question of how we know that the optimum action for the next state is the one with the highest Q-value. The accuracy of Q-values depends on what action we tried and what neighbouring states we explored. However, we lack sufficient knowledge of the best action to take at the initial stage of the training. Therefore, selecting the maximum Q-value as the best action can lead to false positives. Furthermore, the learning will be complicated if non-optimal actions regularly give a higher Q-value than the optimal best action.

Therefore, double DQL employs two networks to separate the action-selection procedure from the generation of target Q-values. First, it uses the prediction network to select the best action for the next state (the action with the highest Q-value). Afterwards, it uses the target network to calculate the target Q-value of taking that action at the next state. As a result, double DQL reduces the overestimation of Q-values and allows for quicker and more consistent learning. Since this method is commonly used in today's DQL and becomes a basic procedure when applying DQL, the structure of double DQL is already illustrated by Figure 2.7 in Section 2.4.3.2.

Moreover, the value of each action at one state needs to be calculated in normal DQL. However, it becomes meaningless if the value of the state is terrible. In other words, the state itself is in bad condition, and all actions will lead to poor results no matter

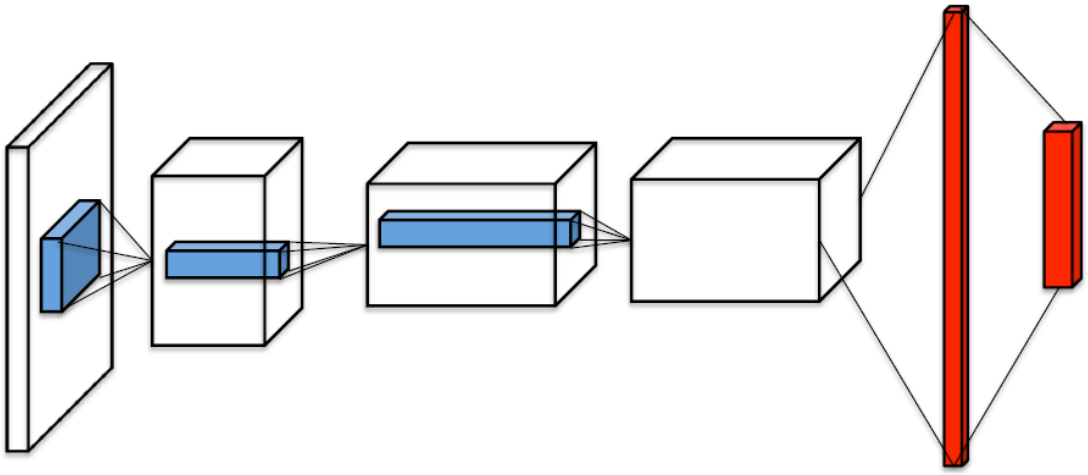

(a) The single stream Q-network.

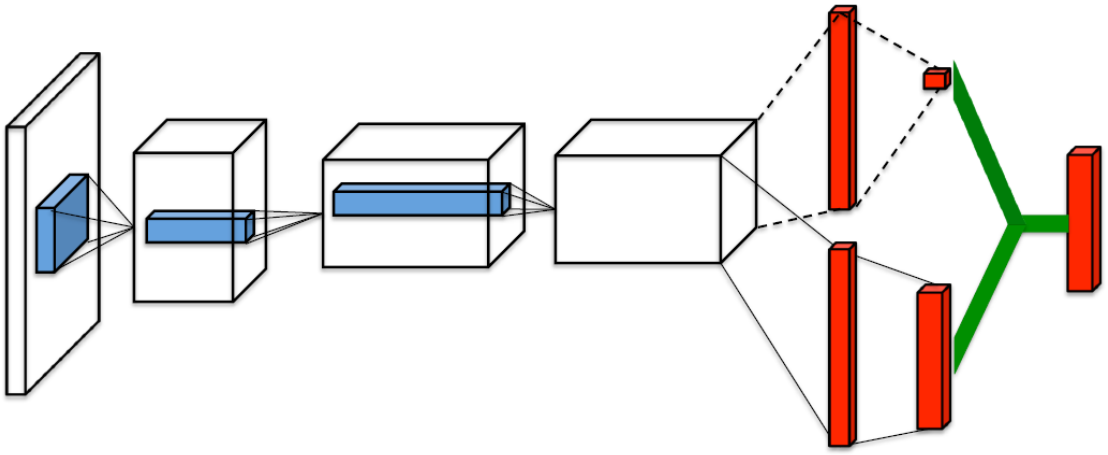

(b) The dueling Q-network.

Figure 2.8: Top: Regular DQL architecture. Bottom: Dueling DQL architecture [4].

how the actions are selected. As a consequence, duelling DQL was proposed in [4] to solve this issue by decomposing $Q(s,a)$ as follow:

$$Q(s,a) = B(s,a) + V(s), \tag{2.21}$$

where $V(s)$ indicates the value of being at a state and $B(s,a)$ is the benefit of taking that action at that state. Different from the single stream Q-network illustrated by Figure 2.8(a) in a regular DQL architecture. The duelling DQL, as shown in Figure 2.8(b), separates the estimator of these two elements into two new streams: one that estimates the state value $V(s)$ and the other estimates the benefit for each action $B(s,a)$.

As a result of decoupling the estimation, the duelling DQL may intuitively understand whether a state is valued or not, without having to study the effect of each action at each state, which is especially advantageous for states where their actions have no significant impact on them. Accordingly, calculating the Q-value of each action at that

state is unnecessary.

2.4.4 Machine Learning in UAV Communication System

UAVs will be an essential component of next-generation wireless communication networks [17]. Compared to traditional ground-based technologies, their use in various communication applications is expected to improve coverage and spectral efficiency. However, this new degree of freedom included in the network will also add new challenges. In this context, the ML framework is expected to provide solutions for the various problems for UAV-based communication purposes. This section reviews relevant research works in which ML techniques have been used on UAV-based communications to improve the various design and functional aspects such as channel modelling and deployment. Moreover, the ML schemes included in this section are not limited to the ML schemes discussed in previous sections.

2.4.4.1 Channel Modelling

Precision prediction of channel behaviour is crucial in wireless networks, particularly in mobile situations. Several ML approaches for predicting UAV channel behaviour and RSS have been reported. The authors of [206, 207] used artificial neural networks (ANNs) and ensemble methods to predict the RSS at the UAVs. Firstly, in [206], a multiple-layer perceptron NN is used and trained by measurement data. Novel training methods are developed based on the combination of self-adaptive differential evolution algorithms with the Levenberg–Marquardt method. The sequential application of these two methods offers better initial starting weights than random weight generation, resulting in better solutions and faster convergence. While the works of [207] focused on ensemble methods for UAV RSS prediction, it is an extension of [206], which developed a new ensemble method relying on five base learners. On the other hand, the study in [208] examines real-time 3D wireless channel modelling of the A2G channel among UAVs and ground nodes using unsupervised learning. Besides, a method that optimises the positioning of UAVs acting as aerial relays in A2G wireless networks was presented in [209]. In particular, to enable UAVs' autonomous path planning by exploiting a finely structured radio map, a joint clustering and regression problem using a maximum likelihood approach were formulated based on the K-segment ray-tracing model. Moreover, the works of [210] extracted the environmental characteristics through 3D image classification based on geo-referenced satellite imaging and 3D point cloud. Then, all these characteristics were fed to the ML-based pathloss model to improve the wireless network deployment by employing light detection and ranging (LiDAR) and ANNs. Furthermore, the authors of [211] considered ML algorithms consisting of the random forest (RandF) and K nearest neighbour (KNN) to study the

application of ML on pathloss prediction for the A2A channels. Another study [212] focused on pathloss prediction for UAV networks communicating with ground nodes in a millimetre-wave channel, where RandF and KNN were employed to realise pathloss and delay spread prediction.

A significant challenge arising not only in UAV networks but also in wireless networks, in general, is interference. The works of [213] studied opportunistic channel access by UAVs. The problem was formulated as a non-cooperative interference mitigation game, and a distributed log-linear learning algorithm was employed to achieve the Nash Equilibrium of the interference mitigation game. A scenario where both ground nodes and UAVs are connected through a cellular is studied in [214]. In particular, each UAV aims to maximize EE and minimize both wireless latency and the interference caused by the ground network along its path. The problem is formulated as a dynamic game among UAVs. A deep RL (DRL) algorithm, based on echo state network (ESN) cells, is proposed to solve this game. Afterwards, the authors of [215] regret-based learning (RBL) dynamic duty cycle selection (DDCS) method for configuring the transmission gaps in LTE-Unlicensed (LTE-U) ABSs, to ensure a satisfactory throughput for all users.

The proper setting of the transmission parameters should be conducted to maintain reliable communication and practical usage of wireless resources. The works in [216] focus on the field of automatic modulation classification (AMC), where the authors proposed a heterogeneous deep model fusion method to solve the AMC problem in a unified framework with convolutional neural network (CNN) and long short-term memory (LSTM). Besides, in massive multiple input and multiple output (MIMO) systems, precoding matrices are essential to improve the performance of the transmission by exploiting the CSI. The major contributions of ML on channel modelling is summarized in Table 2.4

2.4.4.2 Deployment of UAVs

As discussed in previous sections, the deployment of UAVs is also a significant issue that needs to be considered in a UAV-assisted communication network. In [217], the authors proposed a multi-agent QL-based placement algorithm for estimating the 3D optimal placement of the UAVs with respect to the initial positioning of the GUs. Then, mobility and the future positioning of the GUs were predicted by an ESN-based prediction algorithm. Finally, a multi-agent QL-based algorithm was conceived for predicting the position of UAVs in each time slot based on the movement of users. These three steps aim to maximize the throughput and satisfy the rate requirement of GUs by jointly optimizing the trajectory and power control in multiple UAVs scenarios. Then, the authors of [218] employed the nonlinear model predictive control (NMPC)-based framework, an optimization-based trajectory planner for the relay UAV by utilizing the

Table 2.4: Major contribution of ML for UAV channel modelling

Authors	Targets	ML methods
Goudos *et al.* [206, 207]	RSS prediction of UAV	ANN with DE LM training
Wang *et al.* [208]	A2G channel modelling	Unsupervised learning
Chen *et al.* [209]	Radio map construction	Segmented regression
Egi *et al.* [210]	Pathloss prediction in irregular terrains	ANN with LiDAR
Zhang *et al.* [211]	A2A pathloss prediction	KNN and RandF
Yang *et al.* [212]	A2G pathloss prediction	KNN and RandF
Chen *et al.* [213]	Opportunistic channel access by UAV	Distributed log-linear
Challita *et al.* [214]	A2G interference mitigation	ESN-based DRL
Athukoralage *et al.* [215]	Interference management in Wi-Fi and LTE-U networks	RBL
Zhang *et al.* [216]	AMC optimization	DL with CNN and LSTM

communication properties learned from the Gaussian process (GP) method. Besides, a novel QL-based system is designed to directly make movement decisions for a UAV serving multiple users in [219], where the UAV acts as an autonomous agent in the environment to learn the trajectory that maximizes the sum rate of the transmission over the whole flying time. Moreover, a hybrid channel modelling approach in support of the trajectory planning for communication relay UAVs was studied in [220]. The proposed NN-based approach predicted the correct discrete urban environment type that provides essential information to be used in the low altitude platform model.

The QoE-driven 3D deployment and dynamic movement of multiple UAVs were jointly studied in [221] to maximize the sum mean opinion score (MOS) of the users. More specifically, a genetic algorithm based k-means (GAK-means) algorithm was utilised to obtain the cell partition of the users. Then, a QL-based deployment algorithm was proposed, in which each UAV acts as an agent, making its own decision for attaining a 3D position by learning from trial and error. In [222], an unsupervised online self-tuning learning algorithm for joint mobility prediction and object profiling of UAVs was proposed. Afterwards, a UAV-based IoT data harvesting scenario in an urban area was presented in [223], where a resource-constrained ABS was employed to serve multiple static ground nodes. Firstly, an optimised trajectory was devised for the UAV that allows it to learn the propagation parameters. The learning trajectory optimization depends on the dynamic programming techniques and the knowledge of the 3D city map. Then, a joint trajectory and node scheduling problem was formulated based on the learned parameters to maximize the traffic communicated from each node to the UAV. Finally, an iterative algorithm was proposed to solve the optimization problem via a map compression method. The works of [224] consider the case of UAVs as

Table 2.5: Major contribution of ML for UAV deployment

Authors	Targets	ML methods
Liu *et al.* [217]	Average throughput of users	QL
Ladosz *et al.* [218]	Average throughput of ground nodes	GP and NMPC based method
Bayerlein *et al.* [219]	sum rate	QL
Ladosz *et al.* [220]	Quality of communication	NN
Liu *et al.* [221]	QoE and MOS	QL and GAK-means
Peng *et al.* [222]	Mobility prediction and object profiling	Unsupervised learning
Esrafilian *et al.* [223]	Average throughput of ground nodes and path planning	Map compression based method
Colonnese *et al.* [224]	QoE	QL
Dai *et al.* [225]	Sum rate	Distributed learning
Jailton *et al.* [226]	Average throughput of UAVs	ANN
Ghanavi *et al.* [227]	QoS	QL

mobile BSs providing video streaming services within a cellular macro area. The authors devised a QL-based UAV flight planning algorithm to improve the QoE of video users. The authors of [225] investigated the sum-rate maximization with α-fairness for UAV-supported GUs, which are subject to flight region and limited power budget of UAVs. They proposed a robust and distributed learning algorithm to gather useful information about GUs and jointly optimise the power allocation and UAVs' mobility via leveraging the game theory framework. The authors of [226] proposed a flight path planning model, which involves a metaheuristic optimization-based approach. The proposal relied on the ANNs to optimize the positioning of the relay device, so that the throughput between the other devices could be increased. The performance of a downlink A2G communication system was optimised in [227], where user mobility is taken into account. In particular, QL was employed to find the optimal position of the ABS for compensating the QoS loss due to user movements. The major contributions of ML on UAV deployment is summarized in Table 2.5.

2.5 Modulation Schemes

Modulation, impressing the data to be sent on the radio carrier, is the fundamental technique for all wireless communications. The primary purpose of modulation is to integrate as much data into the as little spectrum as possible. This goal, known as spectral efficiency, quantifies how quickly data can be delivered within a given bandwidth. Several techniques for achieving and improving spectral efficiency have evolved. A sine

wave radio carrier may be modulated in three ways: amplitude, frequency, or phase. More advanced approaches combine two or more of these variants to increase spectral efficiency. Moreover, these fundamental modulation schemes are still employed with digital signals today. In this section, two modulation schemes, OFDM and SM, that have been employed in our proposed UAV-assisted communication system will be reviewed.

2.5.1 Orthogonal Frequency Division Multiplexing

OFDM [228, 229] is a digital multi-carrier modulation system that uses multiple subcarriers to expand the idea of single carrier modulation. OFDM employs a large number of closely-spaced orthogonal subcarriers that are transmitted in parallel rather than a single carrier to convey a high-rate stream of data. Using a traditional digital modulation method, each subcarrier is modulated at a low symbol rate (QPSK, 16QAM, etc.). However, combining several subcarriers allows for data rates comparable to standard single-carrier modulation techniques within the same bandwidth.

The frequency division multiplexing (FDM) technique is the foundation of OFDM. Different data streams are mapped onto different parallel frequency channels in FDM. Besides, a frequency guard band separates each FDM channel from the others, which reduces interference between neighbouring channels. Instead of sending data streams serially, OFDM is an effective parallel data transmission technique carried by multiple orthogonal subcarriers with serial to parallel (S/P) conversion. Guard intervals are also used to reduce inter-symbol and inter-channel interference.

2.5.1.1 OFDM Modulation

As aforementioned, OFDM is a sort of multicarrier communication scheme in which multiple subcarriers send data symbols in parallel while sharing the system bandwidth using some form of FDM. The block diagram of the OFDM transmitter is depicted in Figure 2.9. The first step is to convert the serial input data symbols into parallel (S/P) and allocate them to M parallel subbranches, where a_m and b_m represent the data symbols that are allocated to in-phase (I) and quadrature-phase (Q) of m^{th} subbranch. After S/P conversion, each of the M subbranches is modulated onto one of the M subcarriers. Finally, a composite transmitted signal is formed by adding all subbranch signals.

Additionally, the data symbols associated with different subbranches may have different symbol dynamic ranges and are not required to be identical. Furthermore, the modulation scheme can be independently selected on each subbranch. Due to the frequency-selective communication environment, some subcarriers may suffer more

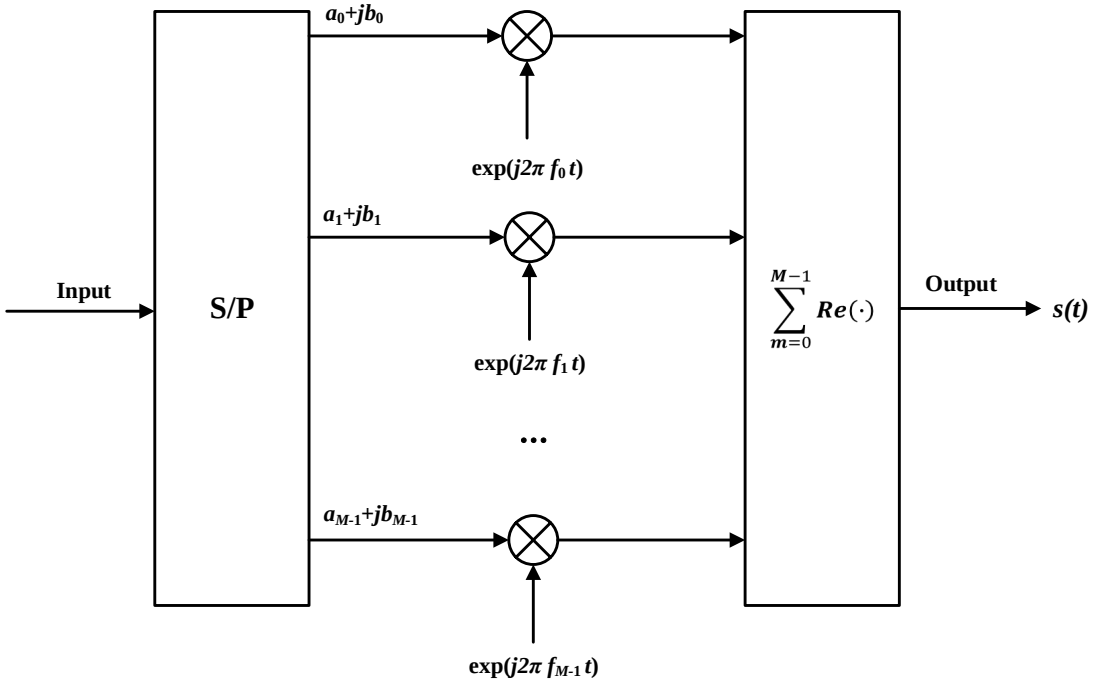

Figure 2.9: Transmitter side block diagram of OFDM system with M number of subcarriers [5].

severe degradation than other subcarriers. Therefore, those subcarriers with higher output signal-to-noise ratio (SNR) may use higher rate modulation schemes, while those with degraded output SNR may use lower rate modulation schemes or cancel the transmission. Consequently, the OFDM signal $s(t)$ in Figure 2.9 can be expressed as [230]:

$$\begin{aligned} s(t) &= \sum_{m=0}^{M-1} \Re\left\{ (a_m + jb_m)\, e^{j2\pi f_m t} \right\}, \\ &= \sum_{m=0}^{M-1} \left[a_m \cos(2\pi f_m t) - b_m \sin(2\pi f_m t) \right]. \end{aligned} \tag{2.22}$$

The OFDM signal can be described as a set of closely spaced FDM subcarriers, the frequency of each subcarrier is selected to form an orthogonal signal set. To maintain orthogonality, the subcarrier signals obey the relationship of [5]:

$$\int_0^{T_s} (a_m + jb_m)\, e^{j2\pi f_m t} \times (a_n + jb_n)^*\, e^{j2\pi f_n t} dt = 0, \tag{2.23}$$

where $m \neq n$ and $(\cdot)^*$ indicates the complex conjugation. As a result, it is simple to find that the M number of frequencies should satisfy [5]:

$$f_m - f_n = \frac{i}{T_s}, \tag{2.24}$$

where $i \geq 1$ is an integer. In OFDM systems, using a frequency spacing equal to the

inverse of the OFDM symbol duration T_s is the standard method of establishing orthogonality of subcarrier signals. Hence, the method of orthogonality of subcarrier signals should be selected to satisfy [5]:

$$\left\{0, \frac{1}{T_s}, \frac{2}{T_s}, \cdots, \frac{M-1}{T_s}\right\}. \tag{2.25}$$

Here, the symbol duration is defined by the following equation [5]:

$$T_s = \left(\sum_{i=0}^{M-1} m_i\right) \times T_b, \tag{2.26}$$

where m_i for $i = 0, 1, \ldots, M-1$ is the number of bits transmitted by the i^{th} subcarrier. Therefore, $\sum_{i=0}^{M-1} m_i$ is the total number of bits transmitted per OFDM symbol. Moreover, T_b is the bit duration of serial input to the S/P converter as illustrated in Figure 2.9.

2.5.1.2 OFDM Demodulation

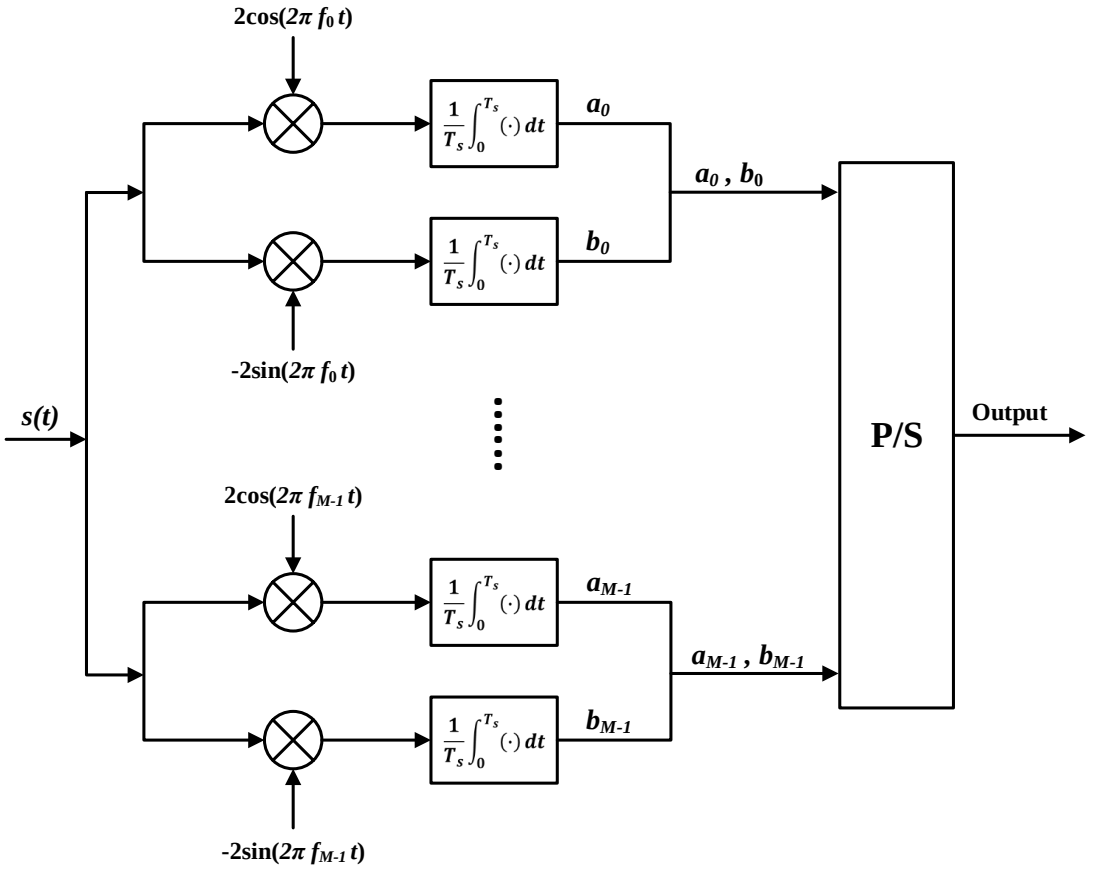

Figure 2.10: Receiver side block diagram of OFDM system with M number of subcarriers [5].

The procedure of OFDM demodulation is illustrated by Figure 2.10. In this system, $2M$ number of correlators and one parallel-to-serial converter (P/S) are included. From Figure 2.10, the recovery process of information symbols is obtained by multiplying corresponding sinusoidal waveforms. For example, in the first subbranch, the symbol a_0 is recovered by first multiplying the OFDM signal $s(t)$ with $2\cos(2\pi f_0 t)$ related to it. Then, the product signal will be sent to a following integrator over a symbol time interval. Hence, the whole process can be expressed by [5]:

$$\begin{aligned}
&\frac{1}{T_s}\int_0^{T_s} s(t)2\cos\left(2\pi f_0 t\right)dt, \\
&\quad= \frac{1}{T_s}\int 0^{T_s}\sum_{m=0}^{M-1}\left[a_m\cos\left(2\pi f_m t\right)-b_m\cos\left(2\pi f_m t\right)\right]2\cos\left(2\pi f_0 t\right)dt, \\
&\quad= \sum_{m=0}^{M-1} a_m\frac{1}{T_s}\int_0^{T_s}\left(\cos\left[2\pi\left(f_m+f_0\right)\right]+\cos\left[2\pi\left(f_m-f_0\right)\right]\right)dt, \\
&\quad- \sum_{m=0}^{M-1} b_m\frac{1}{T_s}\int_0^{T_s}\left(\sin\left[2\pi\left(f_m+f_0\right)\right]+\sin\left[2\pi\left(f_m-f_0\right)\right]\right)dt.
\end{aligned} \tag{2.27}$$

As mentioned before, the subcarrier frequencies are in the form of $\frac{i}{T_s}$. Recall in (2.25), the orthogonality of OFDM system in (2.27) can be reflected by [5]:

$$\begin{aligned}
&\frac{1}{T_s}\int_0^{T_s}\cos\left[2\pi\left(f_m+f_0\right)t\right]dt=0. \\
&\frac{1}{T_s}\int_0^{T_s}\cos\left[2\pi\left(f_m-f_0\right)t\right]dt=\begin{cases}1, & if f_m=f_0; \\ 0, & if f_m\neq f_0.\end{cases} \\
&\frac{1}{T_s}\int_0^{T_s}\sin\left[2\pi\left(f_m+f_0\right)t\right]dt=0. \\
&\frac{1}{T_s}\int_0^{T_s}\sin\left[2\pi\left(f_m-f_0\right)t\right]dt=0.
\end{aligned} \tag{2.28}$$

Consequently, substituting the above results into (2.27), the following equation can be obtained [5]:

$$\frac{1}{T_s}\int_0^{T_s} s(t)2\cos\left(2\pi f_0 t\right)dt=0. \tag{2.29}$$

Similarly, as shown in Figure 2.10, the quadrature-phase symbol b_0 carried by the first subcarrier f_0 can be recovered by the same procedure mentioned above. Therefore, the demodulation scheme of b_0 is given by [5]:

$$\frac{1}{T_s}\int_0^{T_s} s(t)\times\left[-2\sin\left(2\pi f_0 t\right)\right]dt=b_0. \tag{2.30}$$

Hence, all the data symbols carried by their corresponding subcarriers can be recovered. Finally, all those demodulated symbols will pass through the P/S converter, where they are converted from parallel data into serial output data.

Since the subcarrier signals are orthogonal, the demodulation scheme mentioned above shows no need to employ a bandpass filter in an OFDM demodulator for each subcarrier. This property is one of the benefits of employing OFDM because the complexity of the demodulator can be significantly reduced when subcarrier associated filters are not used in the demodulation. In addition, multicarrier modulation and demodulation can be achieved in OFDM systems by employing low-complexity fast Fourier transform (FFT) techniques: inverse discrete Fourier transform (IDFT) and discrete Fourier transform (DFT). Assume we have a M length sequence $\{x(0),\ x(1), \ldots,\ x(M-1)\}$, then, the DFT and IDFT can be defined as: [230]:

$$DFT : X(k) = \frac{1}{\sqrt{M}} \sum_{m=0}^{M-1} x(m) e^{-j\frac{2\pi km}{M}}, k = 0,\ 1, \ldots,\ M-1. \tag{2.31}$$

$$IDFT : x(m) = \frac{1}{\sqrt{M}} \sum_{k=0}^{M-1} X(k) e^{j\frac{2\pi km}{M}}, m = 0,\ 1, \ldots,\ M-1. \tag{2.32}$$

Consequently, the complexity of OFDM system can be further improved.

2.5.2 Orthogonal Frequency Division Multiple Access

Orthogonal frequency division multiple access (OFDMA) [231, 232] divides the channel into smaller frequency allocations, called resource units (RUs). It enables one access point (AP) to synchronize communication with multiple individual clients assigned to specific RUs. By dividing the channel, small frames can be simultaneously transmitted to multiple users in parallel.

OFDMA can be considered as a technology that partitions a channel into smaller subchannels so that simultaneously multi-user transmissions can happen [233]. For example, a 20 MHz channel can be partitioned into nine smaller subchannels. Therefore, the AP can simultaneously serve nine clients by using OFDMA. It is ideal for most network applications and results in better frequency reuse, reduced latency, and increased efficiency [234], which is a much more efficient use of the medium for smaller frames. The simultaneous transmission cuts down on excessive overhead at the medium access control layer and medium contention overhead. The AP can allocate the whole channel to a single user or partition it to serve multiple users simultaneously, based on traffic needs.

2.5.2.1 Resource Unit

Figure 2.11 and Figure 2.13 show how frequency space is assigned to users for data transmission, which helps to clarify the differences between OFDM and OFDMA. When an AP uses OFDM to send data to clients, the entire frequency space is occupied for

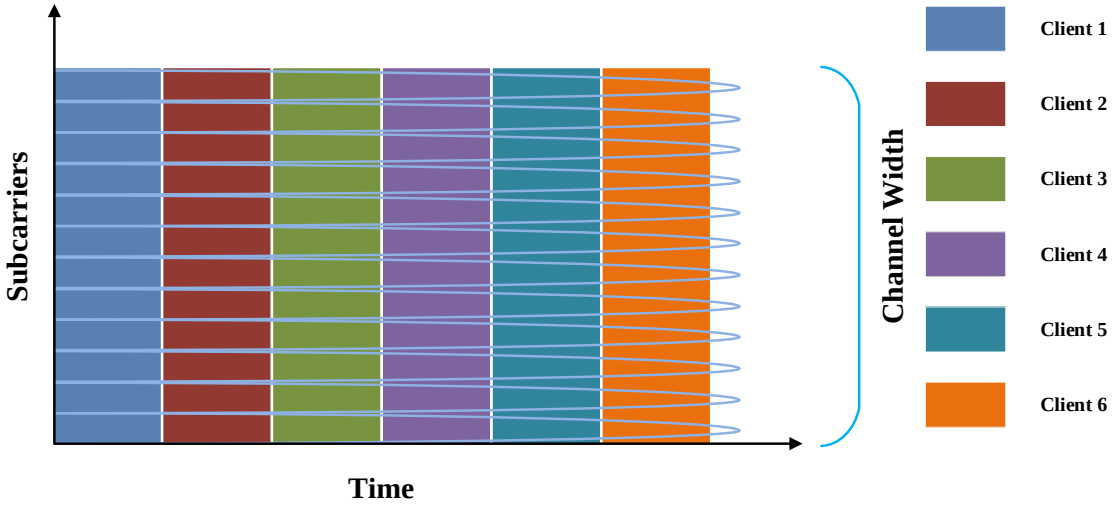

Figure 2.11: Transmissions of OFDM over time [6].

each independent transmission. In the example of Figure 2.11, the AP transmits to 6 clients independently over time. When 20 MHz channel bandwidth is used, all 64 subcarriers will be used for each independent transmission. In other words, the entire channel is needed to communicate between the AP and a single OFDM client.

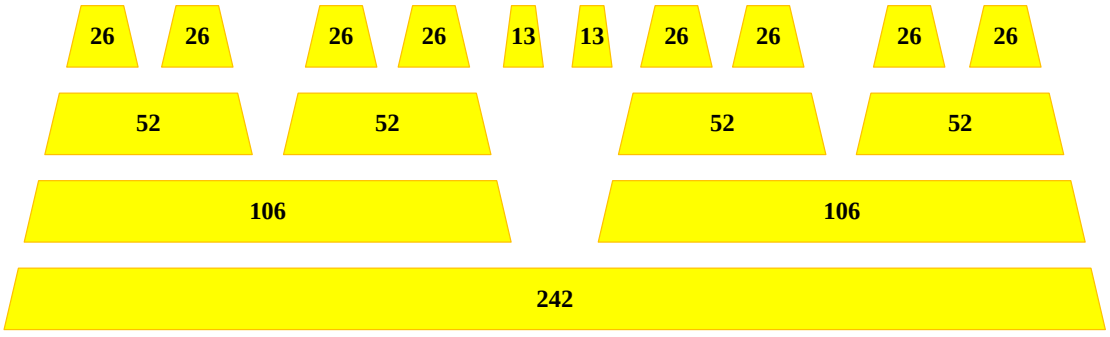

Figure 2.12: Resource units of OFDM system with 20 MHz bandwidth [7].

As previously stated, an OFDMA system considered in [7] has a total of 256 subcarriers. These subcarriers can be divided into RUs, which are smaller subchannels. For example, as illustrated by Figure 2.12, an AP can specify 26, 52, 106, and 242 subcarrier RUs with a 20 MHz frequency bandwidth, which corresponds to 2 MHz, 4 MHz, 8 MHz, and 20 MHz channels, respectively. The AP decides how many RUs are used within a 20 MHz channel, and different combinations can be used. For example, the AP may allocate the whole channel to only one user at a time, or it may partition the channel to serve multiple users simultaneously.

In the example shown in Figure 2.13, the AP first simultaneously transmits to clients 1, 4 and 6. The 20 MHz channel is effectively partitioned into three subchannels. Remember that an ODFMA 20 MHz channel has 256 subcarriers [7], however, the AP is simultaneously transmitted to clients 1, 4 and 6 using two different 52-subcarrier RUs

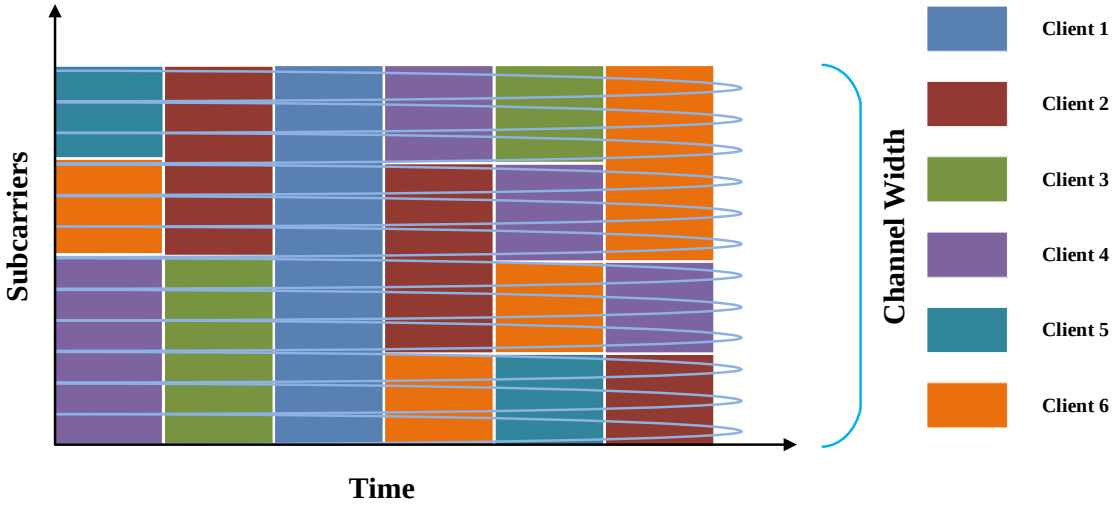

Figure 2.13: Transmissions of OFDMA over time [6].

and one 106-subcarrier RU. In the second transmission, the AP simultaneously transmits downlink to clients 2 and 3. In this case, the ODFMA channel had to be partitioned into two different 106-subcarrier RUs. The AP uses a single 242-tone resource unit to transmit to a single client (client 1) in the third transmission. Using a single RU is effectively using the entire 20 MHz channel. Then, the AP simultaneously transmits downlink to clients 2, 4 and 6 using two 52-subcarrier RUs and one 106-subcarrier RU in the fourth transmission. Afterwards, the AP simultaneously transmits to four clients with four different 52-subcarrier RUs in the fifth transmission. In the sixth transmission, the AP simultaneously transmits downlink to clients 2, 4 and 6. In this instant, the 20 MHz channel is partitioned into three subchannels; two 52-subcarrier RUs are used for clients 2 and 4 and a 106-subcarrier RU for client 6. In addition to 20 MHz channels, 40 MHz, 80 MHz, and even 160 MHz channels can also be partitioned into various combinations of RUs. For example, if an 80 MHz channel was subdivided using 26 subcarrier RUs, 37 clients could theoretically communicate simultaneously using their OFDMA capabilities.

2.5.3 Index Modulation

There has been much interest in the concept of index modulation (IM) in recent years [235, 8]. IM is a spectrum-efficient and energy-efficient but simple digital modulation technology that uses the indices of the associated building blocks of the corresponding communication systems to transmit extra information bits [236]. IM systems provide alternatives to traditional digital modulation techniques that rely on the modulation of the amplitude/phase/frequency of a sinusoidal carrier signal for transmission, as has been widely discussed in communications over the last fifty years.

IM systems can map information bits by altering transmission entities' on/off status, such as transmit antennas, subcarriers, RF mirrors, etc [8]. In other words, IM introduces entirely new dimensions to data transmission. Furthermore, these building blocks can transmit information through the indices via an on/off keying mechanism. As a result, IM schemes can move the saved transmission energy from inactive transmit entities to active transmit entities, resulting in improved error performance compared to traditional schemes that use the same total transmission energy. Additionally, IM methods can convey information in a more energy-efficient manner by deactivating parts of the system's main elements while still utilizing them for data transfer purposes. Finally, because IM introduces additional dimensions for transmitting digital information, the spectral efficiency of the investigated communication system could be efficiently boosted without adding hardware complexity.

SM [235, 237], which considers IM for the transmit antennas of a MIMO system [238, 239], has attracted tremendous attention over the past few years and introduced new directions for the implementation of MIMO systems. Although having very strong and well-established opponents such as vertical Bell Laboratories layered space-time (V-BLAST) [240] and space-time coding (STC) systems [241], SM schemes have quickly shown their potential in terms of spectral and EE and, consequently, have been regarded as possible candidates for next-generation small/large-scale and single/multi-user MIMO, full-duplex, cooperative and cognitive radio systems.

2.5.3.1 Spatial Modulation

As aforementioned, SM utilises the indices of transmit antennas in a MIMO system for sending extra information, which is the most well-known use of IM. Although the origins of SM may be traced back to the early twentieth century, the authors investigated SM-like transmission systems in [242, 243, 244] by utilizing alternative terminology. The term SM was originally used in the research of [245, 246, 247]. The SM idea sparked a fresh wave of alternative digital modulation methods in the years that followed, with several studies published in the literature [235, 237, 248].

In addition to the standard M-ary signal constellations, SM explores a new technique for delivering information through the indices of the transmit antennas of a MIMO system [235]. The traditional MIMO schemes rely on spatial multiplexing to increase the data rate by transmitting different data symbols from different transmit antennas [240], or spatial diversity to improve error performance by receiving multiple copies of the data symbols at different time slots from different transmit/receive antennas [249, 250]. In other words, unlike in SM, the different transmit antennas of a MIMO system are employed for different purposes in these cases. In particular, there are two information-carrying units in SM, the indices of accessible transmit antennas and the

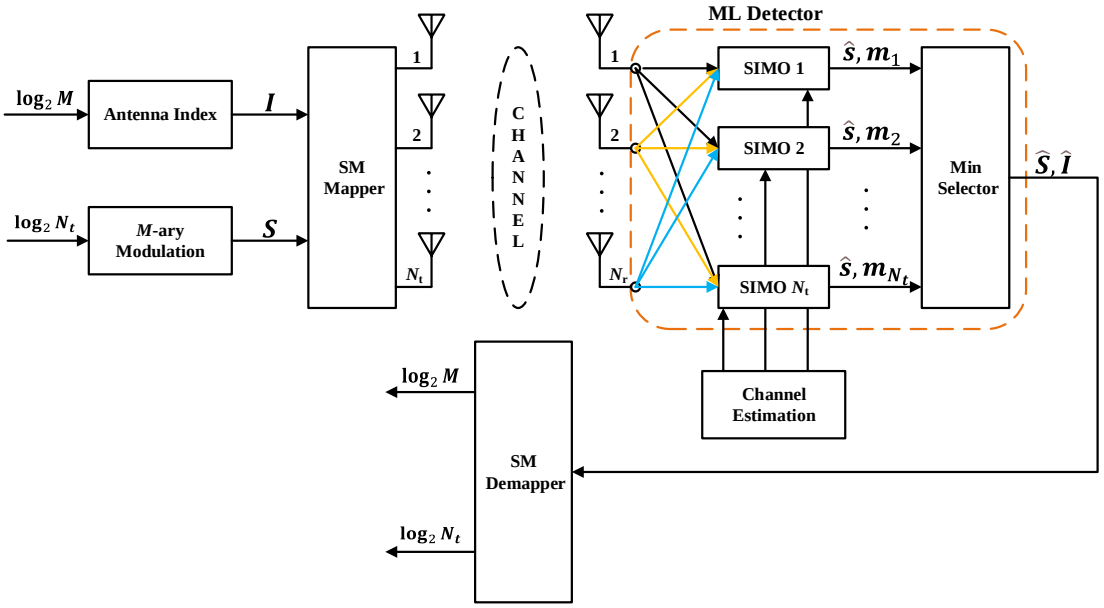

Figure 2.14: SM system model with N_t transmit and N_r receive antennas [8].

M-ary constellation symbols. As depicted in Figure 2.14, a total of

$$\log_2(N_t) + \log_2(M) \tag{2.33}$$

bits enter the transmitter of a SM system within a transmission interval, where N_t and N_r denote the number of transmit and receive antennas, respectively. While M is the size of the considered signal constellation diagram, such as M-ary phase shift keying (M-PSK) or M-ary quadrature amplitude modulation (M-QAM). The first $\log_2(M)$ bits of the incoming bit sequence are traditionally employed to modulate the amplitude and/or phase of a carrier signal. In contrast, the remaining $\log_2(N_t)$ bits of the incoming bit sequence are used to determine the index (I) of the active transmit antenna that transmits the corresponding modulated signal (S). As a result, the baseband transmission vector of SM, with dimensions $N_t \times 1$ is given by:

$$\boldsymbol{S} = [0 \cdots 0\ s\ 0 \cdots 0]^T. \tag{2.34}$$

The sparse structure of the SM transmission vector $\boldsymbol{S}$ presented in (2.34) not only decreases the detection complexity of its maximum likelihood detector in terms of complicated operations but also allows the implementation of compressed sensing-based low/near-optimal detection methods for SM systems.

The SM scheme receiver needs to detect two essential tasks: the active transmit antenna for the demodulation of index bits and the data symbol transmitted over the activated transmit antenna for M-ary signal constellation demodulation. To accomplish these two tasks, the optimal maximum likelihood detector of SM must search jointly over all transmit antennas and constellation symbols [248]. As illustrated by Figure 2.14, the

maximum likelihood detector employed in the SM scheme could be considered as a mixture of N_t single-input and multiple-output maximum likelihood detectors, which correspond to N_t transmit antennas and demodulate the corresponding complex data symbol as $\widehat{s}$. This detector determines the most likely activated transmit antenna by comparing the corresponding minimum decision metrics $(m_1, m_2, \ldots, m_{N_t})$ and provides the detected activated antenna index $(\widehat{l})$ as well as the estimated complex data symbol $(\widehat{s})$ to the SM demapper for retrieving the incoming bit sequence. The rudimentary suboptimal detector of SM, on the other hand, deals with the two tasks mentioned above, one after the other. It first detects the activated transmit antenna, and then it identifies the data symbol transferred over this antenna [246, 251]. As a result, the size of the search space becomes $N_t \times M$ and $N_t + M$ for the maximum likelihood and suboptimal detectors, respectively. Although the suboptimal detector can significantly reduce complexity for an increasing number of transmit antennas and higher-order constellations, its error performance is considerably worse than that of the maximum likelihood detector. Therefore, implementing the suboptimal detector can be problematic for critical applications that require a low error rate. Additionally, the sparse structure of SM transmission vectors enables the implementation of near/sub-optimal low-complexity detection methods for SM systems, such as matched-filter based detection [252] and compressed-sensing based detection [253].

Given the above discussion on SM, MIMO systems can offer attractive advantages over their traditional counterparts by employing SM techniques [**?**, 254, 255, 256]. In the following, the key advantages of SM over classical MIMO systems will be summarized [8]:

- **High spectral efficiency**: The SE of SM exceeds that of single-input single-output systems and orthogonal space-time block codes due to the utilization of transmit antenna indices as an additional method of transmitting the information.
- **High energy efficiency**: The power consumption of the SM transmitter is independent of the number of antennas the transmitter has, while the information can still be transferred via these antennas. In other words, a SM-MIMO system may use a larger number of transmit antennas for data transmission without consuming more energy. SM seems to be a energy-efficient MIMO technology from this standpoint. Compared to V-BLAST, the improvements are up to 46% are reported for different types of BSs equipped with multiple antennas in terms of the EE in Mbits/J [257].
- **Simple transceiver design**: A single RF chain is enough for the SM technique because only one transmit antenna is active during transmission. Additionally, inter-channel interference and inter-antenna synchronization are also removed. As a result, the decoding complexity of the SM receiver rises linearly with the

constellation size and number of transmit antennas in terms of the total number of real multiplications.

- **Operation with flexible MIMO systems**: Unlike the V-BLAST technique, which needs $N_r > N_t$ and zero-forcing type linear detectors to function with minimum mean square error, SM could be designed for any number of transmit and receive antennas. In other words, SM is ideally suited for unbalanced MIMO configurations, such as the downlink of next-generation wireless networks with a larger number of transmit antennas.

Although the SM scheme offers aforementioned appealing advantages, it also has certain drawbacks, which are summarized as follows:

- The SE of V-BLAST grows linearly with N_t, whereas the spectral efficiency of SM increases logarithmically with N_t. As a result, SM requires more transmit antennas to achieve the same spectral efficiency as V-BLAST. More crucially, the spectral efficiency of plain SM cannot compete with that of V-BLAST for higher-order constellation sizes.
- To ensure that a SM scheme operates effectively, the channel coefficients of different transmit antennas must be sufficiently different. In other words, rich scattering environments are required for SM to achieve better error performance. In contrast to classical systems, the bit error rate (BER) performance of SM degrades significantly in situations with higher Rician K or Nakagami-m factors.
- SM transmit the data using the spatial domain, so plain SM cannot offer transmit-diversity as STC systems. Therefore, one solution considers transmit-precoding, which requires channel state information at the transmitter, while another is STC techniques that require at least two transmission phases.

Given the benefits and drawbacks of SM systems discussed above, we can conclude that the SM scheme offers a fascinating trade-off between encoding/decoding complexity, spectral efficiency, and error performance. As a result, SM technologies have been identified as potential options for next-generation wireless communication systems with high spectrum efficiency and low energy consumption.

2.5.3.2 Generalized Spatial Modulation

As outlined in the previous section, one of the primary downsides of SM is its comparatively low spectrum efficiency compared to the traditional V-BLAST system for the same number of transmit antennas. Although the indices of the active transmit antennas in SM can transmit a significant amount of information. Compared to V-BLAST,

SM still has a significant loss in spectral efficiency due to inactive transmit antennas for higher-order modulations and MIMO systems.

The generalised SM (GSM) scheme was one of the first to attempt to boost the spectral efficiency of SM and to alleviate the limitation on the number of transmit antennas, which must be an integer power of two for conventional SM. The number of active transmit antennas is no longer set to one in the GSM method, and the same data symbol is transmitted through a selection of numerous active transmit antennas. Inter-channel interference is also avoided for GSM since the identical data symbol is transmitted from all active transmit antennas. The spectral efficiency of GSM in terms of bits per channel use becomes:

$$\left\lfloor \log_2 \binom{N_a}{N_t} \right\rfloor + \log_2(M), \tag{2.35}$$

where N_a, which satisfies the condition $N_a < N_t$, is the the number of active transmit antennas and $\lfloor \cdot \rfloor$ is the floor operation and $\binom{\cdot}{\cdot}$ stands for the binomial coefficient. It should be noted that SM is a special case of GSM with $N_a = 1$. Considering $\log_2(N_t) \leq \left\lfloor \log_2 \binom{N_a}{N_t} \right\rfloor$ for $N_t = 2^n$ $(n = 1, 2, \ldots)$, the spatial domain can be used in a more effective way by the GSM scheme. For example, consider a case that has $N_t = 8$ transmit antennas. The antenna indices can transmit only three bits in SM. However, GSM can convey six bits with $N_a = 4$. In [258], the concept of GSM has been extended to multiple-active spatial modulation (MA-SM) by transmitting different data symbols from the activated transmit antennas to further improve the spectral efficiency. As a result, the spectral efficiency of the MA-SM scheme is calculated by:

$$\left\lfloor \log_2 \binom{N_a}{N_t} \right\rfloor + N_a \log_2(M), \tag{2.36}$$

which is considerably higher than that of SM given in (2.33). MA-SM is an appealing intermediate solution between two extreme schemes: SM and V-BLAST, which are special cases of MA-SM for $N_a = 1$ and $N_a = N_t$, respectively. Given the growing demand for higher data rates in next-generation wireless networks and its adaptability, GSM appears to be a feasible alternative to the SM and V-BLAST systems, each with advantages and limitations. As a result, GSM techniques have received much attention in recent years and have been demonstrated to outperform V-BLAST in terms of throughput and/or error performance [8].

Chapter 3

Intelligent Caching in UAV-Aided Networks

3.1 Introduction

In this chapter, we propose to use UAVs as flying BSs to increase the probability of having LoS communication links. Moreover, we also investigate the content popularity distribution based on the latent Dirichlet allocation (LDA) learning process, in order to make an effective use of limited storage among BSs. The unique advantage of LDA is that it can be easily used to train a model directly for the property of a completely probabilistic generative model. Besides, due to the fixed size of parameter space in LDA, there is no need to consider the size of the contents. Additionally, LDA largely reduces the size of document feature vectors, which is originally the dimension of the number of vocabularies. Furthermore, a content sharing method among BSs has been considered to provide more chances of content availability. Finally, since the sharing cost (latency) is affected by channel conditions and transmission distances, we propose a method to reduce both request delay and transmission delay to minimize the total delay.

The rest of this chapter is organized as follows. In Section 3.2, we present the system model of our caching-enabled UAV system, while in Section 3.3 we propose three user association methods for the UAV BSs. Afterwards, we analyse our system performance in Section 3.4 followed by our conclusions in Section 3.5.

3.2 System Model

The downlink of cache-enabled network serving a set of mobile GUs via several UAVs acting as flying BSs is shown in Fig. 3.1. As depicted in Figure 3.1, UAVs equipped

with caching storage are connected to terrestrial MBSs, which have more storage and computing resources than the UAVs. Meanwhile, these MBSs are connected to the cloud servers via fibre backhaul links as shown in Figure 3.1. The transmission from MBSs to UAVs is via wireless fronthaul links over licensed cellular band. Additionally, in our model, we consider UAVs as flying BSs, which are used to cache GUs' content in order to reduce duplicate transmissions from BSs to the GUs. This can help to alleviate the mobile traffic and reduce the content delivery latency [259].

However, in order to make a full use of the limited available storage at the UAVs, LDA has been employed to estimate the content popularity distribution based on GUs' browsing history. The LDA has a fixed parameter space, which is suitable for large scale text sets and is easy to use. Moreover, LDA reduces the dimension of document feature vectors [260]. Here, caching is used to store the most popular contents that may be requested by the mobile GUs. By caching predicted contents, the transmission from MBSs to UAVs can be significantly reduced, as UAVs can directly send contents to GUs. Without loss of generality, we assume that each GU requests one content in a single time slot for simplicity, and the LDA training process would be accomplished by the cloud during off-peak period. Finally, unavailable content requests would be sent back to MBSs to support the A2G communication between GUs and UAVs when the requested contents are not cached in the UAVs. In our system, we consider three UAV-user association methods based on the received-SNR, user-preference and minimum-delay. The received-SNR is closely linked with transmission delay while the user-preference influences the caching efficiency, which ultimately affects the request delay. Hence, we develop an effective approach to consider both to achieve the minimum-delay. Furthermore, two databases with different popularity distributions have been investigated to analyse how it can affect the system performance. The following section will introduce the principle of LDA model.

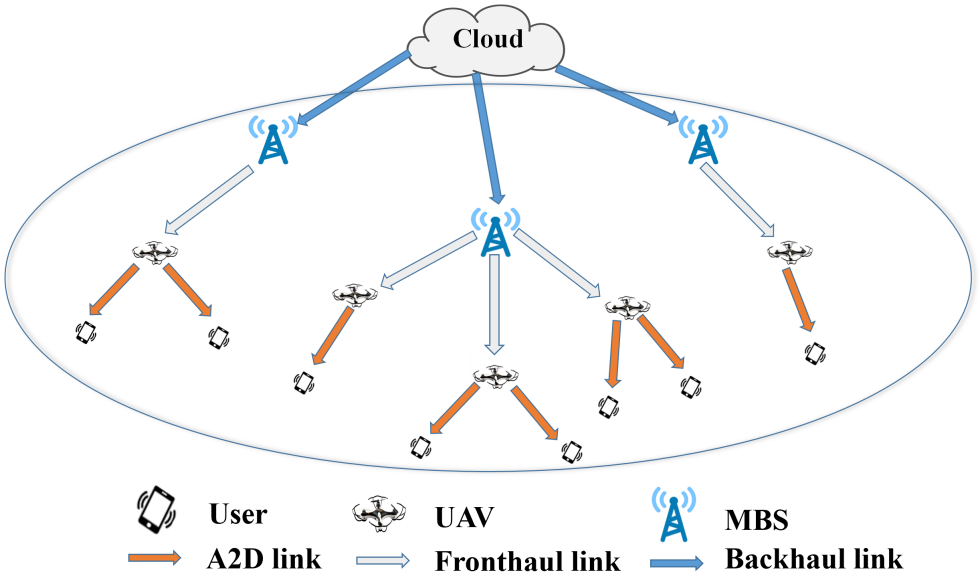

Figure 3.1: Structure of caching-enabled UAV system [9].

3.2.1 Latent Dirichlet Allocation Model

We propose a proactive caching scheme, which utilizes LDA [180, 186, 261] algorithm in accordance with the user preferences for optimizing the caching performance and guaranteeing the QoE. Given the advancement in machine learning and big data analysis, it is beneficial to cache popular contents before the GU requests are generated, since this will help save the time to request contents from far away MBSs. The MBSs are capable of collecting GU data by UAVs and sending them back to the cloud server to perform the training process. Based on this collected information and the training results, UAVs can cache contents accordingly.

Assume that the collected data by the flying BSs during GU communications is represented by Q documents, as shown in Figure 3.2 and the m^{th} document is constructed from a collection of N_q words. Furthermore, T essential topics[1] are assumed in all documents with different probabilities. Please note here that we are concerned with the number of topics and not what the topics are. Therefore, all the subsequent procedures are based on T. Note that m, N_q and T are some of the important parameters. Furthermore, each document (out of the Q available documents) has a Document-Topic distribution[2] based on T topics, while each topic has a Topic-Word distribution. Therefore, with the help of Document-Topic distribution and Topic-Word distribution, we can evaluate the Document-Word distribution, which is also known as the GU's preference.

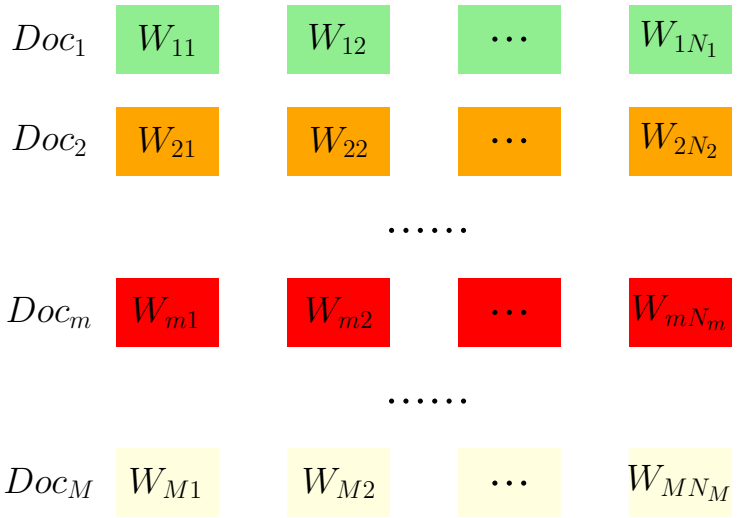

Figure 3.2: Latent Dirichlet Allocation model.

The generative process [182] of LDA will not generate the actual documents, it is the model that explains how a document could be generated by LDA's method. With the

[1] A topic, e.g. football, weather, economy, etc, is considered here as the GU's preference.
[2] Please note that in the following we will refer to probability distribution as distribution.

help of Gibbs samplings [262, 263], LDA is able to evaluate the document-topic distribution and topic-word distribution from the training data. Let us here illustrate the idea using an example, where the generative process mimics the process of generating a file, which is a procedure we utilized to analyse the proportion of each component accounted in those documents. Assuming that some of the latent topics have not been observed in the considered documents and each document has a distribution over these topics. After LDA training in this example, the results show that one document has the following distribution: 50% politics, 40% economy, 8% weather and 2% technology. Besides, for each topic, it has a distribution over the words in the vocabulary, and the vocabulary is composed of words occurring in the documents. For instance, in the weather topic, the word 'temperature' has a higher probability than that of 'money'. Now, considering the same topic distribution mentioned above, we firstly choose a topic according to the distribution, which could be politics. Then, we choose a word following the words distribution corresponding to the politics topic. This becomes the first word of the document and this step is repeated for all the words of the document. Finally, we are able to obtain the distribution of all words (contents) in this document, which means the interests of each GU have been extracted because each document represents a data collected from one GU. According to the distribution of these contents, the most popular contents will be cached in the UAVs. In the following section, we first explain the mobility modelling of the GUs and then we illustrate how we can apply caching on UAVs according to the training results of the LDA process.

3.2.2 Mobility Model

In our proposed system, we assume that all GUs are moving continuously in an area with maximum velocity of $V_{\max}$. Initially, we give each GU a direction and a speed randomly. However, if GUs hit the border, they will change the direction by 180° to keep themselves in this target area. Four UAVs are moving according to the movement of GUs with k-means clustering [264, 265] at a height of h_d [266], which clusters the GUs into four groups and deploys UAVs at the centroids of each group based on the coordinates of GUs in this group. For instance, consider four GUs are in a group and their coordinates on the ground are $\{(1,1),(2,3),(5,2),(4,6)\}$, then the k-means clustering technique will deploy the UAVs at the point $(3,3)$ with a hight of h_d. Also note that, GUs[3] are also randomly distributed in this area. An example of user association by maximum-received-SNR method is illustrated by Figure 3.3.

Here, please note that each group is allocated geographically around one UAV to initialize the system at the very beginning. After that, the GUs would be allocated to their corresponding UAV based on a specific criterion, which will be described in section 3.3. Additionally, the movement of GUs will then be used to determine the contents

[3]The proposed scheme will work for any number of GUs and they do not have to be equal.

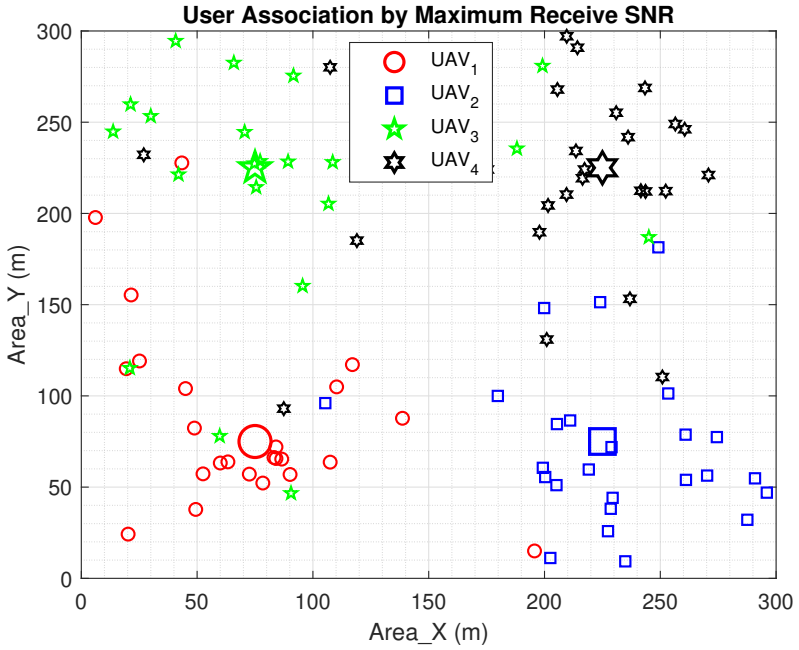

Figure 3.3: An example of user association by maximum-received-SNR, where smaller markers represent GUs and bigger markers represent the UAVs.

that should be cached by the UAVs. More specifically, the movement of GUs could lead to the change of user-UAV association and further cause the change of distributions in each group of associated GUs. However, GU movement does not affect the user-preference method.

We give an example to illustrate how the movement of GUs affect the variation of contents. Assume that two GUs are connected to one of the UAVs, and a total of 4 contents are considered, $C = \{c_1, c_2, c_3, c_4\}$. Furthermore, the popularities of each content are assumed to be different for each GU, which could be represented by $P_1 = \{0.1, 0.25, 0.4, 0.25\}$ and $P_2 = \{0.4, 0.15, 0.4, 0.05\}$ respectively, with the order from 1 to 4. Therefore, the average probability of each content is $P_a = \{0.25, 0.2, 0.4, 0.15\}$ and the contents that should be cached are c_1 and c_3. However, if a new GU moves into this group and the corresponding popularity distribution is $P_3 = \{0.1, 0.5, 0.1, 0.3\}$, then the P_a would change to $\{0.2, 0.3, 0.3, 0.2\}$ and the contents to be cached would be c_2 and c_3. In this model, a total of T topics and N_c words (contents) are considered. Moreover, since the distance between UAVs is much smaller than that from UAVs to BS (We assume that all the UAVs get information from the same BS[4]), a constant request delay D_r per request is assumed [267]. The detailed simulation parameters are listed in Table 3.1.

[4]This does not have to be the case, we did this to simplify the system simulations.

Table 3.1: Simulation parameters

Parameter	Symbol	Value	Parameter	Symbol	Value
Number of GUs	N_u	100	Noise power	σ^2	-95 dBm
Number of UAVs	N_d	4	Carrier frequency	f_c	38 GHz
Number of topics	T	4	Request delay from UAVs to BSs	D_r	8 ms
Number of contents	N_c	100	Bandwidth	B	20 MHz
Transmission power	P_t	$\leq$ 30 dBm	Memory Size	n_m	512000 bits
Area length	L	300 m	Content size	n_c	51200 bits
Path loss exponent	α	2	Speed of light	c	3×10^8 m/s
UAV height	h_d	100 m	Maximum velocity of each GU	$V_{\max}$	2 m/s

3.2.3 Caching Model

For the procedure of caching, all the contents (words) are cached based on their corresponding probabilities. For instance, we assume that there are 4 words in the vocabulary with their probabilities given by $P = \{p_1 = 0.1, p_2 = 0.45, p_3 = 0.05, p_4 = 0.4\}$. Hence, the caching order is $I = \{p_2, p_4, p_1, p_3\}$ which is sorted from high to low based on their probabilities. Based on the memory size, the contents are cached in sequence. Finally, to measure the performance of LDA algorithm, the caching efficiency of each UAV η_d is defined as a function of the GU requests that have been cached in the UAV:

$$\eta_d = \sum_{i=1}^{N_d} P_d(C_d^i) = \sum_{i=1}^{N_d} \frac{\sum_{u=1}^{U_d} P_u(C_d^i)}{U_d}, \tag{3.1}$$

where d is the index of the UAV and u is the index of the GU served by this UAV, N_d is the number of contents that is cached in UAV d, while U_d is the number of GUs allocated to UAV d. Furthermore, $P_d(x)$ and $P_u(x)$ represent the PDFs of the UAV-Content and the User-Content, respectively. Additionally, C_d^i is the i^{th} content cached in UAV d.

Here, we give an example to illustrate the process of calculating caching efficiency for one UAV. Assuming that the memory size of the UAV is 2 units. Hence, only 2 out of 4 words $C_d = \{c_1, c_2\}$ can be cached in the UAV. Besides, 3 GUs are allocated to this UAV and the probabilities of these 2 words for the 3 GUs are indicated by $P_1 = \{0.1, 0.3\}$, $P_2 = \{0.25, 0.05\}$ and $P_3 = \{0.4, 0.3\}$. Then the average probabilities of these 2 words in the UAV is $P_d = \{0.25, 0.22\}$, and the caching efficiency is 47%.

3.2.4 Channel Model

In our system, we use the Rician fading channel model [45, 268], which has a dominant LoS path combined with some NLoS paths. Here, the effect of shadowing is not considered in our system. A Rician channel is described by two parameters: K and Ω, where

$K = \frac{\mu^2}{2\gamma^2}$ is the power ratio of the LoS path and the NLoS paths, while $\Omega = \mu^2 + 2\gamma^2$ is the total power from both LoS and NLoS paths. The probability density function of the Rican fading channel is given by:

$$f(x) = \frac{x}{\gamma^2} \exp\left(-\frac{x^2+\mu^2}{2\gamma^2}\right) I_0\left(\frac{x\mu}{\gamma^2}\right), \tag{3.2}$$

where I_0 is the 0th order modified Bessel function of the first kind. Therefore, the normalized complex-valued Rician channel h can be expressed by [269]:

$$h = \sqrt{\frac{K}{1+K}} \cdot h_{\text{LoS}} + \sqrt{\frac{1}{1+K}} \cdot h_{\text{NLoS}}, \tag{3.3}$$

where h_{LoS} represents the deterministic LoS component, while h_{NLoS} denotes the stochastic NLoS component of the scattered multipath signal. On the other hand, path loss is also considered to describe the signal attenuation due to the signal propagation over large distances. Path loss model is developed by using the numerical methods and the empirical approximations of measured data collected in channel sounding experiments, which is closely related to the environment where the transmitter and receiver are located [270]. In general, the propagation path loss P_l is expressed by [271]:

$$P_l = \left(\frac{4\pi}{\lambda}\right)^2 d^{\alpha}. \tag{3.4}$$

where d is the distance between the transmitter and receiver, α is the path loss exponent which ranges from 2 to 6 and $\lambda = \frac{c}{f_c}$ is the free space wavelength defined as the ratio of the speed of light c in m/s to the carrier frequency f_c in Hz. Therefore, the received signal power P_r given a transmission power P_t is given by [272]

$$P_r = \frac{P_t}{P_l} = P_t \left(\frac{c}{4\pi f_c}\right)^2 \left(\frac{1}{d}\right)^{\alpha}. \tag{3.5}$$

In our system, the UAVs are assumed to operate in a environment at a height of 100 meters [273], where LoS communication links exist for most of the time. Hence, free space path loss exponent $\alpha = 2$ is considered to describe the path loss [44] and P_r is transformed to:

$$P_r = P_t \left(\frac{c}{4\pi d f_c}\right)^2. \tag{3.6}$$

One important criterion to determine the performance of a system is the achievable rate, where the capacity of the Discrete-Input Continuous-Output Memoryless Channel (DCMC) for two-dimensional M-ary complex signals is represented as [274]:

$$C_{DCMC} = \log_2(M) - \frac{1}{M} \sum_{m=1}^{M} E\left[\log_2 \sum_{i}^{M} \exp(\Lambda_i^m)\right], \tag{3.7}$$

where we have:

$$\Lambda_i^m = \frac{-|\sqrt{P_r}h\,(x_m - x_i) + n|^2 + |n|^2}{\sigma^2}, \tag{3.8}$$

where x_m is the M-ary symbol and n is the complex-valued Additive white Gaussian noise (AWGN) having a variance of σ^2.

After obtaining the channel capacity, the transmission time T_t^u needed to send a data content from the associated UAV to a GU u at time slot t can be evaluated as follows:

$$T_t^u = \frac{n_c}{C_t^u \times B} \tag{3.9}$$

where C_t^u is the DCMC capacity of GU u at time slot t and B is the bandwidth.

3.3 User Association Strategies

There are various association methods to assign GUs to the UAVs, when there are multiple GUs and multiple UAVs available. Here, we propose different association methods according to different aspects of system performance, e.g. transmission delay, request delay and caching efficiency. In this section, we propose three user association methods, which are referred to as the maximum-received-SNR, user-preference, and minimum-delay methods. Here, the received-SNR is related to the transmission delay while the user-preference method would affect whether UAVs have to request new contents from BSs or not, which is related to the user-preference method. Besides, we also assume that the distribution of GU interests will not change within a certain period of time. Once the user-UAV association is done, an appropriate modulation scheme could be invoked based on the estimated receive SNR of the transmission link.

3.3.1 User Association by the Maximum-Received-SNR Method

In this method, we consider the received-SNR as the criterion to associate GUs. Consider an example of 4 UAVs with 100 GUs as depicted in Figure 3.3. It can be seen that 4 UAVs are indicated by 4 different shapes and deployed at the center of 4 clusters. Meanwhile, GUs are allocated to one of those UAVs, which are represented by the same shape of the dedicated UAV but in a smaller size, according to the value of received-SNR.

As shown in Algorithm 3, the whole procedure starts with the LDA training, which is done at a BS, to analyse and extract GU preferences based on the browsing history. Here, the GU preferences or interests can be represented by $\boldsymbol{\Theta} = \{\boldsymbol{\vartheta_1}, \boldsymbol{\vartheta_2}, ..., \boldsymbol{\vartheta_u}\}$, where $u \leq N_u$. For each GU u, the interest is indicated by $\boldsymbol{\vartheta_u}$, which can be expressed by $\boldsymbol{\vartheta_u} = (\vartheta_{u1}, \vartheta_{u2}, ..., \vartheta_{uk})$, where $k \leq N_c$. Additionally, ϑ_{uk} is the probability of the k^{th}

Algorithm 3 Operating procedure of maximum-received-SNR method.

```
Training by Latent Dirichlet Allocation
Extract the interest (probability) of each GU
Initialize the number of outage N_o = 0
while t ≤ N_s do
    Deployment by k-means according to coordinates of GUs
    User association by selecting the UAV with the highest SNR
    Cache contents according to θ_u of associated GUs
    Generate real-time requests
    for n from 1 to N_u do
        Check UAV-availability A_u ∈ {0, 1}
        if A_u = 1 then
            d_a^u = d_max
            Select modulation scheme based on C_t^u
        else
            if C_t^u = 0 then
                N_o = N_o + 1
            else
                d_a^u = d_max
                Select modulation scheme based on C_t^u
                Request content from far-away BS
            end if
        end if
    end for
end while
```

content of GU u. Then, we apply the k-means clustering technique based on the coordinates (or A2G distance) of each GU. Given the fact that the path loss P_l, which is determined by distance when f_c is fixed, dominantly affects the received-SNR, the k-means will allocate those GUs with similar A2G distances to the same group and obtain the centroids of each group. Consequently, the UAVs will be dispatched to the cluster centroids for deployment. Afterwards, the GUs would be associated with the UAV, which can provide the best quality of service in terms of the highest received-SNR, as their server by calculating the received-SNR according to the current deployment accomplished by the k-means. Note that the received-SNR depends on both the path loss (or distance) as well as the channel fading. As shown in Figure 3.3, GUs are allocated to the UAV closest to them most of the time. However, some GUs may not be served by the UAV nearest to them due to channel fading, which can cause a degradation on the channel SNR. Furthermore, the UAVs can adaptively deploy themselves with this low-complexity technique by simply recalculating the centroids according to the new coordinates of GUs in each time slot t, where $t \leq N_s$ and N_s is the number of time slots.

Now, UAVs are able to cache the contents according to the interests Θ ("User-Content" distribution) of GUs that have been allocated to them. The next step is to check the UAV-availability A_u of each GU when a new request is generated. If $A_u = 1$, it means the corresponding UAV is linkable and the content has been cached. So, the capacity

C_t^u of each GU at current t^{th} time slot can be simply obtained from their corresponding received-SNR, which is indicated by SNR_u. However, two cases will lead to $A_u = 0$. First, if $C_t^u = 0$, which means the quality of the channel is too bad to establish a stable and reliable links between GU u and the corresponding UAV. Then, the GU u will be counted as outage. Second, when the content has not been cached, a request delay will occur, where the UAV will request this specific content from the BS and then forward to the GU. In this method, the associated UAV d_a^u of GU u will always be d_{max}, where d_{max} is the UAV that can provide the highest SNR.

Let us consider the following example to illustrate the procedure of this user association method. Assume that the memory size of each UAV is 3 units and we have a set of content $S = \{c_1, c_2, c_3, c_4, c_5, c_6, c_7, c_8, c_9, c_{10}, c_{11}, c_{12}\}$. Please note the amount of contents could be any value and the number in the set only represent the index of contents with no order. Based on the 'interests' of GUs in the first group, if the contents in the descending order is $\{c_1, c_{12}, c_5, c_7, c_6, c_4, c_3, c_2, c_9, c_{10}, c_8, c_{11}\}$, then the cached contents of the first UAV should be $D_1 = \{c_1, c_{12}, c_5\}$. In practice, each GU will generate a new request within one time unit, while the UAVs have to check the availability of those requests in the memory. If those requests were not cached in advance, the UAVs have to request for it from higher-level "servers" (BSs around them), which would incur a request delay.

3.3.2 User Association by the User-Preference Method

In this section, user-preference is considered as the criterion to associate users with UAVs. It is different from the purpose of utilizing k-means to accomplish UAV deployment in the scenario of maximum-received-SNR. Thus, users who have similar "interests" would be allocated to the same UAV. As shown in Algorithm 4, the LDA training would be accomplished at the very beginning in accordance with the searching history of all users. Then, based on the number of UAVs N_d, the k-means clustering is applied to divide all the users into N_d groups according to the extracted LDA training results Θ from all users. Therefore, according to the probabilities of contents $\boldsymbol{\theta_u}$ of each GU, those users who hold the most similar "interests" or "distributions" would be clustered into one group. Then, based on the coordinates of users in each clustered group, the UAVs will be deployed at the centroid of the corresponding group.

After each group has been allocated to its dedicated UAV, the corresponding UAV could cache contents based on the content distributions of those users assigned to it. Similarly, the UAV-availability of each GU is checked when a new request is generated at each time slot. If $A_u = 1$, GU u is able to communicate with d_c and get the content directly from the UAV. Otherwise, according to the cases that would cause $A_u = 0$, GU u will be considered as outage when $C_t^u = 0$. On the other hand, the GU can also request the content from a far-away BS if the content is unavailable from the associated UAV. It is

Algorithm 4 Operating procedure of user-preference method.

```
Training by Latent Dirichlet Allocation
Extract the interest (probability) of each GU
Initialize the number of outage N_o = 0
while t ≤ N_s do
    GU clustering by k-means according to θ_u
    Deploy UAVs at centroids of corresponding clusters
    User association by connecting to corresponding UAVs
    Cache contents according to θ_u of associated users
    Generate real-time requests
    for n from 1 to N_u do
        Check UAV-availability A_u ∈ {0, 1}
        if A_u = 1 then
            d_a^u = d_c
            Select modulation scheme based on C_t^u
        else
            if C_t^u = 0 then
                N_o = N_o + 1
            else
                d_a^u = d_c
                Select modulation scheme based on C_t^u
                Request content from far-away BS
            end if
        end if
    end for
end while
```

worth noting that the function of the k-means clustering technique used here is different from that in the other two association methods. In this case, it is only employed for the sake of user-UAV association. As aforementioned, users will firstly be divided into different clusters according to their interests by k-means algorithm and then the UAVs will be dispatched to the centroids of each cluster according to the coordinates of users in each cluster to do user association. It is different from the case that utilises the k-means for clustering and UAV-deployment, as done in the other two user association methods.

Furthermore, consider an example where the memory size of each UAV is 3 units and we have a set of content $S = \{c_1, c_2, c_3, c_4, c_5, c_6, c_7, c_8, c_9, c_{10}, c_{11}, c_{12}\}$. Also, the amount of contents could be any value and the number in the set only represent the index of contents with no order. Based on the 'interests' of users in the first group, if the contents in the descending order is $\{c_7, c_6, c_4, c_1, c_{12}, c_5, c_3, c_2, c_9, c_{10}, c_8, c_{11}\}$, then the cached contents of the first UAV should be $D_1 = \{c_7, c_6, c_4\}$. Finally, If the real-time GU request was not cached in the storage, the UAV has to send a request to the BS to ask for the new content. In reality, it is possible that a certain UAV will serve a large percentage of users if a large group of users are interested in the same thing, which could quickly lead to a performance bottleneck of that specific UAV. For example, if there is only one

group according to the LDA analysis, then the users in this area would have similar interests. In this case, the GU interest factor is a "constant" and we do not need to consider it as a variable. Hence, the communication link quality becomes the key influence and the maximum-received-SNR or minimum-delay method could be applied. Furthermore, the bottleneck issue could be solved by increasing the number of UAVs in this situation.

3.3.3 User Association by the Minimum-Delay Method

In order to provide the best quality of experience, both the transmission delay and the request delay should be considered to minimize the total delay. Algorithm 5 shows the operation procedure of the minimum-delay user association. In this method, k-means is implemented to cluster users into groups based on the coordinates or A2G distances and then find the centroid of each group. Afterwards, all the UAVs will be dispatched to the centroids of these groups and then the same user association method employed in maximum SNR scenario would be adopted to initialize the user-UAV association between users and UAVs, which is only used as a "sketch" or a starting point for the following optimization process. This does not mean users and UAVs are truly associated.

The caching method of UAVs is not in a "local" mode that has been applied in the former two cases due to the limited storage resources on UAVs. In this situation, all the UAVs are considered as a whole and the data synchronization of UAVs will be done periodically. During this process, extra signalling between the UAVs is needed in order to facilitate an information exchange (cached contents and channel condition) and for establishing a proper control of this system as illustrated by Algorithm 3. This signalling information will be transmitted via a control channel and hence it will not affect the transmission from UAVs to users but would consume a small amount of energy.

In this method, we cache the top $\frac{N_d \times n_m}{n_c}$ contents, which have the highest probability to occur instead of caching individually by only considering the top $\frac{n_m}{n_c}$ contents in each subgroup of a UAV. For example, the available memory size for each UAV is 3 units, and so, we have the set of content $S = \{c_{12}, c_{11}, c_{10}, c_9, c_8, c_7, c_6, c_5, c_4, c_3, c_2, c_1\}$, which is ordered by the probability in the descending order, where the index 12 has the highest probability while the index 1 has the lowest probability. Hence, the cached content in each UAV would be $D_1 = \{c_{12}, c_8, c_4\}$, $D_2 = \{c_{11}, c_7, c_3\}$, $D_3 = \{c_{10}, c_6, c_2\}$ and $D_4 = \{c_9, c_5, c_1\}$. It is worth noting that C describes all the contents to be cached, as opposed to the previous two cases where each UAV independently cache the top three contents. In this case, the 4 UAVs are caching in a global way. Then, in order to achieve a minimum total delay scheme, iterations to exchange users among different groups will be applied. According to Algorithm 5, the number of iterations N_i has to be set at the beginning of the process and the value of N_i should be selected to guarantee

Algorithm 5 Operating procedure of minimum-delay method.

Training by Latent Dirichlet Allocation
Extract the interest (probability) of each GU
Initialize the number of outage $N_o = 0$
while $t \leq N_s$ **do**
  Deployment by k-means according to coordinates of users
  Initialise user association by maximum-received-SNR method
  Do caching according to interests of associated users
  for n from 1 to N_i **do**
    Exchange users among different groups
    if $T^c_{sum} > T^e_{sum}$ **then**
      Keep the exchange and move to next GU
    else
      Move to next GU
    end if
  end for
  Generate real-time requests
  for u from 1 to N_u **do**
    Check link-availability $A_l \in \{0, 1\}$
    if $A_l = 1$ **then**
      Check content-availability $A_c \in \{0, 1\}$
      if $A_c = 1$ **then**
        Select modulation scheme based on $C_t^{n_l}$
        Calculate total delay $T^{n_l}_{sum}$ of linkable UAVs
        $d^u_a = \underset{n_l}{\text{argmin}}\ T^{n_l}_{sum}$
      else
        $d^u_a = d_{max}$
        Select modulation scheme based on $C_t^{n_l}$
        Request content from far-away BS
      end if
    else
      $N_o = N_o + 1$
    end if
  end for
end while

the convergence, but it should not be too big as this may increase the complexity of the system. During an iteration, each exchange may lead to a change of the contents in UAVs as mentioned before. Therefore, it affects the theoretical request delay of each GU, $T_r(u)$, which can be calculated as:

$$T_r(u) = \left(1 - \sum_{i=1}^{N_c} P_u(C^i_{d_a})\right) \times D_r. \tag{3.10}$$

Hence, the theoretical request delay of GU u is determined by the probability of contents not cached in the associated UAV d^u_a. Also, the change will directly affect the

transmission delay $T_t(u)$ due to the variation in distance and channel condition between the users and the different UAVs. Finally, the average total delay of the current situation T^c_{sum} and the delay after-exchange T^e_{sum} could be obtained by simply dividing the sum of the two delay values by N_u. Hence, if $T^c_{sum} > T^e_{sum}$, this GU exchange will be kept, otherwise, it will be discarded. Since the number of users are fixed, the value of total delay will continuously go down and converge to a certain level.

After this optimization in Algorithm 5, data communication commences. This iteration is based on the number of users in the area. GU u will firstly check the link-availability A_l, when a new request is generated and it will be set to "1", when at least one of the UAVs can establish communication links, otherwise, it will be "0". Secondly, the content-availability A_c will be checked among those N_l linkable UAVs. If the requested content has been cached in the memory ($A_c = 1$), then we calculate the total delay $T^{n_l}_{sum}$ of all linkable UAVs by choosing appropriate modulation scheme based on the channel capacity of the linkable UAVs, which is denoted by $C^{n_l}_t$, where $n_l = 1, 2, \ldots, N_l$. Afterwards, the UAV with the smallest total delay will be selected as the associated UAV d^u_a. However, if the requested content has not been cached in these N_l UAVs, the UAV d_{max} which is able to provide maximum received-SNR will be selected as the associated UAV. Finally, if $A_l = 0$, it means that the channel condition of all UAVs is not good enough to establish a reliable communication link ($C^u_t = 0$) and this GU u will be counted as outage. Using Algorithm 5, we can achieve a balance between the request delay and the transmission delay to obtain the smallest total delay.

According to the user-UAV association introduced above, it can be found that complexity is closely related to the number of UAVs N_d. From the GU perspective, UAVs will firstly check if this GU is able to establish communication with them, which means totally N_d examinations are required. Then, assume that the GU is able to associate with N_l linkable UAVs, those N_l linkable UAVs have to check the content-availability of its memory based on the requests sent by this GU. Hence, N_l times are required to finish this task. Furthermore, the truly associated UAV will be determined by the comparison of the total delay and therefore $N_l - 1$ times of comparison is required. Finally, the complexity of the proposed user-UAV association is given by:

$$\mathcal{O}\left(N_d + 2N_l - 1\right). \tag{3.11}$$

It can be found that the complexity is almost linearly related to the number of UAVs N_d, which provides us with a relatively low-complexity user-UAV association.

3.4 Performance Results and Evaluation

In this section, we investigate the performance of the proposed schemes in terms of caching efficiency and time delay in a environment that users are moving in a target

area. In order to further investigate how the learning results of LDA training affect the system performance, two databases have been studied. As shown in Figure 3.4, the two databases have quite different distributions. In database 1, some contents have a higher probability compared to others. In this situation, we can say that users are interested in a few specific contents, which could be exploited by the LDA algorithm. However, database 2 has a rather uniform distribution, where all contents have similar probabilities of occurrence. In other words, users do not exhibit any specific interests and hence it would be harder for the LDA to decide which contents to cache from database 2. Moreover, the movement of ground users could lead to the change of user-UAV association and further cause the change of distribution in each group of associated users. In the simulation, the user-preference of each GU will not change but the mobility of GU will cause the change of P_a and the cached content. Besides, the new request is generated by sampling from the GU interests, hence the GU requests are different at each time slot.

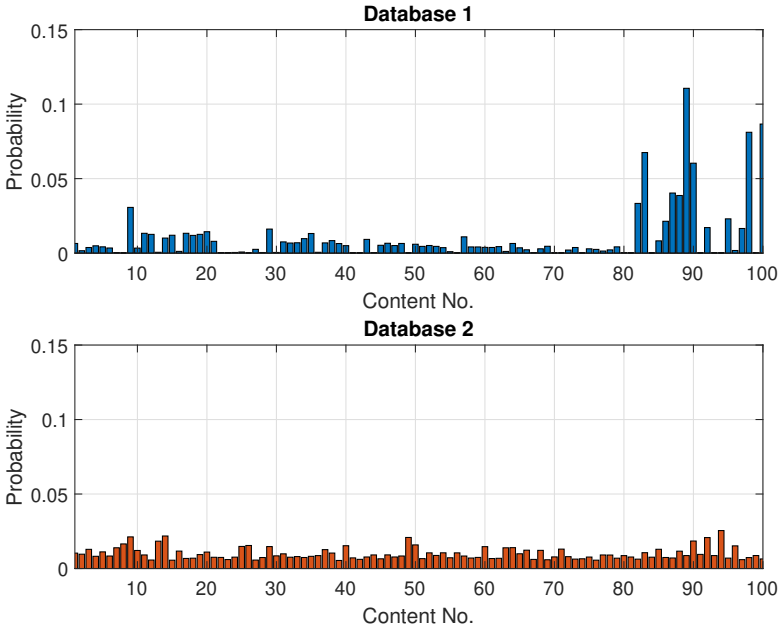

Figure 3.4: The content distributions of the two databases.

In our system, we consider random caching as a benchmark to see how training affects the performance of the caching efficiency. For UAV-user association, the signal strength or received-SNR is a key criterion to associate a GU with a BS in today's communication system, hence, we consider it as the benchmark of transmission delay, as it has the smallest transmission delay. Besides, the system is a cache-enabled system, therefore, the request delay which is affected by the user-preference, would be the second benchmark to measure the performance of request delay, as the user-preference has the smallest request delay. Afterwards, we compare our proposed minimum-delay scheme with them to illustrate the advantages of global caching and global UAV-user association.

The following sections will illustrate how different databases affect the performance, where the notations MD, MS, UP and RC denote minimum-delay, maximum-received-SNR, user-preference and random caching[5], respectively, while d_1 and d_2 represent database 1 and database 2. Note that notations with RC indicate that the relevant schemes employed random caching, while those without RC represent the relevant schemes invoking LDA training for caching.

3.4.1 Channel Capacity

In order to obtain the duration it take to send a content from UAV to GU, we have to know the quality of the channel between UAV and GU as the quality of channel affects the rate of transmission, which is demonstrated by capacity. Figure 3.5 shows the capacity for various modulation schemes when communicating over Rician channel, where it can be seen that the channel capacity increases as SNR increases. However, restricted by modulation schemes, the modulation-dependent DCMC capacity curve would converge to $\log_2(M)$ when the SNR reaches a certain level. Hence, in our proposed system we choose a higher-order modulation type to increase the capacity when the channel quality improves. The Shannon capacity represented by the dashed line is the upper bound, which is independent of the modulation. Our aim is to design a system to approach this upper limit. Therefore, coded modulation is applied to accomplish this task.

As shown in Figure 3.5, the SNRs needed to support the transmission of 3 bits/symbol are 11 dB and 25 dB for 16-QAM and 8-QAM, respectively, where the DCMC capacity curve of the 16-QAM is much closer to the Shannon capacity compared to that of 8-QAM. This means that a scheme using a channel coding having a rate of $\frac{3}{4}$ (1 additionally parity bit for each group of 3 information bits) in conjunction with 16-QAM can perform closer to the Shannon capacity limit, compared to the uncoded 8-QAM scheme. On the other hand, a near Shannon capacity scheme can also be created by using a low rate channel coding in conjunction with higher order modulation schemes, however, it is not advisable because higher order modulation has a higher complexity, which means a higher chance to get errors. The general rule of thumb to transmit k bits using M-QAM is to have $M = 2^{k+1}$. Thus, the transmission of $k = 3$ bits using 16-QAM can be achieved at SNR = 11 dB, using a perfect channel code having a rate of $\frac{k}{k+1} = \frac{3}{4}$.

Based on the aforementioned theory, the transmission delay can be obtained according to the size of contents and the channel conditions. The channel capacity has direct impact on the transmission delay. More explicitly, the SNR increases with the increase of the transmission power, which can support a higher capacity transmission using a

[5]Random caching means we randomly choose the contents to cache without considering the occurrence probabilities of each content.

higher-order modulation. A higher capacity would permit a higher transmission rate, which could reduce the transmission time for the same amount of data.

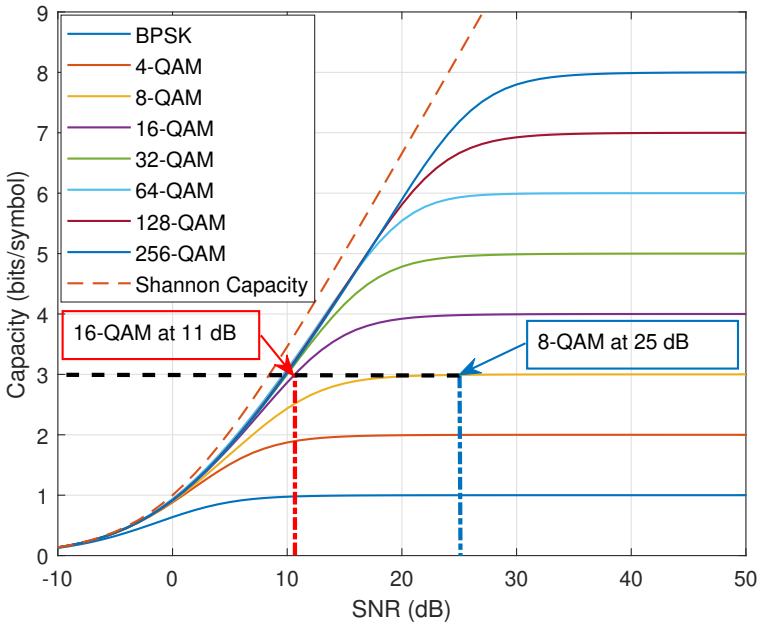

Figure 3.5: The DCMC capacity for various M-QAM schemes when communicating over Rician channel with $K = 3$.

3.4.2 Caching Efficiency

Figure 3.6 shows the average caching efficiency of these UAVs, where it could be found that the caching efficiency of user-preference scenario is higher than that of maximum-received-SNR and minimum-delay scenarios. In the user-preference scenario, those GUs who have similar interests are grouped together to be served by the same UAV and hence, the hit rate of the requested contents would be higher than that of maximum-received-SNR and minimum-delay scenarios. It is worth noting that the caching method in minimum-delay scenario is global, which means the hit rate in each subgroup served by a particular UAV would be lower than that in the other two cases. Additionally, the caching efficiency of random caching in the three scenarios is similar, since in this case all the contents have equal probability and we randomly choose the content for caching. The random caching technique has a low caching efficiency but the system complexity is low, because there is no training required. Here, we assume that GUs' preferences will not change during the simulation period; hence, the caching efficiency of these three scenarios is stable. Moreover, the quality of training will also affect the caching efficiency. More specifically, when the GUs' interests could be distinctively classified, as in database 1, the caching efficiency would be much higher than that of database 2, due to a better training. Finally, LDA training helps us to significantly improve caching

efficiency and enhances the quality of experience compared to the random caching scenario that has no training. As seen in Figure 3.6, the performance of the RC based schemes is independent of the database used. Hence, we will denote RC based schemes without the d_1 or d_2 notation for the rest of our analysis.

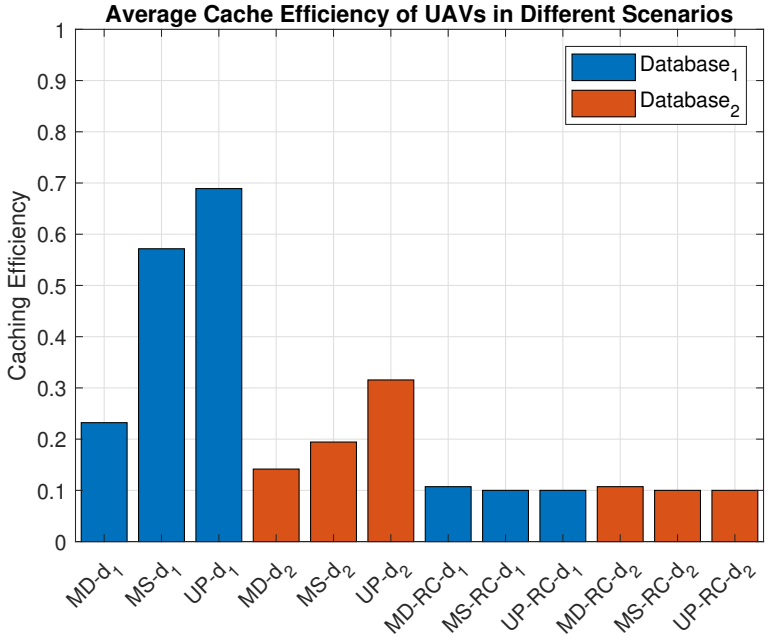

Figure 3.6: Average caching efficiency of UAVs,where the notations MD, MS, UP and RC denote minimum-delay, maximum-SNR, user-preference and random caching, respectively, while d_1 and d_2 represent database 1 and database 2.

3.4.3 Request Delay

Figure 3.7 shows the request delays of the three scenarios as a function of the change of transmission power. From the figure, it could be found that the request delay of maximum-received-SNR and user-preference is stable, which is independent of transmission power. Under the premise of high transmission power, it can be seen that the maximum-received-SNR scheme has the highest request delay because it considers the received-SNR as the primary point but neglects the user-preference. Hence, it needs to request new content more frequently from the BSs than that of the other two scenarios. On the contrary, user-preference scenario achieves a lower request delay as it puts user-preference as the key element, which reduces the number of times of requesting new content from the base station. Note that the request delay for UP and SNR based schemes is independent of the transmission power because both of them are in the local mode and cannot connect to other UAVs.

Additionally, request delay considers the transmission and processing time from a BS to a UAV, which is independent of the transmission power. Therefore, the interest of the GUs (the distributions of the content) is the main factor that affects the request delay. When this interest does not change, the request delay would stay the same. However, since the minimum-delay scenario caches contents in a global way, it is less frequent that the UAVs would ask for new requests from the BSs and hence, it provides the smallest request delay when the transmission power is sufficiently high. However, when a low transmission power is considered, it is hard for GUs to connect to the other UAVs even if the content is available at these other UAVs that could be far away. To elaborate further, as discussed in the previous section, the caching efficiency in the minimum-delay methods is the lowest among the three user association methods. So, the request delay is much higher than that of the other two methods. This is because the system only caches the most popular contents once and it is possible that the contents needed by those users are not cached in their accessible UAVs. Hence, there is a reduced chance to meet their demands.

Indeed, it is good to cache the same content at different UAVs if it is very popular and has extremely high probability, which clarifies the observation that the caching efficiency of MS and UP methods is significantly higher than that of the minimum-delay method. However, the contents needed to be cached are larger than the size of a practical UAV memory. Hence, the minimum-delay method sacrifices some transmission delay and caching efficiency in order to attain significant gains in the request delay as shown in Figure 3.7.

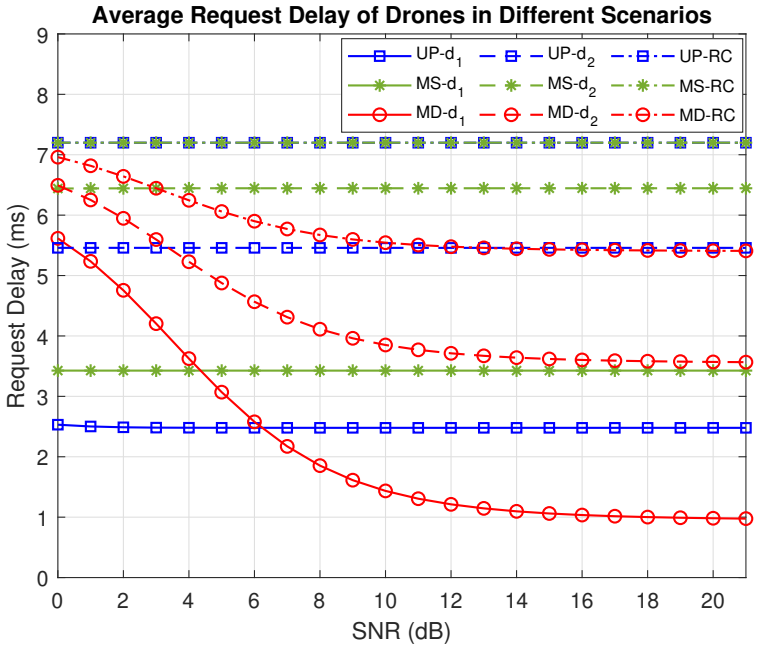

Figure 3.7: Average request delay of UAVs, where the notations MD, MS, UP and RC denote minimum-delay, maximum-SNR, user-preference and random caching, respectively, while d_1 and d_2 represent database 1 and database 2.

3.4.4 Transmission Delay

The transmission delay is the time delay for the transmission of one content from UAVs to GUs. As shown in Figure 3.8, it could be found that the transmission delay will decrease when increasing the transmission power. In our system, we assume perfect channel coding schemes having a code rate of $\frac{k}{k+1}$ to transmit k bits using $M = 2^{k+1}$-QAM to achieve the DCMC capacity as shown in Figure 3.5. The modulation order M would become higher as the transmission power increases, which increases the throughout or transmission rate and reduces the transmission delay. Besides, the caching methods will not affect the transmission delay in the maximum-received-SNR and user-preference scenarios. The transmission delay is the primary consideration in the maximum-received-SNR scenario but not in the user-preference scenario; therefore, the curves of these two scenarios become the lower bound and the upper bound, respectively. Note that the transmission delay is only counted when the content is available. Hence, when the training is good (as in database 1), a lot of GU requests can be fulfilled by the minimum-delay method that consider cooperation among UAVs. However, this translates to a high transmission delay as it becomes even higher than that of user-preference method with the increase of transmission power. By contrast, when the training is poorer (as in database 2 or in the RC scenario), less GU requests can be fulfilled in the minimum-delay method and hence less transmissions are needed, which resulted in a lower transmission delay.

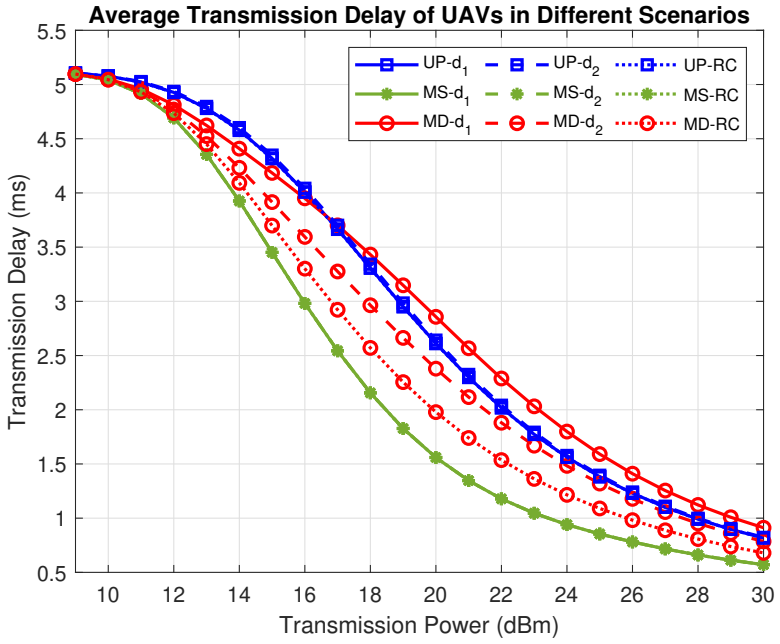

Figure 3.8: Average transmission delay of UAVs, where the notations MD, MS, UP and RC denote minimum-delay, maximum-SNR, user-preference and random caching, respectively, while d_1 and d_2 represent database 1 and database 2.

3.4.5 Total Delay

In Figure 3.9, the total delay is determined by both the request and the transmission delay. When the transmission power is high, transmission delay is low due to improved channel quality. Hence, the request delay becomes more important than the transmission delay when the channel SNR is high. From the curves, we can see that the total delay is closely linked to the training results, where efficient training results can greatly reduce the overall delay, due to a reduced request delay. As expected, the minimum-delay method always provides the best performance in terms of delay except for the low transmission power condition because it requires a reasonably good channel condition to support the shift among different UAVs.

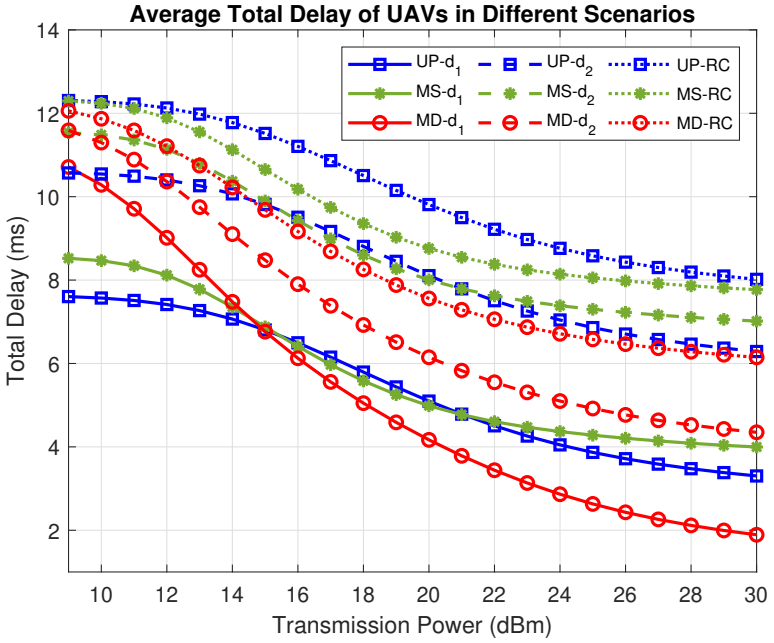

Figure 3.9: Average total delay of UAVs, where the notations MD, MS, UP and RC denote minimum-delay, maximum-SNR, user-preference and random caching, respectively, while d_1 and d_2 represent database 1 and database 2.

3.5 Conclusion

In this chapter, we proposed a UAV-aided intelligent strategy for mobile edge caching in the wireless communication system, which aims to minimize the system delay and hence improve the QoE. The system delay is composed of the transmission delay and the request delay. The transmission delay is determined by GU's receive SNR, while the request delay is related to the cached contents in the UAVs' storage. Three user association methods have been investigated based on the receive SNR, user-preference and

minimum-delay. The results have shown that increasing the received-SNR (transmission power) will largely reduce the transmission delay, while the request delay can be improved by considering user-preference as the main aspect. However, it was found that both methods can only solve part of the issue. Hence, both SNR and user association have been considered to obtain the minimum-delay method. Our simulation results have demonstrated that the proposed method can improve the system's performance in terms of delay.

Chapter 4

Deep Q-learning for UAV Deployment in Dynamic Environments

4.1 Introduction

In Chapter 3, we have designed a caching-enabled UAV communication system by considering UAVs as aerial BSs to reduce the latency of data transmission. Besides, three user association schemes have been analysed for achieving the lowest latency. Moreover, the *k*-means clustering algorithm based deployment algorithm has been employed to adapt to the movement of GUs by utilizing the maneuverability and flexibility of UAVs. However, the realistic deployment issues such as the limited speed of UAVs has not been detailed. It requires impractical fast movement of the UAVs, because a small change on the distribution of GUs can cause a large shift of centroid locations, which makes the UAVs hard to arrive at the new location within practical time. In this context, we aim to solve the frequent position-shift and the impractical fast movement in the deployment of multiple UAVs.

In this chapter, we explore the application of deep reinforcement learning in the deployment of multiple UAVs with multiple targets serving a number of GUs, when operating in a target geographical area with a limited number of UAVs. Besides, the UAV-user association can also affect the network's performance after the deployment of UAVs. Traditionally, the received power based user association rule is the most prevalent one, where a user chooses to associate with the specific BS, which provides the maximum received signal strength [275, 276]. However, given the restrictions of UAV assisted communications systems in terms of limited bandwidth resources and their relatively low transmission power, some of the GUs in a target area might be associated with UAVs

that are far from them. We refer to this as "outliers", whose quality of the communications link is significantly degraded. Thus, in order to solve the issue of "outliers" and to allow the UAVs to work within their capabilities, a new UAV-user association algorithm should be designed. Furthermore, the collision of UAVs has to be taken into consideration to make sure that UAVs are sufficiently far apart to keep the good quality communication links. Besides, the movement of GUs requires UAVs to adaptively adjust the position of deployment to provide stable and reliable services. Finally, the frequent position-shift of UAVs is also a challenge for the adaptive deployment in practice due to the relatively large area and the limited speed of UAVs.

The rest of this chapter is organized as follows. In Section 4.2, we first present the system model, which contains the mobility model of GUs and UAVs, then we present the proposed UAV-user association algorithms. In Section 4.3, we firstly introduce the UAV deployment by k-means clustering techniques and then we propose a DQL based deployment technique. Afterwards, we analyse our simulation results in Section 4.4 followed by our conclusions in Section 4.5.

4.2 System Model

We consider a UAV-assisted downlink communication network in a target square area with a side length of L, where a limited number of UAVs are deployed to operate as aerial BSs to support GUs in this area as shown in Figure 4.1. We assume that these N_d UAVs are able to fly horizontally and hover at a certain altitude h_d [266], where they are capable of knowing each other's location by periodically exchanging information using A2A links. For the connection between the UAV and GUs, a UAV-assisted system has been employed to support multiple GUs simultaneously and the UAVs are backhaul-connected to the core network. The framework of our system is illustrated by Figure 4.1, where several UVAs are supporting ground mobile devices in a given target area. Here, UAVs are capable of exchanging information by A2A links, while all these UAVs are backhaul connected to central servers, which sends control information to the UAVs. Besides, the battery power of the UAV is assumed to be supplied by wireless charging techniques [277], hence, these UAVs are capable of operating for a long period of time.

In our scenario, we consider a limited number of UAVs to provide wireless coverage to the GUs. In most cases, the system performance can be improved by deploying more UAVs, for covering a larger area as well as for providing a higher data rate for the GUs. However, this results in a high cost, in addition to the fact that the control of multiple UAVs becomes more complicated with the increased number of UAVs. In addition, the inter-UAV collision problem becomes more serious as the density of UAVs increases.

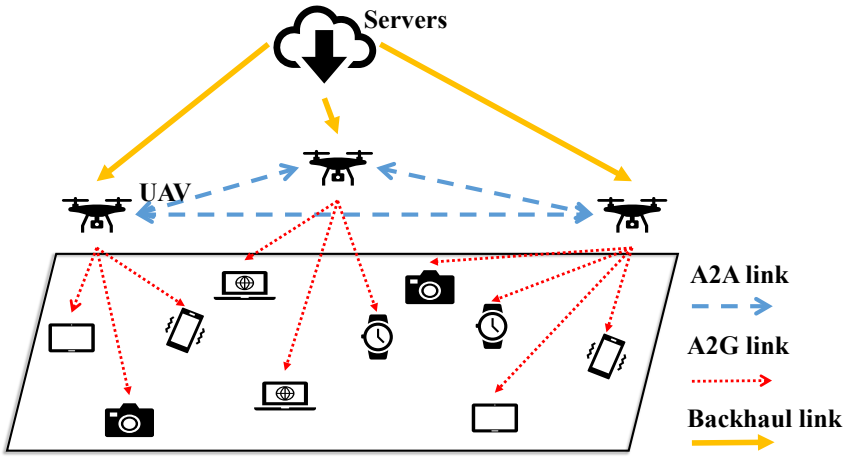

Figure 4.1: UAV-assisted network model that provides service of wireless communication for GUs.

All these aforementioned issues will cause a degradation in the system performance and further lead to a poor user experience.

One potential enabling technique for multiple UAV deployment is the k-means clustering, which is characterised by its scalability, universality and simple implementation [278]. The k-means algorithm is originally used to partition the dataset into k predefined distinct non-overlapping clusters, where each data point belongs to only one cluster [177]. However, the deployment of multiple UAVs is not identical to a clustering problem, since we are considering a limited number of UAVs, which have limited flying speed that forbids them to suddenly move a long distance instantly while tracking the GU movements. Furthermore, the traditional greedy UAV-user association scheme based on the received signal strength will cause some poor association in UAV assisted communication system, where some of the GUs will connect to distant UAVs due to the priority generated from the signal strength and the number of GUs that each UAV can serve. As a consequence, some GUs could not be associated with their preferred UAVs due to this bi-directional selection.

In this contribution, DQL is employed for assisting a limited number of UAVs to adapt to the movement of GUs in a large geographical area. The whole target area will then be divided into small grid cells for application of DQL.

4.2.1 Mobility model

In our system, N_u GUs are moving continuously in an area with a constant velocity[1]. Accordingly, the serving UAVs have to change their formation for adapting to

[1]Please note that the proposed technique readily work for the case of variable user speed, where we consider the assumption of constant speed for the sake of simplifying the discussion.

the movement of GUs. In wireless networks, apart from global positioning system, there are various metrics that could be used to find the location of radio-frequency devices, such as received signal strength [279, 280], time of arrival [281], time difference of arrival [282], frequency difference of arrival [283] and angle of arrival [284]. All these metrics or measurements are assumed in a LoS environment, which is applicable in the UAV assisted system. Based on these metrics, the location information of each GU is available and could be collected by the UAVs. The coordinates of the GUs can then be utilized to determine the deployment position of the UAV.

In each time slot t, the terrestrial coordinate of the n^{th} GU, $n \in N_u$, could be represented by $(x_n(t), y_n(t))$ and the coordinates of the m^{th} UAV, $m \in N_d$, is given by $(x_m(t), y_m(t), h)$, where $t \geq 0$. In the initialization phase at $t = 0$, all GUs are uniformly distributed in the target area. Without loss of generality, we assume that all GUs' coordinates will not change in duration $\Delta_{t,t+1}$, where $\Delta_{t,t+1}$ is the time interval between t and $t+1$. The coordinates $(x_n(t+1), y_n(t+1))$ of the n^{th} GU is determined by the velocity $v_n(t)$ and direction $\theta_n(t)$ in time slot t, which could be represented by:

$$x_n(t+1) = x_n(t) + v_n(t) * \cos(\theta_n(t)), \tag{4.1}$$

$$y_n(t+1) = y_n(t) + v_n(t) * \sin(\theta_n(t)). \tag{4.2}$$

In our model, the whole target area has been discretized into a set of unit square cells with a length of $l_u = \Delta_{t,t+1} \cdot v_d$, where v_d is the speed of the UAV. In our system, the UAV is assumed to hover at the centre of each grid cell within each time slot.

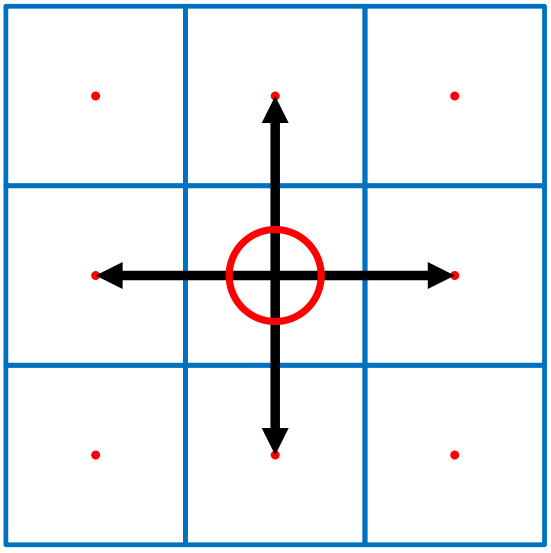

Figure 4.2: Movement strategy of UAV in deep Q-learning.

As shown in Figure 4.2, the UAVs are only allowed to fly to their adjacent grid cells or stay at the current position [217, 285, 286], which is illustrated by black arrows and red circle, respectively. All permitted actions could be summarized by $action =$

$\{Forward, Backward, Left, Right, Hover\}$, while flying diagonally is not allowed due to the speed limit of the UAV and the length of $\Delta_{t,t+1}$.

4.2.2 Channel Model

In our system, the carrier frequency considered is 38 GHz [9, 287, 288, 289], which is capable of providing adequate bandwidth resources. Since UAVs are considered as aerial BSs to serve GUs, the communication between the GUs and the UAVs is in strong LoS propagation environment [290]. Therefore, we consider the Rician fading channel model [45, 268], which has a dominant LoS path combined with some NLoS paths, to measure the signal propagation environment [291, 292, 293]. The Rician channel employed in our A2G communication decomposes the channel into two parts: deterministic LoS component h_{LoS} and stochastic NLoS component h_{NLoS}. The NLoS component is used to represent the scattered multipath propagation of the signals and the Rician K factor is the power ratio of the two components [269]. The channel h is given by:

$$h = \sqrt{\frac{K}{1+K}} \cdot h_{\text{LoS}} + \sqrt{\frac{1}{1+K}} \cdot h_{\text{NLoS}}. \tag{4.3}$$

It is worth noting that h becomes a pure LoS channel when $K = \infty$, while it corresponds to Rayleigh fading channel when $K = 0$. Consequently, we employ a high K value to generate a LoS-dominant channel in our UAV-assisted communication networks [294]. Besides, since we consider the target area in a environment that the LoS link dominate any other links [295], the pathloss between the n^{th} GU and the m^{th} UAV at time slot t can be expressed as [296]:

$$PL_n^m(t) = \left(\frac{4\pi f_c}{c}\right)^2 \left(d_n^m(t)\right)^{\alpha}, \tag{4.4}$$

where f_c is the carrier frequency, c is the speed of light and α $(\alpha \geq 2)$ is the pathloss exponent that indicates the nature of the propagation environment. The A2G distance between the n^{th} GU and the m^{th} UAV during time slot t is denoted by $d_n^m(t)$, which can by obtained as $\sqrt{h_d^2 + \left(r_n^m(t)\right)^2}$, where h_d is the height of the UAVs and $r_n^m(t)$ is the horizontal distance between the n^{th} GU and the m^{th} UAV during time slot t. Therefore, the received signal power $P_{r_n}^m(t)$ at the n^{th} GU from the m^{th} UAV during time slot t given a transmission power P_t is given by [272]:

$$P_{r_n}^m(t) = \frac{P_t}{PL_n^m(t)} = P_t \left(\frac{4\pi f_c}{c}\right)^{-2} \left(d_n^m(t)\right)^{-\alpha}. \tag{4.5}$$

Additionally, the UAVs are assumed to operate at a height of 100 meters [273], where the LoS communication links exist for most of the time. Hence, free space pathloss

exponent $\alpha = 2$ is considered [44] and $P_{r_n}^m(t)$ is transformed to:

$$P_{r_n}^m(t) = P_t \left(\frac{4\pi d_n^m(t) f_c}{c} \right)^{-2}. \tag{4.6}$$

We assume that all UAVs are transmitting with the same power P_t and all the UAVs have the same bandwidth resources. Again, each UAV can simultaneously communicate with multiple GUs by allocating the bandwidth resources to different GUs. Specifically, the bandwidth resources can be divided into N_m^a sub-channels, based on the number of successfully associated GUs of the m^{th} UAV. Here, only when the GU's SNR reaches a certain level $\gamma_{\min}$ that the GU is considered successfully associated to a UAV for supporting communication. Finally, we assume that the interference from other GUs can be successfully cancelled [297].

Hence, the received SNR during time slot t at the receiver side of the n^{th} GU from the m^{th} UAV can be expressed as $\gamma_n^m(t) = P_{r_n}^m(t) \cdot |h|^2/\sigma^2$, where σ^2 represents the noise power. Since $h_{\text{LoS}} = e^{-j\frac{2\pi}{\lambda}d}$ [298], where λ is the wavelength and d indicates the distance between the transmitter and the receiver. According to the (6.1), it is straightforward to find that the power of channel h is approximated to 1 when the LoS component of the channel is much stronger than the NLoS component. In other words, the NLoS part can be neglected. Consequently, the received SNR $\gamma_n^m(t)$ can be simplified to $P_{r_n}^m(t)/\sigma^2$ and the capacity of the n^{th} GU and m^{th} UAV link measured in bits/s/Hz in time slot t is given by:

$$C_n^m(t) = F_n(t) B_n(t) \log_{10}\left(1 + \gamma_n^m(t)\right), \tag{4.7}$$

where $B_N(t)$ is the bandwidth allocated to the n^{th} GU in time slot t and $F_n(t)$ is a flag to indicate if $\gamma_n^m(t)$ could support a basic communication in time slot t, which is determined by:

$$F_n(t) = \begin{cases} 0 & \gamma_n^m(t) < \gamma_{\min}, \\ 1 & \gamma_n^m(t) \geq \gamma_{\min}. \end{cases} \tag{4.8}$$

Accordingly, the overall sum rate of all successfully associated GUs during time slot t is evaluated as:

$$R(t) = \sum_{m=1}^{N_d} \sum_{n=1}^{N_m} C_n^m(t), \tag{4.9}$$

where N_m is the number of GUs allocated to the m^{th} UAV. When the strength of the received signal is weak, some GUs links will be considered as outage even though they have been allocated to one of the UAVs. Thus, the relationship of N_m and N_m^a is given by $N_m \geq N_m^a$.

4.2.3 UAV-user Association Strategy

User association, namely associating a user with a particular serving UAV, could substantially affect the network performance. However, there are various user association methods to assign users to the BSs according to different objectives, realistic constraints and operation environment, when there are multiple users and multiple BSs available. In existing works, the received power based user association method is the most prevalent one, where a GU chooses to associate with a specific BS that provides the maximum received signal strength [276, 299]. In our UAV-aided communication system, the number of UAVs and the bandwidth resources are limited. Therefore, we consider the most widely used user association scheme that considers received signal strength as a measure to link with GUs. However, pure received signal strength will lead to unfairness, since the number of GUs a UAV can support is limited. Hence, a part of GUs will have weak links because they cannot connect to their "favored" UAVs. Therefore, a modification of the current received signal strength based scheme is necessary to improve the communication of these disadvantaged GUs, namely the outliers. Again, we consider a LoS dominant communication environment in our UAV-assisted system, where the signal strength is largely determined by the pathloss and is slightly affected by the NLoS signal propagation. Hence, the received signal is largely up to the A2G distance between the UAV and the GUs. In the following we describe the conventional greedy association method followed by our proposed UAV-user association technique.

4.2.3.1 Greedy UAV-user Association

Let us consider the scenario where there are N_d UAVs, each capable of supporting N_s GUs, and there are $N_d \times N_s$ GUs in a target area. Then, the procedure of the greedy algorithm which only considers the received signal strength is shown in Figure 4.3.

From the flow chart in Figure 4.3, we can see that GUs who have low received SNR will be directly considered as outage, while the GUs that meet that required threshold will prioritize the UAVs according to their received SNR. Hence, smaller distance between the UAV and GU will result in a higher priority. After that, the GUs will initially select their highest priority, this means UAV that could support them with the strongest signal strength will be selected. However, due to the limited UAV service capacity, UAVs will also prioritize GUs according to the quality of communication links, which is essential when the number of GUs that initially choose one of those UAVs is beyond the capacity of the UAV. Hence, this process is a bi-directional selection. Then, only GUs whose first priorities is in the ranking of their corresponding UAVs are able to accomplish this association, otherwise, they have to wait for their next highest priorities and repeat the aforementioned steps until all GUs have been associated.

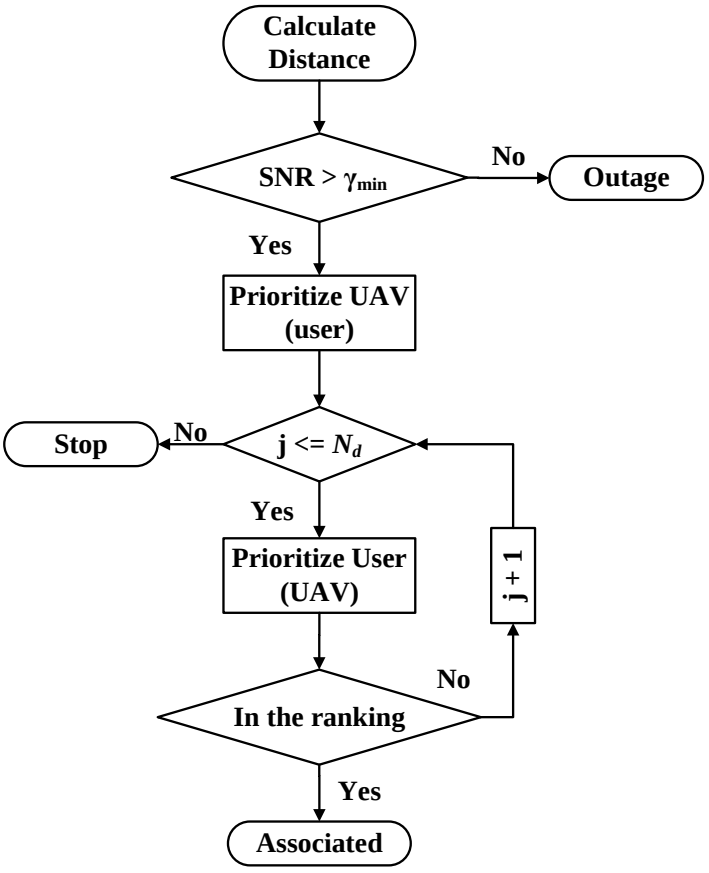

Figure 4.3: Operating procedure of greedy UAV-user association algorithm.

An example of greedy association with four UAVs is shown in Figure 4.4(a), where the UAVs are distinguished by different large size shapes and their corresponding associated GUs will be marked by the same but smaller size shape. Here, we consider the scenario where all the GUs in this square area can be detected by all four UAVs, which means that the channel quality of all GUs is good enough to establish stable and reliable communication links to all UAVS. Then, the GUs can prioritize their favourite UAVs according to the received signal strength. If the signal strength of some GUs is weak, the information contained in the signal cannot be decoded correctly, which means that these GUs are treated as outage and there is no need to consider the association between this GU and UAVs.

According to Figure 4.4(a), there are three "outliers" marked by two red circles, which are associated with unsuitable UAVs. This is caused by the priority in the algorithm, where both UAVs and GUs try their best to connect with the closest GUs or UAVs. More specifically, in the blue "outlier" case, assume that the first priority of the blue square is the green UAV, however, the distance between them is not included in the first N_s closest candidates of this UAV. Then, the blue square GU has to try to associate with its second choice, which is the red UAV. Again, it is still not in the ranking of the red UAV and the same situation occurred at the purple UAV. Finally, it has no choice but to

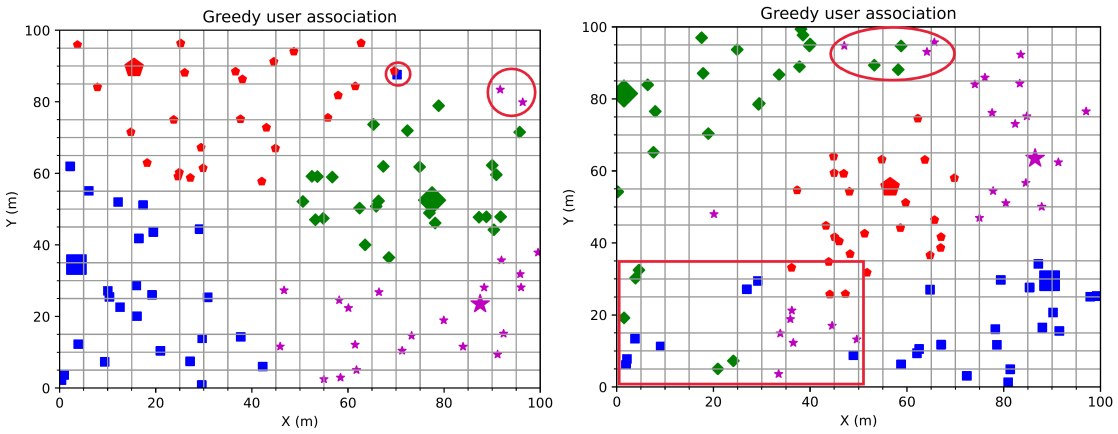

(a) Common condition.

(b) Severe condition.

Figure 4.4: Example of greedy UAV-user association in four UAVs scenario with 100 GUs.

associate with the blue UAV because it still has a space in its ranking list. However, the communications link quality for this specific GU to the blue UAV can be very poor.

As mentioned before, some GUs would be connected with far-away UAVs, and hence this greedy user association rule is unsuitable in our UAV communication system, because the "outliers" would have a very poor communication link with the associated UAV. Although it can be argued that we can achieve a good QoS by sacrificing only a small number of GUs, in Figure 4.4(b) we show a relatively extreme scenario, where, we set one of the UAVs at the top-left corner while the other UAVs are deployed at the lower right, which is aimed at generating a relatively high difference on the received signal strength. At the bottom-left and top-middle of the figure, lots of unsuitable associations occur, when using the greedy user association technique. In this situation, the QoS could be significantly reduced due the "extended" A2G distance. Hence, in the following section, we present our proposed user association technique, that deals with those unsuitable UAV-user association issues that may occur in UAV-aided communication system.

4.2.3.2 Proposed UAV-user Association Strategy

We propose an improved algorithm to avoid the occurrence of unsuitable association, while considering the limited UAV resources. Hence, whether a request from GU is admitted or rejected should be decided according to the priority level of the request and to the availability of the radio resources, with the goal of maximizing the radio resource utilization. Explicitly, instead of choosing the highest received SNR or closest UAV/user to establish communication, we iteratively exchange GUs among different UAVs to achieve a global optimum as shown in the procedure presented in Algorithm 6.

Algorithm 6 Operating procedure of our proposed optimized UAV-user association.

Locate position of each GU
Obtain the quality of communication links (γ_n^m)
for n from 0 to N_u **do**
  if $\max\{\gamma_n^m(t)\} \geq \gamma_{\min}$ **then**
    $F_n(t) = 1$
  else
    $F_n(t) = 0$
  end if
end for
Remove outage GUs ($F_n(t) = 0$)
Initialize the UAV-user association randomly
Calculate the current total A2G distances D_{sum}^c
for i from 0 to N_i **do**
  while $k \leq N_l$ **do**
    Exchange with GUs associated with other UAVs
    Calculate the total distances D_{sum}^e after exchange
    if $D_{\text{sum}}^c > D_{\text{sum}}^e$ **then**
      $D_{\text{sum}}^c = D_{\text{sum}}^e$
      $k = k + 1$
    else
      Move to next other UAV's GU
    end if
  end while
end for

In each time slot t, the m^{th} UAV measures the quality of communication link with the n^{th} GU based on the SNR $\gamma_n^m(t)$ in order to decide if the n^{th} GU can be supported with a reliable and stable link by the m^{th} UAV, i.e. $\gamma_n^m(t) \geq \gamma_{\min}$. If the GU meets the requirement, the flag $F_n(t)$ will be set to 1, otherwise, it will be set to 0 and considered as an outage user. After removing those GUs that cannot connect to the specific UAV, GUs will be randomly allocated to other UAVs at the initialization stage. However, it is worth noting that the initialization process of UAV-user association can be changed according to the actual demand. Explicitly, starting from one of those UAVs and selecting one of the GUs that are associated with this selected UAV, the system (the group of UAVs) will exchange this GU with any other GU associated with other UAVs. Then the total distance of all these GUs is calculated after the change of association. As a result, the current association change would be kept if the current total distance D_{sum}^c is larger than the total distance D_{sum}^e after the exchange, otherwise, it selects next GU of other UAVs and repeat the steps. Again, it is worth noting that the order of UAVs or GUs that the algorithm starts with is not important, because both of them will not affect the final convergence. Finally, after N_i iterations, where N_i is the number of iterations set based on actual demands that can ensure the convergence of system, the total distance will converge to a minimum and an optimized solution can be achieved.

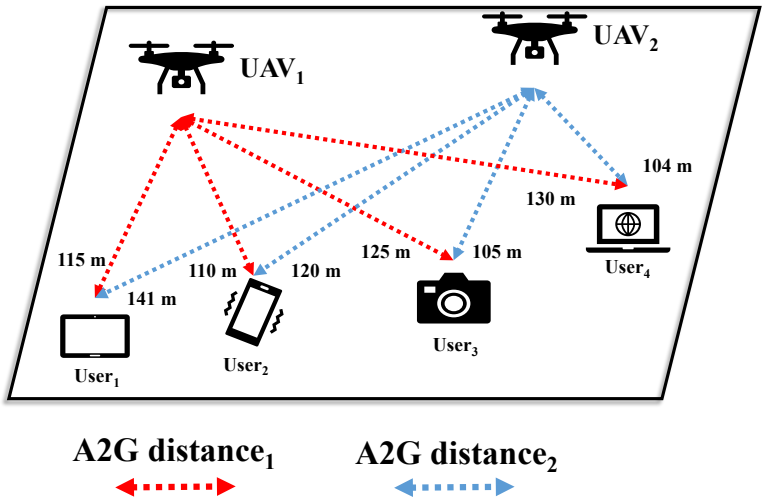

Figure 4.5: Illustration diagram of toy example with four GUs and two UAVs.

For instance in Figure 4.5, we consider an example employing two UAVs in a target area with four GUs and each UAV can only support two GUs. In this example, we assume no outage exists, where each GU can be successfully detected and associated with both UAVs. Then, the A2G distances of each GU is given by $d_1 = [115, 141]$, $d_2 = [110, 120]$, $d_3 = [125, 105]$ and $d_4 = [130, 104]$, where the unit of distances is in meter while d_u is the distance from the u^{th} GU to the two UAVs. More specifically, $d_u = [d_{u_1}, d_{u_2}]$, where d_{u_1} and d_{u_2} are the distances between the u^{th} GU to the first and second UAVs, respectively. According to the algorithm, we start by randomly allocating GUs to UAVs. Without loss of generality, we assume that GU_1 and GU_4 are connected to the UAV_1 while GU_2 and GU_3 are connected to the UAV_2. Hence, the current total distance is given by $D^c_{\text{sum}} = 115 + 130 + 120 + 105 = 470$. Then, the two UAVs start to exchange their GUs, assuming that the first two exchanged GUs are GU_1 and GU_3 and the corresponding total distance is $D^e_{\text{sum}} = 141 + 120 + 125 + 130 = 516$, and this exchange is invalid due to $D^c_{\text{sum}} < D^e_{\text{sum}}$. Next, GU_1 will exchange with GU_2 and the resulting $D^e_{\text{sum}} = 486$ which is still larger than $D^c_{\text{sum}} = 484$. Then, GU_4 will exchange with GU_2 and the resulting total distance is $D^e_{\text{sum}} = 434$, this exchange will be kept because it leads to $D^c_{\text{sum}} > D^e_{\text{sum}}$. The same process is repeated for N_i times or until the system convergence. Finally, a comparison between the greedy and the proposed techniques is shown in Figure 4.6, where it is clear that in our proposed technique, those unreasonable associations have been revised and "outliers" have been reallocated to appropriate UAVs.

4.3 UAV Deployment

In the previous section, the UAV-user association in UAV-aided communication system has been investigated to improve the QoE of GUs. However, the deployment of UAVs

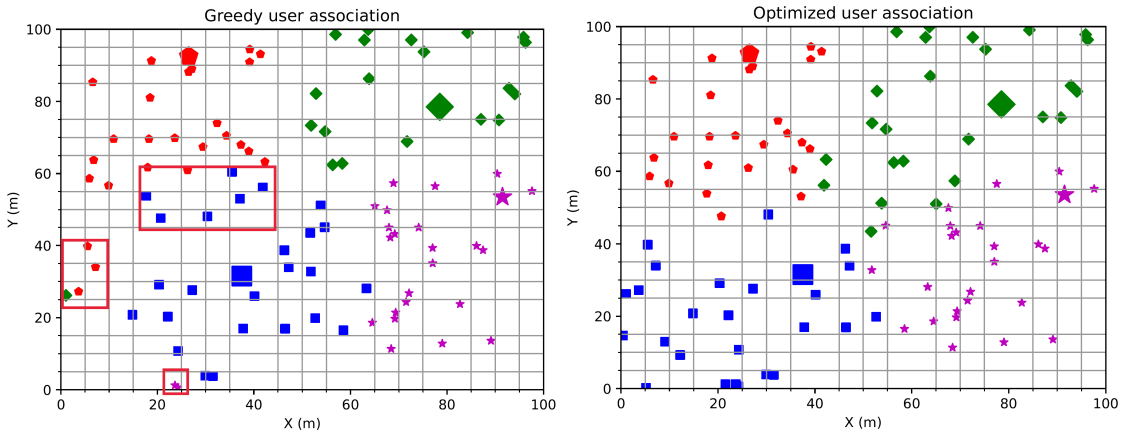

(a) Greedy algorithm. (b) Optimized algorithm.

Figure 4.6: Comparison between the greedy and optimized UAV-user association.

will also affect the quality of the communication links and hence the deployment of multiple UAVs is presented in this section.

4.3.1 Deployment by *k*-means Algorithm

In this section, we present the *k*-means clustering technique, which has been considered in the literature for UAV deployment [300]. In this case, the *k*-mean can be considered as a benchmark of the system performance, since there is the impractical assumption that the UAV can move instantly to a new center of the cluster over a large distance depending on the GU mobility. This algorithm is capable of clustering the GUs into groups according to their ground coordinates. It is an iterative, data-partitioning algorithm that assigns n observations to exactly one of k clusters defined by the centroids, where k is chosen before the algorithm starts. In our system, the k is defined by the number of UAVs, and we assume that all the GUs can be detected by all UAVs.

In Figure 4.7, we show an example of two UAVs serving a number of GUs as aerial BSs, where we show that the *k*-means is capable of finding the centroid of each group using the real-time location of the GUs. However, we show in Figure 4.7 that a sudden-shift would occur if the user distributions are quite different within two consecutive time slots because the distance between the two centroids in the two time slots is significantly changed. Recall that the deployment by based on the centroids obtained from *k*-means. Therefore, if the centroids of two adjacent time slots are quite different which is far beyond the distance a UAV can move within a time slot, the sudden shift occurs. In Figure 4.7, the circle and square are used to represent two UAVs and the size of shapes is used to distinguish two time slots. However, the finite speed of the UAVs limits the distance that a UAV can travel within a time slot and hence practical UAVs cannot move to the target position instantly within a time slot. In Figure 4.7 (b), we

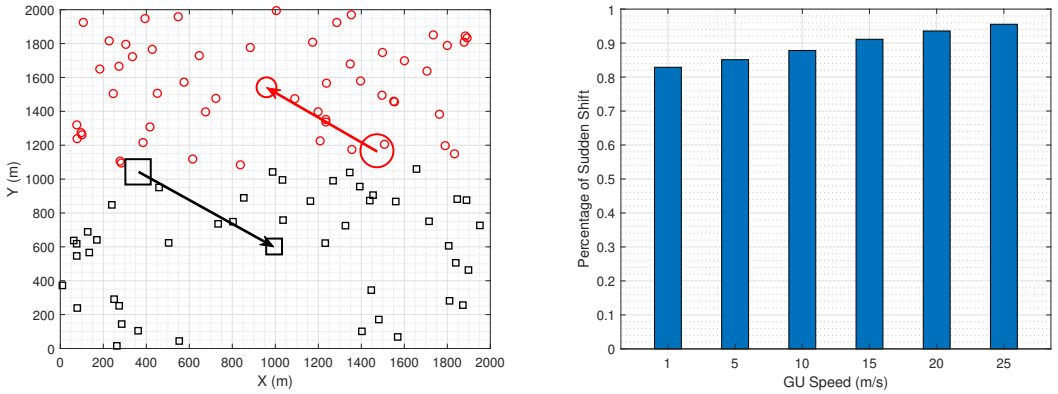

(a) Illustration of sudden-shift occurrences.

(b) Percentage of sudden-shift occurrences.

Figure 4.7: *k*-means clustering aided UAV-user association.

show the percentage of time where there is a sudden-shift of UAV by allowing GUs to move according to the mobility model introduced in section 4.2.1 and counting the times of sudden-shift that occurred in total number of time slots.

When the speed of the UAV is fixed, we define the sudden-shift as the scenario where the distance space between the two *k*-means deployment positions in two time slots is larger than the distance that a UAV can fly within the time slot. It can be observed in Figure 4.7 (b) that there is a high probability of sudden-shift during the operation period. Furthermore, with the increase of GU speed, this phenomenon will occur more frequently, which means that it is hard for UAVs to adapt to the movement of GUs. If the UAV does not move to the cluster centroid as decided by the *k*-means algorithm then the communication performance is affected due to the distance related to pathloss. Therefore, it is necessary to take the speed of UAVs into consideration, which results in a finite speed *k*-means deployment method. In this method, if the distance between two deployment positions is larger than that the UAVs can move, it will only move in the direction illustrated by Figure 4.7 (a) with a certain distance and it will cause degradation of the communication link performance. Hence, in the following section a deep Q-learning based UAV deployment technique will be presented.

4.3.2 Deployment by Deep Q-Learning

Given the challenges of the *k*-means deployment, we consider a DQL based deployment method, which takes the speed of UAVs into consideration by discretizing the movement of UAVs. In this UAV-assisted communication system, all the UAVs are considered as a cooperative unit. Besides, the coordinates of the GUs are shared by all UAVs and the data synchronization of UAVs will be periodically updated to make sure that each UAV has the latest GU information [301, 302, 303]. During this process,

extra signalling between the UAVs is needed in order to facilitate the information exchange, which can include the coordinate of the GUs, the coordinates of the UAVs and the channel conditions. This signalling information will be transmitted via a control channel and hence it will not affect the data transmission from the UAVs to the GUs.

In the DQL algorithm, the agent will continuously interact with the environment and obtain the information from the environment by doing some tests. Please note that, all the information is collected by the UAVs and sent back to the bachhaul server to complete the relatively high-complexity training process due to the limitation of the computation ability and power supply on the UAVs. The whole system is composed of a set of states S and specified set of actions A at each state. Firstly, the time is discretized into equally divided time slots. Then, the agent takes one action $(a(t) \in A)$ at the observed state $(s(t) \in S)$ in time slot t and the state will change to $(s(t+1) \in S)$, which is the initialized state of the next time slot. The agent will get a reward $r(t)$ after taking one action, which is used to evaluate the "value" of that action at that state. Based on the state-action pair in the format of $[state, action, reward, next-state]$, the target of the system is to find out a policy $\pi(s, a)$ that provides the highest reward.

The QL seeks to learn the corresponding Q-value (quality) of a given action-state pair based on the received reward which is indicated by $Q(s, a)$. To calculate the value of these state-action pairs, we use the QL algorithm called action-value function to update the Q-value. As we explore the environment, it will give us improved approximation by iteratively updating $Q(s, a)$ using the Bellman equation [304]:

$$\begin{aligned} Q(s(t), a(t)) = (1 - \alpha_l) Q(s(t), a(t)) + \\ \alpha_l [r(t) + \gamma \max_a Q(s(t+1), a)]. \end{aligned} \tag{4.10}$$

Starting from inside the square parentheses, we first take the reward $r(t)$ we got from our selected action $a(t)$ in (4.10) and add it to the discounted maximum Q-value for next state $s(t+1)$, and subtract it from our current estimate of the Q-value of that state. This step is computing the error between the action we just did and what we believe to be the best action available to us from this new state. Then, we scale the error down by step-size α_l which is also known as the learning rate and add it to our current estimate for $Q(s(t), a(t))$. Finally, we obtain the new estimate for $Q(s(t), a(t))$.

In the proposed DQL system, as shown in Figure 4.8, the state $s(t)$ in each time slot is denoted by the horizontal coordinates of the UAVs $S(t) = [s_1(t),\ s_2(t),\ \ldots,\ s_{N_d}(t)]$ and $s_i(t) \in \{(x_1(t), y_1(t)),\ (x_2(t), y_2(t)),\ \ldots,\ (x_{g\times g}(t), y_{g\times g}(t))\}$, where g is the number of units for each side of the target area and $s_i(t)$ represents the coordinates of the center of the i^{th} grid cell in time slot t. Theoretically, the order of numbering those grid cells will not affect the results, but it could be more understandable to number them according to certain rules, e.g. clockwise or anticlockwise. Due to the high complexity of continuous action space and the limited speed of the UAV, the possible actions

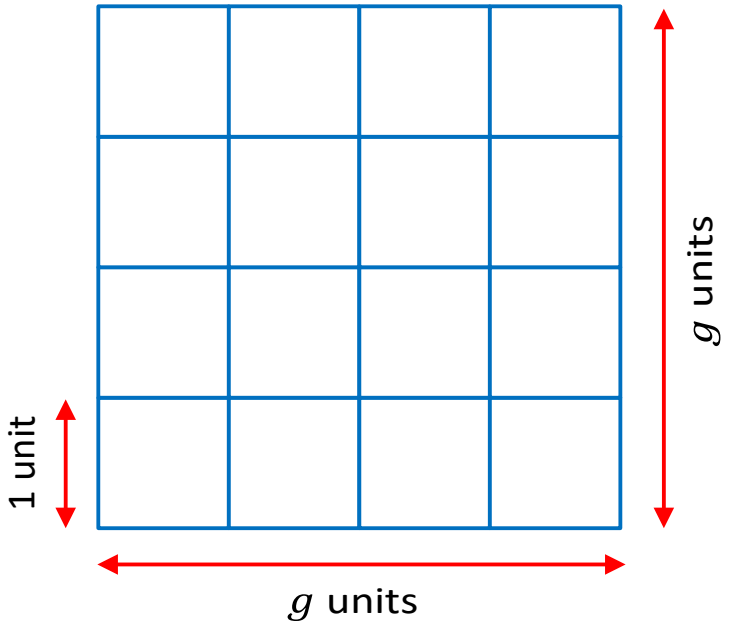

Figure 4.8: Illustration of discretized target area.

are $A = [(0,1),\ (0,-1),\ (-1,0),\ (1,0),\ (0,0)]$, which represents the five actions mentioned in the mobility model. Then, the next states of taking those actions are summarized as:

$$s(t+1) = \begin{cases} s(t) + l_u \cdot (0,1) & \text{Forward,} \\ s(t) - l_u \cdot (0,1) & \text{Backward,} \\ s(t) - l_u \cdot (1,0) & \text{Left,} \\ s(t) + l_u \cdot (1,0) & \text{Right,} \\ s(t) + l_u \cdot (0,0) & \text{Hover.} \end{cases} \tag{4.11}$$

After taking action $a_n(t)$ in time slot t, the transition from state $s(t)$ to $s(t+1)$ generates reward r_t which is defined by three parameters: average transmission rate $R_a(t)$, valid average transmission rate $R_v(t)$ and number of outage GUs $N_o(t)$. The average transmission rate is the mean of all GUs' transmission rate, which is defined by:

$$R_a(t) = \begin{cases} \frac{1}{N_u} \cdot R(t) & N_u > 0, \\ 0 & N_u = 0, \end{cases} \tag{4.12}$$

while the valid average transmission rate is determined by those successfully associated GUs and it can be calculated by:

$$R_v(t) = \begin{cases} \frac{1}{N_u - N_o(t)} \cdot R(t) & N_u > N_o(t), \\ 0 & N_u = N_o(t). \end{cases} \tag{4.13}$$

Here, it is worth noting that the bandwidth resources allocated to each UAV is limited

and each UAV can only connect with GUs whose received SNRs are higher than the threshold $\gamma_{\min}$. Hence, when the distance between the GU and the UAV is very long, this will lead to a weak signal strength due to the high pathloss. As a consequence, if the UAV cannot support a stable and reliable communication link with some GUs, then these GUs will be considered as outage and any bandwidth resources originally allocated to them will be allocated to those successfully associated GUs. This situation will cause $R_a(t) \ll R_v(t)$ when lots of outages exist. However, our target is to cover as many GUs as possible instead of offering high performance communication to a limited number of GUs. To sum up, the reward $r(t)$ at time slot t is calculated by:

$$r(t) = [R_a(t),\ R_v(t),\ N_o(t)] \times \boldsymbol{w}, \tag{4.14}$$

and $\boldsymbol{w}$ is a column vector that contains the weight elements assigned to the row vector $[R_a(t),\ R_v(t),\ N_o(t)]$ respectively, which is given by $\boldsymbol{w} = [w_1,\ w_2,\ w_3]^T$ and $\boldsymbol{w}$ is subject to $w_1 + w_2 + w_3 = 1$. By adjusting the proportion of each element, we are able to train our DQL system with different targets. For example, when the transmission power is very low and lots of GUs are in outage, our target should be for minimising the number of outages. However, if the transmission power is good enough to support all the GUs, our target can be to maximize the average rate of GUs. Therefore, by setting different targets in different situations, it makes our neural network more efficient in finding the appropriate locations to deploy the UAVs.

However, with multiple UAVs flying in close proximity to each other, sharing the same air space, the risk of inter-UAV collisions increases. Hence, it is vital to avoid these collisions while having minimal impact on the UAV-aided communications performance. In Figure 4.9, we show a 4-level classification of collision for UAVs. When the distance between two UAVs is smaller than $2l_u$, it will be identified as collision. Hence, it is clear that we only need to calculate the distance between two ground coordinates to determine the level of collision, since in our system we consider the same flying height for the UAVs. To measure the impact of collision, the four-level criterion is given by:

- Level 0: The distance between two UAVs is equal or greater than $2l_u$, which means no collision occurred.
- Level 1: The distance between two UAVs is $\sqrt{2}l_u$ and it will lead to a slight collision.
- Level 2: The distance between two UAVs is l_u and it will cause a medium collision.
- Level 3: Two UAVs are overlapped, which brings about the worst collision with 0 distance.

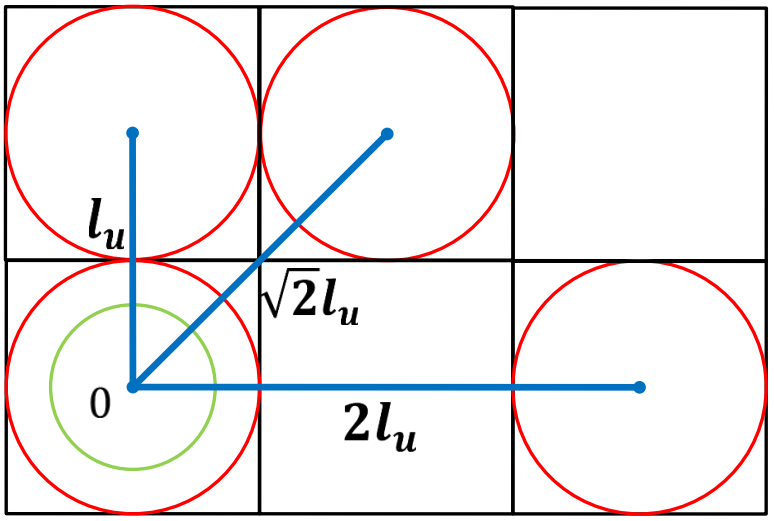

Figure 4.9: Classification of collision level in accordance with the position of UAV.

In our design, we consider collision as a penalty in our proposed system that is represented by:

$$P(t) = \begin{cases} p_0, & Level\ 0 \\ p_1, & Level\ 1 \\ p_2, & Level\ 2 \\ p_3, & Level\ 3 \end{cases} \tag{4.15}$$

where $P(t)$ is a positive constant value in time slot t, while $p_0 < p_1 < p_2 < p_3$, which are used to avoid UAV collision.

The proposed DQL system is illustrated in Algorithm 7. Firstly, we have a replay buffer B with a length of l_B at the servers. We assume that the UAVs do not have enough computation power to finish the training process, and hence the training process will be done at the servers. More specifically, the UAVs will send all collected information back to servers through backhaul links. Then the parameters of the predicted network Q and target network Q' will be initialized. Here, totally N_e episodes will be set and each episode contains N_t time slots. In each episode e, we initialize the state (location) of the UAVs randomly at the beginning. Afterwards, the UAV selects one action $a(t)$ at the given state $s(t)$ based on the ϵ-greedy algorithm in each time slot t. Then, according to the collision level $P(t)$ and the reward $r(t)$ obtained from taking that action $a(t)$ with the corresponding $\boldsymbol{w}$ predefined, the final reward $r(t)$ can be calculated by $r(t) = r(t) - P(t)$. The transition will then be stored in buffer B in the format of $\langle s(t), a(t), r(t), s(t+1) \rangle$. The next step is to randomly choose l_m samples from buffer B and calculate the difference of Q-values between the target network and predicted network. In this step, we employ double-dueling DQL method to calculate the Q-value of both networks in order to reduce the over-estimation and to accelerate the training

process [4, 305]. Now, the loss can be calculated by the squared difference between target Q' and predicted Q, where l_2 is employed here to perform l_2 regularization which is used to address over-fitting and feature selection, and λ_r is used to adjust the level of regularization. Then the gradient descent will be performed to minimize this loss with respect to our actual network parameters. Ultimately, parameters of the target network will be updated by using smoothing factor τ, where $\tau < 1$ and is used to determine the proportion that the parameters of the predicted network will be copied to the target network.

Algorithm 7 UAV deployment by deep Q-learning.

Initialise replay buffer B with a length of l_B in the format of $\langle s(t), a(t), r(t), s(t+1) \rangle$

Initialise predicted action-value function $Q(s, a; \theta)$ arbitrarily
Initialise target action-value function $Q'(s, a; \theta')$ arbitrarily
for episode $e = 1, \ldots, N_e$ **do**
  for t = 1 to N_t **do**
    Initialize the state s_1 randomly
    Select action by ϵ-greedy algorithm

$$a(t) = \begin{cases} argmax_a Q(s(t), a), & \epsilon \\ random, & 1 - \epsilon \end{cases}$$

    Take $a(t)$ to obtain next state $s(t+1)$
    Execute UAV-user association and calculate reward $r(t)$
    Evaluate the level of inter-UAV collision and obtain penalty $P(t)$
    Update $r(t) = r(t) - P(t)$
    Store the transition $\langle s(t), a(t), r(t), s(t+1) \rangle$ in replay buffer B
    Randomly sample l_m mini-batch of transitions from B
    for $i = 1$ to l_m **do**
      Obtain $Q(i; \theta)$ and $Q'(i; \theta')$ according to double-dueling method
    end for
    $Loss = \frac{1}{2l_m} \sum_1^{l_m} \left(Q(i; \theta) - Q'(i; \theta') \right)^2 + \lambda_r \cdot l_2$
    Update target θ' by $\theta' = \tau\theta' + (1 - \tau)\theta$
  end for
end for

In summary, the GUs are continuously moving on the ground based on their direction and velocity, then the UAVs will take actions according to the ϵ-greedy algorithm to move to different positions. At each new deployment position, UAVs perform the proposed UAV-user association and obtain the reward $r(t)$, while the UAVs will record these information in each time slot t and send back to servers. Finally, the UAVs will learn how to take action at different position according to the experiences saved in memory. Therefore, we use our proposed optimized UAV-user association technique to make sure that the association of all GUs in the target area is appropriate and reasonable. Additionally, we use DQL based deployment to find the suitable position to

deploy the UAVs. By combination of this two techniques, we are able to provide our GUs with stable and reliable communication services.

4.4 Performance Results and Evaluation

In this section, we employ $N_d = 2$ and 4 UAVs that are moving in two different square target area with length 200 m and 1000 m, which are virtually divided into 10×10 and 50×50 grid cells, respectively. The area accommodates $N_u = 100$ GUs moving with a constant speed of v_n but in different directions. In our simulation, if GUs hit the border, they will change the direction by 180° to stay in this target area.

Each UAV is allowed to move in a straight line between the current grid cell and the adjacent grid cell with a speed of $v_d = 20$ m/s [306], and one time unit in our simulation corresponds to 1 second. Moreover, each UAV is assumed to fly at a constant altitude of 100 m according to safety consideration. For air to ground communication, we set the carrier frequency to $f_c = 38$ GHz and the pathloss component to $\alpha = 2$, while the bandwidth of each UAV is given by $B = 20$ MHz [307, 296]. Besides, the number of GUs that each UAV can serve is $\frac{N_u}{N_d}$ and the noise power is given by -95 dBm [9, 307]. All the parameters used in our simulation are summarized in Table 4.1.

Table 4.1: Simulation parameters

Parameter	Symbol	Value	Parameter	Symbol	Value
Time slot	$\Delta_{t,t+1}$	1 s	Bandwidth	B	20 MHz
Noise power	σ^2	-95 dBm	Transmission power	P_t	6 to 40 dBm
Carrier frequency	f_c	38 GHz	Pathloss exponent	α	2
UAV height	h_d	100 m	Number of GUs	N_u	100
Number of UAVs	N_d	2 and 4	Velocity of GU	v_n	1 to 25 m/s
Velocity of UAV	v_d	20 m/s	Grid length	l_u	20 m
Mini-batch size	l_m	128	Buffer Size	l_B	1e5
Area length	L	$200 \sim 1000$ m	Learning rate	α_l	0.001
Discount factor	γ	0.99	Smoothing factor	τ	0.01
Size of Layers	N_n	(100, 100, 100)	Number of Layers	N_l	3

The main difference between *k*-means clustering and DQL is that the number of GUs allocated to all UAVs in DQL is identical while the number of GUs allocated to each UAV in *k*-means varied from one to another. Besides, the frequent sudden-shifts in *k*-means makes it difficult for UAVs to adapt in time to the movement of GUs, due to the limitation of UAV speed. Hence, we consider a modification of the *k*-means, which we refer to as 'finite-speed *k*-means', where the distance between two deployment positions is evaluated and then if this distance is larger than the practical distance that a UAV can reach in a time slot, then the UAV moves in the direction of the new position but with a limited distance. This results in a degradation of the communications link performance. Nevertheless, our proposed DQL aided deployment does not suffer from

the sudden-shift required in the *k*-means scenario, because the agent of DQL is able to find an appropriate position to deploy UAVs step by step and the positions chosen by agents are decided from the long-term experience of operation, which means that place is able to provide GUs with good communication services for most of the time.

In Figure 4.10, we consider two scenarios in a given target area with the size of 1 km by 1 km. The left side of Figure 4.10 is a scenario with only 2 UAVs in operation, while the right side depicts a scenario with 4 UAVs. Here, "Fin-k-means" represents the deployment by finite-speed *k*-means algorithm with a fixed speed as that in the "DQL" system within a time slot. Also, three typical transmission power have been selected to illustrate how the density of UAVs affects the distribution of the average downlink rate per GU. It can be seen from the left figures that Fin-k-means deployment method has a longer tail than that of the DQL deployment method, which means that lots of GUs have a poor quality of experience for the communication links when deploying the Fin-k-means algorithm. This shows the limitations of the *k*-means method, where the UAVs cannot move to the desired positions in time, which causes the degradation of communication links as shown in the long tail of the results in Figure 4.10.

While, for the 4-UAV scenario depicted in the right part of Figure 4.10, the downlink rate of the DQL algorithm is shown to be in the tail of Fin-k-means. It is clear that the average downlink rate of both Fin-k-means and DQL has been improved along with the increase of the number of UAVs, although the tail of Fin-k-means scheme still exist. This phenomenon indicates that with the increase in the number of UAVs serving a specific area[2], the average rate of the Fin-k-means is higher that that of the DQL, due to the reduced probability of sudden-shifts as the increased number of UAVs will reduce the distances that UAVs have to move from the current deployment position to the next deployment position as required by the *k*-means algorithm. However, the DQL deployment method cannot update instantly to the movement of GUs due to the nature that the agent learns based on a long-term perspective.

Therefore, when we use a reduced number of UAVs in the target area, the DQL deployment method gives us a better user experience where the average downlink rate of both DQL and Fin-k-means are similar, but the Fin-k-means has a long tail resulting in a large number of GUs experiencing a significantly reduced rate. Although the performance of DQL is not as good as that of Fin-k-means when using 4 UAVs, it is clear that the variance of DQL is much smaller than that of Fin-k-means, which indicates that DQL is more stable and provides GUs with better QoE. In other words, DQL can be employed to reduce the unstable communication links (long-tail) caused by the sudden-shift of Fin-k-means and to provide GUs with a better QoE. The comparison shows that both DQL and Fin-k-means have similar high of downlink rate end

[2]A large amount of UAVs is infeasible due to the high cost and the complexity of control will also increase, hence, it is reasonable to utilize limited number of UAVs to establish communication service

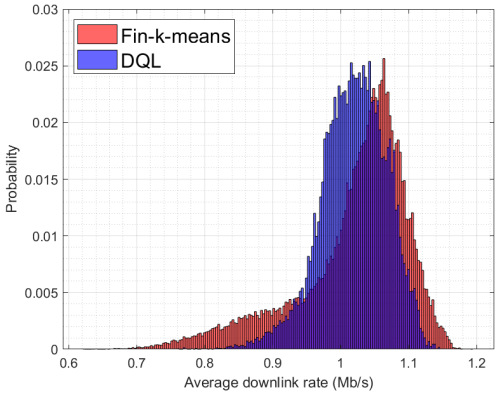

(a) Average downlink rate of 25 dBm using 2 UAVs.

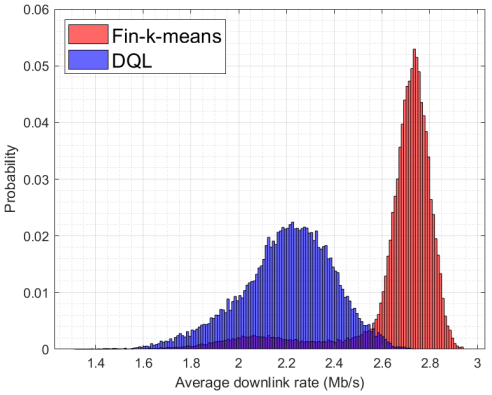

(b) Average downlink rate of 25 dBm using 4 UAVs.

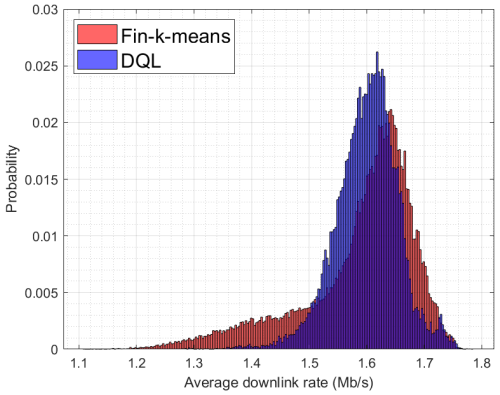

(c) Average downlink rate of 30 dBm using 2 UAVs.

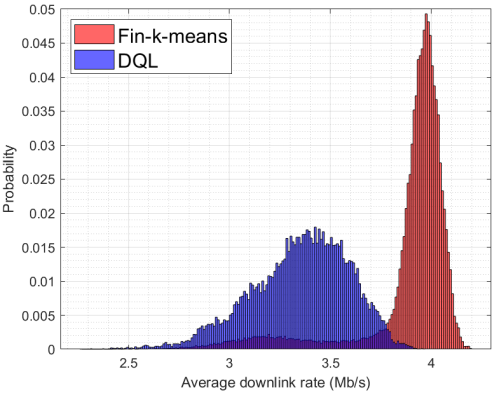

(d) Average downlink rate of 30 dBm using 4 UAVs.

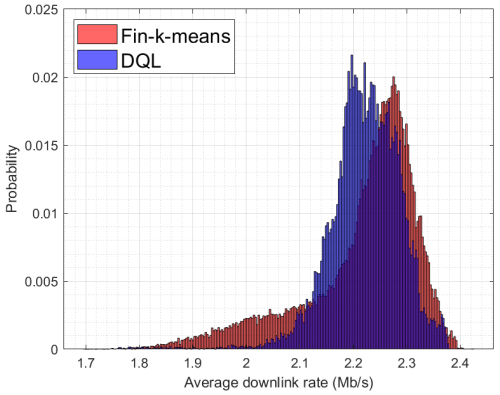

(e) Average downlink rate of 35 dBm using 2 UAVs.

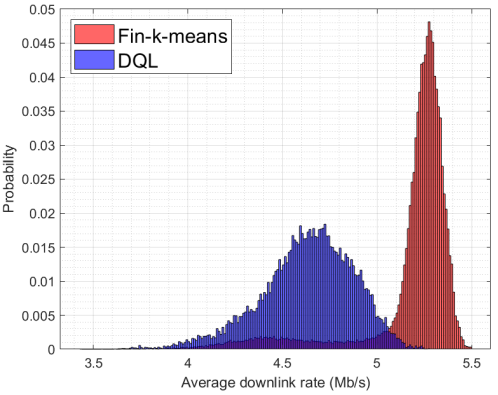

(f) Average downlink rate of 35 dBm using 4 UAVs.

Figure 4.10: The probability distribution of average downlink rate for different transmission power with different number of UAVs in a 1 km by 1 km target area.

but DQL is better at the lower end of downlink rate. Also, it could be found that increasing the number of UAVs can improve the overall performance significantly and immediately. Nevertheless, it is quite complex and expensive to deploy a large number of UAVs to provides communication coverage to GUs in a relatively large target area. Hence, we will focus on how two different deployment methods operate in a relatively small target area but with a limited number of UAVs in the following investigations.

In Figure 4.11, two UAVs are operating in a square target area with the length of 200 m. Figure 4.11 shows two kinds of rates as defined in (4.12) and (4.13) for the Fin-k-means and the DQL schemes. The performance of DQL is indicated by "DQL-x m/s", here, x represents the speed value of GUs in m/s. It could be found in both cases that the speed of GUs has no great impact on the average downlink transmission rate. It is worth noting that we choose the Fin-k-means as the benchmark for a fair comparison due to the consideration of limited UAV speed in practice. This UAV speed is identical in all scenarios, which is 20 m/s. In the Fin-k-means scenario, the occurrence of sudden-shifts is less frequent when GUs are moving slowly, therefore, the curve we select as benchmark is the scenario that all GUs are moving with a speed of 1 m/s due to the best performance it can achieve in this case. For the movement of GUs, we select the range of speed from 1 m/s to 25 m/s.

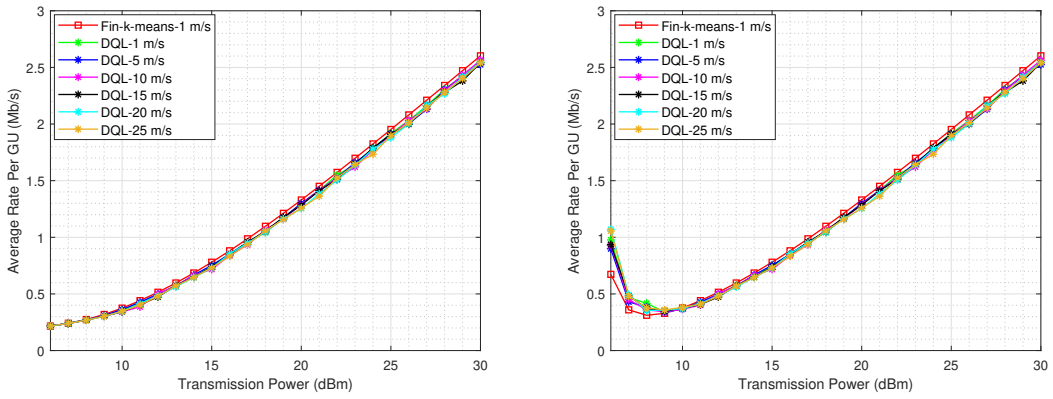

(a) Actual average rate per GU.

(b) Valid average rate per GU.

Figure 4.11: Comparison of the average downlink transmission rate.

From Figure 4.11, all those curves under different GU speed conditions are very close to that of Fin-k-means, when the speed of UAVs is held constant for both Fin-k-means and DQL cases. With the increase of transmission power, the valid average downlink rate would improve. However, for the low transmission power scenario (5 dBm to 10 dBm), due to the small number of GUs that are associated with UAVs, they have more bandwidth resources than that of fully associated GUs with high transmission power. As mentioned before, the limited bandwidth resources will be allocated to GUs equally. Furthermore, only a small amount of GUs are able to successfully associate with UAVs in the scenario of lower transmission power. Therefore, the bandwidth

resources allocated to each user are more than that of higher transmission power. Thus the valid downlink rate goes down and up in the range $6 \sim 10$ dBm.

Figure 4.12 shows the outage probability of GUs which is calculated as the number of outage GUs divided by the total number of GUs in the target area. The DQL based deployment of UAVs are always located at the center of the divided grid cell in the target area, Hence, it is not as flexible as the k-means method that can be deployed at any point in the given target area. In other words, the UAVs of the DQL based scheme would cover fewer GUs than that of the Fin-k-means, since a small difference of position would cause more outages at low transmission power and the DQL method cannot be flexibly deployed, which leads to a deviation most of the time. Similarly, the speed of GUs affects the outage slightly, because DQL considers at which grid cell (location) the UAV can cover most of the GUs most of the time. The important factor here is the density of GUs. If we just focus on a unit area within one time slot, some GUs may walk out while some GUs will walk in, and thus the speed will not affect the outage significantly. Hence, it forms a dynamic balance that gives a stable user distribution.

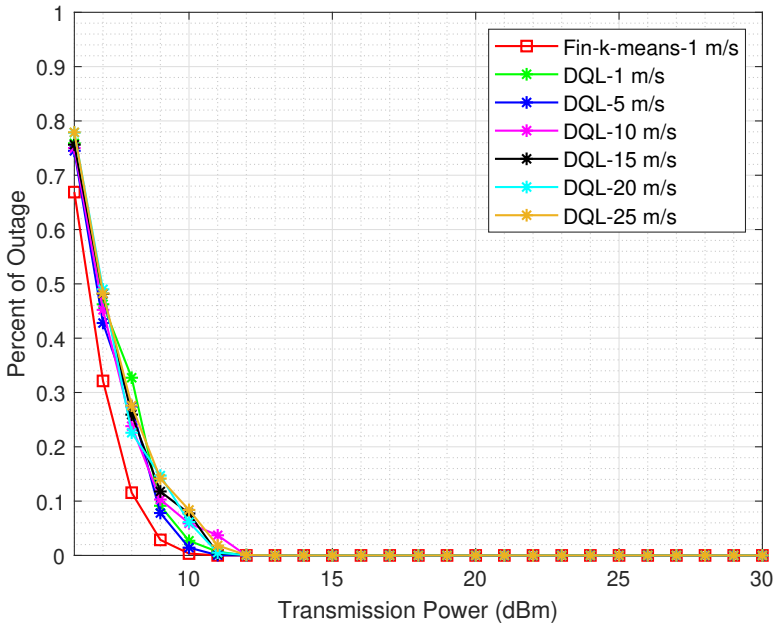

Figure 4.12: Comparison of the outage of GUs.

In Figure 4.13, we show how the number of GUs affects the performance of the average downlink rate per GU, where we choose 5 different power values to represent a different stage of transmission power. Here, the legend is different from that of Figure 4.11 and 4.12. The legend is indicated by "DQL-x" and x represents the number of GUs in the given target area. Also, the Fin-k-means-100 used here consider 100 GUs in the target area as a lower bound and all other parameters are the same. All GUs are assumed to move at 1 m/s and UAVs are working at the speed up to 20 m/s in a 200

m by 200 m area. For the low transmission power scenario (6 dBm to 15 dBm), only a small number of can successfully connected to UAVs, although the limited bandwidth resources will be allocated to GUs equally as aforementioned, it still makes no big difference on the rate. However, with the increase of transmission power scenario, more and more GUs can connect to UAVs. Therefore, the bandwidth resources will finally all be equally allocated to GUs and the average rate of each GU can be improved. Nevertheless, increasing the number of GUs also results in a reduced bandwidth allocated to each user, thus the transmission rate will decrease as the number of GUs increases, when the transmission power is the same. Furthermore, the performance of DQL and that of Fin-k-means are very close under the same transmission power condition.

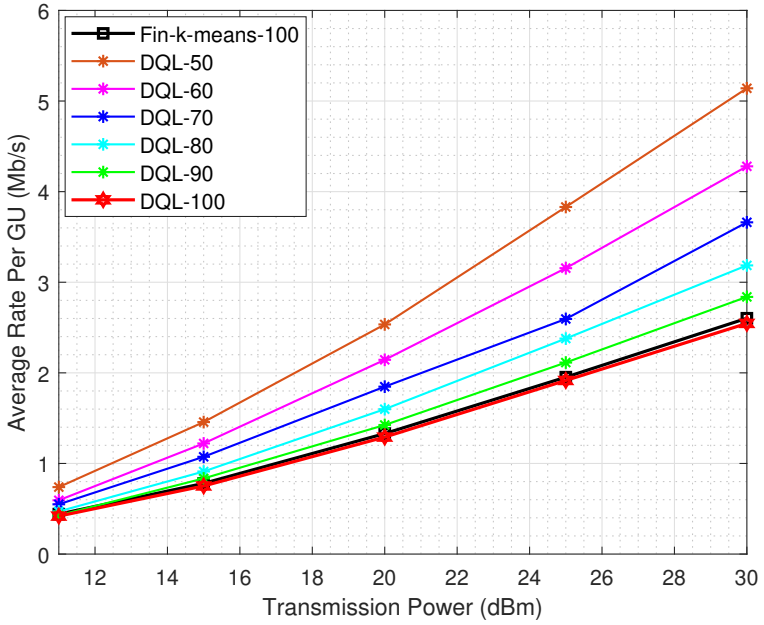

Figure 4.13: Comparison of average downlink transmission rate with different number of GUs.

4.5 Conclusion

In this chapter, we proposed a deep reinforcement learning based algorithm, which enables multiple UAVs in a target area to automatically update their locations according to the distribution of moving GUs. Firstly, to achieve a global optimal QoS for all GUs, by exchanging GUs among different UAVs, an optimal association algorithm has been designed to fix the issue of "outliers" that could occur in the traditional greedy association method. Besides, the issue of collision in multiple UAVs systems could cause a performance degradation in the system, so a four-level criterion has been developed to classify the degree of collision and transform it into the penalty of our DQL system for avoiding the collision. The simulation results show that our proposed system has a

close performance when compared with the k-means clustering method. The k-means clustering can find the centroids of each group of GUs and deploy UAVs at that position, however, it is impractical to do so in reality due to the limited speed of UAVs and high probability of sudden-shifts. Hence, by keep interacting with the environment, our proposed DQL algorithm can find an appropriate position to cover most of the GUs with more stable communication links and to improve the QoE of GUs.

Chapter 5

Low-Complexity Energy-Efficient Aerial Communication Platforms

5.1 Introduction

In Chapter 3 and 4, the UAVs are employed as flying BS to serve GUs in a target area. More explicitly, the memory resource of UAVs has been exploited to realise caching-enabled flying BSs in Chapter 3, which could largely reduce the latency of data transmission. While in Chapter 3, a deep reinforcement learning based deployment schemes has been proposed against the sudden-shift issue of deployment by classic k-means clustering algorithm. However, the limited energy onboard is another factor that restricts the application of UAVs. Therefore, the energy consumption of UAVs is considered from the aspect of wireless communication to reduce the power consumption during data transmission.

In this chapter, UAVs are still considered as flying BSs to increase the probability of having LoS communication links. Meanwhile, in order to support multiple GUs simultaneously and alleviate the performance degradation caused by the multipath channel fading of the NLoS propagation, we employ OFDMA techniques [232, 308]. Furthermore, due to the power limitation of UAVs, it is important to design energy-efficient transmission schemes, and hence we combine the concept of IM with UAV communications to establish an IM-UAV communication system, which treats the activated UAV as index to separately send data bits by conventional data symbols and using the index information. Besides, the deployment of UAVs will also affect the QoS of GUs, hence we propose a gradient descent based deployment algorithm to maximize the sum rate of GUs in the target area. Moreover, the optimal maximum likelihood detection that can provide the best BER performance, requires a high detection complexity. Consequently, a low-complexity detection scheme is required to reduce the detection computational complexity at the receiver side.

The rest of this chapter is organized as follows. In Section 5.2, we present the system model of proposed IM-UAV communication system, Afterwards, we analyze our simulation results in Section 5.3 followed by our conclusions in Section 5.4.

5.2 System Model

In this chapter, we consider a UAV-assisted downlink communication network in a target area, where N_d UAVs are deployed to operate as aerial BSs and each equipped with one transmitter (Tx) antenna to provide wireless communication services to GUs in this area as shown in Figure 5.1. We assume that these N_d UAVs are capable of flying horizontally and hovering at a certain altitude of h_d [266]. In this scenario, UAVs can periodically exchange their location information by air to air (A2A) communciation links [302, 303]. Meanwhile, both OFDMA and SM techniques have been employed to support the A2G communication links between UAVs and GUs simultaneously, as will be detailed later. In the conventional SM, a set of information bits is mapped to a

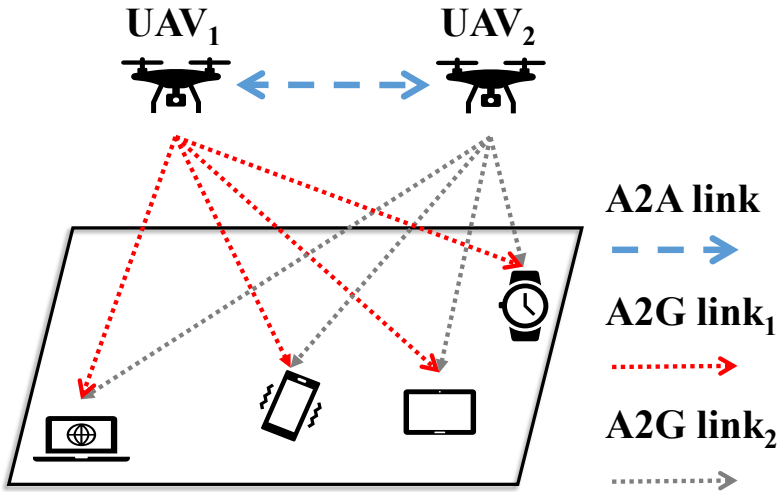

Figure 5.1: UAV-assisted network model that provides service of wireless communication for GUs.

constellation symbol and a spatial symbol. The spatial symbol is utilized to select one combination of activated transmit antennas from all possible combinations at each time slot. Here, the actual combination of active transmit antennas depends on the random incoming data bits [237]. However, in our proposed IM-UAV system, the function of the index bits is different as detailed in the following section. Since OFDMA is implemented in our system to realise multi-user communication, the bandwith resources is divided into small units (subcarriers), which are assigned to GUs according to their real-time requirements [309, 310, 311]. In the proposed system, the indices are utilised to select the UAVs that will be used to modulate the constellation symbols onto those pre-allocated subcarriers.

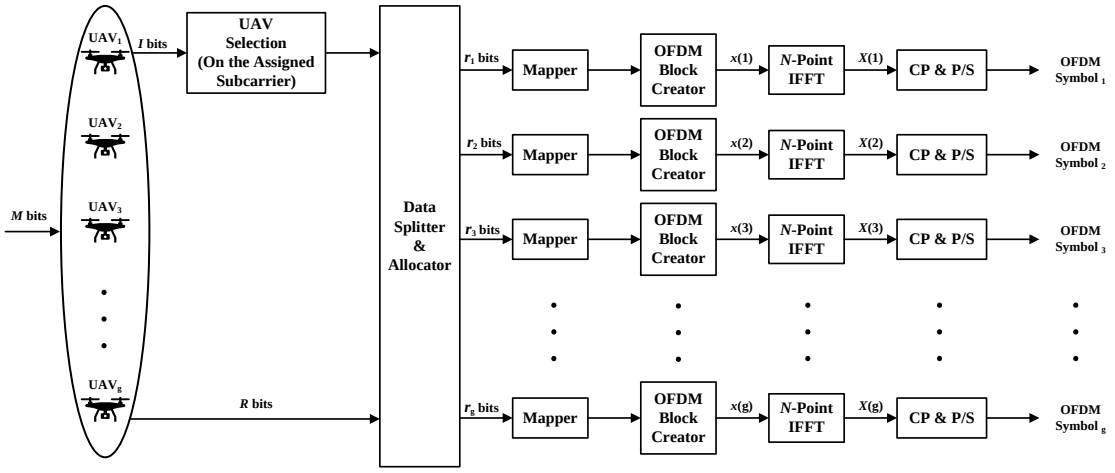

Figure 5.2: Block diagram of the IM-UAV transmitter.

As shown in Figure 5.2, all GUs are served by all UAVs in our system and each GU will be assigned their corresponding subcarrier by using OFDMA scheme. Firstly, the $\boldsymbol{M}$ incoming data bits of all GUs are shared by all UAVs, which will be divided into two parts: the index part that has $\boldsymbol{I}$ bits used to select the transmitting UAVs per subcarrier and the remaining $\boldsymbol{R}$ data bits are used to map to the conventional modulation symbols, such as quadrature phase-shift keying (QPSK). Since all the UAVs are working together to serve all the GUs, the UAVs will use these $\boldsymbol{I}$ bits to correspondingly activate themselves on the assigned subcarriers of the GUs. Then, according to those activated UAVs on the assigned subcarriers, the remaining $\boldsymbol{R}$ bits will be split and mapped onto constellation symbols as shown in Figure 5.2. It is worth noting that the number of constellation symbols assigned to each UAV can be different but the total number of bits transmitted satisfy the constraint:

$$\boldsymbol{R} = \boldsymbol{r}_1 + \boldsymbol{r}_2 + \boldsymbol{r}_3 + \ldots + \boldsymbol{r}_g, \tag{5.1}$$

where g is the number of UAVs and $\boldsymbol{r}_g$ corresponds to the bits transmitted from the g^{th} UAV. Afterwards, each UAV will generate a OFDM block based on its assigned constellation symbols. After this point, each frequency domain OFDM symbol $\boldsymbol{x}(i)$ will be transferred to time domain block $\boldsymbol{X}(i)$ using the inverse fast Fourier transform (IFFT) as depicted in Figure 5.2, where $i \in [1, 2, \ldots, g]$. At the output of the IFFT, cyclic prefix (CP) is appended to each OFDM block [312]. It is worth noting that all these aforementioned steps happen at all UAVs in our system as depicted in Figure 5.2.

In the following, we will explain the "OFDM block creator" processing of Figure 5.2 in the transmitter of the proposed IM-UAV system using the example shown in Figure 5.3. In this specific example, we consider employing 4 UAVs and 8 subcarriers indicated by the boxes in Figure 5.3. For simplicity, we assume that each GU is assigned one subcarrier, thus, totally 8 GUs are served by all 4 UAVs. In this case, only one UAV is activated at a time in the frequency domain. Hence, 2 bits are required for the selection of UAVs.

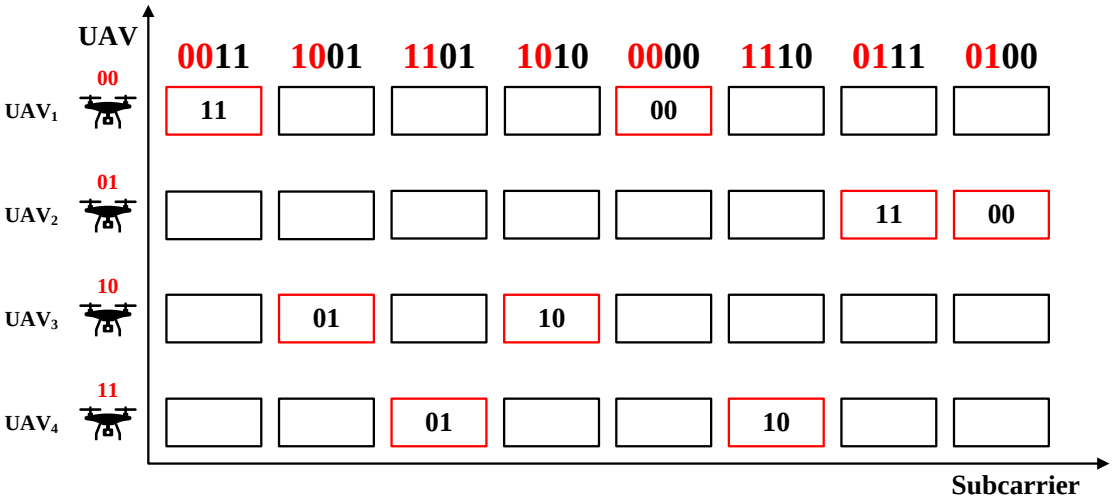

Figure 5.3: Illustration of the IM-UAV block creator using 4 UAVs, 8 RUs and QPSK modulation scheme in the frequency domain.

Additionally, we assume data symbols are modulated using QPSK. Therefore, totally 4 bits are needed for the selection of UAV and the modulation of data symbols for each subcarrier. Here, we assume the incoming information bits requested by each GU on their assigned subcarriers are $(0011, 1001, 1101, 1010, 0000, 1110, 0111, 0100)$[1] and all these information will be shared by A2A links among all UAVs to control the modulation scheme [302, 303]. As shown in Figure 5.3, each UAV is indexed by binary number sequence. Besides, the first two bits of each data bits block marked by red color are used to select one of the UAVs. In each column of boxes, only the corresponding box of the activated UAV is outlined by red. For instance, the data for the first GU in the above example is "0011". Here, we have "00" to indicate the UAV index and "11" for the symbol, which means the first subcarrier is occupied by the first UAV and the following two data bits "11" will be mapped to their constellation symbols and carried by this subcarrier. Again, the four boxes in each column in the illustration of Figure 5.3 are to indicate which UAV will occupy this subcarrier. Afterwards, each UAV has its own OFDM block in the frequency domain followed by the classical OFDM procedures [5]. In the following, we will present the channel model followed by the deployment of IM-UAV communication and then a modified power consumption model and a low-complexity detection scheme will be presented.

5.2.1 Channel Model

Given that the UAVs are considered as aerial BSs to serve GUs, the communication between GUs and UAVs is in strong LoS propagation environment [290]. The strong LoS is usually considered as a cause of low rank channel matrix in MIMO communication system, which brings correlation among MIMO channels, which reduces the capability

[1]Here, each four-bit sequence corresponds to one GU.

of supporting multiple parallel data streams. However, those aerial BSs or UAVs are separately deployed in a target area and it gives enough space to reduce the correlations. According to [298], the channel is largely determined by the distance between the transmitter (UAV) and the receiver (GU) in a LoS environment, since the UAVs are usually separately deployed when in operation and hence the distances from each UAV to the same GU end is different most of the time. Therefore, this will lead to phase differences between different channels as will be detailed in the following. In other words, the receiver side is able to clearly distinguish between different signals from different UAVs.

We consider a downlink MIMO scenario, where each UAV is equipped with one Tx antenna and totally $N_t = N_d$ antennas employed at the transmitter side, which is comprised on the joint UAVs forming a virtual MIMO. Also, N_r receiver (Rx) antennas are employed at each GU and a frequency-flat channel is assumed on the subcarriers due to the OFDMA technique [5]. Hence, the received signal in the frequency domain can be expressed as [313]:

$$\boldsymbol{y} = \sqrt{P_t}\boldsymbol{H}\boldsymbol{x} + \boldsymbol{v}, \tag{5.2}$$

where $\boldsymbol{x}$ denotes the N_t-dimensional transmitted symbol vector, while $\boldsymbol{y}$ denotes the N_r-dimensional received symbol vector. $\boldsymbol{H}$ indicates the $N_r \times N_t$ channel matrix, where each element $|h_{ij}|^2 = 1$ for $i = 1, 2, \ldots, N_r$ and $j = 1, 2, \ldots, N_t$. $\boldsymbol{v}$ is the N_r-dimensional independent identically distributed (i.i.d) zero-mean complex Gaussian noise vector with covariance matrix $\boldsymbol{I}_{N_r}$. P_t is the achievable transmission power at each Tx antenna over a transmission interval.

The Rician MIMO channel is employed in our A2G communication as it decomposes the channel into two parts [314]: deterministic LoS component $\boldsymbol{H}_{\text{LoS}}$ and stochastic NLoS component $\boldsymbol{H}_{\text{NLoS}}$. The NLoS component is used for scattered multipath propagation of signals and the Rician K factor is the ratio of the power of the two components [269]. Hence, the channel matrix $\boldsymbol{H}$ is given by:

$$\boldsymbol{H} = \sqrt{\frac{K}{K+1}} \cdot \boldsymbol{H}_{\text{LoS}} + \sqrt{\frac{1}{K+1}} \cdot \boldsymbol{H}_{\text{NLoS}}. \tag{5.3}$$

Accordingly, in the condition of A2G transmission in our UAV-aided communication system, a relatively large value of K, which ranges from 0.51 to 6.31 [294], will be considered to generate a LoS-dominant channel. The LoS component of $\boldsymbol{H}$ is determined by the LoS distances between the UAV and the GU. A model with 1 Tx antenna and N_r Rx antennas is illustrated by Figure 5.4, where the vertical distance from air to ground is h_d and the coordinate of the Tx antenna is assumed to be (x_t, y_t, h_d). Besides, the Rx antennas at the GU on the ground is considered as a uniform linear array (ULA) [315], which means all antennas are uniformly distributed with an interval of $\frac{\lambda}{2}$ where λ is the wavelength of the carrier. For simplicity, we assume that the coordinate of the first Rx antenna is (x_r, y_r) as the height of Rx antenna is negligible compared with the A2G

distance. As depicted by Figure 5.4, the coordinates of the n_r^{th} Rx antenna can be represented by $(x_r + \frac{\lambda(n_r-1)}{2}, y_r)$, where $n_r \in [1, 2, \ldots, N_r]$ is the index of the Rx antenna.

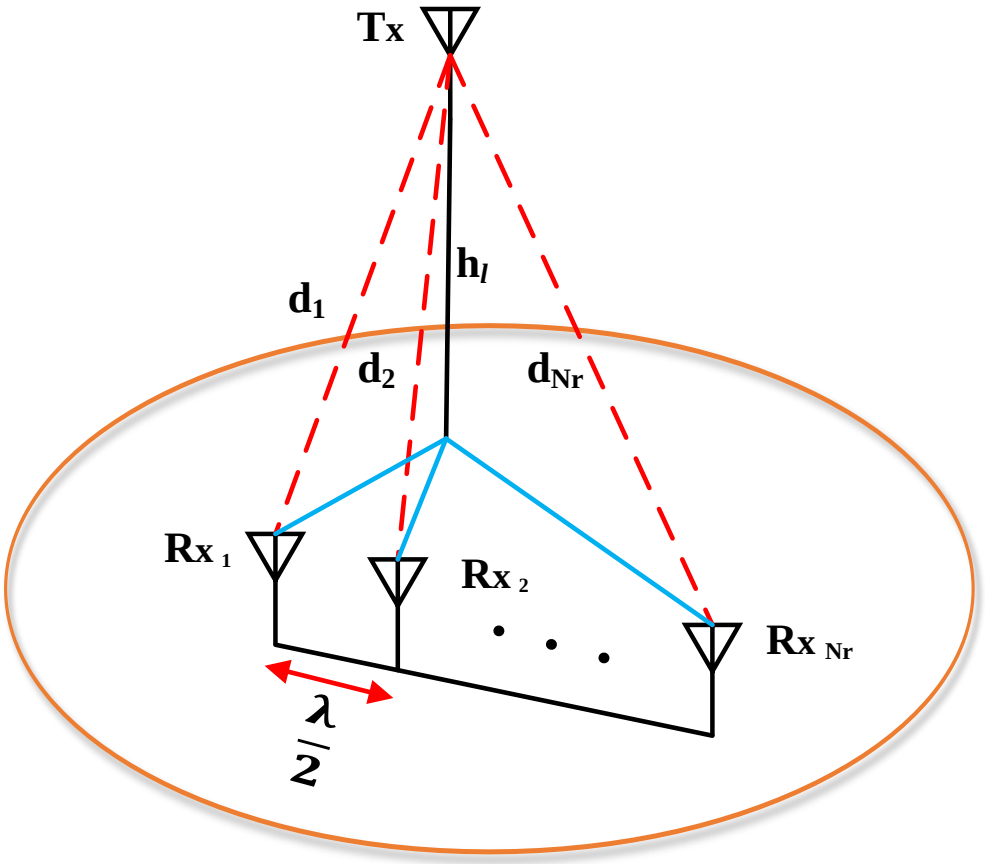

Figure 5.4: Illustration of A2G distances with one aerial Tx antenna and N_r ground Rx antennas of a ULA.

Finally, the distance between the Tx antenna and the n_r^{th} Rx antenna is given by:

$$d_{n_r} = \sqrt{(x_t - x_r - \frac{\lambda(n_r-1)}{2})^2 + (y_t - y_r)^2 + h_d^2}. \tag{5.4}$$

The LoS component vector in this example from the UAV antenna can be expressed by [298]:

$$\boldsymbol{H}_{\text{LoS}} = \left[e^{-j\frac{2\pi}{\lambda}d_1}, e^{-j\frac{2\pi}{\lambda}d_2}, \ldots, e^{-j\frac{2\pi}{\lambda}d_{N_r}}\right]^T, \tag{5.5}$$

where $(\cdot)^T$denotes the transpose. Afterwards, the NLoS part of the channel $\boldsymbol{H}_{\text{NLoS}}$ is caused by multipath propagation, which can be described by Rayleigh fading channel. Therefore, the channel $\boldsymbol{H}$ in (5.3) can be obtained by adding the LoS part and the NLoS part together, while the K factor that indicates the ratio between them is used to describe the channel condition.

Besides, the path loss is commonly considered in A2G communication system, which is closely linked with the environment, where the Tx and Rx are operating [270, 316]. In general, the propagation path loss P_l is expressed by [271]:

$$P_l = \left(\frac{4\pi}{\lambda}\right)^2 d^{\alpha}, \tag{5.6}$$

where d is the distance between the Tx and Rx, the path loss exponent α ranges from 2 to 6 and the free space wavelength $\lambda = \frac{c}{f_c}$ is defined as the ratio of the speed of light c in m/s to the carrier frequency f_c in Hz. Therefore, the received signal power P_r given a transmission power P_t is formulated by [272]:

$$P_r = \frac{P_t}{P_l} = P_t \left(\frac{c}{4\pi f_c}\right)^2 \left(\frac{1}{d}\right)^{\alpha}. \tag{5.7}$$

In our IM-UAV communication system, the UAVs are considered to work at a height of 100 m [273] and the LoS communication links are assumed to exist for most of the time [290]. Hence, free space path loss exponent $\alpha = 2$ is chosen to describe the signal attenuation [44] and P_r is transformed to:

$$P_r = P_t \left(\frac{c}{4\pi d f_c}\right)^2. \tag{5.8}$$

Additionally, the transmission scheme in our proposed IM-UAV communication network is a downlink MIMO system with distributed Tx antennas as we assume each UAV will use one TX antenna to transmit data symbols simultaneously in each transmission interval. Therefore, the signal $\boldsymbol{y}$ received by one GU is given by:

$$\boldsymbol{y} = \sqrt{\boldsymbol{P}_r}\boldsymbol{H}\boldsymbol{x} + \boldsymbol{v}, \tag{5.9}$$

where the signal power $\boldsymbol{P}_r$ at the receiver side is a diagonal matrix in the form of:

$$\boldsymbol{P}_r = \begin{bmatrix} p_{r1} & 0 & \cdots & 0 \\ 0 & p_{r2} & \cdots & 0 \\ \vdots & \vdots & \ddots & \vdots \\ 0 & 0 & \cdots & p_{rN_t} \end{bmatrix}. \tag{5.10}$$

5.2.2 UAV Deployment for the IM-UAV Communication System

In a UAV-assisted communication system, it is important to utilise the maneuverability and flexibility of UAVs, which cannot be realised in traditional fixed BSs, to further improve the QoE of GUs. Therefore, we design a new deployment scheme to improve the sum rate of GUs in the context of our proposed IM-UAV communication system.

Since the channel model of our IM-UAV communication has been provided, the capacity related to this channel can be formulated. When evaluating the capacity of the conventional MIMO systems, the transmitted vector $\boldsymbol{x}$ is assumed to be a zero-mean complex Gaussian random vector [317], which is able to maximize the mutual information between the transmitted and received vectors. Additionally, the normalized transmitted vector $\boldsymbol{x}$ is subject to the power constraint [317, 318, 319]:

$$Tr\left(E\left[\boldsymbol{x}\boldsymbol{x}^H\right]\right) \leq 1, \tag{5.11}$$

where $(\cdot)^H$ denotes the conjugate transpose.

On the other hand, consider the multiple data streams defined as $\boldsymbol{s} = [s_1, s_2, \ldots, s_{N_a}]^T$ that satisfy the unity power constraint, where N_a is the number of activated UAVs, and the form of transmitted vector $\boldsymbol{x}$ is given by [320]:

$$\boldsymbol{x} = \boldsymbol{Q}\boldsymbol{s}, \tag{5.12}$$

where $\boldsymbol{Q} \in \mathbb{C}^{N_t \times N_a}$ such that $\boldsymbol{Q} \in \mathcal{Q} = \left\{\boldsymbol{Q}_1, \boldsymbol{Q}_2, \ldots, \boldsymbol{Q}_{K_{N_a}}\right\}$ and K_{N_a} depends on the structure of the activated UAVs, which is the number of all possible combinations. For example, when considering the example of employing four UAVs and activating one UAV based on the index modulation, then there are $K_{N_a} = 4$ possible combinations that can be represented by:

$$\begin{bmatrix} 1 & 0 & 0 & 0 \\ 0 & 1 & 0 & 0 \\ 0 & 0 & 1 & 0 \\ 0 & 0 & 0 & 1 \end{bmatrix}, \tag{5.13}$$

where $\{\boldsymbol{Q}_1, \boldsymbol{Q}_2, \boldsymbol{Q}_3, \boldsymbol{Q}_4\}$ correspond to the rows of (5.13). Moreover, the power constrain in (5.11) makes the $\boldsymbol{x}$ satisfy the condition:

$$Tr\left(E\left[\boldsymbol{Q}_i\boldsymbol{s}\boldsymbol{s}^H\boldsymbol{Q}_i^H\right]\right) \leq 1. \tag{5.14}$$

The matrix set $\mathcal{Q}$ can be mapped to a set of covariance matrix $\mathcal{V} = \left\{\boldsymbol{V}_1, \boldsymbol{V}_2, \ldots, \boldsymbol{V}_{K_{N_a}}\right\}$. For instance, in the case of fixed N_a number of data streams, the i^{th} covariance matrix of the transmitted vector can be written as:

$$\begin{aligned} \boldsymbol{V}_i &= E\left[\boldsymbol{x}\boldsymbol{x}^H | \boldsymbol{Q} = \boldsymbol{Q}_i\right] \\ &= E\left[\boldsymbol{Q}_i\boldsymbol{s}\boldsymbol{s}^H\boldsymbol{Q}_i^H\right] \\ &= \boldsymbol{Q}_i\boldsymbol{Q}_i^H, \end{aligned} \tag{5.15}$$

for $i = 1, 2, \ldots, K_{N_a}$, where $\boldsymbol{V}_i$ is the covariance of the transmitted vector $\boldsymbol{x}$ by assuming that $\boldsymbol{s}$ has complex Gaussian i.i.d. entries with zero mean and unit variance. This

covariance matrix $\boldsymbol{V}_i$ is related to the achievable rate, which will be used in the following section to calculate the gradient of the achievable rate and deploy the UAVs in the target area.

Based on (5.15) the lower bound of the achievable rate is given by [320]:

$$R_L^M = -\frac{1}{K_{N_a}} \log \left(\prod_{i=1}^{K_{N_a}} \left(\sum_{j=1}^{K_{N_a}} \frac{1}{\pi^{N_r} |\boldsymbol{\Sigma}_i + \boldsymbol{\Sigma}_j|} \right) \right) + \log K_{N_a} - N_r \log (\pi e), \tag{5.16}$$

where $|\cdot|$ indicates the determinant operation, $\boldsymbol{\Sigma}_i = \rho \boldsymbol{H} \boldsymbol{V}_i \boldsymbol{H}^H + \boldsymbol{I}_{N_r}$ for $i = 1, 2, \ldots, K_{N_a}$, where ρ is the signal to noise ratio and $\boldsymbol{I}_{N_r}$ is the N_r-dimensional identity matrix. It can be found that when the structure of the transmission is defined, the element which will affect R_L^M is $\boldsymbol{H}$. As stated in the previous section, the path loss has a steady and significant impact on $\boldsymbol{H}$, which is mainly determined by the distance between the Tx and the Rx. Meanwhile, the locations of the GUs affect the A2G distances, which is related to the path loss. Therefore, the gradient of the achievable rate of GUs can be obtained by taking the derivative of R_L^M with respect to the coordinates (location) of the GUs, then the value of the achievable rate can be optimized by following the gradient descent approach [321].

Firstly, the UAVs will take the derivative of R_L^M with respect to channel $\boldsymbol{H}$ based on the information of GUs location they collected. Here, since we consider a LoS dominant environment, the channel condition or the received signal power is largely dependent on the distance between GUs and UAVs. Even if there is a small NLoS component existing in the channel, we cannot exactly find the relation between the distance and the received signal as it is totally random and uncontrollable. Therefore, we take the derivative of $\boldsymbol{H}_{\text{LoS}}$ instead of $\boldsymbol{H}$. Then, in the rest of this section we use $\boldsymbol{H}$ to denote the LoS component. Here, the derivative of $\boldsymbol{H}$ with respect to the A2G distance $\boldsymbol{D}$ between the UAVs and the GUs will be obtained. Afterwards, the derivative of $\boldsymbol{D}$ with respect to the coordinates (location) of UAVs will be calculated. Finally, the derivative of R_L^M with respect to the coordinates (location) of UAVs can be obtained based on the chain rule.

Then, the derivative of R_L^M with respect to $\boldsymbol{H}$ can be obtained as:

$$\begin{aligned} d\left(R_L^M\right) &= -K_M^{-1} d\left[\log\left(\prod_{i=1}^{K_{N_a}}\left(\sum_{j=1}^{K_{N_a}}\frac{1}{\pi^{N_r}|\boldsymbol{\Sigma}_i+\boldsymbol{\Sigma}_j|}\right)\right)\right] \\ &= -K_{N_a}^{-1}\sum_{i=1}^{K_{N_a}}\frac{d\left(\sum_{j=1}^{K_{N_a}}|\boldsymbol{\Sigma}_i+\boldsymbol{\Sigma}_j|^{-1}\right)}{\sum_{j=1}^{K_{N_a}}|\boldsymbol{\Sigma}_i+\boldsymbol{\Sigma}_j|^{-1}} \\ &= -K_{N_a}^{-1}\sum_{i=1}^{K_{N_a}}\frac{\sum_{j=1}^{K_{N_a}}\left[-|\boldsymbol{\Sigma}_i+\boldsymbol{\Sigma}_j|^{-2}d\left(|\boldsymbol{\Sigma}_i+\boldsymbol{\Sigma}_j|\right)\right]}{\sum_{j=1}^{K_{N_a}}|\boldsymbol{\Sigma}_i+\boldsymbol{\Sigma}_j|^{-1}}, \end{aligned} \tag{5.17}$$

where it can be shown that we only need to calculate the derivative of $|\boldsymbol{\Sigma}_i+\boldsymbol{\Sigma}_j|$ with respect to $\boldsymbol{H}$ if we would like to figure out the derivative of R_L^M with respect to $\boldsymbol{H}$. Therefore, take $\boldsymbol{\Sigma}_i = \rho\boldsymbol{H}\boldsymbol{V}_i\boldsymbol{H}^H + \boldsymbol{I}_{N_r}$ into $|\boldsymbol{\Sigma}_i+\boldsymbol{\Sigma}_j|$ and the derivative of $|\boldsymbol{\Sigma}_i+\boldsymbol{\Sigma}_j|$ with respect to $\boldsymbol{H}$ can be obtained as:

$$\begin{aligned} \frac{\partial|\boldsymbol{\Sigma}_i+\boldsymbol{\Sigma}_j|}{\partial\boldsymbol{H}} &= \frac{\partial|\rho\boldsymbol{H}\left(\boldsymbol{V}_i+\boldsymbol{V}_j\right)\boldsymbol{H}^H+2\boldsymbol{I}_{N_r}|}{\partial\boldsymbol{H}} \\ &= \frac{\partial|\boldsymbol{H}\left(\boldsymbol{V}_i+\boldsymbol{V}_j\right)\boldsymbol{H}^H|}{\partial\boldsymbol{H}}, \end{aligned} \tag{5.18}$$

where the symbol ∂ is used to denote partial derivative. Besides, the coefficient ρ and the identity matrix $\boldsymbol{I}_{N_r}$ can be neglected as they are constant.

Please note that $\boldsymbol{H}$ is a complex matrix, and hence, the derivative of $|\boldsymbol{\Sigma}_i+\boldsymbol{\Sigma}_j|$ is related to the real part and the imaginary part of $\boldsymbol{H}$. Consequently, the derivative of $|\boldsymbol{\Sigma}_i+\boldsymbol{\Sigma}_j|$ with respect to $\boldsymbol{H}$ is given based on the rule of complex derivative in [322]:

$$\begin{aligned} \frac{\partial|\boldsymbol{\Sigma}_i+\boldsymbol{\Sigma}_j|}{\partial\boldsymbol{H}} &= \left(\frac{\partial|\boldsymbol{H}\left(\boldsymbol{V}_i+\boldsymbol{V}_j\right)\boldsymbol{H}^H|}{2\partial\Re\boldsymbol{H}} - i\frac{\partial|\boldsymbol{H}\left(\boldsymbol{V}_i+\boldsymbol{V}_j\right)\boldsymbol{H}^H|}{2\partial\Im\boldsymbol{H}}\right) \\ &= |\boldsymbol{\Sigma}_i+\boldsymbol{\Sigma}_j|\left[\left(\boldsymbol{V}_i+\boldsymbol{V}_j\right)\boldsymbol{H}^H\left(\boldsymbol{\Sigma}_i+\boldsymbol{\Sigma}_j\right)^{-1}\right]^T, \end{aligned} \tag{5.19}$$

and the complex conjugate derivative yields:

$$\begin{aligned} \frac{\partial|\boldsymbol{\Sigma}_i+\boldsymbol{\Sigma}_j|}{\partial\boldsymbol{H}^*} &= \left(\frac{\partial|\boldsymbol{H}\left(\boldsymbol{V}_i+\boldsymbol{V}_j\right)\boldsymbol{H}^H|}{2\partial\Re\boldsymbol{H}} + i\frac{\partial|\boldsymbol{H}\left(\boldsymbol{V}_i+\boldsymbol{V}_j\right)\boldsymbol{H}|}{2\partial\Im\boldsymbol{H}}\right) \\ &= |\boldsymbol{\Sigma}_i+\boldsymbol{\Sigma}_j|\left[\left(\boldsymbol{\Sigma}_i+\boldsymbol{\Sigma}_j\right)^{-1}\boldsymbol{H}\left(\boldsymbol{V}_i+\boldsymbol{V}_j\right)\right], \end{aligned} \tag{5.20}$$

where $\Re$ and $\Im$ refer to the real and imaginary parts. Finally, the derivative of R_L^M with respect to $\boldsymbol{H}$ is given by:

$$\frac{\partial R_L^M}{\partial\boldsymbol{H}} = K_{N_a}^{-1}\sum_{i=1}^{K_{N_a}}\frac{\sum_{j=1}^{K_{N_a}}|\boldsymbol{\Sigma}_i+\boldsymbol{\Sigma}_j|^{-2}\left[\frac{\partial|\boldsymbol{\Sigma}_i+\boldsymbol{\Sigma}_j|}{\partial\boldsymbol{H}}+\frac{\partial|\boldsymbol{\Sigma}_i+\boldsymbol{\Sigma}_j|}{\partial\boldsymbol{H}^*}\right]}{\sum_{j=1}^{K_{N_a}}|\boldsymbol{\Sigma}_i+\boldsymbol{\Sigma}_j|^{-1}}. \tag{5.21}$$

Afterwards, we can calculate the derivative of $\boldsymbol{H}$ with respect to distance $\boldsymbol{D}$. Firstly, the channel matrix $\boldsymbol{H}$ is in the form of:

$$\boldsymbol{H} = \begin{bmatrix} h_{11} & h_{12} & \cdots & h_{1N_t} \\ h_{21} & h_{22} & \cdots & h_{2N_t} \\ \vdots & \vdots & \vdots & \vdots \\ h_{N_r1} & h_{N_r2} & \cdots & h_{N_rN_t} \end{bmatrix}, \tag{5.22}$$

and the corresponding distance matrix is given by:

$$\boldsymbol{D} = \begin{bmatrix} d_{11} & d_{12} & \cdots & d_{1N_t} \\ d_{21} & d_{22} & \cdots & d_{2N_t} \\ \vdots & \vdots & \vdots & \vdots \\ d_{N_r1} & d_{N_r2} & \cdots & d_{N_rN_t} \end{bmatrix}, \tag{5.23}$$

where h_{ij} and d_{ij} represent the channel and the distance from the j^{th} Tx antenna to the i^{th} Rx antenna, respectively, for $i = 1, 2, \ldots, N_r$ and $j = 1, 2, \ldots, N_t$. Hence, the derivative of $\boldsymbol{H}$ with respect to $\boldsymbol{D}$ can be calculated by the point-to-point derivative because only the corresponding d_{ij} of $\boldsymbol{D}$ is related to h_{ij} in $\boldsymbol{H}$ and the derivative of $\boldsymbol{H}$ with respect to $\boldsymbol{D}$ is in the form of:

$$\frac{\partial \boldsymbol{H}}{\partial \boldsymbol{D}} = \begin{bmatrix} \frac{\partial h_{11}}{\partial d_{11}} & \frac{\partial h_{12}}{\partial d_{12}} & \cdots & \frac{\partial h_{1N_t}}{\partial d_{1N_t}} \\ \frac{\partial h_{21}}{\partial d_{21}} & \frac{\partial h_{22}}{\partial d_{22}} & \cdots & \frac{\partial h_{2N_t}}{\partial d_{2N_t}} \\ \vdots & \vdots & \vdots & \vdots \\ \frac{\partial h_{N_r1}}{\partial d_{N_r1}} & \frac{\partial h_{N_r2}}{\partial d_{N_r2}} & \cdots & \frac{\partial h_{N_rN_t}}{\partial d_{N_rN_t}} \end{bmatrix}. \tag{5.24}$$

Recall that the path loss has to be considered in our A2G communication links. So, the element h_{ij} of $\boldsymbol{H}$ including the path loss can be obtained using (5.5) and (5.9), and is given by:

$$h_{ij} = \sqrt{P_r} e^{-j\frac{2\pi}{\lambda} d_{ij}}. \tag{5.25}$$

Hence, the element $\frac{\partial h_{ij}}{\partial d_{ij}}$ of $\frac{\partial \boldsymbol{H}}{\partial \boldsymbol{D}}$ is calculated by:

$$\frac{\partial h_{ij}}{\partial d_{ij}} = \sqrt{P_r} e^{-j\frac{2\pi}{\lambda} d_{ij}} \left[-\frac{\alpha}{d_{ij}} - j\frac{2\pi}{\lambda} \right], \tag{5.26}$$

and the complex conjugate derivative yields:

$$\frac{\partial h_{ij}^*}{\partial d_{ij}} = \sqrt{P_r} e^{j\frac{2\pi}{\lambda} d_{ij}} \left[-\frac{\alpha}{d_{ij}} + j\frac{2\pi}{\lambda} \right]. \tag{5.27}$$

Then, as the height of UAVs is fixed to h_d and each UAV has only one Tx antenna, the coordinate matrix $\boldsymbol{P}_d$ of the UAVs can be represented by:

$$\boldsymbol{P}_d = \begin{bmatrix} P_{d_1} \\ P_{d_2} \\ \vdots \\ P_{d_{N_d}} \end{bmatrix} = \begin{bmatrix} x_{d_1} & y_{d_1} \\ x_{d_2} & y_{d_2} \\ \vdots & \vdots \\ x_{d_{N_d}} & y_{d_{N_d}} \end{bmatrix}. \tag{5.28}$$

Additionally, the coordinate matrix $\boldsymbol{P}_u$ representing the coordinates of the Rx antennas of the u^{th} GU is given by:

$$\boldsymbol{P}_u = \begin{bmatrix} P_{u_1} \\ P_{u_2} \\ \vdots \\ P_{u_{N_r}} \end{bmatrix} = \begin{bmatrix} x_{u_1} & y_{u_1} \\ x_{u_2} & y_{u_2} \\ \vdots & \vdots \\ x_{u_{N_r}} & y_{u_{N_r}} \end{bmatrix}. \tag{5.29}$$

Then, the derivative of $\boldsymbol{D}$ with respect to $\boldsymbol{P}_d$ can be calculated by:

$$\frac{\partial \boldsymbol{D}}{\partial \boldsymbol{P}_d} = \begin{bmatrix} \frac{\partial d_{11}}{\partial P_{d_1}} & \frac{\partial d_{11}}{\partial P_{d_2}} & \cdots & \frac{\partial d_{11}}{\partial P_{d_{N_d}}} \\ \frac{\partial d_{21}}{\partial P_{d_1}} & \frac{\partial d_{21}}{\partial P_{d_1}} & \cdots & \frac{\partial d_{21}}{\partial x_{P_{N_d}}} \\ \vdots & \vdots & \vdots & \vdots \\ \frac{\partial d_{N_r N_d}}{\partial P_{d_1}} & \frac{\partial d_{N_r N_d}}{\partial P_{d_1}} & \cdots & \frac{\partial d_{N_r N_d}}{\partial P_{d_{N_d}}} \end{bmatrix}, \tag{5.30}$$

while the element $\frac{\partial d_{ij}}{P_{d_{n_d}}}$ for $n_d = 1, 2, \ldots, N_d$ is calculated based on (5.4), and can be expressed by:

$$\begin{aligned} \frac{\partial d_{ij}}{P_{d_{n_d}}} &= \frac{\begin{bmatrix} x_{d_{n_d}} - x_{u_{n_r}} & y_{d_{n_d}} - y_{u_{n_r}} \end{bmatrix}}{\sqrt{(x_{d_{n_d}} - x_{u_{n_r}})^2 + (y_{d_{n_d}} - y_{u_{n_r}})^2 + h^2}} \\ &= \begin{bmatrix} \frac{x_{d_{n_d}} - x_{u_{n_r}}}{d_{ij}} & \frac{y_{d_{n_d}} - y_{u_{n_r}}}{d_{ij}} \end{bmatrix}. \end{aligned} \tag{5.31}$$

Consequently, the derivative is in the form of:

$$\frac{\partial \boldsymbol{D}}{\partial \boldsymbol{P}_d} = \begin{bmatrix} \frac{\partial d_{11}}{\partial x_{d_1}} & \frac{\partial d_{11}}{\partial y_{d_1}} & \cdots & \frac{\partial d_{11}}{\partial x_{d_{N_d}}} & \frac{\partial d_{11}}{\partial y_{d_{N_d}}} \\ \frac{\partial d_{21}}{\partial x_{d_1}} & \frac{\partial d_{21}}{\partial y_{d_1}} & \cdots & \frac{\partial d_{21}}{\partial x_{d_{N_d}}} & \frac{\partial d_{21}}{\partial y_{d_{N_d}}} \\ \vdots & \vdots & \vdots & \vdots & \vdots \\ \frac{\partial d_{N_r N_d}}{\partial x_{d_1}} & \frac{\partial d_{N_r N_d}}{\partial y_{d_1}} & \cdots & \frac{\partial d_{N_r N_d}}{\partial x_{d_{N_d}}} & \frac{\partial d_{N_r N_d}}{\partial y_{d_{N_d}}} \end{bmatrix}. \tag{5.32}$$

Finally, the derivative of R_L^M with respect to the location of the UAVs $\boldsymbol{P}_d$ can be obtained as:

$$\frac{\partial R_L^M}{\partial \boldsymbol{H}} \cdot \frac{\partial \boldsymbol{H}}{\partial \boldsymbol{D}} \cdot \frac{\partial \boldsymbol{D}}{\partial \boldsymbol{P}_d} = \frac{\partial R_L^M}{\partial \boldsymbol{P}_d}. \tag{5.33}$$

Hence, since the gradient of R_L^M of the GUs can be obtained and the locations of each UAV will be periodically updated through A2A links, the UAVs can use the gradient descent algorithm to find the position that can maximize the sum rate of all GUs. The whole procedure is summarized in Algorithm 8.

Algorithm 8 Deployment procedure of IM-UAV communication system.

1: **for** n from 1 to N_u **do**
2: Obtain the lower bound of achievable rate R_L^M
3: Take the derivative of R_L^M with respect to channel $\boldsymbol{H}_{\text{LoS}}$ using (5.21)
4: Take the derivative of $\boldsymbol{H}_{\text{LoS}}$ with respect to $\boldsymbol{D}$ according to (5.24)
5: Take the derivative of $\boldsymbol{D}$ with respect to $\boldsymbol{P}_d$ as in (5.32)
6: Obtain the derivative of R_L^M with respect to the location of UAVs $\boldsymbol{P}_d$ through chain rule using (5.33)
7: **end for**
8: Add the gradients of all N_u GUs together to get the final gradient
9: Apply gradient descent algorithm and deploy UAVs to the position when converging

5.2.3 Power Consumption Model

The performance of UAV communication system is fundamentally limited by the on-board energy. The on-board power is mainly consumed by two parts, one is used for flying, while the other is used to establish communication. The major task of this work is about the A2G communications between the UAVs and the GUs. Therefore, it is important to design an energy-efficient UAV communication scheme to reduce the energy consumed per information bit. The calculation of all energy consumed by data transmission in the UAV-assisted communication system is quite different from that in traditional communication system especially in our proposed IM-UAV communication system, since all UAVs in our IM-UAV communication system will be active all the time. For simplicity, the baseband signal processing blocks (e.g., source coding, pulse shaping and digital modulation) have been omitted [323]. Given the UAV is a power limited platform, we care more about the communication energy consumed at the Tx side (UAV) than the Rx side, and hence the energy consumption at the Rx side will not be considered in this chapter.

The total average power consumption along the signal path is composed by two main components [324]: the power consumption of the power amplifier P_a and other circuit blocks P_c. The first term P_a depends on the transmission power P_t and the power consumption of the power amplifier can be calculated by [325]:

$$P_a = \frac{P_t}{\eta}, \tag{5.34}$$

where η is the drain efficiency, which we set as 10% in our system as OFDMA is employed to support multi-user communication [326]. The second term P_c is composed by [327]:

$$P_c = P_{\text{DAC}} + P_{\text{Mix}} + P_{\text{Filt}} + P_{\text{Syn}}, \tag{5.35}$$

where P_{DAC}, P_{Mix}, P_{Filt} and P_{Syn} are the power consumption values for the digital-to-analogue converter (DAC), the mixer, the filter and the frequency synthesizer. Finally, according to the power constraint in (5.11), the total power consumed by the UAVs can be written as:

$$P_{\text{sum}} = N_a P_a + N_d P_c. \tag{5.36}$$

A binary-weighted current-steering DAC is considered in our system [328] and the power consumption of the DAC consists of two components: static power consumption P_s and dynamic power consumption P_d. Firstly, the total output current I_o of a N-bit DAC is closely related to the unit current source, which is denoted by I_u. For the i^{th} bit, totally 2^i unit current resources are needed. Thus, the total number of I_u, which is also known as code k, can be expressed by:

$$k = \sum_{i=0}^{N-1} 2^i b_i, \tag{5.37}$$

where b_i is independent binary random variables taking values of 0 or 1 with percentage of 50%. Here, b_{N-1} is the most significant bit and b_0 is the least significant bit. Therefore, the total output current is given by:

$$I_o = k I_u. \tag{5.38}$$

Consequently, the static power consumption can be calculated by:

$$P_s = V_{\text{dd}} E\left[I_o\right] = \frac{1}{2} V_{\text{dd}} I_u \left(2^N - 1\right), \tag{5.39}$$

where V_{dd} is the power supply voltage.

The dynamic power consumption occurs during the switching process (on or off) between symbols. For simplicity, we assume that each switch has the same parasitic capacitance C_p and each switch has a chance of 50% to change status during a transition. Then, the average value of P_d can be obtained by $P_d = \frac{NC_p f_s V_{\text{dd}}^2}{2}$ for the first-order approximation [329]. The sampling frequency can be approximately taken as $f_s = 2(2B + f_{\text{cor}})$ in our proposed system as we assume it is a low intermediate frequency structure, where f_{cor} is the corner frequency of the $\frac{1}{f}$ noise [325] and B is the bandwidth. Thus, the expression for P_d can be rewritten as:

$$P_d = NC_p \left(2B + f_{\text{cor}}\right) V_{\text{dd}}^2. \tag{5.40}$$

Hence, the total power consumption of the DAC is given by:

$$P_{\mathrm{DAC}} = \beta \left(P_s + P_d \right), \tag{5.41}$$

where β is a correcting factor to incorporate second-order effects. Hence, we are able to calculate the energy consumed by communication, which can be utilised to analyze EE in the following section.

5.2.4 Low-Complexity Detection

For our IM-UAV communication system, the optimal ML detection, which jointly searches all the possible transmit antenna combinations and the modulated symbols, increases exponentially in complexity with the number of UAVs and modulation levels. By contrast, both the maximal-ratio combining and the zero-forcing algorithms have very low-complexity, but their error performance is significantly worse than the ML. In order to reduce the computational complexity but also keep the BER performance satisfactory, we propose a new low-complexity detection scheme that can provide a trade-off between BER performance and complexity. The proposed low-complexity detection scheme utilizes the fact that the signals transmitted from different UAVs have different signal power at the receiver side, which typically exists in UAV-assisted communication networks, to identify signals received from different UAVs. Besides, by additionally considering the phase difference of the data symbols, the detection accuracy can be further improved.

We assume perfect channel knowledge at the GUs and that the GUs are aware of the number of activated UAVs N_a. Therefore, all possible combinations of the channels can be represented by the set:

$$\mathcal{H} = \{ \boldsymbol{h}_1, \boldsymbol{h}_2, \ldots, \boldsymbol{h}_{n_h}, \ldots, \boldsymbol{h}_{N_h} \}, \tag{5.42}$$

where N_h is the number of all channel combinations and can be calculated by:

$$N_h = \left\lfloor \log_2 \binom{N_a}{N_d} \right\rfloor, \tag{5.43}$$

where N_d it the total number of UAVs, $\lfloor \cdot \rfloor$ is the floor operation and $\binom{\cdot}{\cdot}$ stands for the binomial coefficient. For example, if we have 4 UAVs and only 3 of them are activated, the $N_h = 4$ possible combinations of the channels is shown in Table 5.1, where $\boldsymbol{h}_i$ indicates the i^{th} possible combination and h_i indicates the channel of the i^{th} UAV, for $i = 1, 2, 3, 4$.

After the FFT operation at the receiver side, all the N_h possible combinations of the transmitted signals $\hat{\boldsymbol{x}} = [\boldsymbol{x}_1, \boldsymbol{x}_2, \ldots, \boldsymbol{x}_{n_h}, \ldots, \boldsymbol{x}_{N_h}]$ in frequency domain can be obtained

Table 5.1: Example for $N_d = 4$ and $N_a = 3$.

Combinations	Corresponding block
$\boldsymbol{h}_1$	$\{h_1, h_2, h_3\}$
$\boldsymbol{h}_2$	$\{h_2, h_3, h_4\}$
$\boldsymbol{h}_3$	$\{h_1, h_2, h_4\}$
$\boldsymbol{h}_4$	$\{h_1, h_3, h_4\}$

by:

$$\boldsymbol{x}_{n_h} = \boldsymbol{h}_{n_h}^{\dagger} \boldsymbol{y}, \tag{5.44}$$

$$= \boldsymbol{x} + \boldsymbol{h}_{n_h}^{\dagger} \boldsymbol{n}, \tag{5.45}$$

$$= [S_1, S_2, \ldots, S_{n_a}, \ldots, S_{N_a}]^T, \tag{5.46}$$

where $(\cdot)^{\dagger}$ indicates the pseudo inverse operation and $(\cdot)^T$ denotes the transpose. Here, the n_h^{th} possible recovered signal $\boldsymbol{x}_{n_h}$ has a size of N_a and S_{n_a} represents the n_a^{th} data symbol of $\boldsymbol{x}_{n_h}$. Then, the Euclidean distances between the constellation symbols and each possible received data symbol S_{n_a} can be calculated based on the cosine rule in (5.47). Therefore, a Euclidean distance vector $\boldsymbol{D}_s = [d_1, d_2, \ldots, d_{n_h}, \ldots, d_{N_h}]$ can be obtained by calculating all N_h possible combinations in $\hat{\boldsymbol{x}}$, where d_{n_h} is the sum Euclidean distance of all symbols from n_h^{th} combination $\boldsymbol{x}_{n_h}$. Thereafter, based on the sum Euclidean distances that has been obtained, the combinations that has the smallest distance will be considered as the original transmitted data symbol vector.

According to the cosine rule, it states that the third side of a triangle can be obtained when two sides and their enclosed angle are known, which can be evaluated as:

$$\omega^2 = \mu^2 + \lambda^2 - 2\mu\lambda \cos\phi. \tag{5.47}$$

Therefore, it could be shown that the length of ω is only related to the angle ϕ, when μ and λ are fixed. For simplicity, we assume that the modulation scheme used in the system is star-QAM or M-PSK, which keeps all constellation symbols around a ring with fixed amplitudes but different phases. However, if there is a need to use other modulation scheme that is not naturally grouped by amplitudes and phases, it is necessary to "manually" cluster constellation symbols into different groups according to the level of amplitudes. For example, 16-QAM whose constellation symbols form a "square", the detector then has to cluster those symbols into different groups according to their amplitudes and phases. Since cosine is monotonically decreasing in the range $[0, \pi]$, the smallest Euclidean distance between S_{n_a} and the potential constellation symbols can be obtained when the smallest phase difference is achieved. Hence, we name this detection scheme amplitude-phase detection. To further illustrate, let us consider a QPSK modulated system as shown in Figure 5.5. In this example, the modulus of the received data symbol S_{n_c} and the modulus of the constellation symbols are known and fixed,

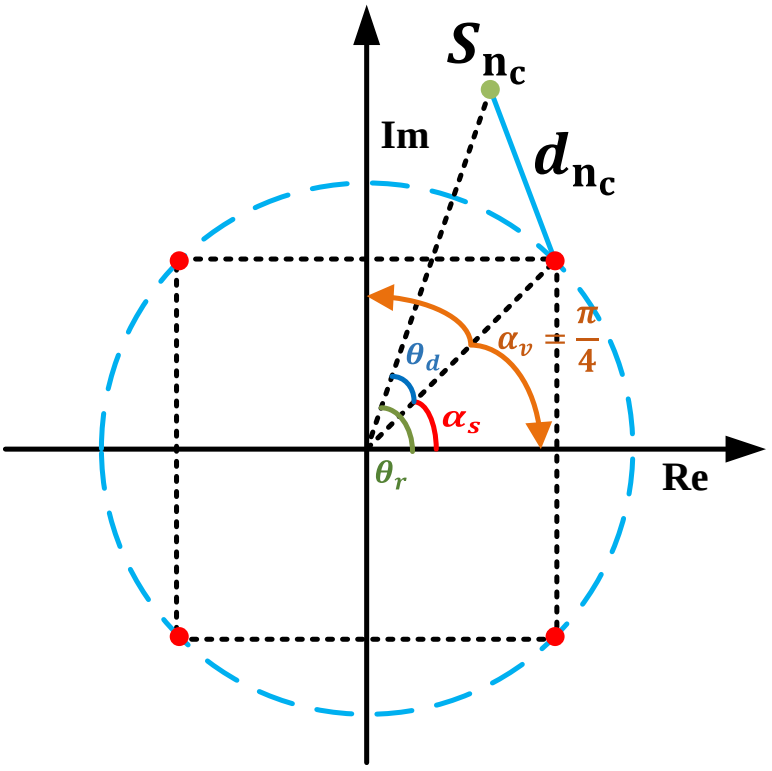

Figure 5.5: Illustration of calculating smallest distance with QPSK by amplitude-phase detection.

and our target is to find the smallest phase difference between S_{n_c} and the constellation symbols. The solution to identify which range the received symbol belongs to is summarized in Algorithm 9.

As shown in Figure 5.5, the detector obtains the phase θ_r of the received symbol and the start phase α_s of the constellation symbols, where the start phase α_s means the smallest angle of constellation symbols in range $[0, 2\pi]$ and $\alpha_s = \frac{\pi}{4}$ in this case. Then, we do the parity check based on the value of α_s and the valid phase range α_v, where α_v indicates the valid phase range of constellation symbols around the same ring, which can be calculated by $\alpha_v = \frac{\pi}{M}$, where M is the modulation order. To further illustrate, we consider the top right constellation symbol on the ring of QPSK in Figure 5.5 as an example. Here, it could be found that when S_{n_c} is located within the phase range of $(0, \frac{\pi}{2})$, the phase difference will be calculated based on this constellation symbol. However, if S_{n_c} is located outside this range, it will choose other constellation symbol as a base to calculate the phase difference. Therefore, it can be seen that the valid phase range is $\frac{\pi}{4}$ on both side of this constellation symbol. Since all constellation symbols around the same ring are space arranged with equal phase difference, the valid phase range is identical for all constellation symbols around the same ring. Finally, the smallest phase difference θ_d between the received symbol and the constellation symbols is related to multiple of α_v, and thus a flag F is set to identify the parity of $\lfloor \theta_r \rfloor$ or $\lfloor \theta_r - \alpha_v \rfloor$. Now, the

smallest distance can also be calculated based on θ_d and the cosine formula presented in (5.47).

Algorithm 9 Operating procedure of minimum phase difference.

1: Obtain the phase θ_r of the received symbol
2: Obtain the start phase α_s of the constellation symbols
3: **if** $\alpha_s = 0$ **then**
4: $\quad F = \frac{|\theta_r - \alpha_v|}{\alpha_v} \mod 2$
5: **else**
6: $\quad F = \frac{|\theta_r|}{\alpha_v} \mod 2$
7: **end if**
8: $\theta_d = |F \times \alpha_v - (\theta_r \mod \alpha_v)|$

Afterwards, all those smallest distances of the received symbols will be added together for each combination and the combination that results in the smallest $\boldsymbol{d}_{n_c}$ will be considered as the detected symbols. Therefore, the index of the activated UAVs can be obtained according to this combination. Finally, we use the corresponding channel combination to do the data bits recovery with ML detection. Our proposed low-complexity detection scheme separately detects the index symbols and data symbols, which largely reduce the complexity of the optimal ML detection.

For example, we consider one scenario that $N_a = 2$ UAVs will be activated and totally I possible combinations of index bits (activated UAV) is considered. Then, if S constellation symbols and T rings are assumed, the search space for the ML detection scheme is $I \times S^{N_a}$, while the search space of the proposed low-complexity detection scheme is $I \times T + S^{N_a}$. Therefore, the search space of our proposed low-complexity detection scheme is significantly smaller than that of ML detection scheme as discussed numerically in the following section.

5.3 Performance Results and Evaluation

In this section, we investigate the performance of our proposed IM-UAV communication system in a 1 km $\times$ 1 km square area with totally $N_u = 18$ GUs and $N_d = 4$ UAVs. For all GUs in this target area, we assume that $N_r = 4$ antennas are mounted on their equipments. UAVs operate at a height of $h_d = 100$ m and each is equipped with one antenna. Then, we set the carrier frequency to $f_c = 5.8$ GHz for the A2G communication, while the path loss exponent α and the Rician K-factor are set to 2 and 3, respectively. Meanwhile, the noise power spectral density (PSD) N_0 is set to -174 dBm/Hz and the transmission power P_t of the UAVs is in the range from 1 dBm to 40 dBm. Additionally, OFDMA is employed to support multi-user communications, where the total bandwidth B allocated to all GUs is 40 MHz. In our system, the whole bandwidth is divided into 512 subcarriers and only 468 of them will be used as data subcarriers to transmit

data bits, while the rest will be set as guard intervals [330]. Moreover, all GUs in our system has the same weight, which means 26 subcarriers will be assigned to each user.

Table 5.2: Simulation parameters

Parameter	Symbol	Value	Parameter	Symbol	Value
K-factor	K	3	Bandwidth	B	40 MHz
Noise PSD	N_0	-174 dBm/Hz	Transmission power	P_t	1 to 40 dBm
Carrier frequency	f_c	5.8 GHz	Path loss exponent	α	2
UAV height	h_d	100 m	Speed of light	c	3×10^8 m/s
Number of UAVs	N_d	4	Number of activated UAVs	N_a	1 to 4
Number of Rx antennas	N_r	4	Number of subcarriers	N_s	512
Number of data subcarriers	N_{ds}	468	Learning rate	l_r	5
Number of GUs	N_u	18	Number of epochs	N_e	300
Correcting factor	β	1	Drain efficiency	η	10%
Power supply	V_{dd}	3 V	Resolution of DAC	N	10 bits
Unit current source	I_u	10 μ A	Parasitic capacitance	C_p	1 pF
Corner frequency	f_{cor}	1 MHz	Power consumption of filter	P_{filt}	2.5 mW
Power consumption of synthesizer	P_{syn}	50 mW	Power consumption of mixer	P_{mix}	30.3 mW

In the following, we first analyze the effect of the UAV deployment on the sum rate of all GUs. Afterwards, the EE of the proposed IM-UAV system will be investigated. Finally, the BER performance of our proposed low-complexity detection scheme will be examined. The detailed simulation parameters are listed in Table 5.2.

In our proposed IM-UAV communication system, the sum rate of all GUs is taken as the objective function for optimising the deployment of UAVs. Figure 5.6(a) and Figure 5.6(b) depict the performance of our proposed deployment schemes in the scenario of 2 activated UAVs out of 4 deployed UAVs. Based on the gradient of the rate in (6.51) with respect to the position of all UAVs, it can be found from Figure 5.6(a) that the sum rate of all GUs in the target area steadily increases by the gradient descent algorithm. Finally, the curve will reach steady state after enough number of epochs, where the epoch is the maximum number of steps the algorithm will run for convergence. The blue curve, which represents the lower bound of the achievable rate, is obtained from (5.16), while the red curve named by 'Real Rate' is obtained from (8) and (14) of [331] to indicate the true rate of the GUs by Cholesky decomposition [182]. It is straightforward to see that the trend of the lower bound and the real rate is consistent and this means the deployment of multiple UAVs does effectively improve the QoS of the downlink rate. In Figure 5.6(b), the distribution of GUs and the location of UAVs in correspondence with this two curves have been illustrated. Here, all UAVs are represented by red circles and GUs are indicated by blue crosses. The hollow red circles are the initial location of UAVs (UAV_I), and the solid ones are the final location (UAV_F) where UAVs will be deployed.

In Figure 5.7(a), we show the average capacity of different activated patterns,where we show 4 curves that represent different activated patterns. Here, the legend "1-UAV"

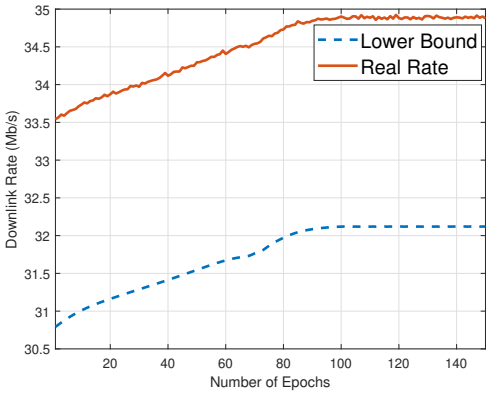

(a) Downlink sum rate of the GUs after deployment with gradient descent.

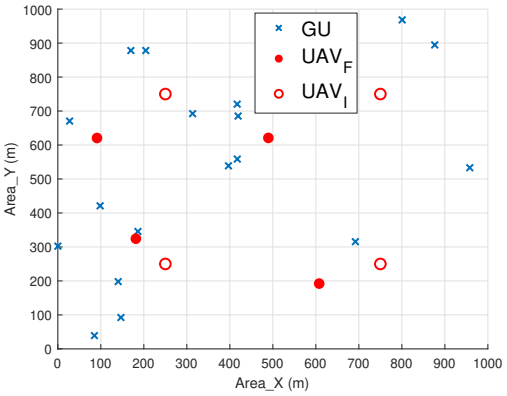

(b) Illustration of UAV's position before and after deployment.

Figure 5.6: Illustration of the deployment of 2 activated UAVs out of 4 deployed UAVs in the proposed IM-UAV communication system with 18 GUs by gradient descent algorithm, where UAV_I and UAV_F indicate the initial locations and the final locations, respectively

means only 1 UAV has been activated among all 4 deployed UAVs and so on. With the increase of transmission power, it can be seen that the capacity will increase. Besides, increasing the number of activated UAVs improves the achievable capacity, as shown in Figure 5.7(a). However, it also can be deduced that the capacity at the level of high transmission power increases slowly, which means the overall increase of information bits is smaller than the increase of the transmission power.

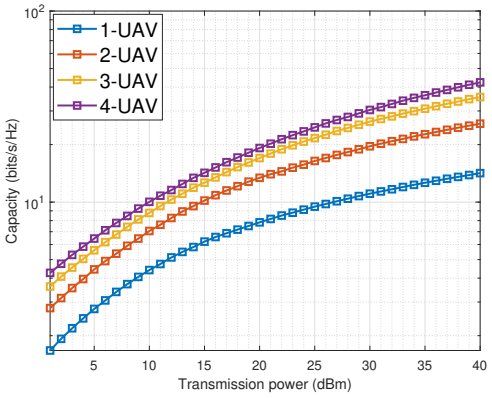

(a) Average capacity.

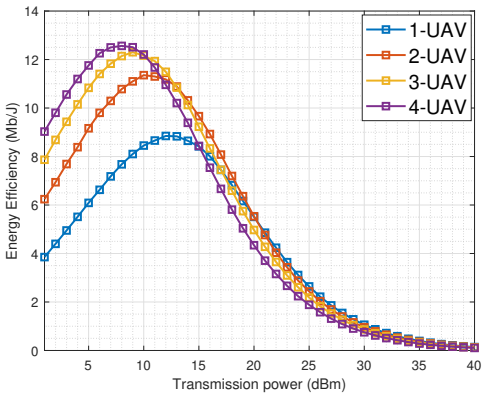

(b) Energy efficiency.

Figure 5.7: Performance illustration of different activated patterns in the proposed IM-UAV communication system with 4 UAVs and 18 GUs.

This phenomenon is also reflected by Figure 5.7(b), where at lower levels of transmission power, the EE of "4-UAV" is the best as it transmits the most information bits with the same transmission power. However, with the increase of transmission power, the trend of all curves increases to a peak and then starts to reduce. Besides, it can be found

that the EE of IM-UAV communication starts to surpass the fully-activated scenario at around 15 dBm transmission power, which is the practical transmission power to consider. Explicitly, the transmission power of common UAVs will not operate in the 5 dBm to 20 dBm range due to the relatively high A2G path loss, where Figure 5.8 also indicates that the BER performance of the system is bad in this range. Hence, it can be concluded that the IM-UAV system attains a higher EE compared to activating all UAVs, in the practical transmission power range as depicted in Figure 5.7(b). Finally, it can also be find that the the EE is quite low when transmitting in a relatively high transmission power, while the improvement of transmission delay requires a relatively high transmission. Hence, there is a trade-off between EE and transmission delay when designing a system with different purposes.

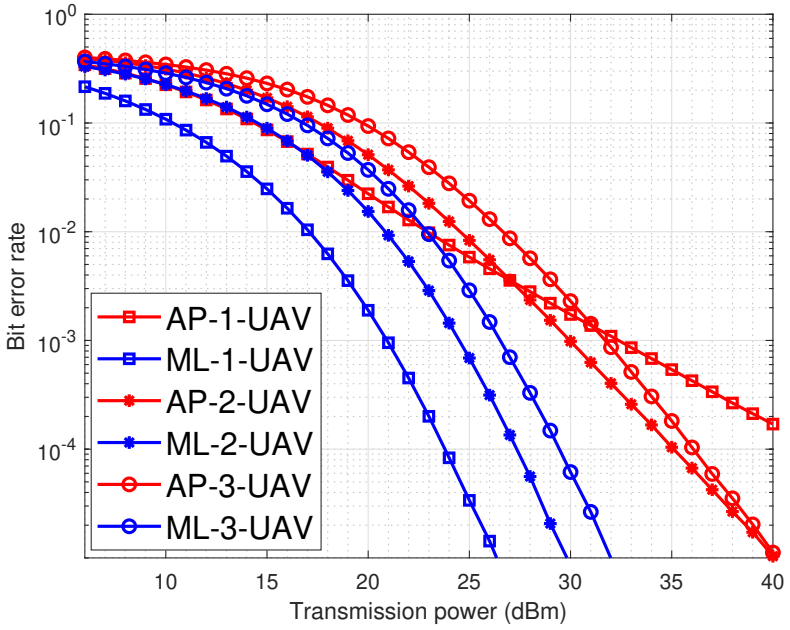

Figure 5.8: BER performance of low-complexity detection and ML detection by 8-PSK in the proposed IM-UAV communication system with 4 UAVs and 18 GUs.

Figure 5.8 shows the BER performance of the proposed low-complexity detection by considering 8-PSK modulation scheme. In this case, we test three activation patterns that activates 1 UAV, 2 UAVs and 3 UAVs, when 4 UAVs are deployed. Below a transmission power of 27 dBm, the low-complexity and ML detection follow the same pattern, where activating more UAVs results in a worse BER performance. However, the performance of 2 activated UAVs and 3 activated UAVs becomes better than that of 1 activated UAV scenario with the increase of the transmission power for the proposed low-complexity detection scheme. This is caused by the characteristics of our proposed detection scheme as we consider both the amplitude and phase of the received signals. In the low transmission power range the signal is deeply affected by the noise, where

activating more UAVs results in a higher transmission rate, which results in more detection errors due to the noise. On the other hand, this phenomenon will be improved with the increase of transmission power because the average path loss of 2 activated UAV and 3 activated UAV is smaller than that of 1 activated UAV scenario and noise is not the dominant factor that affects the BER performance in the higher transmit power scenarios.

Based on the BER comparison between two detection schemes, it can be seen that the degradation of BER performance is mainly caused by the index detection. In our proposed low-complexity detection scheme, we firstly detect the index of activated UAVs by analyzing the amplitude and phase of the constellation symbols. As mentioned before, the complexity of this scheme depends on the level of amplitudes (number of rings) and the corresponding phase differences of constellation symbols around these rings. Therefore, instead of searching all possible combinations of index symbols and data symbols, this amplitude-phase detection scheme will reduce the detection complexity significantly when high order modulation schemes or large number of UAVs have been employed.

Table 5.3: Search space for $N_d = 4$ and $N_a = 3$ by QPSK, 8-PSK and star 16-QAM.

Modulation	ML detection	Low-complexity detection
QPSK	256	68
8-PSK	2048	516
Star 16-QAM	16384	4104

In Table 5.3, a scenario that $N_a = 3$ out of 4 UAVs will be activated has been included to illustrate the complexity of this two detection schemes. It could be found that totally $I = 4$ combinations of index bits or activated UAVs exist, therefore, according to the number of constellation symbols S and the number of rings T for each modulation scheme, the search space can be obtained. However, the reduction of complexity also cause a degradation on BER performance, because the wrong detection of index symbols will cause severe effects on the following detection of data symbols. Therefore, it is a complexity-performance trade-off.

5.4 Conclusion

In this chapter, we proposed an IM based UAV wireless communication system, which aims to increase the EE of power-limited UAV platforms. Furthermore, by combining the UAV communication system with IM, the BER performance of the system could be improved. Besides, based on the proposed IM-UAV communication system, a multi-UAV deployment scheme has been designed to maximize the downlink sum rate of

all GUs. Additionally, we designed a low-complexity detection scheme to separately detect the index symbols and the data symbols, rather than jointly detecting them using the exhaustive search in the IM-UAV scheme.

Chapter 6

Content-Aware Transmission in UAV-Assisted Multicast System

6.1 Introduction

In Chapter 3, we designed a caching-enabled UAV wireless communication system, which utilizes the memory resource onboard to pre-download the popular content for reducing the latency of data transmission. Meanwhile, the OFDMA technique is employed to support multiple GUs simultaneously and to alleviate the performance degradation caused by NLoS propagation (multipath channel fading) in Chapter 5. In this chapter, we further design a new transmission scheme under the content-aware condition (e.g., augmented reality and caching) by considering the two-layer rate splitting (RS) in each subcarrier to effectively utilize the bandwidth resources of UAV. However, the results of this RS based method is proved to either be a pure private scenario or a pure common scenario. Therefore, we directly consider two different subcarrier-sharing (SS) methods instead based on the analysis of RS based method. Firstly, we investigate the private subcarrier-sharing (PSS) scheme, which considers the SS among those GUs who requested the same content. Secondly, we optimize the proportion of contents in each subcarrier by a common subcarrier-sharing (CSS) scheme to further improve the utilization of bandwidth resources. Furthermore, the deployment of UAVs will also affect the QoE of GUs, hence we propose a fixed-point based algorithm to maximize the average rate of GUs in the target area.

6.2 System Model

In this chapter, we consider a UAV-assisted communication system in a downlink scenario to serve a number of GUs in its target area, as shown in Fig. 6.1. In this case,

the UAV is acting as a flying BS serving the GUs[1]. Moreover, the UAV is capable of flying horizontally and hovering at a certain altitude of h_d and it also knows the locations of the GUs [332]. Meanwhile, OFDMA technique is employed to support the A2G communication links between the UAV and the multiple GUs. Here, the bandwith resource is divided into subcarriers, which are assigned to GUs according to their real-time requirements [309].

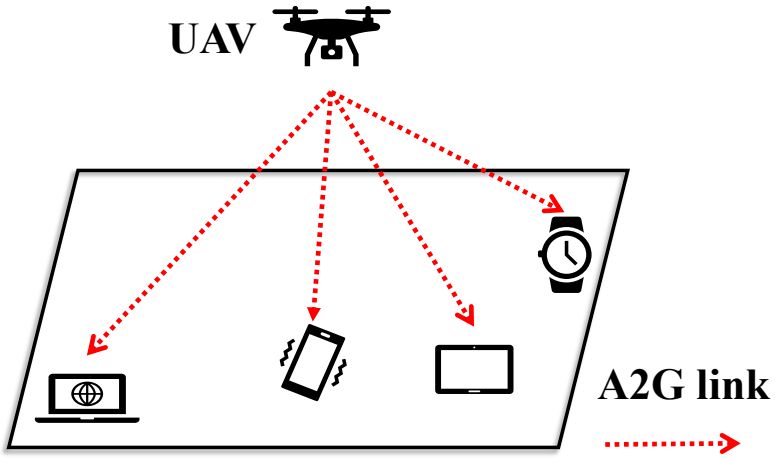

Figure 6.1: UAV-assisted network model that provides service of wireless communication for GUs.

Additionally, we assume that all GUs generate their own request periodically based on their preferences, which can be represented by a set of distributions. Fig. 6.2 shows an example of GU's preference represented by the distribution of available contents. In Fig. 6.2, a total of 50 different contents have been taken into consideration and each can be thought of as a category (e.g. sports, weather, literature.). The probability is used to measure the level of user interests in each content, where the higher the probability, the greater the chance of being requested. However, since the requested contents are all known by the UAV as a flying BS and the bandwidth resources on the UAV is limited, it is necessary to design new transmission schemes to fully utilize the limited bandwidth resources. Besides, the UAV's deployment location also needs to be adjusted to further improve the downlink performance by exploiting the flexibility and maneuverability of the UAV.

Moreover, we consider a capacity-achieving[2] transmission scheme in an OFDMA system, which means that all GUs can achieve the data rate at their full capacity on their assigned subcarrier [333]. Specifically, the whole bandwidth will be equally divided into subcarriers according to the number of GUs N_u and each GU will be assigned one subcarrier. The channel capacity is only related to the received signal power P_r, when

[1]The case illustrated here is one UAV with its associated GUs. However, the scheme can also be applied to a scenario of multiple UAVs and each UAV has their own associated GUs.

[2]We assume that the data bits are transmitted at capacity limit without considering any specific modulation schemes in our system.

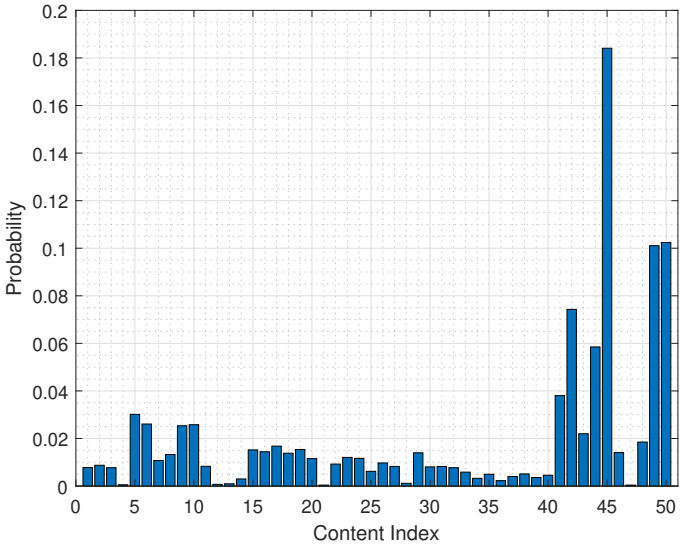

Figure 6.2: An example of GU preference represented by content distribution.

the bandwidth B and the noise power spectral density (PSD) N_0 are fixed. Besides, due to the dynamic A2G distances of the GUs, the different GUs will receive the OFDM modulated signal with different received signal power. Therefore, the capacity of each subcarrier is different for different GUs. For example, consider a system supporting two GUs and each is assigned with one subcarrier, where the received signal power of the first GU is assumed stronger than that of the second GU ($P_r^1 > P_r^2$). In this case, the data throughput that the first GU can be supported based on its assigned subcarrier is higher than that of the second GU. Additionally, we consider the case that each subcarrier is modulated depending on the received signal power of its assigned GU. Hence, the first GU is capable of correctly recovering the information on both subcarriers while the second GU can only recover the information of its own subcarrier. This is because the power needed to demodulate the information of the first subcarrier, which is also the first GU's subcarrier, should be greater than or equal to P_r^1, while the second GU has a lower received power.

In our system, subcarriers are preallocated to GUs before the transmission and the information is encoded based on the channel condition of the GUs. Accordingly, it can be found that one GU can only demodulate the subcarriers that have a reduced received power, which means a lower capacity, in our capacity-achieving communication system. In the following, we will present the channel model of the proposed UAV-assisted communication followed by the structure of our proposed RS-OFDMA. Afterwards, two CS schemes, namely PCS and CCS, will be detailed.

6.2.1 Channel model

Since the UAV is operating as an aerial BS to serve the GUs at a certain height h_d in our system, the communication links between the GUs and the UAV can be considered to be in strong LoS propagation environment [290]. Therefore, the Rician fading channel model [268], which is composed of a dominant LoS path and some non line of sight (NLoS) paths, is considered to model the signal propagation environment [293]. The Rician channel employed in our A2G communication decomposes the channel into two components [314]: deterministic LoS component h_{LoS} and stochastic NLoS component h_{NLoS}. Then, the channel h is given by:

$$h = \sqrt{\frac{K}{1+K}} \cdot h_{\text{LoS}} + \sqrt{\frac{1}{1+K}} \cdot h_{\text{NLoS}}, \tag{6.1}$$

where h_{NLoS} is used to describe the scattered multipath propagation of signals, while the Rician K factor is the power ratio of the LoS path and the NLoS paths. Accordingly, the Rician K factor in our UAV-assisted communication system ranges from 0.51 to 6.31 [294], to generate a LoS dominant channel.

On the other hand, path loss is commonly considered to measure the signal attenuation in A2G communication system. Path loss is closely linked with the environment, where the transmitter and receiver are operating [316]. Generally, the propagation path loss P_l can be expressed by [271]:

$$P_l = \left(\frac{4\pi}{\lambda}\right)^2 d^{\alpha}, \tag{6.2}$$

where d indicates the distance between the transmitter and receiver, while the path loss exponent α, which ranges from 2 to 6, indicates the nature of the propagation environment. The wavelength $\lambda = \frac{c}{f_c}$ is defined as the ratio of the speed of light c in m/s to the carrier frequency f_c in Hz. Therefore, the received signal power P_r given a transmission power P_t is formulated as [272]:

$$P_r = \frac{P_t}{P_l} = P_t \left(\frac{c}{4\pi f_c}\right)^2 \left(\frac{1}{d}\right)^{\alpha}. \tag{6.3}$$

In our UAV-assisted communication system, the UAV is considered to fly at a given altitude of $h_d = 100$ m [273] and the LoS communication links are assumed to exist for most of the time [290]. Under the LoS model, the free space path loss exponent $\alpha = 2$ is chosen to describe the signal attenuation. Then, the received signal power P_r can be represented as:

$$P_r = P_t \left(\frac{c}{4\pi d f_c}\right)^2. \tag{6.4}$$

Additionally, one important criterion to measure the performance of a system is the achievable rate and the channel capacity C in bits per second (bits/s) that uses the

received signal power P_r perturbed by additive white Gaussian noise (AWGN) of PSD N_0 with bandwidth B is given by [334]:

$$C = B \log_2 \left(1 + \frac{P_r}{BN_0}\right). \tag{6.5}$$

6.2.2 Proposed Rate Splitting OFDMA

Inspired by the concept of RS that splits the message into common and private parts, we apply the RS concept to traditional OFDMA modulation in order to improve the throughput due to the fact that a common part will be repeatedly needed by multiple users, which would largely increase the bandwidth utilization.

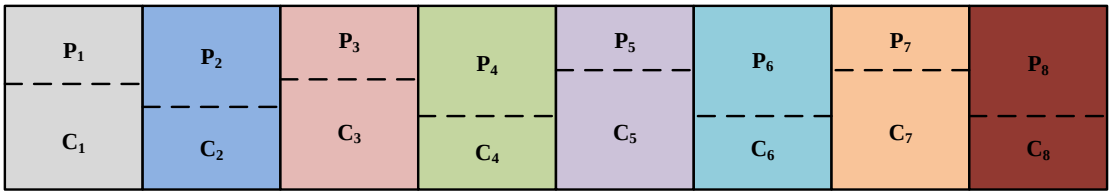

Figure 6.3: A toy example of RS-OFDMA in frequency domain with RS in each subcarrier, where "P" indicates the private message and "C" indicates the common message.

Fig. 6.3 shows the structure of the proposed RS-OFDMA, where instead of separating the users by different power layers in RSMA, the users are partitioned by frequency (subcarriers). Then, we consider a two-layer RS structure in each subcarrier to separate the private and common messages since users are already separated by subcarriers. In each subcarrier, the private message means the content requested by the GU assigned with this subcarrier, while the common message is a mixture of all possible contents considered in this system but with different proportion. Here, the contents conveyed by each subcarrier usually cannot be demodulated by all GUs in a capacity-achieving communication system, especially for the common message. Therefore, the contents modulated on the common part in each subcarrier need to be adjusted based on the number of GUs who can successfully demodulate the information conveyed by each subcarrier and the contents requested by those accessible GUs. As a result, the transmitted signal modulated on the i^{th} subcarrier can be expressed as:

$$x_i = \sqrt{p_i} x_c + \sqrt{1 - p_i} x_p, \tag{6.6}$$

where p_i is the power allocation coefficient of the common message in the i^{th} subcarrier, subject to the constraint $0 \leq p_i \leq 1$, while x_c and x_p represent the common message and the private message, respectively. Consequently, the total received signal of the u^{th}

GU at the i^{th} subcarrier is given by:

$$\begin{aligned} y_u^i &= h_u^i x_i + n_i, \\ &= \sqrt{p_i} h_u^i x_c + \sqrt{1-p_i} h_u^i x_p + n_i, \end{aligned} \tag{6.7}$$

where h_u^i represents the channel gain including the path loss of the u^{th} GU at the i^{th} subcarrier and n_i is the AWGN with variance σ^2 at the i^{th} subcarrier. For simplicity, in the following we assume the index of subcarrier, which intends to transmit the private message to its corresponding GU, equals to the index of its corresponding GU in our system, because only the common part is "public" for all GUs.

As mentioned before, each GU is only allowed to demodulate those subcarriers that have weaker received signal power or weaker channel condition than its allocated subcarrier, in our capacity-achieving system. It is worth noting that we consider the scenario where the weakest channel condition can also support the basic A2G communication. Here, the common message is public for all GUs, while the private message cannot. Besides, it can be seen that the common message in a subcarrier can be demodulated or utilized by more GUs if a weaker channel power is used to modulate the common message. In an extreme case, the system employs the weakest channel among those GUs to modulate the common message, then the common message in each subcarrier is available for all GUs. However, it is highly possible that the sum rate can be lower even though the number of GUs who can access the subcarriers is increased, because the channel condition employed is too weak to support a high-speed data transmission. As a result, a threshold h_T need to be firstly set for the received signal power over all subcarriers before formulating the rate of the common message. In fact, the threshold is used to control the accessibility of the common message in each subcarrier and further affect the sum rate. As an example, let us consider a two-GUs scenario that has $|h_1|^2 > |h_T|^2 > |h_2|^2$. Then, only the first GU can obtain the common message on both subcarriers as well as its private message modulated on its own subcarrier, while the second GU can only obtain the private message on its assigned subcarrier since the common message of all subcarriers is modulated based on h_T.

Based on the above discussion, we know that a GU can only demodulate the subcarriers that have a poorer channel condition. Therefore, to calculate the data rate of the system, a filter vector $\boldsymbol{F}_i$ with a length of N_s needs to be defined to demonstrate the accessibility of the i^{th} subcarrier, which is used to count the utilization of the common message. For instance, we consider a group of 6 GUs and each of them is assigned with one subcarrier. Besides, the channel gain of each GU in a descending order is represented by $|h_2|^2 < |h_3|^2 < |h_1|^2 < |h_5|^2 < |h_6|^2 < |h_4|^2$. Consequently, the filter vector of each

subcarrier can be expressed by:

$$\boldsymbol{F}_1 = [1,1,1,0,0,0]^T, \tag{6.8}$$
$$\boldsymbol{F}_2 = [0,1,0,0,0,0]^T, \tag{6.9}$$
$$\boldsymbol{F}_3 = [0,1,1,0,0,0]^T, \tag{6.10}$$
$$\boldsymbol{F}_4 = [1,1,1,1,1,1]^T, \tag{6.11}$$
$$\boldsymbol{F}_5 = [1,1,1,0,1,0]^T, \tag{6.12}$$
$$\boldsymbol{F}_6 = [1,1,1,0,1,1]^T. \tag{6.13}$$

In (6.8), the power of the first subcarrier p_1 ranks third among all subcarriers, and the two that have stronger received signal power are GU_2 and GU_3. Hence, only the first three positions of $\boldsymbol{F}_1$ have been set to "1".

Meanwhile, the weight vector $\boldsymbol{W}_i \in \mathcal{W}_S$, which is used to indicate the percentage of content in the common part of the i^{th} subcarrier, is given by:

$$\mathcal{W}_S = \{\boldsymbol{W}_1, \boldsymbol{W}_2, \ldots, \boldsymbol{W}_i, \ldots, \boldsymbol{W}_{N_s}\}, \tag{6.14}$$

for $i = 1,2,3,\ldots,N_s$, where $\boldsymbol{W}_i$ represents the weight vector of the i^{th} subcarrier, which is given by:

$$\boldsymbol{W}_i = \left[w_{i1}, w_{i2}, \ldots, w_{ij}, \ldots, w_{iN_c}\right], \tag{6.15}$$

where w_{ij} is the j^{th} content of the i^{th} subcarrier. Additionally, the weight vector $\boldsymbol{W}_i$ is also subject to the constraint:

$$\sum_{j=1}^{N_c} w_{ij} = 1, \tag{6.16}$$

where $0 \leq w_{ij} \leq 1$ and N_c is the number of contents considered in the system. Afterwards, a selection matrix $\boldsymbol{S} \in \mathbb{C}^{N_c \times N_u}$ is necessary to link the N_u GUs with their corresponding contents and the selection matrix $\boldsymbol{S}$ is in the form of:

$$\boldsymbol{S} = \begin{bmatrix} s_{11} & s_{12} & \cdots & s_{1N_u} \\ s_{21} & s_{22} & \cdots & s_{2N_u} \\ \vdots & \vdots & \ddots & \vdots \\ s_{N_c1} & s_{N_c2} & \cdots & s_{N_cN_u} \end{bmatrix}, \tag{6.17}$$

where s_{ju} represents the flag of the j^{th} content from the u^{th} GU, for $j = 1,2,3,\ldots,N_c$ and $u = 1,2,3,\ldots,N_u$. Hence, s_{ju} will be set to "1" if the u^{th} GU asks for the j^{th} content, otherwise, it will be set to "0". To further illustrate the format of $\boldsymbol{S}$, an example that considers 6 GUs with totally 4 contents is included. Firstly, the contents requested by 6 GUs is $\{c_1, c_4, c_3, c_4, c_2, c_4\}$ and the order of these contents is arranged sequentially based on the index of GUs. As a result, the selection matrix for this example is given

by:

$$\boldsymbol{S} = \begin{bmatrix} 1 & 0 & 0 & 0 & 0 & 0 \\ 0 & 0 & 0 & 0 & 1 & 0 \\ 0 & 0 & 1 & 0 & 0 & 0 \\ 0 & 1 & 0 & 1 & 0 & 1 \end{bmatrix}. \tag{6.18}$$

It can be seen that the first, the second and the third contents are requested once by the first, the fifth and the third GUs, respectively. While the forth content is three times requested by the other GUs. Therefore, the position of the requested content in each column of the corresponding GU is set to "1", while the rest will be set to "0".

Since all the factors that will be used have been provided, the derivation of data rate in our proposed RS-OFDMA communication system will be detailed in the following by two scenarios:

6.2.2.1 Scenario 1

In the first scenario of RS-OFDMA, we consider that the private message has a higher power allocation in each subcarrier. Besides, since the bandwidth assigned to each GU is equally divided, the bandwidth is removed from the equations in the following sections. Consequently, the private rate R_p^i and the common rate R_c^i of the i^{th} subcarrier can be given by:

$$R_p^i = \log_2\left(1 + \frac{|h_i|^2 (1 - p_i)}{|h_i|^2 p_i + \sigma^2}\right), \tag{6.19}$$

$$R_c^i = A_i \log_2\left(1 + \frac{|h_T|^2 p_i}{\sigma^2}\right), \tag{6.20}$$

where h_i is channel of the i^{th} GU at the i^{th} subcarrier, which is a metric that is used to modulated the private message at the i^{th} subcarrier. While $A_i = \boldsymbol{W}_i \boldsymbol{S} \boldsymbol{F}_i$ is a coefficient for the utilization measurement of common message in the i^{th} subcarrier named by "sharing times". Back to the definition of A_i, it can be found that $\boldsymbol{W}_i$ represents the proportion of each content, $\boldsymbol{S}$ links the GUs to their corresponding content and $\boldsymbol{F}_i$ helps to find out the accessible GUs of the i^{th} subcarrier. Therefore, the sharing times of each content can be obtained based on the proportion of each content and the number of accessible GUs requesting for this content. Accordingly, it is straightforward to see that A_i is actually the sum sharing times of all contents carried by the i^{th} subcarrier. Therefore, the sum rate of the i^{th} subcarrier can be obtained by:

$$\begin{aligned} R_s^i &= R_p^i + R_c^i \\ &= A_i \log_2\left(|h_T|^2 p_i + \sigma^2\right) \\ &\quad - \log_2\left(|h_i|^2 p_i + \sigma^2\right) + \mathcal{C}_1, \end{aligned} \tag{6.21}$$

where $\mathcal{C}_1 = \log_2\left(|h_i|^2 + \sigma^2\right) - A_i \log_2\left(\sigma^2\right)$. Hereafter, the derivative of R_s^i with respect to p_i can calculated as:

$$\frac{\partial R_s^i}{\partial p_i} = \frac{A_i |h_T|^2}{|h_T|^2 p_i + \sigma^2} - \frac{|h_i|^2}{|h_i|^2 p_i + \sigma^2}. \tag{6.22}$$

Hence, the optimum value p_e of the power allocation coefficient p_i for R_s^i can be obtained by setting $\frac{\partial R_s^i}{\partial p_i} = 0$, which is given by:

$$p_e = \frac{|h_i|^2 - A_i |h_T|^2}{A_i - 1} \cdot \frac{\sigma^2}{|h_T|^2 |h_i|^2}. \tag{6.23}$$

Since $A \geq 1$, we have three conditions if $|h_T|^2 < \frac{\sigma^2}{A-1}$:

$$\begin{cases} p_e > 1, & \text{if } |h_i|^2 > \frac{A_i |h_T|^2 \sigma^2}{\sigma^2 - (A_i - 1)|h_T|^2}; \\ 0 \leq p_e \leq 1, & \text{if } A_i |h_T|^2 \leq |h_i|^2 \leq \frac{A_i |h_T|^2 \sigma^2}{\sigma^2 - (A_i - 1)|h_T|^2}; \\ p_e < 0, & \text{if } |h_i|^2 < A_i |h_T|^2. \end{cases} \tag{6.24}$$

However, it always satisfies the condition that $p_e \leq 1$ if $|h_T|^2 \geq \frac{\sigma^2}{A_i - 1}$. Hence, we have:

$$\begin{cases} 0 \leq p_e \leq 1, & \text{if } |h_i|^2 \geq A_i |h_T|^2; \\ p_e < 0, & \text{if } |h_i|^2 < A_i |h_T|^2. \end{cases} \tag{6.25}$$

Besides, R_s^i is monotonically increasing when $p_e < 0$ and it is monotonically decreasing when $p_e > 1$. Therefore, if we aim to maximize the sum rate of all users, the value of p_i must satisfy the following constraint:

$$\begin{cases} p_i = 0, & \text{if } p_e \geq 1; \\ p_i = 1, & \text{if } p_e \leq 0; \\ p_i = \underset{p_i \in \{0,1\}}{\arg\max}\, R_s^i\left(p_i\right), & \text{if } 0 < \ p_e < 1. \end{cases} \tag{6.26}$$

6.2.2.2 Scenario 2

The second scenario considers that the common part has a higher power allocation. Therefore, the private rate $R_p^{i'}$ and the common rate $R_c^{i'}$ of the i^{th} subcarrier are given by:

$$R_p^{i'} = \log_2\left(1 + \frac{|h_i|^2 p_i'}{\sigma^2}\right), \tag{6.27}$$

$$R_c^{i'} = A_i \log_2\left(1 + \frac{|h_T|^2 \left(1 - p_i'\right)}{|h_T|^2 p_i' + \sigma^2}\right). \tag{6.28}$$

Accordingly, the sum rate of the i^{th} subcarrier can be expressed by:

$$\begin{aligned} R_s^{i'} &= R_p^{i'} + R_c^{i'}, \\ &= -A_i \log_2\left(|h_T|^2 p_i' + \sigma^2\right) \\ &\quad + \log_2\left(|h_i|^2 p_i' + \sigma^2\right) + \mathcal{C}_2, \end{aligned} \tag{6.29}$$

where $\mathcal{C}_2 = A_i \log_2\left(|h_T|^2 + \sigma^2\right) - \log_2\left(\sigma^2\right)$. Hereafter, the derivative of $R_s^{i'}$ with respect to p_i' is calculated by:

$$\frac{\partial R_s^{i'}}{\partial p_i'} = -\frac{A_i |h_T|^2}{|h_T|^2 p_i' + \sigma^2} + \frac{|h_i|^2}{|h_i|^2 p_i' + \sigma^2}, \tag{6.30}$$

where the optimum value p_e' can be obtained by setting $\frac{\partial R_s^{i'}}{\partial p_i'} = 0$, which is computed as:

$$p_e' = \frac{|h_i|^2 - A_i |h_T|^2}{A_i - 1} \cdot \frac{\sigma^2}{|h_T|^2 |h_i|^2}. \tag{6.31}$$

Since $A_i \geq 1$, we have three conditions if $|h_T|^2 < \frac{\sigma^2}{A_i - 1}$:

$$\begin{cases} p_e' > 1, & \text{if } |h_i|^2 > \frac{A_i |h_T|^2 + \sigma^2}{\sigma^2 - (A_i - 1)|h_T|^2}; \\ 0 \leq p_e' \leq 1, & \text{if } A_i |h_T|^2 \leq |h_i|^2 \leq \frac{A_i |h_T|^2 + \sigma^2}{\sigma^2 - (A_i - 1)|h_T|^2}; \\ p_e' < 0, & \text{if } |h_i|^2 < A_i |h_T|^2. \end{cases} \tag{6.32}$$

However, it always satisfies the condition that $p_e' \leq 1$ if $|h_T|^2 \leq \frac{\sigma^2}{A_i - 1}$. Hence, we have:

$$\begin{cases} 0 \leq p_e' < 1, & \text{if } |h_i|^2 \geq A_i |h_T|^2; \\ p_e' < 0, & \text{if } |h_i|^2 < A_i |h_T|^2. \end{cases} \tag{6.33}$$

Besides, $R_s^{i'}$ is monotonically increasing when $p_e' > 1$ and it is monotonically decreasing when $p_e' < 0$. Therefore, if we aim to maximize the sum rate of all users, the value of p_i' must satisfy the following constraint:

$$\begin{cases} p_i' = 1, & \text{if } p_e' \geq 1; \\ p_i' = 0, & \text{if } p_e' \leq 0; \\ p_i' = \underset{p_i' \in \{0,1\}}{\arg\max}\, R_s^{i'}\left(p_i'\right), & \text{if } 0 < \ p_e' < 1 \end{cases} \tag{6.34}$$

Therefore, it could be found that the power allocation coefficient is either 1 or 0 based on (6.26) and (6.34), which means that the i^{th} subcarrier should transmit all private message or all common message based on the condition of the threshold h_T and the channel gain of the i^{th} subcarrier h_i. In other words, the subcarrier should serve GUs either privately or publicly based on the channel condition, and hence there is no combination

of them to serve GUs in a hybrid way. Inspired by this results, the idea of directly sharing the contents in subcarriers among all GUs to increase the utilization of limited bandwidth resources is proposed. In the following two sections, two CS schemes will be introduced in details.

6.2.3 Proposed Private Content-Sharing Scheme

The first CS scheme is inspired from the first conclusion of RS-OFDMA, namely each subcarrier will only carry the information of the content that is requested by its corresponding GU. Therefore, it can be found that this scheme is operated in a relatively "private" way, which can be referred to as private CS (PCS).

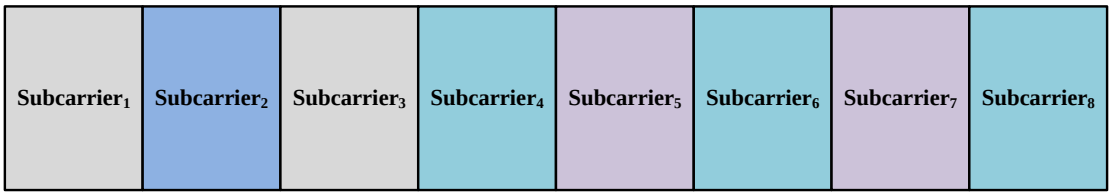

Figure 6.4: Illustration of content-sharing in the frequency domain of OFDMA communication system.

As shown Fig. 6.4 the subcarriers that carried the same kind of contents have been marked by the same colors in CS scheme. Instead of considering to transmit the contents in a hybrid way (private and common), the system directly shares the contents requested by each GU. As a result, the data rate could be improved if we allow those GUs who request the same content to share their contents with each other. For instance, we take the GUs who are requesting the same "Grey" content in the first and third subcarriers as an example, if the corresponding two GUs can only demodulate their allocated subcarriers, the same data need to be transmitted repeatedly on their subcarriers. However, the data rate can be increased if they are allowed to share their subcarriers, because the UAV can now transmit two packages of this content. Here, it is worth noting that the content need to be transmitted by several data packages. Therefore, the GU with a higher channel gain can directly obtain the first data from the GU that has a lower channel gain and obtain the second one by his own subcarrier in our capacity-achieving communication system, which means the GUs with higher channel gain can utilise the data package from other GUs who requested the same content and reduce the duplicate transmissions.

So far, it is straightforward to see that most of the subcarriers can be shared by other GUs if available. In order to calculate the average data rate of the PCS scheme, we take the 4^{th}, 6^{th} and 8^{th} subcarriers that all requested the "Aqua" content in Fig. 6.4 and we assume that the capacity of each subcarrier is in the descending order of 4-6-8. Then, the corresponding sharing times of these 3 subcarriers is 1, 2 and 3, because only these

3 GUs need this content while the others do not. It could be found that the utilization of subcarriers is significantly improved. Finally, the average rate R_A of all GUs in PCS transmission scheme can be formulated as:

$$R_A = \frac{1}{N_u} \sum_{i=1}^{N_s} A_i \log_2 \left(1 + \frac{|h_i|^2}{\sigma^2}\right), \tag{6.35}$$

where A_i is the sum sharing times of the i^{th} subcarrier. However, to further improve the average data rate of PCS, we propose an advanced CS method, referred to as common CS (CCS).

6.2.4 Proposed Common Content-Sharing Scheme

As mentioned before, the GU in PCS can only obtain the information from the subcarriers of GUs that request the same content but have weaker received signal strength. However, GUs will not be restricted by the category of contents since all subcarriers are able to carry all related contents in a pure "common" way, which means GUs are capable of demodulating all available subcarriers. Then, the utilization of each subcarrier can be further improved. Besides, the data rate can also be controlled by adjusting the proportion of contents in each subcarrier. Here, an example of one subcarrier with 5 contents represented by different colors is shown in Fig. 6.5 to illustrate the format of CCS in one subcarrier, where the message is composed by all contents considered in the system but different proportion.

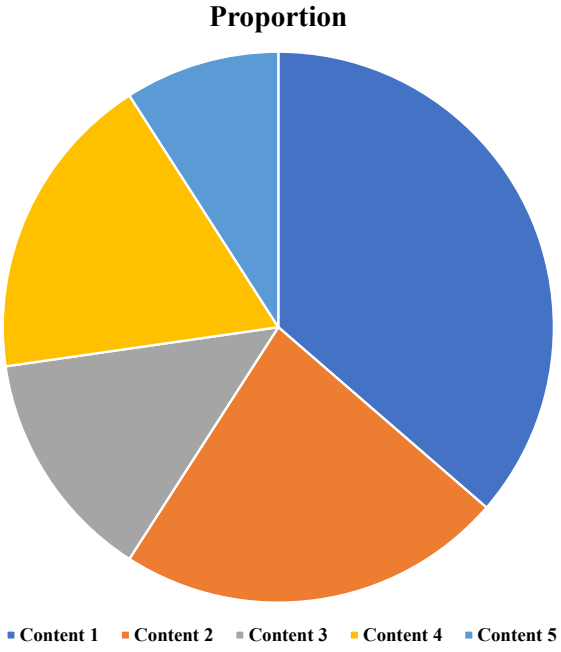

Figure 6.5: An example of content proportion in one subcarrier with 5 contents.

Similar to the common part in RS-OFDMA, a filter vector $\boldsymbol{F}_i$ is used to select those accessible GUs for the i^{th} subcarrier. Accordingly, the rate of the i^{th} subcarrier in CCS scheme can be calculated by:

$$\begin{aligned} R_i &= \boldsymbol{W}_i \boldsymbol{S} \boldsymbol{F}_i \log_2 \left(1 + \frac{|h_i|^2}{\sigma^2}\right), \\ &= A_i \log_2 \left(1 + \frac{|h_i|^2}{\sigma^2}\right), \end{aligned} \tag{6.36}$$

where A_i is the sharing times of the i^{th} subcarrier. Consequently, the average data rate R_A of the CCS scheme can also be expressed by:

$$R_A = \frac{1}{N_u} \sum_{s=1}^{N_s} R_i = \frac{1}{N_u} \sum_{i=1}^{N_s} A_i \log_2 \left(1 + \frac{|h_i|^2}{\sigma^2}\right). \tag{6.37}$$

Our objective is to maximize the average data rate R_A by optimizing the weight vector of each subcarrier, under the weight constraint stated by (6.16) and the individual minimum rate requirement R_m of the GUs. Hence, it is necessary to formulate the rate of each GU before the optimization. Firstly, the rate of the u^{th} GU is defined by R_u. Then, the subcarrier based weight vector $\boldsymbol{W}_i$ should be transferred to the content based format, which is given by:

$$\boldsymbol{W}_c = [w_{c1}, w_{c2}, \ldots, w_{ci}, \ldots, w_{cN_s}], \tag{6.38}$$

where w_{ci} is the weight of the c^{th} content in the i^{th} subcarrier. Therefore, the weight vector of the u^{th} GU is given by $\boldsymbol{W}_u \in \mathcal{W}_C = \{\boldsymbol{W}_1, \boldsymbol{W}_2, \ldots, \boldsymbol{W}_c, \ldots, \boldsymbol{W}_{N_c}\}$. Besides, the capacity vector $\boldsymbol{V}$ that indicates the capacity of each subcarrier is of the form:

$$\boldsymbol{V} = [v_1, v_2, \ldots, v_i, \ldots, v_{N_s}]^T, \tag{6.39}$$

where v_i is the capacity of the i^{th} subcarrier obtained by (6.5) and the rate of the u^{th} GU can be written accordingly as:

$$R_u = \boldsymbol{W}_u \left(\boldsymbol{F}_u \cdot \boldsymbol{V}\right). \tag{6.40}$$

As defined before, it is worth noting that $\boldsymbol{F}_u = \boldsymbol{F}_i$ since the index of subcarriers (i) is identical to the index of the GUs (u). Mathematically, the average data rate maximization problem can be formulated as:

$$\max_{\mathcal{W}_c} \frac{1}{N_u} \sum_{i=1}^{N_s} A_i \log_2 \left(1 + \frac{|h_i|^2}{\sigma^2}\right), \tag{6.41a}$$

$$\text{s.t. } R_u \geq R_{\min}. \tag{6.41b}$$

Recall that A_i is the sharing times of the i^{th} subcarrier, which can be represented by:

$$\begin{aligned} A_i &= w_{i1}n_{i1} + w_{i2}n_{i2} + \cdots + w_{iN_c}n_{iN_c}, \\ &= \boldsymbol{W}_i\boldsymbol{N}_i, \\ &= \boldsymbol{W}_i\boldsymbol{S}\boldsymbol{F}_i, \end{aligned} \tag{6.42}$$

where $\boldsymbol{N}_i = \boldsymbol{S}\boldsymbol{F}_i$ is a vector that represents the number of accessible GUs requesting for each content in the i^{th} subcarrier, which is given by:

$$\boldsymbol{N}_i = \left[n_{i1}, n_{i2}, \ldots, n_{ij}, \ldots, n_{iN_c}\right]^T, \tag{6.43}$$

where n_{ij} is the number of accessible GUs requesting for j^{th} content in the i^{th} subcarrier. As a result, it can be found that the sharing times of the i^{th} subcarrier can be obtained from the percentage of each content in the i^{th} subcarrier $\boldsymbol{W}_i$ and the number of accessible GUs requesting for each content in the i^{th} subcarrier $\boldsymbol{N}_i$. Therefore, the optimization of the average data rate in CCS is translated into a linear programming problem by adjusting the weight of contents in each subcarrier as $\boldsymbol{N}_i$ is a fixed value for each subcarrier [335].

6.3 UAV Deployment

In the case of a UAV-assisted communication system, the advantages of rapid establishment and controlled mobility should be utilized to enhance the communication quality of GUs when compared with traditional fixed terrestrial BSs. Therefore, we propose two different deployment schemes to optimize the average rate of our proposed CS transmission schemes in a content-aware scenario. Here, we need to emphasize that the user association [275, 276] has been done before the deployment and the deployment scheme is considered according to the associated GUs. Hence, a one-UAV scenario is provided here to illustrate the progress of UAV deployment. Firstly, inspired from the traditional k-means clustering algorithm, a fixed-point based deployment scheme is designed for the PCS transmission scheme. Afterwards, a traverse-search based deployment is proposed for the CCS transmission scheme.

Here, we consider a LoS dominant communication environment in our UAV-assisted communication system, which means that the received signal power is determined by the path loss between the UAV and the GUs. It is worth noting that the fast fading is unpredictable and uncontrollable during the communication. Besides, the time scales of the fast fading and the UAV deployment is different, in other words, the fast fading is always changing during the process of deployment. Therefore, we only consider the h_{LoS} and the path loss to optimize the deployment of UAV. Firstly, we assume that

the UAV is flying at a fixed height of h_d, and the coordinate of the UAV can be expressed by $\boldsymbol{G} = [x_a, y_a, h_d]$. Similarly, the coordinate of the u^{th} GU can be represented by $\boldsymbol{U}_u = [x_u, y_u, 0]$. Here, the height of GUs is negligible compared with the A2G distance. Additionally, we also define the terrestrial coordinates $\tilde{\boldsymbol{G}} = [x_a, y_a]$ and $\tilde{\boldsymbol{U}}_u = [x_u, y_u]$ to represent the terrestrial coordinates of the UAV and the GUs, respectively. Therefore, the A2G distance d_u between the u^{th} GU and the UAV is given by:

$$\begin{aligned} d_u &= \sqrt{(x_a - x_u)^2 + (y_a - y_u)^2 + h_d^2}, \\ &= \|\boldsymbol{G} - \boldsymbol{U}_u\|. \end{aligned} \tag{6.44}$$

Besides, h_{LoS} can be expressed by [298]:

$$h_{\text{LoS}} = e^{-j\frac{2\pi}{\lambda}d}, \tag{6.45}$$

where d is the distance in meter between the transmitter and the receiver. Consequently, the received signal power of the i^{th} subcarrier in the LoS dominant environment is given by:

$$\begin{aligned} P_{r_s} &= P_t |h_{\text{LoS}}|^2 \left(\frac{c}{4\pi d_u f_c}\right)^2, \\ &= P_t \left(\frac{c}{4\pi d_u f_c}\right)^2. \end{aligned} \tag{6.46}$$

The traditional k-means clustering algorithm uses the squared Euclidean distance to find out the mean of the points in that cluster iteratively. Here, we choose the capacity as the "distance metric" in our PCS based communication system, where the deployment of the UAV can be transformed to the following optimisation problem:

$$\max_{\tilde{\boldsymbol{G}}} \sum_{u=1}^{N_u} A_u \log_2 \left(1 + \frac{P_t}{\sigma^2} \left(\frac{4\pi f_c \|\boldsymbol{G} - \boldsymbol{U}_u\|}{c}\right)^{-\alpha}\right), \tag{6.47}$$

where A_u is the sharing times of the u^{th} subcarrier, while $\tilde{\boldsymbol{G}}$ is the ground coordinates of the UAV and can be represented by $\tilde{\boldsymbol{G}} = (x_a, y_a)$. Furthermore, the transmit power P_t is large enough to cover all GUs in the target area, which means the received signal to noise power ratio (SNR) is high. Therefore, we may use the following approximation:

$$\max_{\tilde{\boldsymbol{G}}} \sum_{u=1}^{N_u} A_u \log_2 \left(\frac{P_t}{\sigma^2} \left(\frac{4\pi f_c \|\boldsymbol{G} - \boldsymbol{U}_u\|}{c}\right)^{-\alpha}\right), \tag{6.48}$$

which is equivalent to:

$$\max_{\tilde{\boldsymbol{G}}} -\alpha \sum_{u=1}^{N_u} A_u \log_2 \|\boldsymbol{G} - \boldsymbol{U}_u\|. \tag{6.49}$$

As mentioned before, the free space path loss exponent $\alpha = 2$ is selected in the LoS dominant environment. Thus, (6.49) can be further simplified as:

$$\min_{\tilde{\boldsymbol{G}}} \sum_{u=1}^{N_u} A_u \log_2 \|\boldsymbol{G} - \boldsymbol{U}_u\|^2. \tag{6.50}$$

Taking the gradient with respect to $\boldsymbol{G}$ and set to zero, we have:

$$\sum_{u=1}^{N_u} \frac{A_u(\tilde{\boldsymbol{G}} - \tilde{\boldsymbol{U}}_u)}{\|\boldsymbol{G} - \boldsymbol{U}_u\|^2} = \boldsymbol{0}. \tag{6.51}$$

Simplifying the above equation, we obtain:

$$\tilde{\boldsymbol{G}} = \frac{\sum_{u=1}^{N_u} \frac{A_u \tilde{\boldsymbol{U}}_u}{\|\boldsymbol{G} - \boldsymbol{U}_u\|^2}}{\sum_{u=1}^{N_u} \frac{A_u}{\|\boldsymbol{G} - \boldsymbol{U}_u\|^2}}. \tag{6.52}$$

Afterwards, we use fixed-point iteration to obtain the solution as follow [336]:

$$\tilde{\boldsymbol{G}}^{(t+1)} = \frac{\sum_{u=1}^{N_u} \frac{A_u \tilde{\boldsymbol{U}}_u}{\|\boldsymbol{G}^{(t)} - \boldsymbol{U}_u\|^2}}{\sum_{u=1}^{N_u} \frac{A_u}{\|\boldsymbol{G}^{(t)} - \boldsymbol{U}_u\|^2}}. \tag{6.53}$$

It can be seen that $\tilde{\boldsymbol{G}}$ is the linear combination of $\tilde{\boldsymbol{U}}_u$ and $\tilde{\boldsymbol{U}}_u$ is a convex hull. Therefore, the UAV will be restricted in the convex hull (target area) and will be rapidly dragged into the convex hull even if the initial point is selected outside the convex hull. Furthermore, we set $\boldsymbol{E} = \frac{A_u(\tilde{\boldsymbol{G}} - \tilde{\boldsymbol{U}}_u)}{\|\boldsymbol{G} - \boldsymbol{U}_u\|^2}$ and the Hessian matrix with respect to $\boldsymbol{G}$ based on $\boldsymbol{E}$ can be expressed by:

$$\begin{aligned} \frac{\partial \boldsymbol{E}}{\partial \boldsymbol{G}} &= \frac{A_u \left(2\boldsymbol{I}\|\boldsymbol{G} - \boldsymbol{U}_u\|^2 - 4(\tilde{\boldsymbol{G}} - \tilde{\boldsymbol{U}}_u)(\tilde{\boldsymbol{G}} - \tilde{\boldsymbol{U}}_u)^T\right)}{\|\boldsymbol{G} - \boldsymbol{U}_u\|^4}, \\ &= \frac{A_u \left(2\boldsymbol{I}\|\boldsymbol{G} - \boldsymbol{U}_u\|^2 - 4\|\tilde{\boldsymbol{G}} - \tilde{\boldsymbol{U}}_u\|^2 \boldsymbol{Z}\boldsymbol{Z}^T\right)}{\|\boldsymbol{G} - \boldsymbol{U}_u\|^4}, \end{aligned} \tag{6.54}$$

where $\boldsymbol{Z} = \frac{\tilde{\boldsymbol{G}} - \tilde{\boldsymbol{U}}_u}{\|\tilde{\boldsymbol{G}} - \tilde{\boldsymbol{U}}_u\|}$ is the direction vector of $\tilde{\boldsymbol{G}} - \tilde{\boldsymbol{U}}_u$, which can also be represented in parametric form: $\boldsymbol{Z} = [\cos\theta, \sin\theta]$ and the direction angle θ can be obtained by $\theta = \arccos(\cos\theta)$. Then, the expectation of (6.54) is calculated by:

$$\begin{aligned} \mathbb{E}\left\{\frac{\partial \boldsymbol{E}}{\partial \boldsymbol{G}}\right\} &= \frac{2A_u\boldsymbol{I}}{\|\boldsymbol{G} - \boldsymbol{U}_u\|^4} \left(\|\boldsymbol{G} - \boldsymbol{U}_u\|^2 - \|\tilde{\boldsymbol{G}} - \tilde{\boldsymbol{U}}_u\|^2\right), \\ &= \frac{2A_u\boldsymbol{I}h_d^2}{\|\boldsymbol{G} - \boldsymbol{U}_u\|^4}. \end{aligned} \tag{6.55}$$

Additionally, it is worth noting that the expectation of $\boldsymbol{Z}\boldsymbol{Z}^T$ satisfy the following condition:

$$\mathbb{E}\left\{\boldsymbol{Z}\boldsymbol{Z}^T\right\} = \begin{bmatrix} \cos\theta^2 & \cos\theta\sin\theta \\ \cos\theta\sin\theta & \sin\theta^2 \end{bmatrix} = \frac{1}{2}\boldsymbol{I}, \tag{6.56}$$

when a large number of GUs are uniformly distributed in a target area. Therefore, it can be seen that (6.55) is positive definite and the objective function (6.50) is convex, which means that the proposed deployment can always "converge" to the global optimum position.

The above deployment process is also applicable in the classic OFDMA scenarios by simply setting the coefficient A_u to 1. Here, it can be found that both of the cases have a constant A_u, where the sum of A_u is a constant no matter how the location of the UAV changes. To further illustrate this phenomenon, we consider that three GUs request the same content under this condition. Then, the corresponding sharing times A_u must be one of the cases illustrated by Table 6.1 based on the order of received signal power. Therefore, it is clear that the sum of A_u is always a constant even during the process of deployment, i.e. $\sum_u^{N_u} A_u = 6$.

Table 6.1: The combinations of weight vector when 3 GUs request the same content in content-sharing scheme.

w_1	w_2	w_3
1	2	3
1	3	2
2	1	3
2	3	1
3	1	2
3	2	1

However, this is not the case in the CCS scenario. As shown in Fig. 6.6, the sum of sharing times at different deployment locations of UAV in a scenario of 50 GUs in a 1 km $\times$ 1 km target area is not a constant any more. Also, the red point in both subfigures indicates the position that gives us the highest sum of A_i or A_u.The reason for the variation of the sum of sharing times at different locations is the optimization process. At different locations, the optimization process cannot guarantee that the weight vector $\boldsymbol{W}_i$ is fixed because different positions will result in different capacity for the GU. Therefore, to meet the demand of the basic data requirement R_m, the system has to adjust the weight of each content, which will cause the variation of the weight vector. Besides, the change of locations will also change the filter vector, and further affect the sum of sharing times.

Since the sum of A_i is related to the location of UAV, the deployment scheme proposed in previous scheme is not applicable for the CCS case any more. Therefore, we design a traverse-search based deployment scheme for our proposed CCS scenario. Firstly, we divide the whole target area into small grids as shown in Fig. 6.7. Afterwards, all possible locations (points) are tested and then the point where maximum average data rate can be achieved, as illustrated in Fig. 6.6, is selected as the final deployment

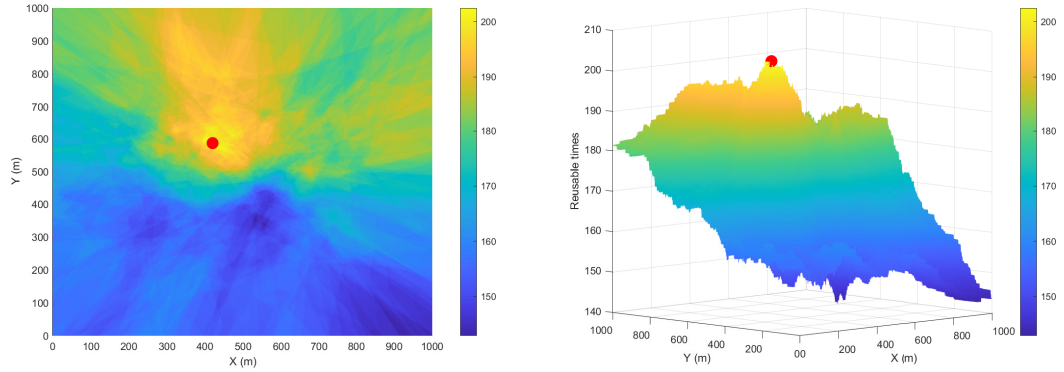

(a) 2D figure. (b) 3D figure.

Figure 6.6: The sum of sharing times in CCS scenario at different deployment locations in 1 km $\times$ 1 km area with 50 subcarriers.

location. Consequently, the computation complexity is directly related to the size of the grids. Fortunately, this procedure can be accomplished by sending the location information back to the terrestrial BS via backhaul links as the computation ability of terrestrial BS is much stronger than that on the UAV or it can also be accomplished by UAV itself if the UAV's computation ability is good enough to support this process.

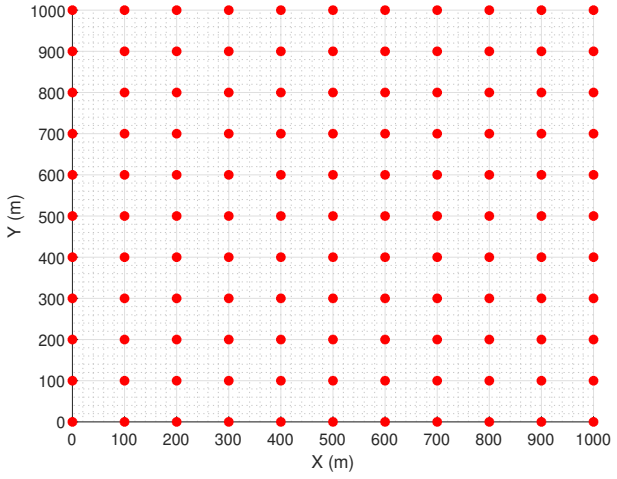

Figure 6.7: The grids of 1 km $\times$ 1 km target area with a space of 100 m for traverse-search in CCS scenario.

6.4 Performance Results and Evaluation

In this section, we investigate the performance of our proposed content-aware communication system in a 1 km $\times$ 1 km square area with a total of $N_u = 50$ GUs uniformly distributed on the ground. Besides, the UAV flies at a height of $h_d = 100$ m and operate at a frequency band of $f_c = 5.8$ GHz for the A2G communication. Under the LoS

model, the path loss exponent α is set to 2. Meanwhile, the noise PSD N_0 is set to -174 dBm/Hz and the transmission power P_t of the UAVs is 26 dBm. Additionally, OFDMA is employed to support multi-user communications, where the total bandwidth B allocated to all GUs is 40 MHz. In our system, the whole bandwidth is equally divided into $N_s = 50$ subcarriers and each GU will be assigned one subcarrier. Moreover, we assume that the interests of GUs are stable within a long period, which means the distribution of GUs interests is fixed in our simulation time[3]. In the following, we first analyze the effect of the UAV deployment based on the average rate of all GUs. Afterwards, the average rate of each transmission scheme will be investigated. The detailed simulation parameters are listed in Table 6.2.

Table 6.2: Simulation parameters

Parameter	Symbol	Value
Bandwidth	B	40 MHz
Noise PSD	N_0	-174 dBm/Hz
Carrier frequency	f_c	5.8 GHz
Path loss exponent	α	2
Transmission power	P_t	26 dBm
UAV height	h_d	100 m
Speed of light	c	3×10^8 m/s
Number of UAV	N_d	1
Number of GUs	N_u	50
Number of subcarriers	N_s	50

In our proposed content-aware transmission schemes, the average rate of each GU is taken as the objective function for optimising the UAV deployment. Fig. 6.8 depicts the performance of our proposed deployment schemes in the scenario of one UAV with 50 GUs in the target area. In our simulation, we tested 3 different deployment schemes, which are classic k-means algorithm, fixed-point algorithm and traverse-search algorithm. In Fig. 6.8, the fixed-point deployment scheme is applied on two scenarios, where we use non-content-sharing (NCS) to indicate the scenario that uses fixed-point deployment scheme without CS, while use PCS and CCS to indicate the scenario with CS. Besides, the proposed CS transmission schemes are also included to further illustrate the effects of the requested contents on deployment results. Then, in order to reveal the generality of our proposed deployment scheme, we randomly set the initial points of the fixed-point deployment scheme with two different snapshots as seen in Fig. 6.8(a) and Fig. 6.8(b). Here, two different snapshots means the locations of GUs and the requested contents are different. Additionally, the GUs are classified by the

[3]The UAV has to request the new contents from the core network if new contents are requested by GUs. Therefore, this will cause a request delay since the new contents have not been cached in advance but the proposed transmission scheme can still be applied when the new contents are obtained.

requested times of contents, which is pointed out by the number in the legend. For example, those GUs marked by small blue "▽" in Fig. 6.8(a) means that their requested contents occurred only once, but it is worth noting that the same requested times does not mean they requested the same content.

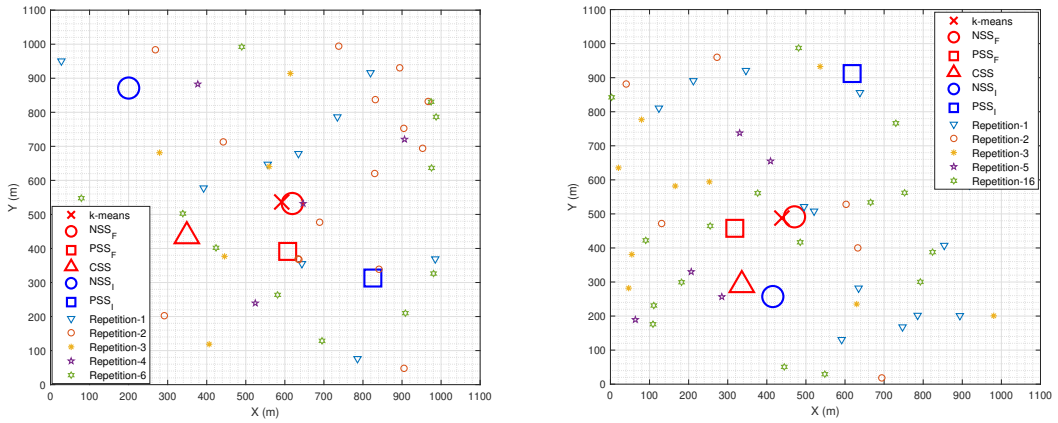

(a) Snapshot 1.

(b) Snapshot 2.

Figure 6.8: Illustration of the UAV deployment with 50 GUs and $R_{min} = 2$ Mbits/s by the proposed deployment algorithm, where NCS, PCS and CCS denote non-content-sharing, private content-sharing and common content-sharing, respectively. While the repetition-x indicates that the requested times of contents for GUs represented by the same markers is x. Moreover, the subscripts I and F indicate the initial locations and the final locations, respectively.

As shown in Fig. 6.8(a) and Fig. 6.8(b), we consider a scenario that 50 GUs are in a target area served by one UAV with different deployment schemes under the constraint of $R_{min} = 2$ Mbits/s. It could be found that the final deployment locations of k-means and fixed-point under NCS are very close under LoS dominant condition as the capacity is directly related to the A2G distances. Besides, the sharing times of the contents, which are indicated by repetition-x in Fig. 6.8, plays an important role in the deployment of UAV in each setup. Compared to the first two deployment schemes that stay at the centroids of all GUs, the final deployment position of PCS is more bias to those GUs with requested contents of high sharing times. However, CCS is accomplished based on an exhaustive search on the whole area, the final deployment position is the location it obtains the maximum average rate. Unlike PCS, CCS may not show any bias to specific group of GUs as the R_{min} is also a key factor to affect the decision of final position, and hence it cannot deploy the UAV by purely considering the frequency of contents.

Additionally, Fig. 6.9 illustrates the convergence progress of fixed-point deployment algorithm in NCS scenario. For conciseness, the scenario of PCS will not be repeatedly illustrated here to show the same property. It can be found from Fig. 6.9(a) and Fig. 6.9(b) that two different initial points (within and outside convex hull) have been selected to test the performance of the proposed fixed-point deployment scheme in the

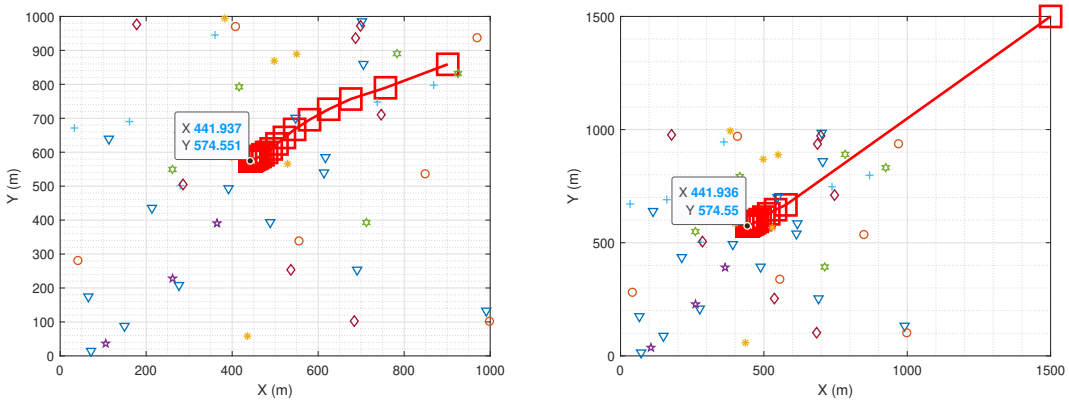

(a) Within convex hull. (b) Outside convex hull.

Figure 6.9: Convergence progress of the UAV deployment with 50 GUs by fixed-point deployment algorithm in NCS method.

same distribution of GUs. These two figures show that the UAVs will iteratively converge to the final deployment position no matter where the initial point is selected. Besides, it can be seen that the convergence is very fast. If we consider other iterative algorithm, such as gradient algorithm, the speed of convergence will be very slow when the step size is too small. On the other hand, the final results may not be satisfactory if the step size is too big. Therefore, our proposed deployment scheme can rapidly and precisely find the position where the maximum average rate can be achieved.

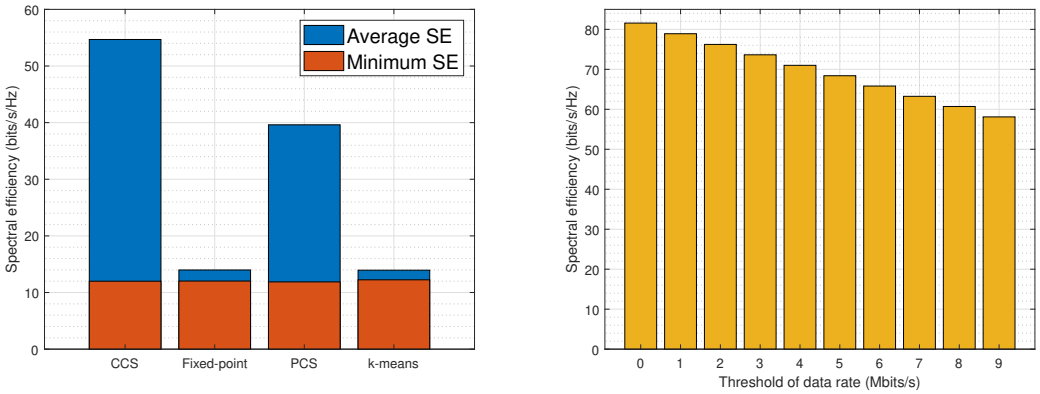

(a) Comparison of average SE. (b) Average SE of different thresholds.

Figure 6.10: Illustration of average SE by different deployment schemes and transmission schemes, where NCS and *k*-means all indicate the NCS scenario but with different deployment schemes.

In Fig. 6.10, the average SE is obtained by Monte Carlo simulation, where we run a large number of setups with different locations of GUs with different requested contents for testing the performance of our system. Fig. 6.10(a) shows the average SE of different investigated transmission and deployment schemes. From the aspect of UAV

deployment, it can be seen that the average SE of *k*-means and fixed-point deployment schemes are very close, which means that both distance based and the capacity-achieving deployment scheme give us similar performance in a LoS dominant environment without CS. However, if PCS is considered in the data transmission with fixed-point deployment scheme, the average data rate is almost tripled when compared to the previous two cases. Besides, it is worth noting that *k*-means is solely depend on the A2G distance and cannot be combined with the proposed the PCS scheme. Moreover, the minimum data rate threshold will affect the performance. Hence, we set $R_{min} = 9.6$ Mbits/s (12 bits/s/Hz) based on the average minimum data rate of the first two scenarios for a fair comparison. It is worth noting that the R_{min} is not obtained from the minimum data value of all setups, it was calculated by collecting the minimum data rate in each setup and the average of these minimum values was taken. Therefore, it is clear to see from Fig. 6.10(a) that the average SE of PCS is more than twice as much as that of *k*-means and NCS. Additionally, the average SE of CCS under this R_{min} condition is close to 1.5 times of PCS, which further improves the SE of GUs. Furthermore, it could be found from Fig. 6.10(b) that the increase of threshold R_{min} will gradually reduce the average SE of CCS, which means that the system cannot exploit more subcarrier resources from those GUs with low-frequency requested contents when their data rate demand is higher. In other words, the optimization need to increase the weight of those low-frequency requested contents in subcarriers to achieve the minimum SE set by R_{min}. Consequently, this will conversely reduce the weight of those high-frequency requested contents since the sum of weight is fixed to 1.

6.5 Conclusion

In this chapter, we proposed two CS transmission schemes, namely PCS and CCS, in a UAV-assisted wireless communication, which aims to increase the average SE of GUs. Afterwards, based on the proposed PCS and CCS scheme, we designed two deployment schemes to find the appropriate UAV position that maximizes the average SE of GUs. The simulation results indicate that our proposed PCS and CCS transmission scheme will significantly improve the average SE and that the deployment schemes are able to help the UAV to find the appropriate deployment position. The simulation results prove that our proposed two CS transmission schemes outperform the traditional transmission scheme by 25 bits/s/Hz and 40 bits/s/Hz, respectively.

Chapter 7

Conclusion and Future Work

7.1 Thesis Conclusion

In this thesis, we initially seeked to reduce the system latency of the UAV-assisted wireless communication system to enhance the GUs' QoE by taking mobile edge caching on UAVs into consideration. Both transmission delays and request delays were taken into account in the system. The received SNR by the GUs determines the transmission delay, whereas the request delay depends on the cached contents in the storage of the UAVs. Three user association methods have been investigated based on the received SNR, user preference, and minimum delay. The results have shown that increasing the received SNR (transmission power) will reduce transmission delay. Meanwhile, the request delay can also be improved by considering user preference as the central aspect. However, it turns out that neither of these two strategies can fully address the problem. Therefore, we proposed a global caching method that collaboratively utilizes the storage resources on UAVs to achieve a minimum delay by considering both received SNR and user preference.

Additionally, we devised an approach based on deep reinforcement learning that enables multiple UAVs in a target area to update their positions automatically based on the distribution of moving GUs. First, to achieve a global optimal QoS for all GUs by swapping GUs among the problem of "outliers" that may arise in the conventional greedy association method, which only considers the strongest received signal power. In addition, the collision challenge in multiple UAVs systems may degrade system performance. Thus a four-level criterion has been created to identify the collision intensity and convert it into the penalty of our DQL system for avoiding the collision. The simulation results demonstrate that our proposed method performs similarly to the k-means clustering technique described in Chapter 3. The k-means clustering algorithm can locate the centre of each group of GUs and deploy UAVs accordingly. It is impractical,

however, due to the limited speed of UAVs and the probability of sudden shifts. Consequently, by interacting with the environment, our proposed DQL method can locate an optimal position to cover the majority of GUs with more robust communication links and enhance the QoE of GUs.

Then, the constraint of onboard energy stimulates the development of a more energy-efficient information transmission method, and the deployment of multiple UAVs might negatively impact the QoE of GUs. Therefore, we proposed an approach that combines the concept of IM with UAV communications systems to improve EE. In addition, based on the proposed IM-UAV communication system, a gradient descent based UAV deployment scheme was designed to optimize the sum rate of GUs in the target area. On the other hand, maximum likelihood detection for the IM-UAV necessitates a high computational complexity for detection at the GUs while offering the best possible performance. In order to reduce the computational complexity on the receiver side, we proposed a low-complexity detection scheme that can detect index symbols and data symbols separately. The simulation results demonstrate that the proposed deployment method can attain the appropriate positions to deploy the UAVs. At the same time, the EE is also enhanced by combining IM with a UAV communication system.

Finally, we presented two CS transmission techniques, PCS and CCS, based on the OFDMA methodology employed in Chapter 5 for a UAV-assisted wireless communication in the content-aware scenario in Chapter 3. This two proposed transmission schemes aim to increase the average data rate of GUs. Afterwards, based on the proposed CS transmission scheme, we developed two deployment schemes to determine the optimal UAV position for maximizing the average data rate of GUs. The simulation results indicate that our proposed CS transmission scheme would significantly increase the average data rate. Meanwhile, the deployment strategies will assist the UAV in finding the appropriate deployment position.

7.2 Future Work

In this thesis, we have investigated the feasibility of considering UAVs as ABSs to support GUs with different targets, such as latency, QoE, EE and data rate. In this section, we will briefly discuss several future research ideas.

7.2.1 Content Update of UAVs

In Chapter 3, we have investigated the potential of applying caching on UAVs to reduce the transmission latency, where LDA was employed to find out the interests of GUs. However, the preferences of GUs is considered as a "constant" in the system. Therefore,

it is worth considering the scenario where the preferences of GUs are slowly varying and the strategy of updating the contents should be taken into consideration. Besides, different content popularity analysis algorithms may also affect the content cached in UAVs. Hence, there is a need to investigate the performance of different popularity analysis algorithms and test how they affect the caching efficiency.

7.2.2 Hybrid Deployment of UAVs

In this thesis, the distribution of GUs is mainly considered as a uniform distribution. However, it is highly possible that GUs are not uniformly distributed in the service area in reality. Hence, the deployment of UAVs may have to operate in a hybrid way, for example, a swarm of UAVs may have to decoupled into several sub-swarms or solely to serve GUs according to the distribution of GUs.

7.2.3 Joint Optimization of Deployment and Caching

Moreover, the moving pattern of GUs may also help to determine the contents to be cached in UAVs. More explicitly, the prediction of GUs' trajectory should be able to help UAVs adjust their positions in advance. Besides, it can be seen that the contents cached on UAVs can also be updated accordingly before the arrival of GUs, which largely improve the QoE of GUs.

7.2.4 Strategy of Resource Allocation

Additionally, the bandwidth of each GU is identical in our systems for simplicity. However, the allocation of bandwidth resources will also affect the system performance. For example, if we hope to maximize the minimum data rate of GUs in the system, then, the bandwidth resources allocated to those that have poor channel conditions are usually more than that of GUs having good channel condition. Therefore, the strategy of resource allocation can be taken into consideration according to specific design target.

7.2.5 Multi-Dimensional Index Modulation

In Chapter 5, the IM was employed on UAVs to activate UAVs on corresponding subcarriers, where each UAV can only modulate data symbols onto the allocated subcarriers according to the index bits. However, it is worth considering multi-Dimensional IM to further improve the EE. For example, we can consider OFDM-IM, which is also known as subcarrier IM, in the frequency domain to add more index bits by using only

part of the assigned subcarriers to transmit data symbols while keeping the remainings empty.

7.2.6 Interference Cancellation

In this thesis, the A2G interference issue was not considered in our UAV-assisted communication system. How to mitigate the severe A2G interference is deemed a significant challenge in practically realizing cellular-connected UAVs. Although various interference mitigation techniques have been studied in terrestrial networks, they may be ineffective or insufficient to deal with UAVs' new and more severe interference issues. Owing to their unique LoS-dominant A2G channels, new and more sophisticated interference mitigation techniques are needed to achieve efficient spectrum sharing between the existing GUs and UAVs in future cellular networks.

References

[1] N. Abbas, Y. Zhang, A. Taherkordi, and T. Skeie, "Mobile edge computing: A survey," *IEEE Internet of Things Journal*, vol. 5, no. 1, pp. 450–465, 2017.

[2] J. Lee, J.-H. Kang, S. Jun, H. Lim, D. Jang, and S. Park, "Ensemble modeling for sustainable technology transfer," *Sustainability*, vol. 10, no. 7, p. 2278, 2018.

[3] R. S. Sutton and A. G. Barto, *Reinforcement learning: An introduction*. MIT press, 2018.

[4] Z. Wang, T. Schaul, M. Hessel, H. Hasselt, M. Lanctot, and N. Freitas, "Dueling network architectures for deep reinforcement learning," in *International conference on machine learning*. PMLR, 2016, pp. 1995–2003.

[5] L.-L. Yang, *Multicarrier communications*. John Wiley & Sons, 2009.

[6] D. Coleman, *Wi-Fi 6 For Dummies, Extreme Networks Special Edition*. John Wiley & Sons, 2020.

[7] R. . Schwarz, "White paper: IEEE 802.11ax technology introduction," *IEEE 802.11ax*, 2020.

[8] E. Basar, M. Wen, R. Mesleh, M. Di Renzo, Y. Xiao, and H. Haas, "Index modulation techniques for next-generation wireless networks," *IEEE access*, vol. 5, pp. 16 693–16 746, 2017.

[9] M. Chen, M. Mozaffari, W. Saad, C. Yin, M. Debbah, and C. S. Hong, "Caching in the sky: Proactive deployment of cache-enabled unmanned aerial vehicles for optimized quality-of-experience," *IEEE Journal on Selected Areas in Communications*, vol. 35, no. 5, pp. 1046–1061, 2017.

[10] H. Wang, G. Ding, F. Gao, J. Chen, J. Wang, and L. Wang, "Power control in UAV-supported ultra dense networks: Communications, caching, and energy transfer," *IEEE Communications Magazine*, vol. 56, no. 6, pp. 28–34, 2018.

[11] C. V. N. Index, "Global mobile data traffic forecast update, 2017–2022 white paper," *Cisco: San Jose, CA, USA*, 2019.

[12] S. Wang, X. Zhang, Y. Zhang, L. Wang, J. Yang, and W. Wang, "A survey on mobile edge networks: Convergence of computing, caching and communications," *IEEE Access*, vol. 5, pp. 6757–6779, 2017.

[13] K. P. Valavanis and G. J. Vachtsevanos, *Handbook of unmanned aerial vehicles*. Springer, 2015.

[14] R. W. Beard and T. W. McLain, *Small unmanned aircraft: Theory and practice*. Princeton university press, 2012.

[15] E. Yanmaz, S. Yahyanejad, B. Rinner, H. Hellwagner, and C. Bettstetter, "Drone networks: Communications, coordination, and sensing," *Ad Hoc Networks*, vol. 68, pp. 1–15, 2018.

[16] R. Gupta, A. Nair, S. Tanwar, and N. Kumar, "Blockchain-assisted secure UAV communication in 6G environment: Architecture, opportunities, and challenges," *IET communications*, vol. 15, no. 10, pp. 1352–1367, 2021.

[17] X. Jiang, M. Sheng, Z. Nan, X. Chengwen, L. Weidang, and W. Xianbin, "Green UAV communications for 6G: A survey," *Chinese Journal of Aeronautics*, 2021.

[18] X. Wang, M. Chen, T. Taleb, A. Ksentini, and V. C. Leung, "Cache in the air: Exploiting content caching and delivery techniques for 5G systems," *IEEE Communications Magazine*, vol. 52, no. 2, pp. 131–139, 2014.

[19] K. Zhang, S. Leng, Y. He, S. Maharjan, and Y. Zhang, "Mobile edge computing and networking for green and low-latency Internet of Things," *IEEE Communications Magazine*, vol. 56, no. 5, pp. 39–45, 2018.

[20] Y. Dai, D. Xu, S. Maharjan, G. Qiao, and Y. Zhang, "Artificial intelligence empowered edge computing and caching for internet of vehicles," *IEEE Wireless Communications*, vol. 26, no. 3, pp. 12–18, 2019.

[21] M. Chen and Y. Hao, "Task offloading for mobile edge computing in software defined ultra-dense network," *IEEE Journal on Selected Areas in Communications*, vol. 36, no. 3, pp. 587–597, 2018.

[22] Y. Zeng, R. Zhang, and T. J. Lim, "Wireless communications with unmanned aerial vehicles: Opportunities and challenges," *IEEE Communications Magazine*, vol. 54, no. 5, pp. 36–42, 2016.

[23] Y. Guo, L. Duan, and R. Zhang, "Cooperative local caching under heterogeneous file preferences," *IEEE Transactions on Communications*, vol. 65, no. 1, pp. 444–457, 2016.

[24] J. Qiao, Y. He, and X. S. Shen, "Proactive caching for mobile video streaming in millimeter wave 5g networks," *IEEE Transactions on Wireless Communications*, vol. 15, no. 10, pp. 7187–7198, 2016.

[25] R. I. Bor-Yaliniz, A. El-Keyi, and H. Yanikomeroglu, "Efficient 3-D placement of an aerial base station in next generation cellular networks," in *2016 IEEE international conference on communications (ICC)*. IEEE, 2016, pp. 1–5.

[26] "Supporting IoT with rate-splitting multiple access in satellite and aerial-integrated networks], author=Lin, Zhi and Lin, Min and De Cola, Tomaso and Wang, Jun-Bo and Zhu, Wei-Ping and Cheng, Julian, journal=IEEE Internet of Things Journal, volume=8, number=14, pages=11123–11134, year=2021, publisher=IEEE."

[27] E. Danish, V. De Silva, A. Fernando, C. De Alwis, and A. Kondoz, "Content-aware resource allocation in OFDM systems for energy-efficient video transmission," *IEEE Transactions on Consumer Electronics*, vol. 60, no. 3, pp. 320–328, 2014.

[28] H. Wu, N. Zhang, Z. Wei, S. Zhang, X. Tao, X. Shen, and P. Zhang, "Content-aware cooperative transmission in HetNets with consideration of base station height," *IEEE Transactions on Vehicular Technology*, vol. 67, no. 7, pp. 6048–6062, 2018.

[29] S. Baidya, Y. Chen, and M. Levorato, "eBPF-based content and computation-aware communication for real-time edge computing," in *IEEE INFOCOM 2018-IEEE Conference on Computer Communications Workshops (INFOCOM WKSHPS)*. IEEE, 2018, pp. 865–870.

[30] P. Dinh, T. M. Nguyen, C. Assi, and W. Ajib, "Joint beamforming and location optimization for cooperative content-aware UAVs," in *2019 IEEE Wireless Communications and Networking Conference (WCNC)*. IEEE, 2019, pp. 1–7.

[31] P. Dinh, T. M. Nguyen, S. Sharafeddine, and C. Assi, "Joint location and beamforming design for cooperative UAVs with limited storage capacity," *IEEE Transactions on Communications*, vol. 67, no. 11, pp. 8112–8123, 2019.

[32] C. H. Liu, Z. Chen, J. Tang, J. Xu, and C. Piao, "Energy-efficient UAV control for effective and fair communication coverage: A deep reinforcement learning approach," *IEEE Journal on Selected Areas in Communications*, vol. 36, no. 9, pp. 2059–2070, 2018.

[33] M. Mozaffari, W. Saad, M. Bennis, Y.-H. Nam, and M. Debbah, "A tutorial on UAVs for wireless networks: Applications, challenges, and open problems," *IEEE Communications Surveys & Tutorials*, 2019.

[34] H. Wu, Y. Wen, J. Zhang, Z. Wei, N. Zhang, and X. Tao, "Energy-efficient and secure air-to-ground communication with jittering UAV," *IEEE Transactions on Vehicular Technology*, vol. 69, no. 4, pp. 3954–3967, 2020.

[35] Y. Cai, Z. Wei, R. Li, D. W. K. Ng, and J. Yuan, "Joint trajectory and resource allocation design for energy-efficient secure UAV communication systems," *IEEE Transactions on Communications*, vol. 68, no. 7, pp. 4536–4553, 2020.

[36] D. Bamburry, "Drones: Designed for product delivery," *Design Management Review*, vol. 26, no. 1, pp. 40–48, 2015.

[37] O. K. Sahingoz, "Networking models in flying ad-hoc networks (fanets): Concepts and challenges," *Journal of Intelligent & Robotic Systems*, vol. 74, no. 1-2, pp. 513–527, 2014.

[38] W. Zafar and B. M. Khan, "Flying ad-hoc networks: Technological and social implications," *IEEE Technology and Society Magazine*, vol. 35, no. 2, pp. 67–74, 2016.

[39] I. Bucaille, S. Héthuin, A. Munari, R. Hermenier, T. Rasheed, and S. Allsopp, "Rapidly deployable network for tactical applications: Aerial base station with opportunistic links for unattended and temporary events absolute example," in *MILCOM 2013-2013 IEEE military communications conference*. IEEE, 2013, pp. 1116–1120.

[40] A. Orsino, A. Ometov, G. Fodor, D. Moltchanov, L. Militano, S. Andreev, O. N. Yilmaz, T. Tirronen, J. Torsner, G. Araniti *et al.*, "Effects of Heterogeneous Mobility on D2D-and Drone-Assisted Mission-Critical MTC in 5G." *IEEE Communications Magazine*, vol. 55, no. 2, pp. 79–87, 2017.

[41] U. Siddique, H. Tabassum, E. Hossain, and D. I. Kim, "Wireless backhauling of 5G small cells: Challenges and solution approaches," *IEEE Wireless Communications*, vol. 22, no. 5, pp. 22–31, 2015.

[42] H. Menouar, I. Guvenc, K. Akkaya, A. S. Uluagac, A. Kadri, and A. Tuncer, "UAV-enabled intelligent transportation systems for the smart city: Applications and challenges," *IEEE Communications Magazine*, vol. 55, no. 3, pp. 22–28, 2017.

[43] L. Zhou, H. Ma, Z. Yang, S. Zhou, and W. Zhang, "Unmanned aerial vehicle communications: Path-loss modeling and evaluation," *IEEE Vehicular Technology Magazine*, vol. 15, no. 2, pp. 121–128, 2020.

[44] R. Amorim, H. Nguyen, P. Mogensen, I. Z. Kovács, J. Wigard, and T. B. Sørensen, "Radio channel modeling for UAV communication over cellular networks," *IEEE Wireless Communications Letters*, vol. 6, no. 4, pp. 514–517, 2017.

[45] D. W. Matolak and R. Sun, "Air–ground channel characterization for unmanned aircraft systems—Part I: Methods, measurements, and models for over-water settings," *IEEE Transactions on Vehicular Technology*, vol. 66, no. 1, pp. 26–44, 2016.

[46] R. Sun and D. W. Matolak, "Air–ground channel characterization for unmanned aircraft systems part II: Hilly and mountainous settings," *IEEE Transactions on Vehicular Technology*, vol. 66, no. 3, pp. 1913–1925, 2016.

[47] D. W. Matolak and R. Sun, "Air–ground channel characterization for unmanned aircraft systems—Part III: The suburban and near-urban environments," *IEEE Transactions on Vehicular Technology*, vol. 66, no. 8, pp. 6607–6618, 2017.

[48] "[wlcp2-06: Modelling the likelihood of line-of-sight for air-to-ground radio propagation in urban environments."

[49] J. Holis and P. Pechac, "Elevation dependent shadowing model for mobile communications via high altitude platforms in built-up areas," *IEEE Transactions on Antennas and Propagation*, vol. 56, no. 4, pp. 1078–1084, 2008.

[50] A. A. Khuwaja, Y. Chen, N. Zhao, M.-S. Alouini, and P. Dobbins, "A survey of channel modeling for UAV communications," *IEEE Communications Surveys & Tutorials*, vol. 20, no. 4, pp. 2804–2821, 2018.

[51] A. D. Panagopoulos, P.-D. M. Arapoglou, and P. G. Cottis, "Satellite communications at Ku, Ka, and V bands: Propagation impairments and mitigation techniques," *IEEE Communications Surveys & Tutorials*, vol. 6, no. 3, pp. 2–14, 2004.

[52] P. Chini, G. Giambene, and S. Kota, "A survey on mobile satellite systems," *International Journal of Satellite Communications and Networking*, vol. 28, no. 1, pp. 29–57, 2010.

[53] W. Khawaja, I. Guvenc, and D. Matolak, "UWB channel sounding and modeling for UAV air-to-ground propagation channels," in *2016 IEEE global communications conference (GLOBECOM)*. IEEE, 2016, pp. 1–7.

[54] X. Cai, J. Rodríguez-Piñeiro, X. Yin, N. Wang, B. Ai, G. F. Pedersen, and A. P. Yuste, "An empirical air-to-ground channel model based on passive measurements in LTE," *IEEE Transactions on Vehicular Technology*, vol. 68, no. 2, pp. 1140–1154, 2018.

[55] A. Al-Hourani and K. Gomez, "Modeling cellular-to-UAV path-loss for suburban environments," *IEEE Wireless Communications Letters*, vol. 7, no. 1, pp. 82–85, 2017.

[56] J. H. Bae, Y. S. Kim, N. Hur, and H. M. Kim, "Study on air-to-ground multipath channel and mobility influences in UAV based broadcasting," in *2018 International Conference on Information and Communication Technology Convergence (ICTC)*. IEEE, 2018, pp. 1534–1538.

[57] D. Becker, U.-C. Fiebig, and L. Schalk, "Wideband channel measurements and first findings for low altitude drone-to-drone links in an urban scenario," in *2020 14th European Conference on Antennas and Propagation (EuCAP)*. IEEE, 2020, pp. 1–5.

[58] J. Košmerl and A. Vilhar, "Base stations placement optimization in wireless networks for emergency communications," in *2014 IEEE international conference on communications workshops (ICC)*. IEEE, 2014, pp. 200–205.

[59] A. Al-Hourani, S. Kandeepan, and S. Lardner, "Optimal LAP altitude for maximum coverage," *IEEE Wireless Communications Letters*, vol. 3, no. 6, pp. 569–572, 2014.

[60] M. Alzenad, A. El-Keyi, F. Lagum, and H. Yanikomeroglu, "3-D placement of an unmanned aerial vehicle base station (UAV-BS) for energy-efficient maximal coverage," *IEEE Wireless Communications Letters*, vol. 6, no. 4, pp. 434–437, 2017.

[61] P. K. Sharma and D. I. Kim, "UAV-enabled downlink wireless system with non-orthogonal multiple access," in *2017 IEEE Globecom Workshops (GC Wkshps)*. IEEE, 2017, pp. 1–6.

[62] M. F. Sohail, C. Y. Leow, and S. Won, "Non-orthogonal multiple access for unmanned aerial vehicle assisted communication," *IEEE Access*, vol. 6, pp. 22 716–22 727, 2018.

[63] T. Hou, Y. Liu, Z. Song, X. Sun, and Y. Chen, "Multiple antenna aided NOMA in UAV networks: A stochastic geometry approach," *IEEE Transactions on Communications*, vol. 67, no. 2, pp. 1031–1044, 2018.

[64] M. Mozaffari, W. Saad, M. Bennis, and M. Debbah, "Unmanned aerial vehicle with underlaid device-to-device communications: Performance and tradeoffs," *IEEE Transactions on Wireless Communications*, vol. 15, no. 6, pp. 3949–3963, 2016.

[65] ——, "Wireless communication using unmanned aerial vehicles (UAVs): Optimal transport theory for hover time optimization," *IEEE Transactions on Wireless Communications*, vol. 16, no. 12, pp. 8052–8066, 2017.

[66] ——, "Efficient deployment of multiple unmanned aerial vehicles for optimal wireless coverage," *IEEE Communications Letters*, vol. 20, no. 8, pp. 1647–1650, 2016.

[67] D. Yang, Q. Wu, Y. Zeng, and R. Zhang, "Energy tradeoff in ground-to-UAV communication via trajectory design," *IEEE Transactions on Vehicular Technology*, vol. 67, no. 7, pp. 6721–6726, 2018.

[68] J. Lyu, Y. Zeng, and R. Zhang, "Cyclical multiple access in UAV-aided communications: A throughput-delay tradeoff," *IEEE Wireless Communications Letters*, vol. 5, no. 6, pp. 600–603, 2016.

[69] Q. Wu, Y. Zeng, and R. Zhang, "Joint trajectory and communication design for multi-UAV enabled wireless networks," *IEEE Transactions on Wireless Communications*, vol. 17, no. 3, pp. 2109–2121, 2018.

[70] Y. Zeng and R. Zhang, "Energy-efficient UAV communication with trajectory optimization," *IEEE Transactions on Wireless Communications*, vol. 16, no. 6, pp. 3747–3760, 2017.

[71] Q. Wu and R. Zhang, "Common throughput maximization in UAV-enabled OFDMA systems with delay consideration," *IEEE Transactions on Communications*, vol. 66, no. 12, pp. 6614–6627, 2018.

[72] S. Zhang, Y. Zeng, and R. Zhang, "Cellular-enabled UAV communication: Trajectory optimization under connectivity constraint," in *2018 IEEE International Conference on Communications (ICC)*. IEEE, 2018, pp. 1–6.

[73] A. Khandekar, N. Bhushan, J. Tingfang, and V. Vanghi, "LTE-advanced: Heterogeneous networks," in *2010 European wireless conference (EW)*. IEEE, 2010, pp. 978–982.

[74] T. Qu, D. Xiao, and D. Yang, "A novel cell selection method in heterogeneous LTE-advanced systems," in *2010 3rd IEEE International Conference on Broadband Network and Multimedia Technology (IC-BNMT)*. IEEE, 2010, pp. 510–513.

[75] M. El Helou, S. Lahoud, M. Ibrahim, K. Khawam, B. Cousin, and D. Mezher, "A hybrid approach for radio access technology selection in heterogeneous wireless networks," *Wireless Personal Communications*, vol. 86, no. 2, pp. 789–834, 2016.

[76] H. Kim, G. de Veciana, X. Yang, and M. Venkatachalam, "Alpha-optimal user association and cell load balancing in wireless networks," in *2010 Proceedings IEEE INFOCOM*. IEEE, 2010, pp. 1–5.

[77] K. Son, H. Kim, Y. Yi, and B. Krishnamachari, "Base station operation and user association mechanisms for energy-delay tradeoffs in green cellular networks," *IEEE journal on selected areas in communications*, vol. 29, no. 8, pp. 1525–1536, 2011.

[78] L. Chiaraviglio, D. Ciullo, M. Meo, M. A. Marsan, and I. Torino, "Energy-aware UMTS access networks," 2008.

[79] M. A. Marsan, L. Chiaraviglio, D. Ciullo, and M. Meo, "Optimal energy savings in cellular access networks," in *2009 IEEE International Conference on Communications Workshops*. IEEE, 2009, pp. 1–5.

[80] S. Zhou, J. Gong, Z. Yang, Z. Niu, and P. Yang, "Green mobile access network with dynamic base station energy saving," in *ACM MobiCom*, vol. 9, no. 262, 2009, pp. 10–12.

[81] E. Oh and B. Krishnamachari, "Energy savings through dynamic base station switching in cellular wireless access networks," in *2010 IEEE Global Telecommunications Conference GLOBECOM 2010*. IEEE, 2010, pp. 1–5.

[82] M. A. Marsan and M. Meo, "Energy efficient management of two cellular access networks," *ACM SIGMETRICS Performance Evaluation Review*, vol. 37, no. 4, pp. 69–73, 2010.

[83] O. Esrafilian and D. Gesbert, "Simultaneous user association and placement in multi-UAV enabled wireless networks," in *WSA 2018; 22nd International ITG Workshop on Smart Antennas*. VDE, 2018, pp. 1–5.

[84] X. Xi, X. Cao, P. Yang, J. Chen, T. Quek, and D. Wu, "Joint user association and UAV location optimization for UAV-aided communications," *IEEE Wireless Communications Letters*, vol. 8, no. 6, pp. 1688–1691, 2019.

[85] Y. Qian, F. Wang, J. Li, L. Shi, K. Cai, and F. Shu, "User association and path planning for UAV-aided mobile edge computing with energy restriction," *IEEE Wireless Communications Letters*, vol. 8, no. 5, pp. 1312–1315, 2019.

[86] F. Cheng, D. Zou, J. Liu, J. Wang, and N. Zhao, "Learning-based user association for dual-UAV enabled wireless networks with D2D connections," *IEEE Access*, vol. 7, pp. 30 672–30 682, 2019.

[87] Y. Sun, T. Wang, and S. Wang, "Location optimization and user association for unmanned aerial vehicles assisted mobile networks," *IEEE Transactions on Vehicular Technology*, vol. 68, no. 10, pp. 10 056–10 065, 2019.

[88] H. El Hammouti, M. Benjillali, B. Shihada, and M.-S. Alouini, "Learn-as-you-fly: A distributed algorithm for joint 3D placement and user association in multi-UAVs networks," *IEEE Transactions on Wireless Communications*, vol. 18, no. 12, pp. 5831–5844, 2019.

[89] F. Boccardi, R. W. Heath, A. Lozano, T. L. Marzetta, and P. Popovski, "Five disruptive technology directions for 5G," *IEEE communications magazine*, vol. 52, no. 2, pp. 74–80, 2014.

[90] M. T. Beck, M. Werner, S. Feld, and S. Schimper, "Mobile edge computing: A taxonomy," in *Proc. of the Sixth International Conference on Advances in Future Internet*. Citeseer, 2014, pp. 48–55.

[91] M. Satyanarayanan, "Mobile computing: the next decade," in *Proceedings of the 1st ACM workshop on mobile cloud computing & services: social networks and beyond*. ACM, 2010, p. 5.

[92] H. T. Dinh, C. Lee, D. Niyato, and P. Wang, "A survey of mobile cloud computing: architecture, applications, and approaches," *Wireless communications and mobile computing*, vol. 13, no. 18, pp. 1587–1611, 2013.

[93] M. Patel, B. Naughton, C. Chan, N. Sprecher, S. Abeta, A. Neal *et al.*, "Mobile-edge computing introductory technical white paper," *White paper, mobile-edge computing (MEC) industry initiative*, pp. 1089–7801, 2014.

[94] Y. C. Hu, M. Patel, D. Sabella, N. Sprecher, and V. Young, "Mobile edge computing—A key technology towards 5G," *ETSI white paper*, vol. 11, no. 11, pp. 1–16, 2015.

[95] Y. Mao, C. You, J. Zhang, K. Huang, and K. B. Letaief, "A survey on mobile edge computing: The communication perspective," *IEEE Communications Surveys & Tutorials*, vol. 19, no. 4, pp. 2322–2358, 2017.

[96] G. I. P. Association *et al.*, "5G Vision-The 5G Infrastructure Public Private Partnership: the next generation of communication networks and services," *White Paper, February*, 2015.

[97] T. H. Luan, L. Gao, Z. Li, Y. Xiang, G. Wei, and L. Sun, "Fog computing: Focusing on mobile users at the edge," *arXiv preprint arXiv:1502.01815*, 2015.

[98] J. Erman, A. Gerber, M. Hajiaghayi, D. Pei, S. Sen, and O. Spatscheck, "To cache or not to cache: The 3G case," *IEEE Internet Computing*, vol. 15, no. 2, pp. 27–34, 2011.

[99] S. Woo, E. Jeong, S. Park, J. Lee, S. Ihm, and K. Park, "Comparison of caching strategies in modern cellular backhaul networks," in *Proceeding of the 11th annual international conference on Mobile systems, applications, and services*. ACM, 2013, pp. 319–332.

[100] B. A. Ramanan, L. M. Drabeck, M. Haner, N. Nithi, T. E. Klein, and C. Sawkar, "Cacheability analysis of HTTP traffic in an operational LTE network," in *2013 Wireless Telecommunications Symposium (WTS)*. IEEE, 2013, pp. 1–8.

[101] D. Barbará and T. Imieliński, "Sleepers and workaholics: caching strategies in mobile environments," in *ACM Sigmod Record*, vol. 23, no. 2. ACM, 1994, pp. 1–12.

[102] E. Baştuğ, M. Bennis, E. Zeydan, M. A. Kader, I. A. Karatepe, A. S. Er, and M. Debbah, "Big data meets telcos: A proactive caching perspective," *Journal of Communications and Networks*, vol. 17, no. 6, pp. 549–557, 2015.

[103] A. Chattopadhyay, B. Błaszczyszyn, and H. P. Keeler, "Gibbsian on-line distributed content caching strategy for cellular networks," *IEEE Transactions on Wireless Communications*, vol. 17, no. 2, pp. 969–981, 2017.

[104] Q. Li, C. Lu, B. Cao, and Q. Zhang, "Caching resource management of mobile edge network based on Stackelberg game," *Digital Communications and Networks*, vol. 5, no. 1, pp. 18–23, 2019.

[105] J. Yao, T. Han, and N. Ansari, "On mobile edge caching," *IEEE Communications Surveys & Tutorials*, vol. 21, no. 3, pp. 2525–2553, 2019.

[106] J. Tadrous and A. Eryilmaz, "On optimal proactive caching for mobile networks with demand uncertainties," *IEEE/ACM Transactions on Networking*, vol. 24, no. 5, pp. 2715–2727, 2015.

[107] P. Blasco and D. Gündüz, "Learning-based optimization of cache content in a small cell base station," in *2014 IEEE International Conference on Communications (ICC)*. IEEE, 2014, pp. 1897–1903.

[108] J. Wu, Z. Zhang, Y. Hong, and Y. Wen, "Cloud radio access network (C-RAN): a primer," *IEEE network*, vol. 29, no. 1, pp. 35–41, 2015.

[109] W. Jiang, G. Feng, and S. Qin, "Optimal cooperative content caching and delivery policy for heterogeneous cellular networks," *IEEE Transactions on Mobile Computing*, vol. 16, no. 5, pp. 1382–1393, 2016.

[110] J. Zhao, X. Sun, Q. Li, and X. Ma, "Edge caching and computation management for real-time internet of vehicles: An online and distributed approach," *IEEE Transactions on Intelligent Transportation Systems*, vol. 22, no. 4, pp. 2183–2197, 2020.

[111] Z. Chen, N. Pappas, and M. Kountouris, "Probabilistic caching in wireless D2D networks: Cache hit optimal versus throughput optimal," *IEEE Communications Letters*, vol. 21, no. 3, pp. 584–587, 2016.

[112] N. Giatsoglou, K. Ntontin, E. Kartsakli, A. Antonopoulos, and C. Verikoukis, "D2D-aware device caching in mmWave-cellular networks," *IEEE Journal on Selected Areas in Communications*, vol. 35, no. 9, pp. 2025–2037, 2017.

[113] K. Wu, M. Jiang, F. She, and X. Chen, "Relay-aided request-aware distributed packet caching for device-to-device communication," *IEEE Wireless Communications Letters*, vol. 8, no. 1, pp. 217–220, 2018.

[114] W. Jiang, G. Feng, S. Qin, T. S. P. Yum, and G. Cao, "Multi-agent reinforcement learning for efficient content caching in mobile D2D networks," *IEEE Transactions on Wireless Communications*, vol. 18, no. 3, pp. 1610–1622, 2019.

[115] Z. Li, J. Chen, and Z. Zhang, "Socially aware caching in D2D enabled fog radio access networks," *IEEE Access*, vol. 7, pp. 84 293–84 303, 2019.

[116] S. Zhang and J. Liu, "Optimal probabilistic caching in heterogeneous IoT networks," *IEEE Internet of Things Journal*, vol. 7, no. 4, pp. 3404–3414, 2020.

[117] S. A. R. Zaidi, M. Ghogho, and D. C. McLernon, "Information centric modeling for two-tier cache enabled cellular networks," in *2015 IEEE International Conference on Communication Workshop (ICCW)*. IEEE, 2015, pp. 80–86.

[118] S. Wang, X. Zhang, K. Yang, L. Wang, and W. Wang, "Distributed edge caching scheme considering the tradeoff between the diversity and redundancy of cached content," in *2015 IEEE/CIC International Conference on Communications in China (ICCC)*. IEEE, 2015, pp. 1–5.

[119] J. George and S. Sebastian, "Cooperative caching strategy for video streaming in mobile networks," in *2016 International Conference on Emerging Technological Trends (ICETT)*. IEEE, 2016, pp. 1–7.

[120] Z. Chang, Y. Gu, Z. Han, X. Chen, and T. Ristaniemi, "Context-aware data caching for 5G heterogeneous small cells networks," in *2016 IEEE International Conference on Communications (ICC)*. IEEE, 2016, pp. 1–6.

[121] M. Gregori, J. Gómez-Vilardebó, J. Matamoros, and D. Gündüz, "Wireless content caching for small cell and D2D networks," *IEEE Journal on Selected Areas in Communications*, vol. 34, no. 5, pp. 1222–1234, 2016.

[122] A. Khreishah, J. Chakareski, and A. Gharaibeh, "Joint caching, routing, and channel assignment for collaborative small-cell cellular networks," *IEEE Journal on Selected Areas in Communications*, vol. 34, no. 8, pp. 2275–2284, 2016.

[123] K. Li, C. Yang, Z. Chen, and M. Tao, "Optimization and analysis of probabilistic caching in n-tier heterogeneous networks," *IEEE Transactions on Wireless Communications*, vol. 17, no. 2, pp. 1283–1297, 2017.

[124] T. Hou, G. Feng, S. Qin, and W. Jiang, "Proactive content caching by exploiting transfer learning for mobile edge computing," *International Journal of Communication Systems*, vol. 31, no. 11, p. e3706, 2018.

[125] H. Zhao, Y. Wang, and R. Sun, "Task proactive caching based computation offloading and resource allocation in mobile-edge computing systems," in *2018 14th International Wireless Communications & Mobile Computing Conference (IWCMC)*. IEEE, 2018, pp. 232–237.

[126] T. X. Tran and D. Pompili, "Adaptive bitrate video caching and processing in mobile-edge computing networks," *IEEE Transactions on Mobile Computing*, vol. 18, no. 9, pp. 1965–1978, 2018.

[127] L. Ale, N. Zhang, H. Wu, D. Chen, and T. Han, "Online proactive caching in mobile edge computing using bidirectional deep recurrent neural network," *IEEE Internet of Things Journal*, vol. 6, no. 3, pp. 5520–5530, 2019.

[128] M. Yan, C. A. Chan, W. Li, L. Lei, A. F. Gygax, and I. Chih-Lin, "Assessing the energy consumption of proactive mobile edge caching in wireless networks," *IEEE Access*, vol. 7, pp. 104 394–104 404, 2019.

[129] R. Pabst, B. H. Walke, D. C. Schultz, P. Herhold, H. Yanikomeroglu, S. Mukherjee, H. Viswanathan, M. Lott, W. Zirwas, M. Dohler *et al.*, "Relay-based deployment concepts for wireless and mobile broadband radio," *IEEE Communications magazine*, vol. 42, no. 9, pp. 80–89, 2004.

[130] X. Wang, Y. Bao, X. Liu, and Z. Niu, "On the design of relay caching in cellular networks for energy efficiency," in *2011 IEEE Conference on Computer Communications Workshops (INFOCOM WKSHPS)*. IEEE, 2011, pp. 259–264.

[131] W. Gao, G. Cao, A. Iyengar, and M. Srivatsa, "Supporting cooperative caching in disruption tolerant networks," in *2011 31st International Conference on Distributed Computing Systems*. IEEE, 2011, pp. 151–161.

[132] A. A. Zewail and A. Yener, "Coded caching for combination networks with cache-aided relays," in *2017 IEEE International Symposium on Information Theory (ISIT)*. IEEE, 2017, pp. 2433–2437.

[133] S.-J. Cao, J. Chen, Y. Wu, and K. Wang, "Coded Caching for Relay Networks: The Impact of Caching Memories," in *2020 IEEE Information Theory Workshop (ITW)*. IEEE, 2021, pp. 1–5.

[134] S.-H. Park, O. Simeone, and S. S. Shitz, "Joint optimization of cloud and edge processing for fog radio access networks," *IEEE Transactions on Wireless Communications*, vol. 15, no. 11, pp. 7621–7632, 2016.

[135] "Cloud-aided wireless networks with edge caching: Fundamental latency tradeoffs in fog radio access networks], author=Tandon, Ravi and Simeone, Osvaldo, booktitle=2016 IEEE International Symposium on Information Theory (ISIT), pages=2029–2033, year=2016, organization=IEEE."

[136] L. Lu, Y. Jiang, M. Bennis, Z. Ding, F.-C. Zheng, and X. You, "Distributed edge caching via reinforcement learning in fog radio access networks," in *2019 IEEE 89th Vehicular Technology Conference (VTC2019-Spring)*. IEEE, 2019, pp. 1–6.

[137] Y. Jiang, Y. Hu, M. Bennis, F.-C. Zheng, and X. You, "A mean field game-based distributed edge caching in fog radio access networks," *IEEE Transactions on Communications*, vol. 68, no. 3, pp. 1567–1580, 2019.

[138] J. Yan, Y. Jiang, F. Zheng, F. R. Yu, X. Gao, and X. You, "Distributed edge caching with content recommendation in fog-RANs via deep reinforcement learning," in *2020 IEEE International Conference on Communications Workshops (ICC Workshops)*. IEEE, 2020, pp. 1–6.

[139] B. Chen, C. Yang, and G. Wang, "Cooperative device-to-device communications with caching," in *2016 IEEE 83rd Vehicular Technology Conference (VTC Spring)*. IEEE, 2016, pp. 1–5.

[140] M. Erol-Kantarci, "Cache-at-relay: energy-efficient content placement for next-generation wireless relays," *International Journal of Network Management*, vol. 25, no. 6, pp. 454–470, 2015.

[141] J. Yao and N. Ansari, "QoS-aware joint BBU-RRH mapping and user association in cloud-RANs," *IEEE Transactions on Green Communications and Networking*, vol. 2, no. 4, pp. 881–889, 2018.

[142] M. Peng, Y. Sun, X. Li, Z. Mao, and C. Wang, "Recent advances in cloud radio access networks: System architectures, key techniques, and open issues," *IEEE Communications Surveys & Tutorials*, vol. 18, no. 3, pp. 2282–2308, 2016.

[143] H. Ahlehagh and S. Dey, "Video-aware scheduling and caching in the radio access network," *IEEE/ACM Transactions on Networking (TON)*, vol. 22, no. 5, pp. 1444–1462, 2014.

[144] E. Bastug, M. Bennis, and M. Debbah, "Living on the edge: The role of proactive caching in 5G wireless networks," *IEEE Communications Magazine*, vol. 52, no. 8, pp. 82–89, 2014.

[145] N. Zhao, F. Cheng, F. R. Yu, J. Tang, Y. Chen, G. Gui, and H. Sari, "Caching UAV assisted secure transmission in hyper-dense networks based on interference alignment," *IEEE Transactions on Communications*, vol. 66, no. 5, pp. 2281–2294, 2018.

[146] X. Xu, Y. Zeng, Y. L. Guan, and R. Zhang, "Overcoming endurance issue: UAV-enabled communications with proactive caching," *IEEE Journal on Selected Areas in Communications*, vol. 36, no. 6, pp. 1231–1244, 2018.

[147] N. Golrezaei, A. F. Molisch, A. G. Dimakis, and G. Caire, "Femtocaching and device-to-device collaboration: A new architecture for wireless video distribution," *IEEE Communications Magazine*, vol. 51, no. 4, pp. 142–149, 2013.

[148] L. Marini, J. Li, and Y. Li, "Distributed caching based on decentralized learning automata," in *2015 IEEE International Conference on Communications (ICC)*. IEEE, 2015, pp. 3807–3812.

[149] F. Cheng, G. Gui, N. Zhao, Y. Chen, J. Tang, and H. Sari, "UAV-relaying-assisted secure transmission with caching," *IEEE Transactions on Communications*, vol. 67, no. 5, pp. 3140–3153, 2019.

[150] A. Gharaibeh, A. Khreishah, B. Ji, and M. Ayyash, "A provably efficient online collaborative caching algorithm for multicell-coordinated systems," *IEEE Transactions on Mobile Computing*, vol. 15, no. 8, pp. 1863–1876, 2015.

[151] W. Gao, G. Cao, A. Iyengar, and M. Srivatsa, "Cooperative caching for efficient data access in disruption tolerant networks," *IEEE Transactions on Mobile Computing*, vol. 13, no. 3, pp. 611–625, 2013.

[152] R. Pedarsani, M. A. Maddah-Ali, and U. Niesen, "Online coded caching," *IEEE/ACM Transactions on Networking*, vol. 24, no. 2, pp. 836–845, 2015.

[153] M. M. Amiri, Q. Yang, and D. Gündüz, "Coded caching for a large number of users," in *2016 IEEE Information Theory Workshop (ITW)*. IEEE, 2016, pp. 171–175.

[154] T. Ho and D. Lun, *Network coding: an introduction*. Cambridge University Press, 2008.

[155] M. M. Amiri, Q. Yang, and D. Gündüz, "Decentralized coded caching with distinct cache capacities," in *2016 50th Asilomar Conference on Signals, Systems and Computers*. IEEE, 2016, pp. 734–738.

[156] X. Liu, J. Zhang, X. Zhang, and W. Wang, "Mobility-aware coded probabilistic caching scheme for MEC-enabled small cell networks," *IEEE Access*, vol. 5, pp. 17 824–17 833, 2017.

[157] I. Psaras, W. K. Chai, and G. Pavlou, "Probabilistic in-network caching for information-centric networks," in *Proceedings of the second edition of the ICN workshop on Information-centric networking*, 2012, pp. 55–60.

[158] ——, "In-network cache management and resource allocation for information-centric networks," *IEEE Transactions on Parallel and Distributed Systems*, vol. 25, no. 11, pp. 2920–2931, 2013.

[159] S. Tarnoi, K. Suksomboon, W. Kumwilaisak, and Y. Ji, "Performance of probabilistic caching and cache replacement policies for content-centric networks," in *39th Annual IEEE Conference on Local Computer Networks*. IEEE, 2014, pp. 99–106.

[160] B. Blaszczyszyn and A. Giovanidis, "Optimal geographic caching in cellular networks," in *2015 IEEE international conference on communications (ICC)*. IEEE, 2015, pp. 3358–3363.

[161] M. Ji, G. Caire, and A. F. Molisch, "Fundamental limits of caching in wireless D2D networks," *IEEE Transactions on Information Theory*, vol. 62, no. 2, pp. 849–869, 2015.

[162] "[in-network caching of internet-of-things data."

[163] H. Che, Y. Tung, and Z. Wang, "Hierarchical web caching systems: Modeling, design and experimental results," *IEEE journal on Selected Areas in Communications*, vol. 20, no. 7, pp. 1305–1314, 2002.

[164] R. Urgaonkar, S. Wang, T. He, M. Zafer, K. Chan, and K. K. Leung, "Dynamic service migration and workload scheduling in edge-clouds," *Performance Evaluation*, vol. 91, pp. 205–228, 2015.

[165] D. Niu, Z. Liu, B. Li, and S. Zhao, "Demand forecast and performance prediction in peer-assisted on-demand streaming systems," in *2011 Proceedings IEEE INFOCOM*. IEEE, 2011, pp. 421–425.

[166] Z. Wang, L. Sun, C. Wu, and S. Yang, "Enhancing internet-scale video service deployment using microblog-based prediction," *IEEE Transactions on Parallel and Distributed Systems*, vol. 26, no. 3, pp. 775–785, 2014.

[167] M. Rowe, "Forecasting audience increase on youtube," 2011.

[168] H. Nakayama, Z. M. Fadlullah, N. Ansari, and N. Kato, "A novel scheme for WSAN sink mobility based on clustering and set packing techniques," *IEEE Transactions on Automatic Control*, vol. 56, no. 10, pp. 2381–2389, 2011.

[169] H. Nishiyama, T. Ngo, N. Ansari, and N. Kato, "On minimizing the impact of mobility on topology control in mobile ad hoc networks," *IEEE Transactions on Wireless Communications*, vol. 11, no. 3, pp. 1158–1166, 2012.

[170] R. Wang, X. Peng, J. Zhang, and K. B. Letaief, "Mobility-aware caching for content-centric wireless networks: Modeling and methodology," *IEEE Communications Magazine*, vol. 54, no. 8, pp. 77–83, 2016.

[171] X. Lin, J. Xia, and Z. Wang, "Probabilistic caching placement in UAV-assisted heterogeneous wireless networks," *Physical Communication*, vol. 33, pp. 54–61, 2019.

[172] T. Zhang, Y. Wang, Y. Liu, W. Xu, and A. Nallanathan, "Cache-enabling UAV communications: Network deployment and resource allocation," *IEEE Transactions on Wireless Communications*, vol. 19, no. 11, pp. 7470–7483, 2020.

[173] S. Gu, X. Sun, Z. Yang, T. Huang, W. Xiang, and K. Yu, "Energy-aware coded caching strategy design with resource optimization for satellite-UAV-vehicle integrated networks," *IEEE Internet of Things Journal*, 2021.

[174] "[multi-uav content caching strategy and cooperative, complementary content transmission based on coalition formation game."

[175] J. MacQueen *et al.*, "Some methods for classification and analysis of multivariate observations," in *Proceedings of the fifth Berkeley symposium on mathematical statistics and probability*, vol. 1, no. 14. Oakland, CA, USA, 1967, pp. 281–297.

[176] H. S. Black and J. Edson, "Pulse code modulation," *Transactions of the American Institute of Electrical Engineers*, vol. 66, no. 1, pp. 895–899, 1947.

[177] S. Lloyd, "Least squares quantization in PCM," *IEEE transactions on information theory*, vol. 28, no. 2, pp. 129–137, 1982.

[178] P.-E. Danielsson, "Euclidean distance mapping," *Computer Graphics and image processing*, vol. 14, no. 3, pp. 227–248, 1980.

[179] E. F. Krause, "Taxicab geometry," *The Mathematics Teacher*, vol. 66, no. 8, pp. 695–706, 1973.

[180] D. M. Blei, A. Y. Ng, and M. I. Jordan, "Latent dirichlet allocation," *Journal of machine Learning research*, vol. 3, no. Jan, pp. 993–1022, 2003.

[181] M. Steyvers and T. Griffiths, "Probabilistic topic models," *Handbook of latent semantic analysis*, vol. 427, no. 7, pp. 424–440, 2007.

[182] C. M. Bishop, *Pattern recognition and machine learning*. springer, 2006.

[183] W. M. Darling, "A theoretical and practical implementation tutorial on topic modeling and gibbs sampling," in *Proceedings of the 49th annual meeting of the association for computational linguistics: Human language technologies*, 2011, pp. 642–647.

[184] E. I. George and R. E. McCulloch, "Variable selection via Gibbs sampling," *Journal of the American Statistical Association*, vol. 88, no. 423, pp. 881–889, 1993.

[185] C. K. Carter and R. Kohn, "On Gibbs sampling for state space models," *Biometrika*, vol. 81, no. 3, pp. 541–553, 1994.

[186] G. Heinrich, "Parameter estimation for text analysis," Technical report, Tech. Rep., 2005.

[187] Y. Teh, M. Jordan, M. Beal, and D. Blei, "Sharing clusters among related groups: Hierarchical Dirichlet processes," *Advances in neural information processing systems*, vol. 17, 2004.

[188] T. L. Griffiths and M. Steyvers, "Finding scientific topics," *Proceedings of the National academy of Sciences*, vol. 101, no. suppl 1, pp. 5228–5235, 2004.

[189] L. P. Kaelbling, M. L. Littman, and A. W. Moore, "Reinforcement learning: A survey," *Journal of artificial intelligence research*, vol. 4, pp. 237–285, 1996.

[190] M. A. Wiering and M. Van Otterlo, "Reinforcement learning," *Adaptation, learning, and optimization*, vol. 12, no. 3, p. 729, 2012.

[191] B. Mehlig, "Machine learning with neural networks," *arXiv preprint arXiv:1901.05639*, 2019.

[192] R. Y. Rubinstein and D. P. Kroese, *Simulation and the Monte Carlo method*. John Wiley & Sons, 2016.

[193] R. S. Sutton, D. Precup, and S. Singh, "Between MDPs and semi-MDPs: A framework for temporal abstraction in reinforcement learning," *Artificial intelligence*, vol. 112, no. 1-2, pp. 181–211, 1999.

[194] S. P. Singh and R. S. Sutton, "Reinforcement learning with replacing eligibility traces," *Machine learning*, vol. 22, no. 1, pp. 123–158, 1996.

[195] J. G. March, "Exploration and exploitation in organizational learning," *Organization science*, vol. 2, no. 1, pp. 71–87, 1991.

[196] C. J. C. H. Watkins, "Learning from delayed rewards," 1989.

[197] R. Bellman, "Dynamic programming," *Science*, vol. 153, no. 3731, pp. 34–37, 1966.

[198] M. L. Puterman, *Markov decision processes: discrete stochastic dynamic programming*. John Wiley & Sons, 2014.

[199] T. W. Sandholm and R. H. Crites, "Multiagent reinforcement learning in the iterated prisoner's dilemma," *Biosystems*, vol. 37, no. 1-2, pp. 147–166, 1996.

[200] M. Wunder, M. L. Littman, and M. Babes, "Classes of multiagent q-learning dynamics with epsilon-greedy exploration," in *ICML*, 2010.

[201] L. K. Hansen and P. Salamon, "Neural network ensembles," *IEEE transactions on pattern analysis and machine intelligence*, vol. 12, no. 10, pp. 993–1001, 1990.

[202] V. Mnih, K. Kavukcuoglu, D. Silver, A. A. Rusu, J. Veness, M. G. Bellemare, A. Graves, M. Riedmiller, A. K. Fidjeland, G. Ostrovski *et al.*, "Human-level control through deep reinforcement learning," *nature*, vol. 518, no. 7540, pp. 529–533, 2015.

[203] Y. LeCun, Y. Bengio, and G. Hinton, "Deep learning," *nature*, vol. 521, no. 7553, pp. 436–444, 2015.

[204] M. A. Nielsen, *Neural networks and deep learning*. Determination press San Francisco, CA, USA, 2015, vol. 25.

[205] H. Van Hasselt, A. Guez, and D. Silver, "Deep reinforcement learning with double q-learning," *arXiv preprint arXiv:1509.06461*, 2015.

[206] S. K. Goudos, G. V. Tsoulos, G. Athanasiadou, M. C. Batistatos, D. Zarbouti, and K. E. Psannis, "Artificial neural network optimal modeling and optimization of UAV measurements for mobile communications using the L-SHADE algorithm," *IEEE Transactions on Antennas and Propagation*, vol. 67, no. 6, pp. 4022–4031, 2019.

[207] S. K. Goudos and G. Athanasiadou, "Application of an ensemble method to UAV power modeling for cellular communications," *IEEE Antennas and Wireless Propagation Letters*, vol. 18, no. 11, pp. 2340–2344, 2019.

[208] J.-L. Wang, Y.-R. Li, A. B. Adege, L.-C. Wang, S.-S. Jeng, and J.-Y. Chen, "Machine learning based rapid 3D channel modeling for UAV communication networks," in *2019 16th IEEE Annual Consumer Communications & Networking Conference (CCNC)*. IEEE, 2019, pp. 1–5.

[209] J. Chen, U. Yatnalli, and D. Gesbert, "Learning radio maps for UAV-aided wireless networks: A segmented regression approach," in *2017 IEEE International Conference on Communications (ICC)*. IEEE, 2017, pp. 1–6.

[210] Y. Egi and C. E. Otero, "Machine-learning and 3D point-cloud based signal power path loss model for the deployment of wireless communication systems," *IEEE Access*, vol. 7, pp. 42 507–42 517, 2019.

[211] Y. Zhang, J. Wen, G. Yang, Z. He, and X. Luo, "Air-to-air path loss prediction based on machine learning methods in urban environments," *Wireless Communications and Mobile Computing*, vol. 2018, 2018.

[212] G. Yang, Y. Zhang, Z. He, J. Wen, Z. Ji, and Y. Li, "Machine-learning-based prediction methods for path loss and delay spread in air-to-ground millimetre-wave channels," *IET Microwaves, Antennas & Propagation*, vol. 13, no. 8, pp. 1113–1121, 2019.

[213] J. Chen, Q. Wu, Y. Xu, Y. Zhang, and Y. Yang, "Distributed demand-aware channel-slot selection for multi-UAV networks: A game-theoretic learning approach," *IEEE Access*, vol. 6, pp. 14 799–14 811, 2018.

[214] U. Challita, W. Saad, and C. Bettstetter, "Interference management for cellular-connected UAVs: A deep reinforcement learning approach," *IEEE Transactions on Wireless Communications*, vol. 18, no. 4, pp. 2125–2140, 2019.

[215] D. Athukoralage, I. Guvenc, W. Saad, and M. Bennis, "Regret based learning for UAV assisted LTE-U/WiFi public safety networks," in *2016 IEEE Global Communications Conference (GLOBECOM)*. IEEE, 2016, pp. 1–7.

[216] D. Zhang, W. Ding, B. Zhang, C. Xie, H. Li, C. Liu, and J. Han, "Automatic modulation classification based on deep learning for unmanned aerial vehicles," *Sensors*, vol. 18, no. 3, p. 924, 2018.

[217] X. Liu, Y. Liu, Y. Chen, and L. Hanzo, "Trajectory design and power control for multi-UAV assisted wireless networks: A machine learning approach," *IEEE Transactions on Vehicular Technology*, vol. 68, no. 8, pp. 7957–7969, 2019.

[218] P. Ladosz, H. Oh, G. Zheng, and W.-H. Chen, "Gaussian process based channel prediction for communication-relay UAV in urban environments," *IEEE Transactions on Aerospace and Electronic Systems*, vol. 56, no. 1, pp. 313–325, 2019.

[219] H. Bayerlein, P. De Kerret, and D. Gesbert, "Trajectory optimization for autonomous flying base station via reinforcement learning," in *2018 IEEE 19th International Workshop on Signal Processing Advances in Wireless Communications (SPAWC)*. IEEE, 2018, pp. 1–5.

[220] P. Ladosz, H. Oh, G. Zheng, and W.-H. Chen, "A hybrid approach of learning and model-based channel prediction for communication relay UAVs in dynamic urban environments," *IEEE Robotics and Automation Letters*, vol. 4, no. 3, pp. 2370–2377, 2019.

[221] X. Liu, Y. Liu, and Y. Chen, "Reinforcement learning in multiple-UAV networks: Deployment and movement design," *IEEE Transactions on Vehicular Technology*, vol. 68, no. 8, pp. 8036–8049, 2019.

[222] H. Peng, A. Razi, F. Afghah, and J. Ashdown, "A unified framework for joint mobility prediction and object profiling of drones in UAV networks," *Journal of Communications and Networks*, vol. 20, no. 5, pp. 434–442, 2018.

[223] O. Esrafilian, R. Gangula, and D. Gesbert, "Learning to communicate in UAV-aided wireless networks: Map-based approaches," *IEEE Internet of Things Journal*, vol. 6, no. 2, pp. 1791–1802, 2018.

[224] S. Colonnese, F. Cuomo, G. Pagliari, and L. Chiaraviglio, "Q-SQUARE: A Q-learning approach to provide a QoE aware UAV flight path in cellular networks," *Ad Hoc Networks*, vol. 91, p. 101872, 2019.

[225] H. Dai, H. Zhang, M. Hua, C. Li, Y. Huang, and B. Wang, "How to deploy multiple UAVs for providing communication service in an unknown region?" *IEEE Wireless Communications Letters*, vol. 8, no. 4, pp. 1276–1279, 2019.

[226] J. Jailton, T. Carvalho, J. Araújo, and R. Francês, "Relay positioning strategy for traffic data collection of multiple unmanned aerial vehicles using hybrid optimization systems: A FANET-based case study," *Wireless Communications and Mobile Computing*, vol. 2017, 2017.

[227] R. Ghanavi, E. Kalantari, M. Sabbaghian, H. Yanikomeroglu, and A. Yongacoglu, "Efficient 3D aerial base station placement considering users mobility by reinforcement learning," in *2018 IEEE Wireless Communications and Networking Conference (WCNC)*. IEEE, 2018, pp. 1–6.

[228] Y. G. Li and G. L. Stuber, *Orthogonal frequency division multiplexing for wireless communications*. Springer Science & Business Media, 2006.

[229] S. B. Weinstein, "The history of orthogonal frequency-division multiplexing [History of Communications]," *IEEE Communications Magazine*, vol. 47, no. 11, pp. 26–35, 2009.

[230] S. Weinstein and P. Ebert, "Data transmission by frequency-division multiplexing using the discrete Fourier transform," *IEEE transactions on Communication Technology*, vol. 19, no. 5, pp. 628–634, 1971.

[231] L. M. Hoo, B. Halder, J. Tellado, and J. M. Cioffi, "Multiuser transmit optimization for multicarrier broadcast channels: asymptotic FDMA capacity region and algorithms," *IEEE Transactions on Communications*, vol. 52, no. 6, pp. 922–930, 2004.

[232] H. Yin and S. Alamouti, "OFDMA: A broadband wireless access technology," in *2006 IEEE sarnoff symposium*. IEEE, 2006, pp. 1–4.

[233] C. Y. Wong, R. S. Cheng, K. B. Lataief, and R. D. Murch, "Multiuser OFDM with adaptive subcarrier, bit, and power allocation," *IEEE Journal on selected areas in communications*, vol. 17, no. 10, pp. 1747–1758, 1999.

[234] H. Holma and A. Toskala, *LTE for UMTS: OFDMA and SC-FDMA based radio access*. John Wiley & Sons, 2009.

[235] R. Y. Mesleh, H. Haas, S. Sinanovic, C. W. Ahn, and S. Yun, "Spatial modulation," *IEEE Transactions on vehicular technology*, vol. 57, no. 4, pp. 2228–2241, 2008.

[236] E. Basar, "Index modulation techniques for 5G wireless networks," *IEEE Communications Magazine*, vol. 54, no. 7, pp. 168–175, 2016.

[237] A. Younis, N. Serafimovski, R. Mesleh, and H. Haas, "Generalised spatial modulation," in *2010 conference record of the forty fourth Asilomar conference on signals, systems and computers*. IEEE, 2010, pp. 1498–1502.

[238] E. Biglieri, R. Calderbank, A. Constantinides, A. Goldsmith, A. Paulraj, and H. V. Poor, *MIMO wireless communications*. Cambridge university press, 2007.

[239] *Fundamentals of massive MIMO], author=Marzetta, Thomas L, year=2016, publisher=Cambridge University Press*.

[240] P. W. Wolniansky, G. J. Foschini, G. D. Golden, and R. A. Valenzuela, "V-BLAST: An architecture for realizing very high data rates over the rich-scattering wireless channel," in *1998 URSI international symposium on signals, systems, and electronics. Conference proceedings (Cat. No. 98EX167)*. IEEE, 1998, pp. 295–300.

[241] H. Jafarkhani, *Space-time coding: theory and practice*. Cambridge university press, 2005.

[242] H. Haas, E. Costa, and E. Schulz, "Increasing spectral efficiency by data multiplexing using antenna arrays," in *The 13th IEEE International Symposium on Personal, Indoor and Mobile Radio Communications*, vol. 2. IEEE, 2002, pp. 610–613.

[243] S. Song, Y. Yang, Q. Xionq, K. Xie, B.-J. Jeong, and B. Jiao, "A channel hopping technique I: Theoretical studies on band efficiency and capacity," in *2004 International Conference on Communications, Circuits and Systems (IEEE Cat. No. 04EX914)*, vol. 1. IEEE, 2004, pp. 229–233.

[244] Y. Lee, S. Yun *et al.*, "Interchannel interference avoidance in MIMO transmission by exploiting spatial information," in *2005 IEEE 16th International Symposium on Personal, Indoor and Mobile Radio Communications*, vol. 1. IEEE, 2005, pp. 141–145.

[245] R. Mesleh, H. Haas, C. Ahn, and S. Yun, "Spatial modulation-OFDM," in *Proc. of the International OFDM Workshop*, 2006, pp. 30–31.

[246] R. Mesleh, H. Haas, C. W. Ahn, and S. Yun, "Spatial modulation-a new low complexity spectral efficiency enhancing technique," in *2006 First International Conference on Communications and Networking in China*. IEEE, 2006, pp. 1–5.

[247] S. Ganesan, R. Mesleh, H. Ho, C. W. Ahn, and S. Yun, "On the performance of spatial modulation OFDM," in *2006 Fortieth Asilomar Conference on Signals, Systems and Computers*. IEEE, 2006, pp. 1825–1829.

[248] J. Jeganathan, A. Ghrayeb, and L. Szczecinski, "Spatial modulation: Optimal detection and performance analysis," *IEEE Communications Letters*, vol. 12, no. 8, pp. 545–547, 2008.

[249] S. M. Alamouti, "A simple transmit diversity technique for wireless communications," *IEEE Journal on selected areas in communications*, vol. 16, no. 8, pp. 1451–1458, 1998.

[250] V. Tarokh, H. Jafarkhani, and A. R. Calderbank, "Space-time block codes from orthogonal designs," *IEEE Transactions on Information theory*, vol. 45, no. 5, pp. 1456–1467, 1999.

[251] N. R. Naidoo, H. Xu, and T. A.-M. Quazi, "Spatial modulation: optimal detector asymptotic performance and multiple-stage detection," *IET communications*, vol. 5, no. 10, pp. 1368–1376, 2011.

[252] Q. Tang, Y. Xiao, P. Yang, Q. Yu, and S. Li, "A new low-complexity near-ML detection algorithm for spatial modulation," *IEEE Wireless Communications Letters*, vol. 2, no. 1, pp. 90–93, 2012.

[253] C.-M. Yu, S.-H. Hsieh, H.-W. Liang, C.-S. Lu, W.-H. Chung, S.-Y. Kuo, and S.-C. Pei, "Compressed sensing detector design for space shift keying in MIMO systems," *IEEE Communications Letters*, vol. 16, no. 10, pp. 1556–1559, 2012.

[254] M. Di Renzo, H. Haas, A. Ghrayeb, S. Sugiura, and L. Hanzo, "Spatial modulation for generalized MIMO: Challenges, opportunities, and implementation," *Proceedings of the IEEE*, vol. 102, no. 1, pp. 56–103, 2013.

[255] P. Yang, M. Di Renzo, Y. Xiao, S. Li, and L. Hanzo, "Design guidelines for spatial modulation," *IEEE Communications Surveys & Tutorials*, vol. 17, no. 1, pp. 6–26, 2014.

[256] M. Renzo, H. Haas, A. Ghrayeb, L. Hanzo, and S. Sugiura, "Spatial modulation for multiple-antenna communication," 2016.

[257] A. Stavridis, S. Sinanovic, M. Di Renzo, and H. Haas, "Energy evaluation of spatial modulation at a multi-antenna base station," in *2013 IEEE 78th Vehicular Technology Conference (VTC Fall)*. IEEE, 2013, pp. 1–5.

[258] J. Wang, S. Jia, and J. Song, "Generalised spatial modulation system with multiple active transmit antennas and low complexity detection scheme," *IEEE Transactions on Wireless Communications*, vol. 11, no. 4, pp. 1605–1615, 2012.

[259] T. X. Tran, A. Hajisami, P. Pandey, and D. Pompili, "Collaborative mobile edge computing in 5G networks: New paradigms, scenarios, and challenges," *IEEE Communications Magazine*, vol. 55, no. 4, pp. 54–61, 2017.

[260] T. Masada, S. Kiyasu, and S. Miyahara, "Comparing LDA with PLSI as a dimensionality reduction method in document clustering," in *International Conference on Large-Scale Knowledge Resources*. Springer, 2008, pp. 13–26.

[261] T. Hofmann, "Probabilistic latent semantic analysis," *arXiv preprint arXiv:1301.6705*, 2013.

[262] I. Porteous, D. Newman, A. Ihler, A. Asuncion, P. Smyth, and M. Welling, "Fast collapsed gibbs sampling for latent dirichlet allocation," in *Proceedings of the 14th ACM SIGKDD international conference on Knowledge discovery and data mining*. ACM, 2008, pp. 569–577.

[263] M. Hoffman, F. R. Bach, and D. M. Blei, "Online learning for latent dirichlet allocation," in *advances in neural information processing systems*, 2010, pp. 856–864.

[264] J. A. Hartigan and M. A. Wong, "Algorithm AS 136: A k-means clustering algorithm," *Journal of the royal statistical society. series c (applied statistics)*, vol. 28, no. 1, pp. 100–108, 1979.

[265] D. Arthur and S. Vassilvitskii, "k-means++: The advantages of careful seeding," Stanford, Tech. Rep., 2006.

[266] A. Fotouhi, H. Qiang, M. Ding, M. Hassan, L. G. Giordano, A. Garcia-Rodriguez, and J. Yuan, "Survey on uav cellular communications: Practical aspects, standardization advancements, regulation, and security challenges," *IEEE Communications Surveys & Tutorials*, 2019.

[267] S. Redana, Ö. Bulakci, A. Zafeiropoulos, A. Gavras, A. Tzanakaki, A. Albanese, A. Kousaridas, A. Weit, B. Sayadi, B. T. Jou *et al.*, "5G ppp architecture working group: View on 5G architecture," 2019.

[268] H. Zhang, L. Song, Z. Han, and H. V. Poor, "Cooperation techniques for a cellular internet of unmanned aerial vehicles," *IEEE Wireless Communications*, vol. 26, no. 5, pp. 167–173, 2019.

[269] C. Tepedelenlioglu, A. Abdi, and G. B. Giannakis, "The ricean K factor: estimation and performance analysis," *IEEE Transactions on Wireless Communications*, vol. 2, no. 4, pp. 799–810, 2003.

[270] T. J. Rouphael, *RF and digital signal processing for software-defined radio: a multi-standard multi-mode approach*. Newnes, 2009.

[271] T. S. Rappaport, "Mobile radio propagation: Large-scale path loss," *Wireless communications: principles and practice*, pp. 107–110, 2002.

[272] B. S. Chaudhari and M. Zennaro, *LPWAN Technologies for IoT and M2M Applications*. Academic Press, 2020.

[273] L. Gupta, R. Jain, and G. Vaszkun, "Survey of important issues in UAV communication networks," *IEEE Communications Surveys & Tutorials*, vol. 18, no. 2, pp. 1123–1152, 2015.

[274] L. Hanzo, S. X. Ng, W. Webb, and T. Keller, *Quadrature amplitude modulation: From basics to adaptive trellis-coded, turbo-equalised and space-time coded OFDM, CDMA and MC-CDMA systems*. IEEE Press-John Wiley, 2004.

[275] Q. Ye, B. Rong, Y. Chen, M. Al-Shalash, C. Caramanis, and J. G. Andrews, "User association for load balancing in heterogeneous cellular networks," *IEEE Transactions on Wireless Communications*, vol. 12, no. 6, pp. 2706–2716, 2013.

[276] D. Liu, L. Wang, Y. Chen, M. Elkashlan, K.-K. Wong, R. Schober, and L. Hanzo, "User association in 5G networks: A survey and an outlook," *IEEE Communications Surveys & Tutorials*, vol. 18, no. 2, pp. 1018–1044, 2016.

[277] M. Lu, M. Bagheri, A. P. James, and T. Phung, "Wireless charging techniques for UAVs: A review, reconceptualization, and extension," *IEEE Access*, vol. 6, pp. 29 865–29 884, 2018.

[278] "Mobility and location-aware stable clustering scheme for UAV] networks, author=Bhandari, Sabin and Wang, Xianbin and Lee, Richard, journal=IEEE Access, volume=8, pages=106364–106372, year=2020, publisher=IEEE."

[279] J. Talvitie, M. Renfors, and E. S. Lohan, "Distance-based interpolation and extrapolation methods for RSS-based localization with indoor wireless signals," *IEEE transactions on vehicular technology*, vol. 64, no. 4, pp. 1340–1353, 2015.

[280] F. Bandiera, A. Coluccia, and G. Ricci, "A cognitive algorithm for received signal strength based localization," *IEEE Transactions on signal processing*, vol. 63, no. 7, pp. 1726–1736, 2015.

[281] I. Sharp and K. Yu, "Indoor TOA error measurement, modeling, and analysis," *IEEE Transactions on Instrumentation and Measurement*, vol. 63, no. 9, pp. 2129–2144, 2014.

[282] A. Gaber and A. Omar, "A study of wireless indoor positioning based on joint TDOA and DOA estimation using 2-D matrix pencil algorithms and ieee 802.11 ac," *IEEE Transactions on Wireless Communications*, vol. 14, no. 5, pp. 2440–2454, 2014.

[283] J. M. Kelner, P. Gajewski, and C. Ziółkowski, "Spatial localisation of radio wave emission sources using Signal Doppler Frequency (SDF) technology," in *2012 Military Communications and Information Systems Conference (MCC)*. IEEE, 2012, pp. 1–4.

[284] Y. Sharma and V. Gulhane, "Hybrid mechanism for multiple user indoor localization using smart antenna," in *2015 fifth international conference on advanced computing & communication technologies*. IEEE, 2015, pp. 602–607.

[285] Q. Liu, L. Shi, L. Sun, J. Li, M. Ding, and F. Shu, "Path planning for UAV-mounted mobile edge computing with deep reinforcement learning," *IEEE Transactions on Vehicular Technology*, vol. 69, no. 5, pp. 5723–5728, 2020.

[286] H. V. Abeywickrama, Y. He, E. Dutkiewicz, B. A. Jayawickrama, and M. Mueck, "A Reinforcement Learning Approach for Fair User Coverage Using UAV Mounted Base Stations Under Energy Constraints," *IEEE Open Journal of Vehicular Technology*, vol. 1, pp. 67–81, 2020.

[287] Z. Xiao, P. Xia, and X.-G. Xia, "Enabling UAV cellular with millimeter-wave communication: Potentials and approaches," *IEEE Communications Magazine*, vol. 54, no. 5, pp. 66–73, 2016.

[288] L. Zhang, H. Zhao, S. Hou, Z. Zhao, H. Xu, X. Wu, Q. Wu, and R. Zhang, "A survey on 5G millimeter wave communications for UAV-assisted wireless networks," *IEEE Access*, vol. 7, pp. 117 460–117 504, 2019.

[289] C. Zhang, W. Zhang, W. Wang, L. Yang, and W. Zhang, "Research challenges and opportunities of UAV millimeter-wave communications," *IEEE Wireless Communications*, vol. 26, no. 1, pp. 58–62, 2019.

[290] J. Lyu, Y. Zeng, R. Zhang, and T. J. Lim, "Placement optimization of UAV-mounted mobile base stations," *IEEE Communications Letters*, vol. 21, no. 3, pp. 604–607, 2016.

[291] C. You and R. Zhang, "3D trajectory optimization in Rician fading for UAV-enabled data harvesting," *IEEE Transactions on Wireless Communications*, vol. 18, no. 6, pp. 3192–3207, 2019.

[292] T. Shen and H. Ochiai, "A UAV-aided data collection for wireless powered sensor network over Rician fading channels," in *2019 16th IEEE Annual Consumer Communications & Networking Conference (CCNC)*. IEEE, 2019, pp. 1–5.

[293] Y. Liu, K. Xiong, Y. Lu, Q. Ni, P. Fan, and K. B. Letaief, "UAV-Aided Wireless Power Transfer and Data Collection in Rician Fading," *IEEE Journal on Selected Areas in Communications*, vol. 39, no. 10, pp. 3097–3113, 2021.

[294] S. Zhu, T. S. Ghazaany, S. M. Jones, R. A. Abd-Alhameed, J. M. Noras, T. Van Buren, J. Wilson, T. Suggett, and S. Marker, "Probability Distribution of Rician *K*-Factor in Urban, Suburban and Rural Areas Using Real-World Captured Data," *IEEE Transactions on Antennas and Propagation*, vol. 62, no. 7, pp. 3835–3839, 2014.

[295] V. V. Chetlur and H. S. Dhillon, "Downlink coverage analysis for a finite 3-D wireless network of unmanned aerial vehicles," *IEEE Transactions on Communications*, vol. 65, no. 10, pp. 4543–4558, 2017.

[296] Z. Wang, L. Duan, and R. Zhang, "Adaptive deployment for UAV-aided communication networks," *IEEE transactions on wireless communications*, vol. 18, no. 9, pp. 4531–4543, 2019.

[297] W. Mei and R. Zhang, "Aerial-Ground Interference Mitigation for Cellular-Connected UAV," *IEEE Wireless Communications*, vol. 28, no. 1, pp. 167–173, 2021.

[298] "Characterization of line-of-sight MIMO channel for fixed wireless communications], author=Liu, Leilei and Hong, Wei and Wang, Haiming and Yang, Guangqi and Zhang, Nianzu and Zhao, Hongxin and Chang, Jing and Yu, Cheng and Yu, Xutao and Tang, Hongjun and others, journal=IEEE Antennas and Wireless Propagation Letters, volume=6, pages=36–39, year=2007, publisher=IEEE."

[299] D. Fooladivanda and C. Rosenberg, "Joint resource allocation and user association for heterogeneous wireless cellular networks," *IEEE Transactions on Wireless Communications*, vol. 12, no. 1, pp. 248–257, 2012.

[300] X. Li and L. Xing, "Use of Unmanned Aerial Vehicles for Livestock Monitoring based on Streaming K-Means Clustering," *Ifac-Papersonline*, vol. 52, no. 30, pp. 324–329, 2019.

[301] M. Rieke, T. Foerster, J. Geipel, and T. Prinz, "High-precision positioning and real-time data processing of UAV systems," *International Archives of the Photogrammetry, Remote Sensing and Spatial Information Sciences*, vol. 38, no. 1/C22, 2011.

[302] T. Tomic, K. Schmid, P. Lutz, A. Domel, M. Kassecker, E. Mair, I. L. Grixa, F. Ruess, M. Suppa, and D. Burschka, "Toward a fully autonomous UAV: Research platform for indoor and outdoor urban search and rescue," *IEEE robotics & automation magazine*, vol. 19, no. 3, pp. 46–56, 2012.

[303] S. Ullah, K.-I. Kim, K. H. Kim, M. Imran, P. Khan, E. Tovar, and F. Ali, "UAV-enabled healthcare architecture: Issues and challenges," *Future Generation Computer Systems*, vol. 97, pp. 425–432, 2019.

[304] A. K. Dixit, J. J. Sherrerd *et al.*, *Optimization in economic theory*. Oxford University Press on Demand, 1990.

[305] H. Hasselt, "Double q-learning," *Advances in neural information processing systems*, vol. 23, pp. 2613–2621, 2010.

[306] A. Fotouhi, M. Ding, and M. Hassan, "Dynamic base station repositioning to improve performance of drone small cells," in *2016 IEEE Globecom Workshops (GC Wkshps)*. IEEE, 2016, pp. 1–6.

[307] M. D. Nguyen, T. M. Ho, L. B. Le, and A. Girard, "UAV placement and bandwidth allocation for UAV based wireless networks," in *2019 IEEE Global Communications Conference (GLOBECOM)*. IEEE, 2019, pp. 1–6.

[308] D. Lopez-Perez, A. Valcarce, G. De La Roche, and J. Zhang, "OFDMA femtocells: A roadmap on interference avoidance," *IEEE communications magazine*, vol. 47, no. 9, pp. 41–48, 2009.

[309] K. Seong, M. Mohseni, and J. M. Cioffi, "Optimal resource allocation for OFDMA downlink systems," in *2006 IEEE International Symposium on Information Theory*. IEEE, 2006, pp. 1394–1398.

[310] G. Li and H. Liu, "Downlink radio resource allocation for multi-cell OFDMA system," *IEEE transactions on wireless communications*, vol. 5, no. 12, pp. 3451–3459, 2006.

[311] I. C. Wong and B. L. Evans, "Optimal downlink OFDMA resource allocation with linear complexity to maximize ergodic rates," *IEEE Transactions on Wireless Communications*, vol. 7, no. 3, pp. 962–971, 2008.

[312] G. L. Stuber, J. R. Barry, S. W. Mclaughlin, Y. Li, M. A. Ingram, and T. G. Pratt, "Broadband MIMO-OFDM wireless communications," *Proceedings of the IEEE*, vol. 92, no. 2, pp. 271–294, 2004.

[313] G. J. Foschini, "Layered space-time architecture for wireless communication in a fading environment when using multi-element antennas," *Bell labs technical journal*, vol. 1, no. 2, pp. 41–59, 1996.

[314] "Capacity obtained from multiple-input multiple-output channel measurements in fixed wireless environments at 2.5 GHz], author=Erceg, Vinko and Soma, Pitchaiah and Baum, Daniel S and Paulraj, Arogyaswami J, booktitle=2002 IEEE International Conference on Communications. Conference Proceedings.

ICC 2002 (Cat. No. 02CH37333), volume=1, pages=396–400, year=2002, organization=IEEE."

[315] P. Stoica, R. L. Moses *et al.*, "Spectral analysis of signals," 2005.

[316] S. Suman, S. Kumar, and S. De, "Path loss model for UAV-assisted RFET," *IEEE Communications Letters*, vol. 22, no. 10, pp. 2048–2051, 2018.

[317] E. Telatar, "Capacity of multi-antenna gaussian channels," *European transactions on telecommunications*, vol. 10, no. 6, pp. 585–595, 1999.

[318] A. Goldsmith, S. A. Jafar, N. Jindal, and S. Vishwanath, "Capacity limits of MIMO channels," *IEEE Journal on selected areas in Communications*, vol. 21, no. 5, pp. 684–702, 2003.

[319] S. Vishwanath, N. Jindal, and A. Goldsmith, "Duality, achievable rates, and sum-rate capacity of Gaussian MIMO broadcast channels," *IEEE Transactions on information theory*, vol. 49, no. 10, pp. 2658–2668, 2003.

[320] A. A. Ibrahim, T. Kim, and D. J. Love, "On the achievable rate of generalized spatial modulation using multiplexing under a Gaussian mixture model," *IEEE Transactions on Communications*, vol. 64, no. 4, pp. 1588–1599, 2016.

[321] S. Ruder, "An overview of gradient descent optimization algorithms," *arXiv preprint arXiv:1609.04747*, 2016.

[322] K. B. Petersen, M. S. Pedersen *et al.*, "The matrix cookbook," *Technical University of Denmark*, vol. 7, no. 15, p. 510, 2008.

[323] S. Cui, A. J. Goldsmith, and A. Bahai, "Energy-constrained modulation optimization for coded systems," in *GLOBECOM'03. IEEE Global Telecommunications Conference (IEEE Cat. No. 03CH37489)*, vol. 1. IEEE, 2003, pp. 372–376.

[324] ——, "Modulation optimization under energy constraints," in *IEEE International Conference on Communications, 2003. ICC'03.*, vol. 4. IEEE, 2003, pp. 2805–2811.

[325] T. H. Lee, *The design of CMOS radio-frequency integrated circuits*. Cambridge university press, 2003.

[326] M. Parker, *Digital Signal Processing 101: Everything you need to know to get started*. Newnes, 2017.

[327] S. Cui, A. J. Goldsmith, and A. Bahai, "Energy-efficiency of mimo and cooperative mimo techniques in sensor networks," *IEEE Journal on selected areas in communications*, vol. 22, no. 6, pp. 1089–1098, 2004.

[328] M. Gustavsson, J. J. Wikner, and N. Tan, *CMOS data converters for communications*. Springer Science & Business Media, 2000, vol. 543.

[329] S. Cui, A. J. Goldsmith, and A. Bahai, "Energy-constrained modulation optimization," *IEEE transactions on wireless communications*, vol. 4, no. 5, pp. 2349–2360, 2005.

[330] Rohde-Schwarz. (2020) IEEE 802.11ax TECHNOLOGY INTRODUCTION. [Online]. Available: https://www.rohde-schwarz.com/uk/solutions/test-and-measurement/wireless-communication/wireless-connectivity/wlan-wifi/wlan-ieee-802.11ax-testing/white-paper-ieee-802.11ax-technology-introduction_253050.html

[331] T. L. Narasimhan and A. Chockalingam, "On the capacity and performance of generalized spatial modulation," *IEEE Communications Letters*, vol. 20, no. 2, pp. 252–255, 2015.

[332] L. Liu, S. Zhang, and R. Zhang, "CoMP in the sky: UAV placement and movement optimization for multi-user communications," *IEEE Transactions on Communications*, vol. 67, no. 8, pp. 5645–5658, 2019.

[333] M. Zhang, M. El-Hajjar, and S. X. Ng, "Intelligent Caching in UAV-Aided Networks," *IEEE Transactions on Vehicular Technology*, 2021.

[334] C. E. Shannon, "A mathematical theory of communication," *ACM SIGMOBILE mobile computing and communications review*, vol. 5, no. 1, pp. 3–55, 2001.

[335] R. J. Vanderbei *et al.*, *Linear programming*. Springer, 2020.

[336] A. Granas and J. Dugundji, *Fixed point theory*. Springer Science & Business Media, 2013.